AD-A255 380

(2)

FINAL REPORT FOR 1991

MECHANICS OF COMPOSITE MATERIALS FOR SPACECRAFT

George J. Dvorak and Mark S. Shephard

DTIC
ELECTE
AUG 3 1 1992
S A D

This document has been approved for public release and sale; its distribution is unlimited.

Submitted to

Mechanics Division
Office of Naval Research
800 North Quincy Street
Arlington, Virginia

Contract Number N00014-90-J-1918

92-23937

92 8 28 040

DTIC QUALITY INSPECTED 5

Accesion For
NTIS CRA&I ☑
DTIC TAB ☐
Unannounced ☐
Justification .....
By .....
Distribution /
Availability Codes
Dist | Avail and / or Special
A-1

ONR Contract Information

ONR Contract Number: N00014-90-J-1918
Scientific Officer: Dr. Yapa Rajapakse
Principal Investigators: Dr. George J. Dvorak and Dr. Mark S. Shephard
Project Duration: June 1, 1991 to December 31, 1991

Description of the Scientific Research Goals

During this seven month project efforts continued on the development of advanced analytical and numerical techniques which can be effectively combined to provide advanced thermo-mechanical modeling of composite materials with nonlinear constituents. The areas of emphasis during this period were:

- development of thermoplastic and thermoviscoplastic models of composite materials using transformation strains
- finite element formulation of bimodal plasticity model in combination with various forms of dimensional reduction
- idealization control for composite materials

Significant Results of the Project

Thermoplastic and Thermoviscoplastic Models of Composite Materials using Transformation Strains

This part of the research program focused on development and implementation of an innovative approach for nonlinear problems in multiphase media to replace classical solutions which rely on finite element analysis of representative volumes. The latter approach has been employed in our previous research work in the context of the Periodic Hexagonal Array (PHA) model [9, 14] and required substantial computational effort.

The new approach evolved from our research in uniform fields and transformation fields in two-phase and multi-phase elastic media [5, 6, 7, 8] and leads to a simple solution of nonlinear thermomechanical problems in multiphase media. In particular, thermal and inelastic strains in the phases are treated as transformation strains and the inelastic deformation problem is reduced to an elasticity problem for the transformation strain in the phases. When such strains are taken as piecewise uniform in the discretized microstructure, problems of this kind lead to a system of linear algebraic equations which involve certain eigenstrain influence coefficients and the given instantaneous constitutive relations of the inelastic phases. The influence coefficients depend on the microstructure and on elastic constants of the phases, and are therefore constant. These influence coefficients can be evaluated for any given representative volume element.

This solution strategy is advantageous when the representative volume is subjected to many incremental loading steps under homogeneous boundary conditions. The results coincide with those obtained by conventional finite element analysis, but can be found more efficiently. In particular, in viscoplastic analysis of composites where the inelastic strain in the phases is derived

from the thermoviscoplasticity theory which was developed under the current project [1], or other theories with a similar framework, the local stress and strain rates depend on the overall applied thermomechanical load and the current local fields. In this way, the solution can be found fairly easily in the new method. In contrast, evaluation of the local fields with the PHA model and the finite element method requires evaluation of a local instantaneous stiffness matrix which is a function of the local stress or strain rate. This causes certain numerical complications since the local stress and strain rates vary continually.

In the reporting period, we have fully developed computational schemes for evaluation of the local fields in fibrous media with elastic-plastic and viscoplastic phases using the transformation strain approach described above. Expansion of the transformation strain method to symmetric laminated plates was also formulated. The approach for laminates treats the collection of subelements present in all the layers as one multiphase media subjected to certain constraints which are derived from the micromechanical model for each layer, such as the PHA model, and the constraints imposed on the strains in the plane of the laminate. In this way, the procedure developed for nonlinear analysis of multiphase media is applicable to laminates when the appropriate influence coefficients derived from the laminate analysis are used.

Finite Element Formulation of Bimodal Plasticity Model in Combination with Various Forms of Dimensional Reductions

The two mode semi-phenomenological model underlying bi-modal plasticity should give a distinct computational advantage to models such as the periodic hexagonal array (PHA) model in which a local finite element solution is required. However, the combination of the need to always check both modes at a point and the complexity of resolving the slip planes for the matrix dominated mode introduced substantial increases in the computational effort required to apply this model. In particular, the need to construct and solve the roots of a quartic polynomial introduced substantial computational expense [16]. The original implementation of the bi-modal plasticity model introduces only a small computational improvement over the coarse mesh PHA model. A more careful examination of the implementation of these procedures has identified a number of areas where specific improvements can be introduced. Those implemented to date cut the computational effort of bi-modal plasticity in half, thus increasing the attractiveness of the model. Additional improvements are possible.

Plate and shell formulations, and the equivalent reduced dimension finite element formulations operate in a five dimensional stress space. Since the basic bi-modal plasticity model was formulated in a full six dimensional stress space, specific modifications were required to eliminate the sixth component so it could be used with these finite elements [2].

These versions of the bi-modal plasticity model were then used with both three-dimensional solid and our previously developed discrete layer theory element [4] finite elements on various test cases [2, 3, 13]. With total loads taken to from four to seven times that causing initial yield, a number of solution quantities were compared. Since the linear fibers provide the majority of the structural stiffness, the overall deformations showed only a small influence due to matrix yielding. The difference between the solid and discrete layer shell idealizations were not noticeable. Examination of resultant bending moments along supports showed a more pronounced influence to the nonlinear material behavior with redistributions of nearly fifteen percent. Examination of

the stresses through the thickness showed a more pronounced redistribution in specific locations due to the material nonlinearities. The local stresses also demonstrated the biggest difference between the solid and discrete layer shell idealizations. Although direct inplane stresses were nearly the same for both idealizations as the load was increased well past initial matrix yield, the through the thickness shear stresses showed major differences as the load increased. These differences can be important in the prediction of failure modes which are dependent on the values of the transverse shear stresses.

In addition to the above studies, a detailed examination of the formation and distribution of both the fiber and matrix dominated modes in the layers of both a thin and thick transverse load plate were examined [12].

Idealization Control for Composite Materials

The goal of the majority of our development efforts to date have focused on the specific idealizations associated with the mixing models in the presence of nonlinear constituents, and the through the thickness kinematic assumptions on plate and shell type formulations. The experience gained in combining these two levels of idealization [3, 12] clearly indicates that the reliable modeling of the physical behavior of composite structures requires the balanced consideration of each of the analysis idealizations used to go from the physical system to the numerical analysis models. The goal of our efforts on this portion of the project was to begin to build on our expertise in adaptive finite element techniques and idealization control methodologies [11, 15] to develop idealization control techniques for nonlinear composite materials.

Specification and categorization of the idealization steps associated with the analysis of composites with nonlinear material behavior is complicated by both the complexity of the idealizations needed and the close interrelationships among the idealization steps. The prediction of the performance of composite structures must explicitly account for the physical scales that control the behavior of interest. There are a variety of methodologies available to account for these physical scales in an analysis. Of particular interest in composite structures with material nonlinearities is accounting for micromechanical behavior. The methods available to account for micromechanical level nonlinearities include:

- application of micromechanical mixing models using idealized micro-geometry and boundary conditions to predict the macromechanical constitutive relationship at the material points in the macromechanical model
- application of local micromechanical level models coupled with macromechanical models
- application of micromechanical models throughout the entire analysis domain

The second analysis idealization steps critical to the effective analysis of composite materials are dimensional reductions.

Initial efforts in composite idealization control have focused on implementing and extension of our currently available techniques within a general analysis idealization control framework [15]. In addition Professor Fish at RPI has begun extending his superposition concepts to control the multiscale idealizations common to composite materials [10]. The combination of these two key capabilities, is allowing us to use a new approach for the adaptive control of the multiscale idealizations needed for the effective analysis of composite materials [12].

References

[1] Y. A. Bahei-El-Din, R. S. Shah, and G. J. Dvorak. Numerical analysis of the rate-dependent behavior of high temperature fibrous composites. In S. N. Singhal, W. F. Jones, and C. T. Herakovich, editors, *Mechanics of Composites at Elevated and Cryogenic Temperatures*, volume AMD-118, pages 67–78. 1991.

[2] M. W. Beall and M. S. Shephard. Advanced finite element formulations for composite shells. In *Proceedings of the American Society of Composites 6th Technical Conference on Composite*, pages 360–369, 1991.

[3] M. W. Beall, J. F. Wu, and M. S. Shephard. Lamina level nonlinear composite mixing models in finite element computations. In J. N. Reddy, editor, *Enhancing Analysis Techniques for Composite Materials*, pages 197–200, New York, 1991. ASME.

[4] K. Dorninger. A nonlinear layered shell finite element with improved transverse shear behavior. Technical Report SCOREC Report # 4-1991, Scientific Computation Research Center, Rensselaer Polytechnic Institute, Troy, NY 12180-3590, 1991.

[5] G. J. Dvorak. On uniform fields in heterogeneous media. *Proc. Royal Soc. London*, A 431:89–110, 1990.

[6] G. J. Dvorak. Plasticity theories for fibrous composite materials. In R. K. Everett and R. J. Arsenault, editors, *Metal Matrix Composites*, volume 2, pages 1–77. Academic Press, Boston, 1991.

[7] G. J. Dvorak. Transformation field analysis of inelastic composite materials. *Proceedings of the Royal Society, London*, A437:311–326, 1992.

[8] G. J. Dvorak and Y. Benveniste. On transformation strains and uniform fields in multiphase elastic media. *Proceedings of the Royal Society, London*, A437:291–310, 1992.

[9] G. J. Dvorak and J. A. Teply. Periodic hexagonal array models for plasticity of composite materials. In *Plasticity Today: Modeling, Methods and Applications*, pages 623–642. Elsevier, Amsterdam, 1985.

[10] J. Fish and S. Markolefas. The s-version of the finite element method for multilayer laminates. *Int. J. Numer. Meth. Engng.*, 33:1081–1105, 1992.

[11] M. S. Shephard, P. L. Baehmann, M. K. Georges, and E. V. Korngold. Framework for the reliable generation and control of analysis idealizations. *Comp. Meth. Appl. Mech. Engng.*, 82:257–280, 1990.

[12] M. S. Shephard and M. W. Beall. Analysis idealization control for composite materials with nonlinear materials. In S. G. Advani, W. R. Blain, W. P. de Wilde, J. W. Gillespie, Jr., and O. H. Griffin, Jr., editors, *Computer Aided Design in Composite Material Technology III*, pages 313–330. Computational Mechanics Pub. and Elsevier Applied Science, 1992.

[13] M. S. Shephard, J. Fish, and M. W. Beall. Idealization control for the analysis of composite materials. *Computing Systems in Engng.*, to appear, 1992.

[14] J. L. Teply and G. J. Dvorak. Bounds on the overall instanteous properties of elastic-plastic composites. *J. Mech. Phys. Solids*, 36(1):29–58, 1988.

[15] R. Wentorf, A. Budhiraja, R. R. Collar, M. S. Shephard, and P. L. Baehmann. Two prototypes testing the use of an expert system in the control of structural analysis

idealizations. In E. N. Houstis, J. R. Rice, and R. Vichnevetsky, editors, *Intelligent Scientific Software*, pages 283–326. North Holland, Amsterdam, 1992.

[16] J. F. Wu. *Numerical Techniques for the Elastic Plastic Analysis of Fibrous Metal Matrix Composites*. PhD thesis, Civil Engineering, Rensselaer Polytechnic Institute, Troy, NY, 1991.

List of Publications/Reports/Presentations

Publications

[1] Y. A. Bahei-El-Din and G. J. Dvorak. New results in bimodal plasticity of fibrous composite materials. In A. S. Khan and M. Tokuda, editors, *Advances in Plasticity*, pages 121–127. Pergamon Press, 1989.

[2] Y. A. Bahei-El-Din and G. J. Dvorak. A review of plasticity theory of fibrous composite materials. In W. S. Johnson, editor, *Metal Matrix Composites: Testing, Analysis and Failure Modes, ASTM-STP 1032*, pages 103–129. American Society for Testing and Materials, Philadelphia, 1989.

[3] Y. A. Bahei-El-Din, G. J. Dvorak, and R. S. Shah. Numerical analysis of the elastic-plastic behavior of fibrous metal matrix composites. In W. K. Liu, P. Smolinski, R. Ohayon, J. Navickas, and J. Gvildys, editors, *Computational Experiments*, volume 176, pages 125–131.

[4] Y. A. Bahei-El-Din, G. J. Dvorak, and J. F. Wu. Dimensional stability of metal-matrix laminates. *Composites Science and Technology*, 43:207–219, 1992.

[5] Y. A. Bahei-El-Din, R. S. Shah, and G. J. Dvorak. Numerical analysis of the rate-dependent behavior of high temperature fibrous composites. In S. N. Singhal, W. F. Jones, and C. T. Herakovich, editors, *Mechanics of Composites at Elevated and Cryogenic Temperatures*, volume AMD-118, pages 67–78. 1991.

[6] M. W. Beall and M. S. Shephard. Advanced finite element formulations for composite shells. In *Proceedings of the American Society of Composites 6th Technical Conference on Composite*, pages 360–369, 1991.

[7] M. W. Beall, J. F. Wu, and M. S. Shephard. Lamina level nonlinear composite mixing models in finite element computations. In J. N. Reddy, editor, *Enhancing Analysis Techniques for Composite Materials*, pages 197–200, New York, 1991. ASME.

[8] G. J. Dvorak. Plasticity theories for fibrous composite materials. In R. K. Everett and R. J. Arsenault, editors, *Metal Matrix Composites*, volume 2, pages 1–77. Academic Press, Boston, 1991.

[9] G. J. Dvorak, Y. A. Bahei-El-Din, R. S. Shah, and H. Nigam. Experiments and modeling in plasticity of fibrous composites. In G. J. Dvorak, editor, *Inelastic Deformation of Composite Materials*, pages 270–293. Springer-Verlag, New York, 1991.

[10] M. S. Shephard and M. W. Beall. Analysis idealization control for composite materials with nonlinear materials. In S. G. Advani, W. R. Blain, W. P. de Wilde, J. W. Gillespie, Jr., and

O. H. Griffin, Jr., editors, *Computer Aided Design in Composite Material Technology III*, pages 313–330. Computational Mechanics Pub. and Elsevier Applied Science, 1992.

[11] M. S. Shephard, J. Fish, and M. W. Beall. Idealization control for the analysis of composite materials. *Computing Systems in Engng.*, to appear, 1992.

[12] J. F. Wu, Y. A. Bahei-El-Din, G. J. Dvorak, and M. S. Shephard. A bimodal plasticity model for fibrous composites implemented in ABAQUS - I. fiber-dominated mode. In *Proceedings of the ABAQUS Users' Conference*, pages 519–527. Hibbitt, Karlsson & Sorensen, Inc.

[13] J. F. Wu, M. S. Shephard, G. J. Dvorak, and Y. A. Bahei-El-Din. A material model for the finite element analysis of metal matrix composites. *Composites Science and Technology*, 35:347–366, 1989.

Presentations by Dr. Dvorak

[1] A new approach in nonlinear micromechanical analysis of heterogeneous media. Chicago, Illinois, July 1991. First U.S. National Congress on Computational Mechanics.

[2] Invited lecture at plasticity 91. Grenoble, France, August 12-16 1991. Third International Symposium of Plasticity and its Current Applications.

[3] Engineering education in the united states. Czechoslovakia, Prague, August 29 1991. Klokner Institute of the Czech Technical University in Prague.

[4] Fatigue damage and shakedown in metal matrix composite laminates. Czechoslovakia, Prague, September 2 1991. Conference on New Trends in Structural Mechanics, Institute of Theoretical Applied Mechanics, Czechoslovakia Academy of Sciences.

[5] Experimental evaluation of yield surfaces and plastic strains in a metal matrix composite. Albany, New York, October 6-9 1991. American Society of Composites Meeting.

[6] Fatigue and shakedown in metal matrix composites. Gainesville, Florida, November 6-8 1991. 28th Annual Technical Meeting of the Society of Engineering Science.

[7] On some exact results in thermoplasticity of composite material. Atlanta, Georgia, December 4 1991. ASME/WAM.

[8] Thermal stresses in elastic-plastic composites with coated fibers. Atlanta, Georgia, December 6 1991. ASME/WAM.

[9] Overview of mechanics of composites program. Troy, New York, January 20 1992. Italian Visitors.

[10] Mechanics of hot isostatic pressing. Troy, New York, February 21 1992. Center for Composite Materials and Structures.

[11] Experimental plasticity of fibrous metal matrix composites. University of Oklahoma, Norman, Oklahoma, April 23 1992. University of Oklahoma, Third Charles E. Foster Lecture.

[12] Mechanics of hot isostatic pressing. San Antonio, Texas, April 27 1992. Southwest Research Institute.

[13] Mechanics of hot isostatic pressing. College Station, Texas, April 28 1992. Texas A&M University.

[14] Uniform strain fields in heterogeneous material. Houston, Texas, April 29 1992. Rice University.

[15] A new approach to inelastic analysis of heterogeneous media. Tempe, Arizona, April 30 1992. ASME Summer Mechanics and Materials Meeting.

[16] On effective properties of piezoelectric composites. Leesburg, Virginia, May 19 1992. ONR Workshop on Active Materials and Structures.

[17] Transformation field analysis of heterogeneous media. Arlington, Virginia, June 30 1992. ONR Review Meeting.

[18] Mechanics of fracture in metal matrix composites and mechanics of hot isostatic pressing. State College, Pennsylvania, July 2 1992. Penn State University.

Presentations by Dr. Shephard

Listed limited to only the presentations on composites — mesh generation and adaptive methods lectures not given

[1] Lamina level nonlinear mixing models in finite element computations. Atlanta, GA, December 6, 1991. ASME.

[2] Framework for the analysis of composites with explicit idealization control. Tempe Arizona, April 30 1992. 1992 ASME Applied Mechanics, Materials and Aerospace Summer Meeting.

[3] Analysis idealizatipon control for composite materials with nonlinear behavior. Newark, Delaware, May 14 1992. 3rd Int. Conf. on CAD in Composite Material Technology.

[4] An analysis idealization control framework to support engineering modeling and design. Troy, NY, May 20 1992. ARO Workshop on Adaptive Methods in Partial Differential Equations.

Presentations by Dr. Bahei-El-Din

[1] Symposium on the mechanics of composites at elevated and cryogenic temperatures. Columbus, Ohio, June 16-19 1991. ASME Applied Mechanics Division.

[2] Local stresses in high temperature fibrous composites. Chicago, Illinois, July 21-24 1991. First U.S. National Congress on Computational Mechanics.

[3] Invited lecture, mechanics of materials branch. Hampton, Virginia, January 21 1992. NASA Langley Research Center.

[4] Invited lecture, aluminum company of america. Alcoa Technical Center, Pennsylvania, January 22 1992. Aluminum Company of America.

SELECTED PUBLICATIONS

IDEALIZATION CONTROL FOR THE ANALYSIS OF COMPOSITE MATERIALS

M. S. Shephard, J. Fish and M. W. Beall

Scientific Computation Research Center
Rensselaer Polytechnic Institute
Troy, NY 12180-3590

Abstract—The various idealization steps required to go from the physical description of a composite structures to the numerical analyses used to predict thermo-mechanical response are overviewed. A general methodology for the reliable control of these idealizations steps in proposed. One component of this methodology is a general analysis idealization control system which can easily combine a variety of analytic (numeric) and knowledge-based procedures through a goal manager and analysis strategist. The second component of the methodology is the use of idealization regions typically added to lower level analysis models using superposition techniques. A simple example that demonstrates some of the concepts is presented.

INTRODUCTION

The reliable modeling of the physical behavior of composite structures requires the balanced consideration of each of the analysis idealizations used to go from the physical system to the numerical analysis models. Specification and categorization of the idealization steps associated with the analysis of composite materials with nonlinear material behavior is complicated by both the idealizations needed and the close interrelationships among the idealization steps. This paper discusses a set of techniques currently under development to control these idealizations.

The prediction of the performance of composite structures must explicitly account for the physical scales that control the behavior of interest. There are a variety of methodologies available to account for these physical scales in an analysis. Of particular interest in composite structures with material nonlinearities is accounting for micromechanical behavior. The methods available to account for micromechanical level nonlinearities include:

- application of micromechanical mixing models, using idealized micro-geometry and boundary conditions, to predict the macromechanical constitutive relationship at the material points in the macromechanical model
- application of local micromechanical level models coupled with macromechanical models
- application of micromechanical models throughout the entire analysis domain

Since most composite structures are small in at least one direction, dimensional reduction is also an important analysis idealization which is commonly applied.

The techniques under development build on two key capabilities. The first is an overall idealization control modeling methodology [1, 2, 3] which combines analytic and knowledge-based applications with the model representations of the composite structure. A goal manager is used to specify the analyses to be performed and the analyses are controlled by an analysis strategist responsible for performing, evaluating and improving the analysis idealizations. The second capability, which is key to the efficient and reliable application of analysis strategies appropriate for composite materials, is multiscale solution procedures based on the mesh superposition-method (s-method) [4, 5, 6]. The s-method for analysis idealization control expands the concepts of hierarchical mesh overlays to control mesh discretizations, to hierarchic idealization overlays where the overlays introduce specific local improvements in the analysis idealizations. In the case of composite materials this includes local elimination of dimensional reductions and the explicit representation of micro-structure.

The combination of the overall idealization control methodology with the mesh superposition method allows the reliable performance of analyses throughout the design process where the level of idealization control used is that needed at that point in the design process.

CONTROL OF ANALYSIS IDEALIZATIONS

Analysis Idealization

The application of engineering analysis typically incorporates a number of idealizations to reduce the physical behavior of a system to a set of algebraic equations that can be solved manually or on a computer. Each step of idealization used in an engineering analysis process introduces some level of approximation. The reliability of an analysis depends on the ability to understand and control the errors introduced by each step of idealization [7, 8, 9].

The accuracy of a solution is a function of the measure(s) of accuracy of interest. It is therefore important to qualify the error of interest, e_α, in an appropriate norm as

$$\underline{e}_\alpha = \left\| \underline{u} - \underline{u}_{app} \right\|_\alpha \tag{1}$$

where $\underline{u}$ is the exact solution, $\underline{u}_{app}$ is the approximate solution, and $\|v\|_\alpha$ is the norm written in terms of the variable v. Typically several norms of the solution results are of interest.

The first step to estimate the errors in engineering analysis is to enumerate the contributing sources as

$$e_\alpha = e_\alpha(\Psi, \psi, \Phi, \Omega, D, \beta, \Delta) \tag{2}$$

where Ψ is the basic mathematical model selected to represent the physical behavior of interest, ψ represents the physical scale the mathematical model is solved upon and the alterations to the basic mathematical model associated with representation of lower scales, Φ are the dimensional reductions and associated alterations to the mathematical model to eliminate physical dimensions, Ω is the domain of the analysis, D are the material property parameters, β are the boundary conditions (also initial conditions when time is one of the dimensions of the problem), and Δ represents the discretization used for the analysis.

Since the exact solution to a requested analysis is generally not known, it is only possible to obtain estimates of the solution error. The goal of idealization error control is to ensure that

$$E_{\alpha_i} \leq \Upsilon_{\alpha_i} \qquad\qquad i = 1, 2, 3, ..., m \tag{3}$$

where Υ_{α_i} is the desired error limit for the i^{th} norm, E_{α_i} is the value of the error estimate for the i^{th} norm, with $E_{\alpha_i} \rightarrow e_{\alpha_i}$ as the solution procedure is refined, and $E_{\alpha_i} \simeq e_{\alpha_i}$ for a solution of acceptable cost.

The techniques available to aid in the control of idealization errors include analytically-based error estimation, hierarchic model comparisons, analytically-based results for ideal situations, sensitivity analysis, statistical methods, comparison to known physical limits, test results and reasonable limits, and rules based on experience and intuition[8]. Analytically-based error estimation and hierarchic model comparisons provide the greatest promise for the reliable estimation of the idealization error contributions. Analytically-based error estimators have been developed to provide reliable control of

some of the finite element discretization errors. However, techniques of similar reliability are not readily available to control other idealization error contributions. The combination of analytically-based error estimation and hierarchic model comparisons is a promising approach for the control of the other idealizations critical to the analysis of composite structures.

Framework for Analysis Idealization Control in Engineering Design

The ability to apply idealization control during engineering design requires a system framework which can house various levels of analysis idealization control along with intelligent design methodologies and engineering analysis tools. The framework of an engineering modeling system for mechanical objects (IDEALZ) that is specifically structured to support the idealizations used in engineering modeling and analysis is described in references [1, 2, 3]. The system architecture is consistent with the architectures being considered to support design modeling systems in reference [10].

The heart of the system is the representation of the object being designed and the modelers that support that representation. To support the functions necessary in the design evolution of an object, its representation is housed in linked functional and geometric model structures, each of which are controlled by the appropriate modelers. The other operational components of the modeling system are the applications. The applications include analysis procedures to answer performance questions, algorithms to alter the design based on analysis results, and procedures to plan the manufacturing processes, etc. Applications are separated into two groups based on the technology underlying their implementation, not on the functions addressed. The first group is analytically-based applications. The majority of the applications in this group are numerical analysis and optimization procedures. The second group is knowledge-based applications. Knowledge-based applications operate from codified heuristics placed in rule sets.

The task of analysis idealization control falls to the goal manager and the analysis strategist which guide the operation of the system. The goal manager and the analysis strategists interact with the models, applications, and databases to track the various activities that have been performed and guide the application of those that are requested. The first task of the goal manager is to accept a request to perform an operation, and determine if the basic information and capabilities required to perform the task exist. It then invokes the strategist which is responsible for formulating and controlling the idealization steps required to perform the requested analysis. The goal manager is

responsible for maintaining information about the status of the analysis goals used for the design and the goals that have been performed previously.

ANALYSIS IDEALIZATION CONTROL FOR COMPOSITE STRUCTURES

The close interaction of the methods of idealization control applied to composite materials tends to make one idealization process flow into the next and makes the idealization processes dependent upon each other. Although this makes the process of idealization categorization difficult, and in some cases seemingly arbitrary, it affords an opportunity to incorporate idealization evaluation processes that can provide useful insight into multiple idealization steps.

Mathematical model. The derivation of the base mathematical model begins with a clear enumeration of the physical laws deemed critical to the description of the physical behavior at hand. In the case of the thermo-mechanical behavior of heterogeneous materials the minimum scale that must be addressed in any analysis idealization must be considered. In structural composites of the overall scale considered here, the minimum level is deemed to be orders of magnitude above that of the individual atomic units. This assumption allows us to employ classic continuum mechanics in terms of i) equilibrium of mechanical forces, ii) kinematic relationships relating internal deformations (strains) to displacements, and iii) constitutive relations between internal forces and deformations. These relationships must be satisfied at any scale for which they are constructed. They are valid down to constituent levels where the minimum dimensions of the constituents considered are well above atomic dimensions. Such assumptions may not be reasonable in extremely small scale structures such as micromachines or ultra-thin multichip interconnects.

Physical scale of the solution and representation of lower scales. By their very nature, the thermo-mechanical analysis of heterogeneous materials at a macromechanical level must explicitly account for the micromechanical structure and properties of the constituents. In some simple linear cases, this may be through simple models which are easy to apply. However, in more advanced situations much more explicit consideration of the micromechanical level behavior is needed. For example, metal matrix composites can not be properly designed without explicit consideration of the material nonlinearities. These materials demonstrate nonlinear behavior early in the load-deformation process, and the extension of linear results past the limit of linearity is not conservative [11, 12].

The determination of a homogenization method and its bounds of validity appropriate for the problem at hand must consider:

- the accuracy level required for the terms in the homogenized constitutive model developed
- the geometry of the microstructure
- the well posedness of the mathematical model with respect to local damage models due to the possible loss of ellipticy
- the material behavior of the constituents
- the need to use the information generated during the homogenization process to predict local field information after the global field is determined
- the gradients in the solution parameters with respect to the size of the microconstituents used in the homogenization process

A number of analytic procedures are available to perform the homogenization of idealized micromechanical geometries when the constituent materials are linear elastic [13]. In many cases these procedures can be shown to produce tight bounds on the macromechanical constitutive relations. However, they often do not provide accurate estimates of the detailed local stresses and strains for other than the idealized geometric configuration assumed.

When one or more of the constituent materials becomes nonlinear, analytically derived homogenization expressions require solution through numerical iteration. One such model is the vanishing fiber diameter model which has the two deficiencies of not being able to accurately model behavior dominated by transverse stresses and not being able to provide accurate local values.

An alternative approach to the development of homogenization procedures when the constituents become nonlinear is phenomenological micromechanic models such as bimodal plasticity [11]. This model uses the inner envelop of a micromechanical level fiber dominated mode and matrix dominated mode. The numerical implementation of such a procedure can be made quite efficient, however, it is not likely that such approach will provide accurate predictions of local field quantities.

Numerical models using more realistic micro-geometries have recently received considerable attention for the homogenization of nonlinear constituents. One such model is the periodic hexagonal array model [14] in which a local finite element discretization is used in the construction of a macromechanical constitutive model based on the constituent properties. Although a computationally demanding model, the periodic hexagonal array model does provide accurate prediction of the overall properties, and, if the local

discretization is fine enough, a good estimation of the local field quantities. Another micromechanical level analyses based on a finite element implementation of mathematical homogenization [15] is given by Guedes and Kikuchi [16].

Most homogenization procedures rely on a level of uniformity of the local fields at each point of evaluation. If the gradients of the critical solution parameters are too high, the accuracy and validity of the homogenization process is in question.

The ability to evaluate the idealization errors associated with homogenization is strongly dependent on the homogenization process used. Mathematical analysis procedures can be used in some cases to bound specific elastic constants. The ability to define such bounds is often lost by the introduction of nonlinear material behavior of the constituents. The use of finite element techniques for the solution of the homogenized problem provides an interesting method to employ discretization error control techniques to evaluate the homogenization errors [16].

Separate evaluation procedures are required when the high local gradients invalidate the micromechanical uniform periodicity of the entire homogenization process.

Dimensional reductions. Since the effective use of composite materials must account for the directional nature of the material, most composite components are thin in at least one direction. Therefore, the development of analysis idealizations must deal with the reduction of the through the thickness direction. This introduces the complexities of the plate and shell type of assumptions which all utilize at least one representational inconsistency which leads to complexities in the representation of transverse shear and/or introduce representational difficulties at boundaries and junctures in shells. These problems become even more critical in composite materials [17].

One approach to the control of idealization errors associated with dimensional reduction is to convert it into a discretization process. Instead of stating specific assumptions on the through the thickness direction, a convergent discretization through the thickness is used which allows the development of estimates of the error introduced by truncating the expansion at a given point [18, 19]. Since many of the finite element discretizations of laminated shells [20] employ semi-discretizations where there are laminate level through the thickness discrete assumptions applied, the use of an expansion through the thickness is possible.

Often the need to improve the through the thickness idealization is limited to critical areas. In these cases is advisable to employ different levels of through the thickness idealization locally. For example at shell boundaries or at junctures complete three-dimensional representations could be used to improve the solution accuracy [21].

Alternatively, two level models can be used to determine local parameters and to provide feedback to locally improve the through the thickness idealization. Noor has successfully demonstrated such a procedure [22, 6] for composite shells.

Domain. Domain simplifications in the analysis of composite materials can arise at each scale level considered. At the macromechanical level there are the standard domain simplifications of ignoring fillets, small cutouts, etc. An additional concern in the evaluation of the influence of these procedures is the directional nature of composites will complicate the evaluation of idealization procedures. For example, typical dimensions for assuming Saint-Venant's principle holds can be much greater for anisotropic materials.

At the micromechanical scale it is common to employ geometric simplifications of the shape and distribution of the constituents in the specification of the idealization used in the homogenization process. Consideration must be given to the influence of these approximations on the determination of macromechanical material parameters. Often the approximations used have only a small influence on these parameters. In some cases, consideration must also be given to the influence of micromechanical domain approximations on the estimation of local quantities such as stress concentration factors that may be used in criteria to estimate the initiation of local nonlinear behavior and/or damage.

Material properties. The accuracy of the material parameters in a macromechanical constitutive relation are a function of the homogenization process and the accuracy of the constituent material parameters, including the representation of interfaces or interphases. Therefore, the accuracy of representation of the material parameters must consider the constituents and the representation, if any, of the constituent interfaces. Once the constituent material parameters have been combined through homogenization to produce a macromechanical constitutive relation, it is also necessary to examine the ability of that relationship to represent the material behavior.

Although the mathematical model places constraints on the overall form of the constituent constitutive relations, there are a wide range of possible models that can be selected when material nonlinearities must be represented. The selection of these models must consider both the model's ability to represent the experimentally measured material response, and the validity and influence of that model on the nonlinear solution processes that must be applied to that model during thermo-mechanical analyses. At this time there has been a limited amount of work on the qualification of the idealization errors associated with nonlinear material models [23, 24].

Boundary and initial conditions. The representation of boundary conditions must

account for the homogenization and dimensional reduction processes. The dimensional reduction processes introduce a number of problems in the specification of boundary conditions [25]. The issues of boundary condition representation become even more complex in composite materials if edge effects are considered. Another issue of particular importance associated with the specification of boundary conditions is when a local micromechanical level analysis needs to obtain boundary conditions determined by a global macromechanical analysis.

Discretization. The control of discretization errors for composite materials at a particular level becomes complicated by the desire to control the discretization errors as they relate to variables at different scales where different discretizations may be used at the different levels of scale. Even with these complications it is clear that error control based on a posteriori error estimation is the most reliable method to qualify and control idealizations.

COMPOSITE STRUCTURES IDEALIZATION CONTROL USING SUPERIMPOSED REGIONS

An Approach to a-posteriori Idealization Control

The approach to analysis idealization outlined here is an extension of the basic concepts used in adaptive discretization error control coupled with hierarchical models applied through hierarchic superposition methods. The basic assumption underlying the approach is the ability to selectively apply improvements to locally enrich idealizations in much the same manner the basis functions can be enriched over portions of a finite element mesh to obtain a given level of discretization control.

To consider such an idealization control process, one must consider the exact solution to the analysis problem. This solution would be obtained by the *most-comprehensive idealization* if all *idealization expansions* are allowed to go to their limit. For example, in a case where only dimensional reduction and spatial discretization errors are introduced, the exact solution to the *most-comprehensive idealization* would have a three-dimensional discretization with an infinite number of degrees-of-freedom. It is clear that the exact solution to the *most-comprehensive idealization* cannot be obtained. However, the goal of adaptive idealization control is to have a reliable estimate of the error between the *current idealization*, for which we have a solution, and the exact solution to the *most-comprehensive idealization*. These estimates will be obtained by employing various forms

of *higher-level idealizations* which would, in the limit, become the solution to the *most-comprehensive idealization*.

A major objective of this approach is to develop practical computational techniques to construct and solve the required higher-level idealizations in a computationally efficient manner. A promising approach to achieve this is by a hybridization of *a posteriori* discretization error estimation procedures with hierarchic modeling methodologies. As a by-product, a measure of the local idealization error, termed here as *a posteriori local idealization error estimators*, will be developed. This concept is analogous to the elemental *a posteriori* discretization error estimators, in which two numerical schemes are compared on the element level and the local error of a lower degree scheme is approximately taken as the difference between the two.

The philosophy behind the proposed local idealization error estimates is similar to that of their discretization counterpart, namely, if the solution is locally enriched, the solution outside the local region is not significantly affected, and thus the bulk of the error can be computed on the local level assuming insignificant changes outside the local region are taking place, thus reducing the problem of error estimation to one of manageable size. Discretization error indicators based on this approach were found to be very efficient, especially in linear applications, making us believe that application of these ideas in the context of hierarchic modeling will be efficient as well.

The basic steps in the *a posteriori* idealization error estimation procedure are i) model subdivision into *idealization regions*, ii) error estimation on individual *idealization regions* and iii) estimation of the total idealization error

Model subdivision. There are two levels of model subdivision used. The first is the lowest level used for the numerical discretization, e.g., the finite element mesh. The second subdivision consists of what are referred to as *idealization regions*. The *idealization region* is the local unit over which local a posteriori idealization error estimation is performed. In general, the *idealization regions* may be of arbitrary shape (Fig. 1) and can be independent of the finite element mesh. However, it may often be advantageous to align the boundaries of the idealization region with the boundary of finite elements to maximize computational efficiency.

The idealization regions are defined to isolate portions of the model where it may be necessary to introduce hierarchic improvements in the idealization used in the global analysis. Figure 1 depicts one such example where the global idealization has introduced geometric simplifications that ignored a crack tip and small circular cutout. These

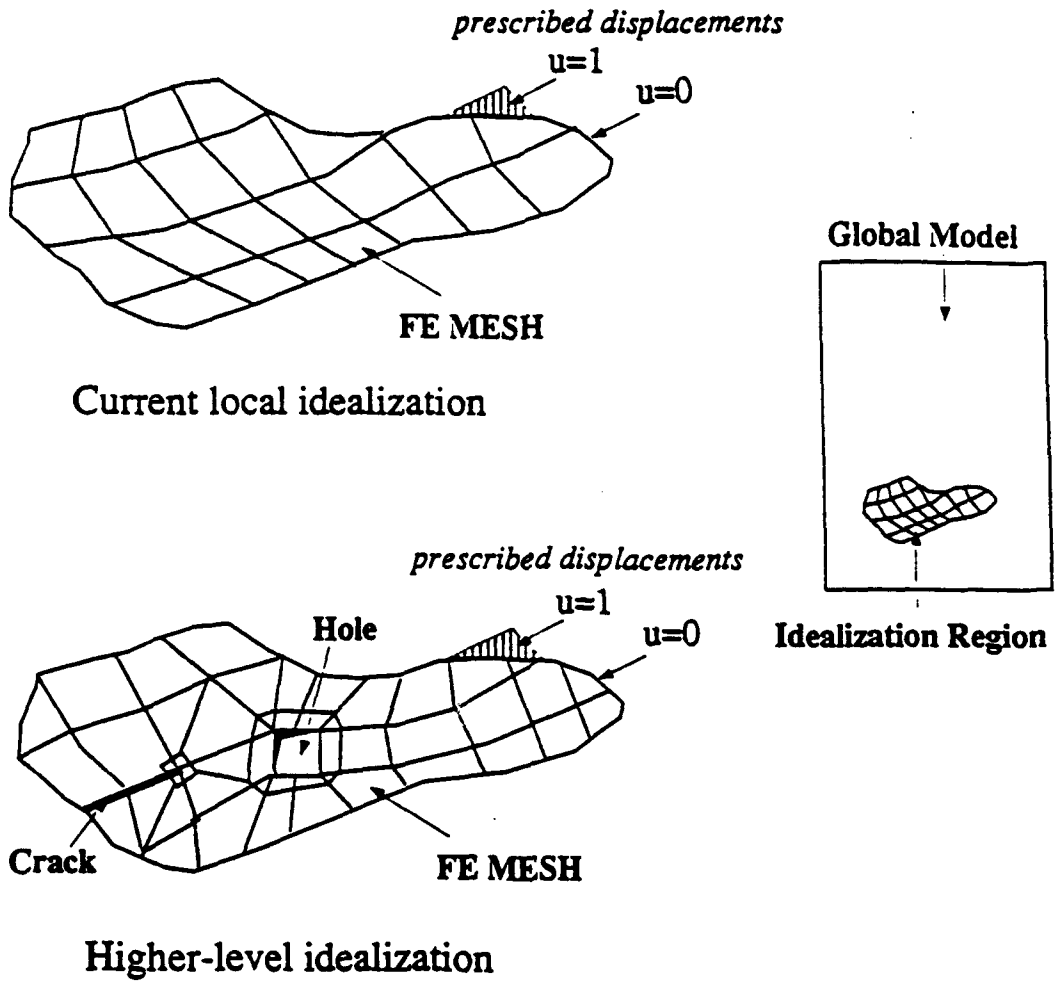

Figure 1 Idealization regions

geometric features can be introduced into an improved idealization locally using an appropriately selected idealization region.

Reliable computational techniques require that these regions be defined based on a combination of a priori and a posteriori information. The a priori information is knowledge of the individual localized idealizations performed in a step of the analysis. For example, knowledge of the local geometric simplifications in the example of Figure 1 can be used in the determination of an idealization region that isolates them, allowing further local investigation. The a posteriori information to be used must be derived from the solution results of the global analysis model. These results, combined with

a knowledge of the local idealizations performed, must be used to derive simple error indicators which key the need to define idealization regions allowing an explicit estimation of the idealization errors. For example, the stress in the area of a small hole ignored in a global analysis can be multiplied by a conservative stress concentration factor to see if a more careful consideration of the idealization error due to ignoring that hole is required [68]. Another simple example would be to use knowledge of global stress magnitudes and gradients to see if an idealization region needs to be defined to more carefully estimate the influence of edge effects at critical locations on the boundary of a composite structure.

Error estimation in a single idealization region. In general, the errors in the *idealization region* can be estimated by comparing the behavior of the *most-comprehensive idealization* to the *current idealization* model in the idealization region. One way the behavior of such a local idealization region may be quantified is in terms of its overall and local responses.

The quality of the overall behavior of a given idealization region may be assessed by its ability to accurately represent the interaction with the remaining global idealization. A given idealization model can be considered to have an accurate overall behavior if, for all possible prescribed displacement modes applied on its boundary, the traction resultants in the *current idealization* model and its higher level counterpart are within the required error tolerance. The difference in these traction values measured in appropriate norms can be used to estimate the quality of the overall behavior in the idealization region. Obviously, in the implementation of such error estimation procedure, the prescribed displacement field will consist of a finite number of degrees-of-freedom expressed in terms of finite element shape functions applied on the boundary of the idealization region as shown in Fig.1.

On the other hand, the ability of a given local idealization model to accurately resolve some critical local behavior, such as a maximum stress, must be assessed using various sup-norms, depending on the goal of analysis. In many cases, a *current idealization* model can accurately resolve the overall behavior of an idealization region, but may err badly in predicting some critical pointwise values. A typical example is a problem of a small scale yielding zone at the tip of a crack. If the characteristic size of the idealization region is much greater than the size of the plasticity zone, the overall behavior of the idealization element might not be significantly affected by the material nonlinearity.

Although this procedure will reduce the error estimation to a local level, numerical solution of the *most-comprehensive* local idealization model subjected to a variety of

loading conditions as shown in Fig. 1 is not realistic, especially in the case of large idealization regions and nonlinear material and kinematical mathematical models. Therefore, efforts must be devoted to further reduce the computational cost of the local error estimation.

So far, the formulation of the local error estimation was based on the idea that since the displacement field at the boundary of the idealization region is unknown *a priori* the behavior of the local model can only be assessed by subjecting it to all possible prescribed fields. By drawing the analogy to the elemental discretization error estimators, it is reasonable to assume that, for the purpose of error estimation, it is sufficient to assess the behavior of the local model by only subjecting it to the displacement field found from the global solution of the *current idealization model*. This reduces the computation of the local error estimation to a single boundary value problem over the domain of the local idealization region.

To provide effective idealization estimates the relative contribution of various individual idealizations associated with the reduction of the *most-comprehensive local idealization* model to the *current local idealization*, must be obtained without explicit comparison of these two models. For example, consider a linear laminated plate as a *current idealization*, and a fully nonlinear layerwise solid as the *most-comprehensive idealization*. In this case, solution of a single three-dimensional nonlinear problem is more expensive than solving both a nonlinear laminated plate problem (to examine the effect of nonlinearities) and a linear layerwise solid model (to examine the effect of the refined through-the-thickness modeling). These two contributions added together in some meaningful way should be able to determine the total local idealization error.

Remark 1: The philosophy behind this approach is analogous to that of the residual error discretization error indicators, except that the actual idealization is compared not only to the higher level discretization models, but also, to other higher level local idealization schemes. Note that the idealization error, although it may be large, can be orthogonal or "almost orthogonal" to one or more higher level idealization models. In other words, one may have a poor idealization of a physical phenomenon, but by enriching the actual idealization model in a certain manner (for example, accounting for geometric nonlinearities in a plate where the deflections are much smaller than the thickness) no significant improvement in the solution will be achieved. For this class of problems, estimation of the relative contributions of various idealizations associated with the reduction of the most-comprehensive local model to the current local idealization will be more efficient than comparing these two models.

It is currently assumed that only the errors in the overall behavior of the local idealization region will be needed to steer the process of *global (or first level) adaptivity*, since only these errors may directly affect the global response and the force redistribution within the model. The detailed response within the local idealization region can be recovered by means of postprocessing techniques such as subjecting the local model to the boundary conditions obtained from the global solution. Adaptive techniques may be employed to solve the local boundary value problem, which is referred here as a *second level (local) adaptivity*. This approach will enable the further reduction of the problem of error estimation to one of a manageable complexity, while retaining its essential characteristics.

Estimation of the total idealization error. Idealization error estimates for the whole problem domain are to be obtained by adding the contributions from all idealization regions in some meaningful way to be determined as a part of this research. The effectiveness of this approach must be verified by computing the *idealization error effectivity index*, defined as the ratio of the estimated idealization error to the "exact" error which can be approximated by employing a close approximation to the *most-comprehensive global idealization* model

Remark 2: Special care must be exercised while estimating errors due to the scale reduction, where the homogenized (macro) and heterogeneous (micro) models are considered as lower and higher level representations, respectively. Idealization errors resulting from scale reduction cannot be assessed without explicitly considering the homogenization procedure as indicated below.

Assessment of Idealization Errors Due to Scale Reduction

The techniques to derive the effective properties of heterogeneous media is a well established field starting from the simple model of Rule of Mixtures (RM), followed by the Composite Spheres (CS) model of Hashin [26], the Self Consistent (SC) method of Budianski [27] and Hill [28], the Generalized Self Consistent (GSC) method of Christensen [29], the Mori-Tanaka (MT) method which has many contributors, but the simplest form has been given by Benveniste [30], and finally the Periodic Hexagonal Array (PHA) of Dvorak and Teply [14]. The primary objective here is to assess the errors introduced by scale reduction when one of the homogenization procedures is used, and consequently, to develop an adaptive strategy for nearly optimal scale representation.

For the purpose of developing a unified framework to control homogenization errors it is convenient to view the scale reduction as a five-step process:

1. Macrostructure idealization as a spatial repetition of representative volume elements (RVE) of the microstructure.
2. Idealization of prescribed fields of the RVE assuming that it is subjected to prescribed uniform (periodic) field.
3. Solution of the boundary value problem of RVE for all prescribed uniform fields.
4. Solution of the boundary value problem of an equivalent homogeneous volume EHV for the same prescribed uniform fields.
5. Extraction of material properties from the energy equivalence between EHV and RVE.

Remark 3: In practice homogenization models based on the solution of the inclusion problem (fiber embedded in the infinite matrix media (SC), fiber embedded in the homogenized composite media (MT), fiber embedded in the two-phase (matrix and composite) media (GSC)) are based on finding concentration factors relating averages of local fields to overall fields [24].

Four of these steps introduce some level of approximation. A brief description given below indicates what each source of error is and how to control these errors.

Periodicity assumption. Periodicity is referred herein as a geometric repetition of representative volume with no restriction made on uniformity of local fields. In most composites geometric periodicity is only an approximation. Various mathematical approaches to control these errors exist, but will not be extensively addressed in this paper.

Solution of the boundary value problem for RVE. The errors introduced in this step depend on the type of homogenization procedure employed. The CS, SC, GSC and MT homogenization techniques employ analytically-based results for idealized situations to solve microscopic boundary value problems. The PHA method involves solution of the boundary value problem of the representative volume element using a finite element method. In this case, a standard discretization error control procedure can be used to control the errors at this step. Furthermore, since, with reasonable discretization the PHA model is more accurate than any of the above analytically-based methods, especially for inelastic problems [24], it can serve as a higher level hierarchical model for all homogenization techniques.

Solution of the boundary value problem for EHV. At this step we prescribe a uniform overall strain field on the boundary of the equivalent homogeneous volume. No errors are introduced at this step if the geometry of the EHV can be exactly represented by a finite element mesh, and the finite elements employed in the discretization pass the 'patch' test (which test their ability to exactly represent constant fields).

Idealization of prescribed fields on RVE. Theoretically, the problem of simplification of boundary conditions and loading applied on the RVE can be treated by means of hierarchical modeling. By this technique the microscopic boundary value problem can be solved for both actual and idealized (uniform and periodic) prescribed fields applied on the boundary of RVE. The difference in the solution measured in an appropriate norm can be used to quantify the errors introduced due to the idealization of prescribed fields. Further research is required to assess the idealization errors introduced in this step.

Energy equivalence. At this step, the energies absorbed in RVE and EHV are compared in order to extract material properties. For linear problems this step introduces no errors. However, when one of the phases deforms plastically, its homogeneity is lost, local properties become stress-dependent within the phase and their instantaneous values need to be found at many loading points. In such a case it is only possible to define instantaneous properties of EHV from the instantaneous properties of phases. This is accomplished by comparing the energy rates in both models [14]. The error in this step is tightly linked to the mathematical idealization of the material model and the specification of material and state parameters.

Remark 4: Special care must be exercised to account for degradation of effective material properties (as a result of damage in microstructure), which may result in strain softening phenomenon [31, 32]. It has been shown that strain softening dissipates no energy, and thus a failure is localized to a region of a vanishing size. The mathematical model becomes ill-posed since the governing equations change type, which manifests itself in severe mesh-size dependence in the finite element solution. For real materials this is an unrealistic feature and demonstrates one of the difficulties we encounter in modeling failure processes of materials. Regularization of these ill-conditioned mathematical equations by enriching the fundamental mechanics of failure process is a critical step in reliable modeling. This can be achieved either by regularization through localization limiters techniques [33], or by incorporating rate sensitivity into the material model [32], or by the use of embedded shear banding techniques of the type proposed by Pietruszak and Mroz [34] and Belytschko, Fish and Engelmann [31].

Framework for Multiscale Computational Techniques

In practical problems modeling of physical phenomenon has to be performed at several scales in order to capture both the overall and local features of the prototype. For example, an airplane shown in Fig. 2 is approximately 30m long, while the diameter of the fastener hole is approximately 2.5mm. In order to determine the force redistribution

between the various structural components, fasteners, lugs and other interconnecting parts must be accurately modeled at a scale which is three orders of magnitude smaller than the entire aircraft. Furthermore, if various failure modes such as delamination or matrix yielding at the free edge of the fastener made of more than 100 layers (not unusual in aircraft structures) are of interest, the interconnecting parts should be modeled as an assemblage of three dimensional lamina models. And finally, prediction of micromechanical failure modes such microbuckling, microcracking, or fiber breaking necessitates considerations at even smaller scales. The useful life and cost of maintenance of the structure depends on the quality of modeling at each scale and the ability of a reliable transfer of the appropriate information between various modeling levels. In this section we briefly summarize the basic ideas of such multiscale computational techniques termed in the references [5, 6, 35, 36, 4] as the s-version of the finite element method.

The basic idea of the s-version of the finite element method is that a portion of domain, where unacceptable idealization errors have been identified, is overlaid by a patch(s) of local idealization regions as shown in Fig. 3. The solution in the entire problem domain Ω is obtained by superimposing displacements resulting from the global analysis model $\underline{u}^G$ defined on Ω with the displacements $\underline{u}^L$ on local idealization regions Ω_L. The total displacement field $\underline{u}$ is approximated by adding the two fields

$$\underline{u} = \underline{u}^G + \underline{u}^L \text{ in } \Omega_L \tag{4}$$

where

$$\underline{u}^L = 0 \text{ on } \Gamma_{GL} \tag{5}$$

and

$$u_k^G + u_k^L = g_k \text{ on } \Gamma_{g_k} \; k = 1, \ldots, n_{sd} \tag{6}$$

where Γ is the boundary of the problem domain Ω, which consists of the prescribed displacement boundary Γ_{g_k} and the prescribed traction boundary Γ_{h_k}. Γ_{GL} is the boundary between the global and local analysis models, and g_k are prescribed displacements on Γ_{g_k}. Condition (5) is required in order to satisfy compatibility between the global and local analysis models.

Both the global (macroscopic in Fig.3) and the local (microscopic Fig.3) displacement fields are discretized using hierarchical C^0 continuous shape functions on finite element meshes as

$$u_k^G = N_{kA}^G(s,t) d_A \tag{7}$$

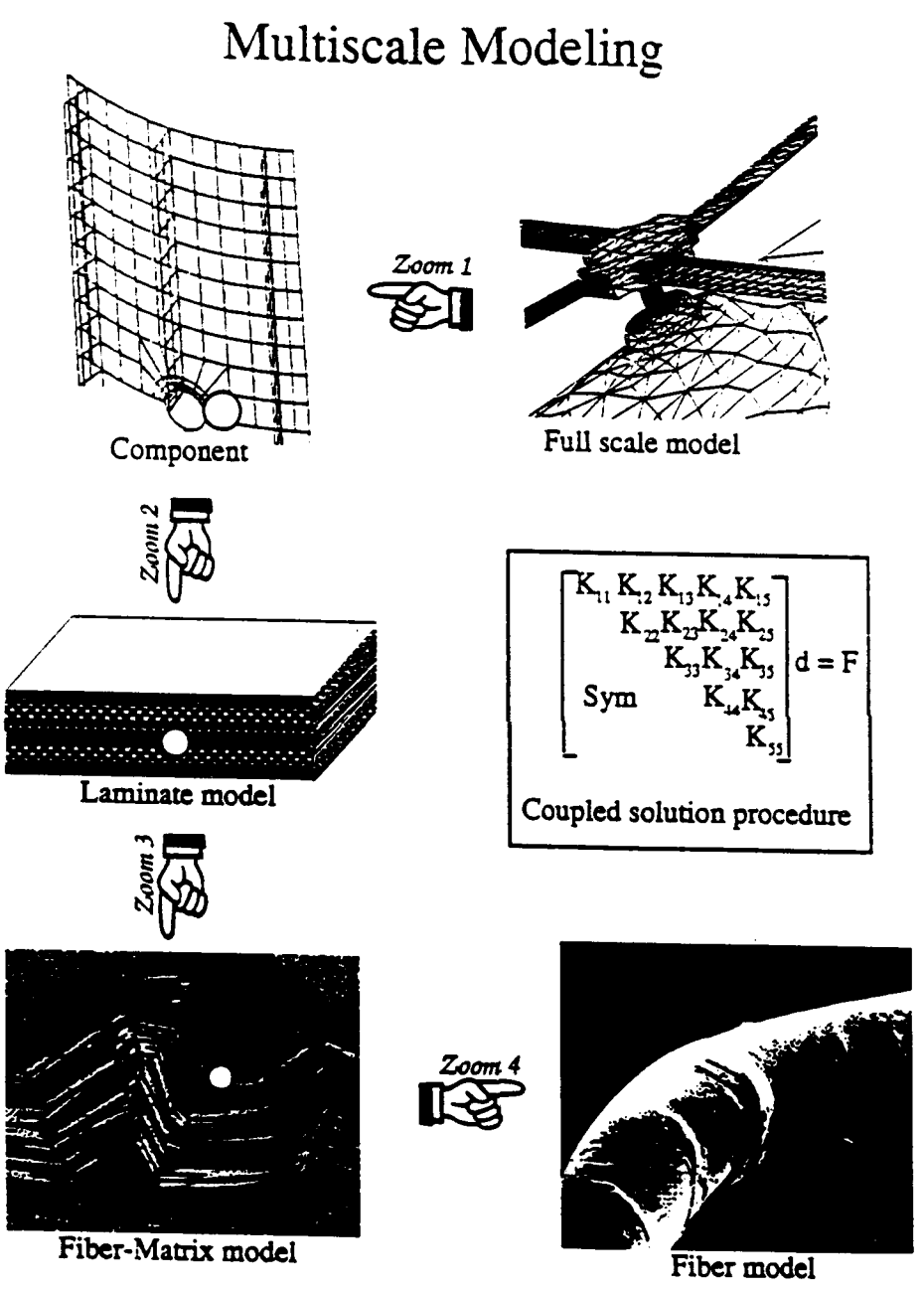

Figure 2 Multiple scales of a composite aircraft

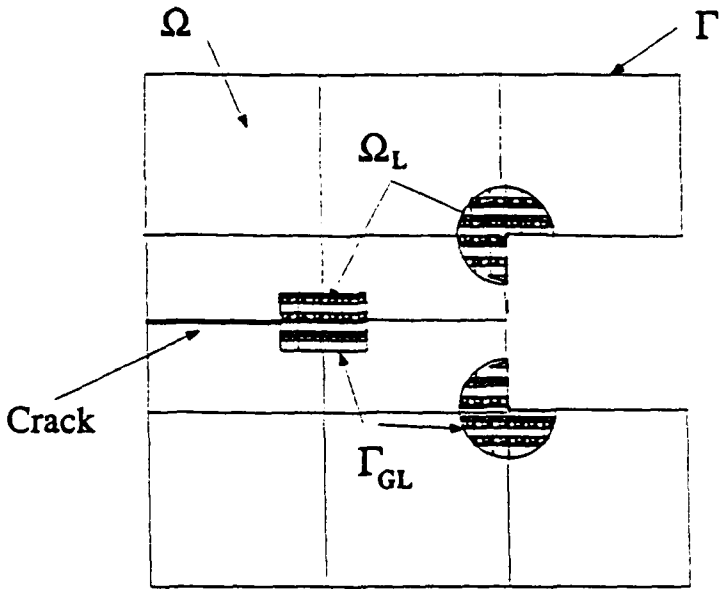

Figure 3 Multiscale modeling by the s-method

$$u_k^L = N_{kA}^L(s,t)a_A \tag{8}$$

where d_A and a_A are the degrees-of-freedom in the global and local finite element meshes, respectively. The lower case subscripts indicate spatial components, while the upper case subscripts indicate degrees-of-freedom. Standard tensorial notation is used with summation over the repeated indices.

The compatibility condition (5), is imposed by constraining the nodal and side degrees-of-freedom on the boundary between the meshes

$$a_A|_{\Gamma_{GL}} = 0 \tag{9}$$

The discrete equilibrium equations can be obtained by the principle of virtual work, which for linear elasticity problems, states

$$\int_{\Omega-\Omega_L} \delta u_{(i,j)} D_{ijkl} u_{(k,l)} d\Omega + \int_{\Omega_L} \delta u_{(i,j)} \mathcal{D}_{ijkl} u_{(k,l)} d\Omega - \int_{\Gamma_{h_i}} \delta u_i h_i d\Gamma - \int_{\Omega} \delta u_i b_i d\Omega = 0 \ \forall \ \delta \mathbf{u} \tag{10}$$

In equation (10) the D_{ijkl} and $\mathcal{D}_{ijkl}$ represent homogenized and heterogeneous constitutive tensors, respectively, b_i and t_i are the body forces and prescribed tractions, respectively, and the prefix δ designates a variation. Discrete equations are obtained by substituting interpolants eqs.(7, 8) into variational statement eq.(10) and requiring arbitrariness of local and global variations. For details of see [37, 38].

Remark 5: Several strategies can be employed to control the location of the superimposed mesh. One approach is to construct the superimposed heterogeneous mesh from a fixed amount of representative volumes, corresponding to those which would give the highest value of the homogenization error indicators. Alternatively, one could decide *a priori* on the homogenization error indicator value, say $\gamma\left(E^{\text{het}} - E^{\text{hom}}\right)_{\text{max}}$ where $0 \leq \gamma \leq 1$, above which all the representative volumes which produce a larger error would be included in the superimposed model.

ILLUSTRATIVE RESULTS

The purpose of this section is to illustrate the process of idealization error control. A very simple problem was selected to investigate some of the issues in developing this type of system. Much work remains to be done in the area of developing reliable and accurate idealization error estimation proceedures and the overall control system. For the purposes of this demonstration some simple idealization error indicators are used. The general idea for this example was to model a problem as simply as possible and then use that solution and some simple post processing techniques to enhance our knowledge of how the problem should be modeled. In this example the idealizations considered are the modeling of material properties, dimensional reduction, physical scale and discretization.

Problem Definition

The problem investigated here is that of a flat plate, with three sides clamped and one simply supported, subject to a uniform pressure load. The plate is made of boron/aluminum with a fifty percent volume fraction. A (0/90)s lay-up is used in this example. The geometry of the plate is as indicated in Fig. 4.

System Description

The geometric model in this example was generated using the geometric modeler CATIA [39]. Interfaces to CATIA have been developed for both the model manipulations required to construct idealized geometries, which are controlled by the goal manager and

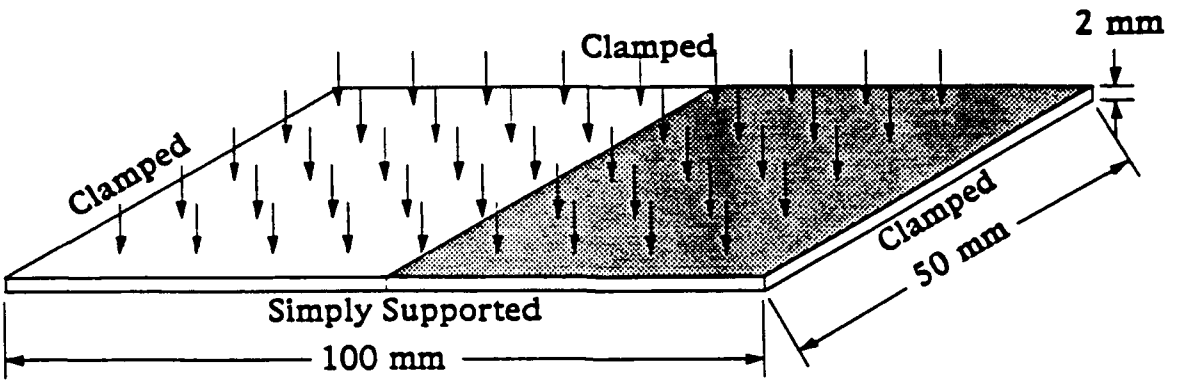

- Flat Plate
- Boron/Aluminum (50% v.f.)
- (0/90)s Layup

Figure 4 Plate Geometry for Example Problem

strategist [40] and for mesh generation using the Finite Octree [41] mesh generator. The ABAQUS [42] finite element analysis program and the Mesh Superposition Research Code [4, 5, 6] were used to perform the analyses in this example. In the future many different types of analysis codes and modelers will be integrated into the system to allow for the use of the most appropriate analysis procedures for a given analysis goal. All of these programs are tied together to provide a system which can both adaptively change the representation of the model to reflect different idealization and provide adaptive meshing capabilities.

The process starts with the definition of the problem to be analyzed. This definition must include a geometric description, attributes and a functional model. From this problem definition and any a priori information known about the problem, an initial set of idealization regions is created and initial idealizations are defined on the idealization regions. After this initial information is given to the system the adaptive idealization process can start.

At each cycle of the adaptive idealization process the following steps must be performed:

1. Determine and specify the appropriate idealizations over the appropriate idealization regions.
2. Convert the physical model to a numerical model through the specified idealization processes.

3. Obtain the numerical solution.
4. Evaluate the idealization error estimate or indicator for each idealization in each idealization region.
5. Redefine the idealization regions and idealizations and return to step 2.

Initial Model

There are four idealizations that will be investigated in this problem. The first idealization investigated is the material behavior. The assumption of elastic behavior in this material is incorrect at most reasonable load levels since plasticity in the matrix occurs long before the material approaches its usable limits. However, it has been observed [43] that even when plasticity occurs in the matrix, the overall deformation of the plate is primarily governed by the elastic response of the fibers. In this example the elastic material properties are calculated using a Mori-Tanaka mixing model. The second idealization is that of dimensional reduction. In this problem the plate relatively thin (h/L = 25) thus for the initial analysis a first order shear deformation model will be used. The appropriate initial dimensional reduction is then that of a two dimensional plate. The third idealization is the mesh discretization used for the analysis. Mesh discretization error is controlled using adaptive mesh refinement procedures. The fourth idealization is the scale of analysis. This issue will be addressed using a global/local analysis procedure and s-method finite element analysis [4, 5, 6]. The initial scale used in this analysis assumes that the material is homogeneous on the lamina level. Further refinement of this idealization will consider the existence of both fibers and matrix in the material.

For this problem the initial idealization regions cover the entire domain of the plate. There is one defined for the material property idealization and one for the dimensional reduction. In the course of an adaptively idealized analysis these idealization regions will be subdivided and refined when there are areas with different idealizations.

Mesh Discretization

The mesh for this model was automatically generated and refined using the Finite Octree mesh generator [41] and a simple adaptive algorithm to define the areas of mesh refinement. The adaptive meshes are shown in Fig. 5

Material Model

For this particular problem, if we account for yielding in the matrix, we would not expect the gross behavior of the plate to change significantly since the elastic response of

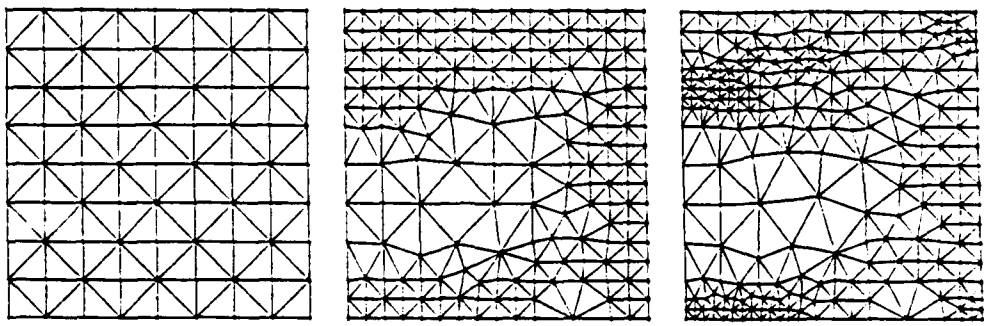

Figure 5 Adaptively Refined Meshes for Flat Plate

the fibers will still be the dominant factor. However, stress resultants and local stresses will change strongly with the nonlinear material behavior. How important these changes are depends on the goals of the analysis. If the goal of the analysis is to find the displacement at the center of the plate to within a few percent, the elastic material model may be sufficient. However, if the goal is to investigate some local stresses at a point in the plate or to determine the reaction forces and their distributions at the supports with great precision, then such an analysis may not be adequate. We can obtain an indication of the error due to the material model by using the stresses predicted by the problem solved using the elastic model. In this case, it was determined where, in relation to the initial yield surface of the composite, the stresses from the elastic model were. The initial yield surface used is that given by the bimodal plasticity material model [11]. Note that this is a very inexpensive procedure compared to doing the analysis with the nonlinear material model itself. Figure 6 shows the areas where plasticity will have occurred anywhere through the thickness using this criterion. The actual plastic areas would be expected to be somewhat larger than those shown here since there will be a certain redistribution of load away from the inelastic areas. This information can then be used to redefine the idealization regions for the material properties and, in those regions where plasticity was predicted, change the idealization.

Dimensional Reduction

The first order shear deformation theory used in this analysis generally gives good results for the inplane stress quantities, however the predictions for transverse quantities are usually poor. These poor predictions for transverse stresses may not be too important unless these stresses reach too large a magnitude. Large transverse shear stresses may indicate an area where delaminations may occur or grow. Also large transverse shear

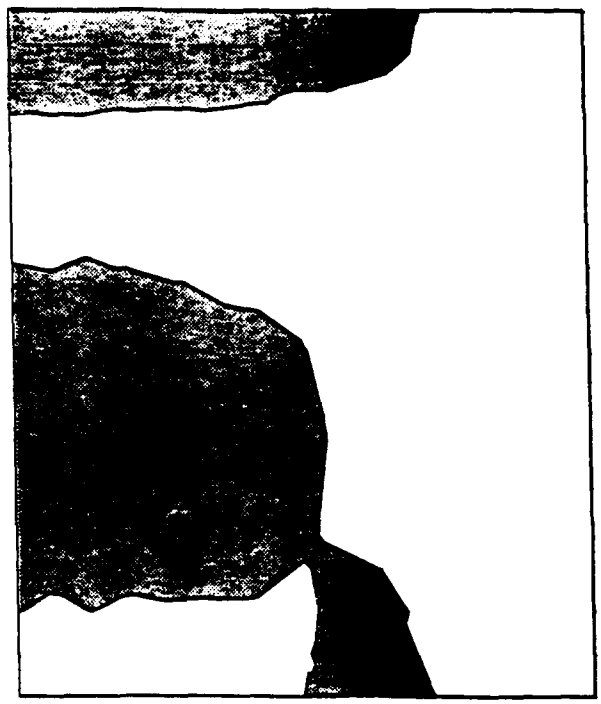

Figure 6 Areas of Plasticity for Plate Example

stresses may initiate plasticity in the matrix. A more accurate stress field can be calculated from the one predicted by shear deformation theory by finding transverse stresses that satisfy the equilibrium equations locally [44]. For the problem at hand the transverse stresses were calculated to satisfy the equilibrium equations through the thickness of the plate. Since the occurrence of large transverse shear stresses are of concern, the magnitude of the greatest shear stress was found through the thickness of the plate at each integration point. The results of this are shown in Fig. 7. If the transverse shear stress is high enough there is the need to model that particular area in more detail. In particular we might choose to use a layerwise plate model or a three dimensional solid model of the plate in that area.

The new idealized model in this example could include a three-dimensional idealization region. An example of such a refined model is shown in Fig. 8.

Scale of Analysis

To assess the micromechanical response (stresses and strains) of the heterogeneous

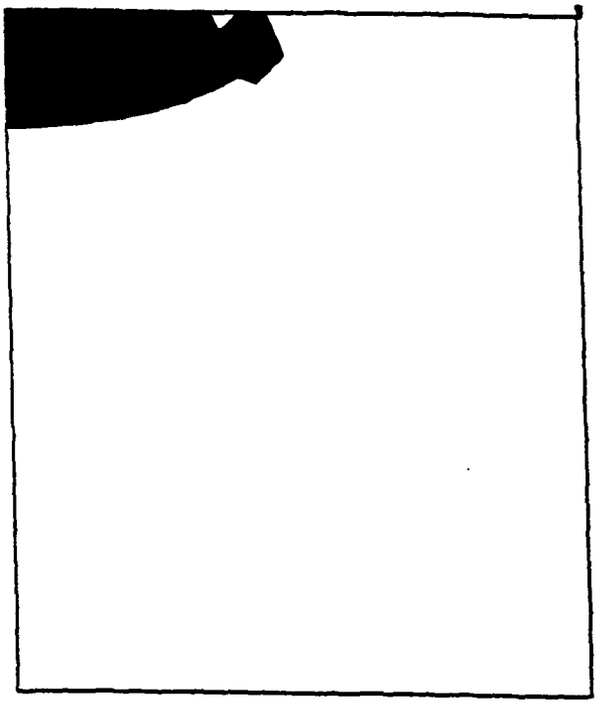

Figure 7 Areas with high transverse shear stress

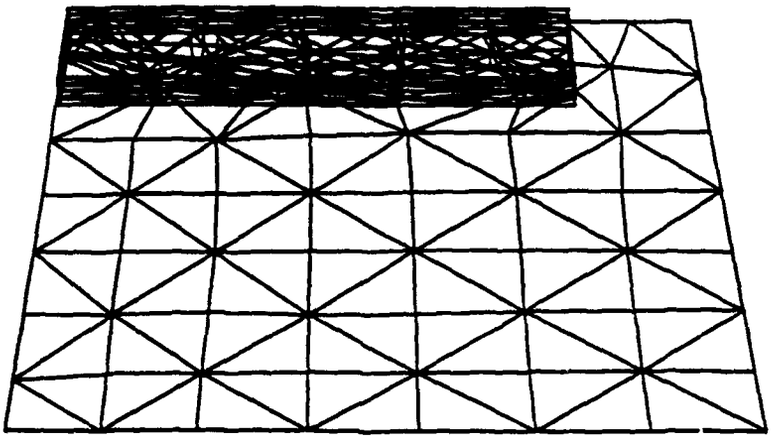

Figure 8 Model after idealization region defined

constituents (fibers and matrix) we employ a multiscale finite element method for locally nonperiodic medium developed in references [37, 38]. By this technique, in the portion of the problem domain where the material is formed by a spatial repetition of the base cell and the macroscopic solution is smooth, a double scale asymptotic expansion and solution periodicity are assumed. Consequently, mathematical homogenization theory is used to uncouple the microscopic problem from the global solution. It has been found that the reactions on the plane normal to the simply supported edge are significantly smaller than the other planes. Therefore, a two-dimensional idealization was deemed adequate. This analysis was performed by extracting the tractions thought the thickness of the plate near the edge of the global model and applying them to the local model.

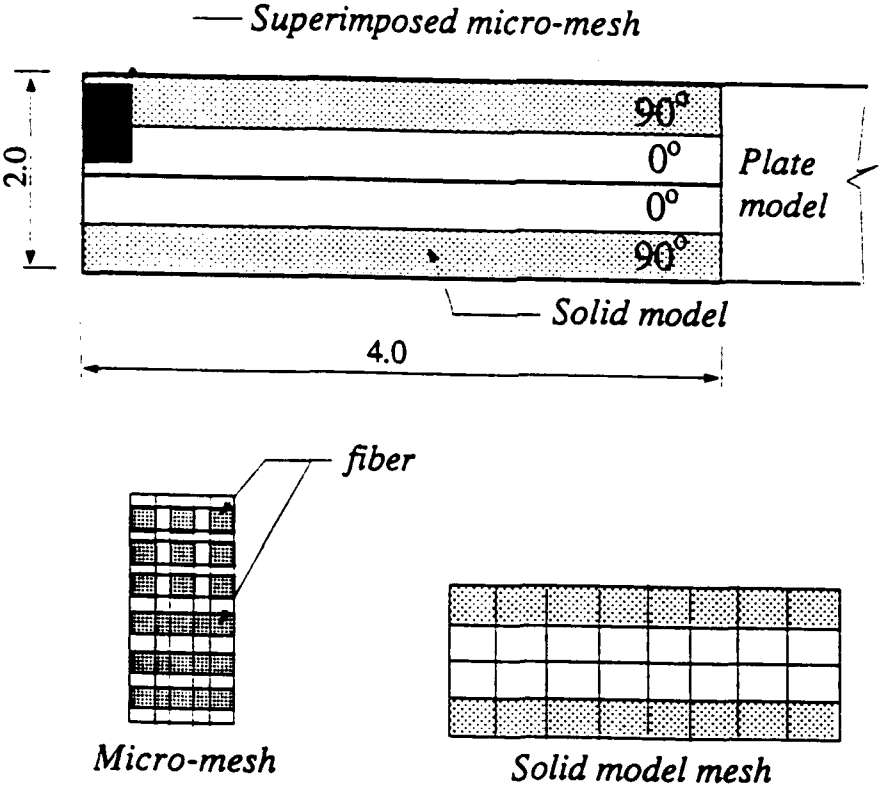

Figure 9 Idealization used for micromechanical level idealization region

In the immediate vicinity of the singularity (interface between 0/90 layers at the edge as shown in Fig. 9) it is assumed that the periodic solution does not exist and the approximation space is decomposed into macroscopic and microscopic fields.

Compatibility between the two regions is explicitly enforced. For formulation detail, comparison to other techniques and validation tests see [37, 38]. Figure 10 depicts the distribution of shear and normal stresses in the superimposed region. As expected higher stresses are found in the vicinity of the singularity with stress concentration in the fiber phase.

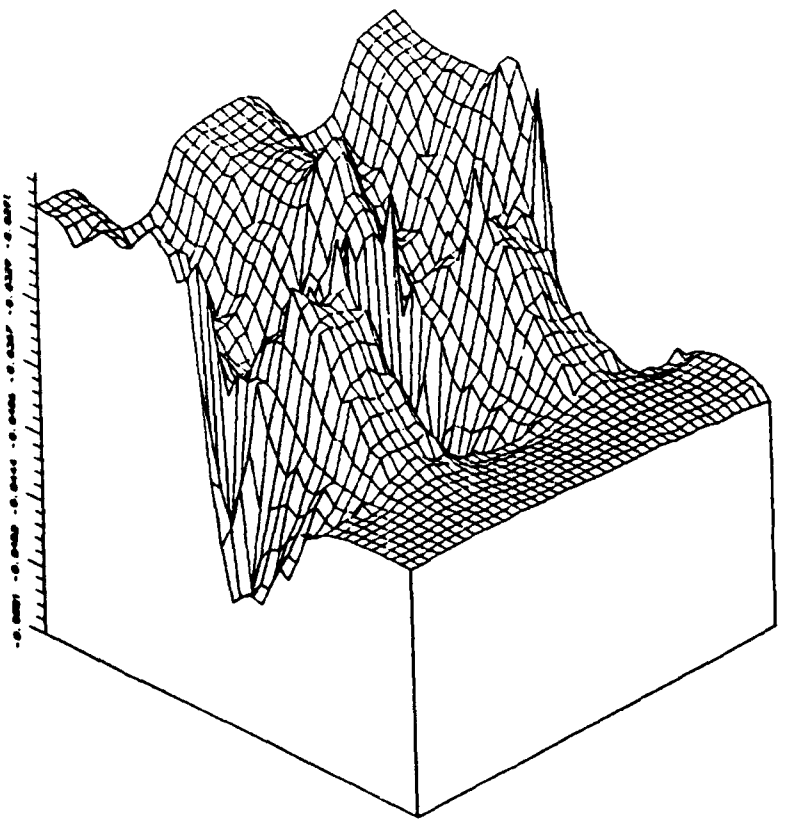

Figure 10 Shear stresses in microstructure at free edge

CLOSING REMARKS

A broad consideration of the various classes of idealizations used in the analysis of composite structures has been presented as well as a framework to provide the reliable control of these idealizations. The overall analysis idealization control framework allows the inclusion of a wide variety of idealization control techniques and can easily build on a variety of analysis procedures implemented in different software packages. The use of

idealization regions and adaptive idealization region control, in much the same manner as finite elements in adaptive discretization control, has been introduced for use in the reliable control of analysis idealizations. The use of these idealization regions within the context of a superposition method has also been discussed. A simple example problem was used to partly demonstrate the application of multiple analysis idealization control.

ACKNOWLEDGMENTS

The work on the development of finite element analysis capabilities for composites including nonlinear material mixing models was partially supported by the Office of Naval Research under grant N000014–85–K-0733, Dr. Yapa Rajapakse, project monitor. Also the support of the National Science Foundation under the Research Initiation Award ECS-9003093 is gratefully acknowledged. The work on the development of the analysis idealization control framework is supported by the Affiliates of the Scientific Computation Research Center.

REFERENCES

[1] M. S. Shephard, E. V. Korngold, and R. Wentorf. Design systems supporting engineering idealizations. In *Geometric Modeling for Product Engineering*, pages 279–300. North-Holland, Amsterdam, 1990.

[2] R. Wentorf, A. Budhiraja, R. R. Collar, M. S. Shephard, and P. L. Baehmann. Two prototypes testing the use of an expert system in the control of structural analysis idealizations. Technical Report SCOREC Report #20-1990, Scientific Computation Research Center, Rensselaer Polytechnic Institute, Troy, NY 12180-3590, 1990.

[3] R. Wentorf and S. M. S. Automated analysis idealization control. In *CONCURRENT ENGINEERING: Automation, Tools, and Techniques*, page TBA. John Wiley, New York, 1992.

[4] J. Fish and S.Markolefas. Adaptive s-version for linear elastostatics. *Comp. Meth. Appl. Mech. Engng.*, 1992. to appear.

[5] J. Fish. The s-version of the finite element method. *Computers and Structures*, page to appear, 1992.

[6] J. Fish and S. Markolefas. The s-version of the finite element method for multilayer laminates. *Int. J. Numer. Meth. Engng.*, 33:1081–1105, 1992.

[7] I. Babuska. Adaptive mathematical modeling. In J. E. Flaherty, P. J. Paslow, M. S. Shephard, and J. D. Vasilakis, editors, *Adaptive Methods for Partial Differential Equations*, pages 1-14. SIAM, 1989.

[8] M. S. Shephard, P. L. Baehmann, M. K. Georges, and E. V. Korngold. Framework for the reliable generation and control of analysis idealizations. *Comp. Meth. Appl. Mech. Engng.*, 82:257-280, 1990.

[9] B. A. Szabo. On errors of idealization in finite element analysis of structural connections. In J. E. Flaherty, P. J. Paslow, M. S. Shephard, and J. D. Vasilakis, editors, *Adaptive Methods for Partial Differential Equations*, pages 15-28. SIAM, 1989.

[10] J. R. Dixon, E. C. Libardi, and E. H. Nielsen. Unresolved research issues in development of design-with-features. In *Geometric Modeling for Product Engineering*, pages 183-196. North-Holland, Amsterdam, 1990.

[11] G. J. Dvorak and Y. A. Bahei-El-Din. A bimodal theory of fibrouous composite materials. *Acta Mechanica*, 69:219-241, 1987.

[12] J. L. Teply and G. J. Dvorak. Bounds on the overall instanteous properties of elastic-plastic composites. *J. Mech. Phys. Solids*, 36(1):29-58, 1988.

[13] R. M. Christensen. *Mechanics of Composite Materials*. John Wiley and Sons, New York, 1979.

[14] G. J. Dvorak and J. A. Teply. Periodic hexagonal array models for plasticity of composite materials. In *Plasticity Today: Modeling, Methods and Applications*, pages 623-642. Elsevier, Amsterdam, 1985.

[15] A. Benssousan, J. L. Lions, and G. Papanicoulou. *Asymptotic Analysis for Periodic Structures*. North Holland, Amsterdam, 1978.

[16] J. M. Guedes and N. Kikuchi. Preprocessing and postprocessing for materials based on the homogenization method with adaptive finite element methods. *Comp. Meth. Appl. Mech. Engng.*, 83:143-198, 1990.

[17] A. K. Noor and W. S. Burton. Assessment of shear deformation theories for multilayered composite plates. *Applied Mechanics Review*, 42(1):1-13, 1990.

[18] I. Babuska, B. A. Szabo, and R. L. Actis. Hierarchic models for laminated composites. *Int. J. Numer. Meth. Engng.*, 33(3):503-535, 1992.

[19] M. Vogelius. On mathematical modeling - dimensional reduction. Technical report, Institute for Physical Science and Technology, University of Maryland, College Park, Maryland, 1980. Tech. Note BN-940.

[20] A. K. Noor and W. S. Burton. Assessment of computational models for multilayered composite shells. *Applied Mechanics Review*, 43(4):67-97, 1990.

[21] K. J. Bathe, N. S. Lee, and M. L. Bucalem. On the use of hierarchical models in engineering analysis. *Comp. Meth. Appl. Mech. Engng.*, 82:5-26, 1990.

[22] A. K. Noor and J. M. Peters. A posteriori estimates for shear correction factors in multilayered composite cylinders. *J. Engng. Mechanics Div., ASCE*, 115(6):1225-1244, 1989.

[23] C. S. Desai, G. W. Wathugala, K. G. Sharma, and L. Woo. Factors affecting reilability of computer solutions with hierarchical single surface constitutive models. *Comp. Meth. Appl. Mech. Engng.*, 82:115-137, 1990.

[24] G. J. Dvorak. Plasticity theories for fibrous composite materials. In *Metal Matrix Composites, Vol. 2, Mechanisms and Properties*, pages 1-77. Academis Press, 1991.

[25] I. Babuska. The problem of modeling elastomechanics in engineering. *Comp. Meth. Appl. Mech. Engng.*, pages 155-182, 1990.

[26] Z. Hashin. The elastic moduli of heterogeneous materials. *J.Appl. Mech*, 29:143, 1962.

[27] B. Budiansky. On the elastic moduli of some heterogeneous materials. *J.Mech. Phys. Solids*, 13:223, 1965.

[28] R. Hill. A self-consistent mechanics of composite materials. *J.Mech. Phys. Solids*, 13(213), 1965.

[29] R. M. Cristensen and K. H. Lo. Solution for effective shear properties in three phase sphere and cylinder models. *J.Mech.Phys.Solids*, 27(4), 1979.

[30] Y. Benveniste. A new approach to the application of Mori-Tanaka's theory in composite materials. *Mechanics of Materials*, 6:147, 1987.

[31] T. Belytschko, J. Fish, and B. E. Engelman. A finite element with embedded localization zones. *Comp. Meth. Appl. Mech. Engng.*, 70(59-89), 1988.

[32] A. Needleman. Material rate dependence and mesh sensitivity in localization problems. Technical report, January 1987. Report ONR-N00014-86-K-0235/1.

[33] Z. P. Bazant and G. Pijauder-Cabot. Nonlocal damage: continuum model and localization instability. Technical report, Northwestern University, Evanston, IL, 1987. Center for Concrete and Geomaterials.

[34] S. T. Pietruszak and Z. Mroz. Finite element analysis of deformation of strain softening materials. *Int. J. Numer. Meth. Engng.*, 17:327-334, 1981.

[35] J. Fish, N. Fares, and A. Nath. Elastic cracktip fields in a heterogeneous fiber reinforced composite. *International Journal of Fracture*, 1992. to appear.

[36] J. Fish. Hierarchical modeling of discontinuous fields. *Communications in Applied Numerical Methods*, 1992. to appear.

[37] J. Fish and A. Wagiman. Multiscale finite element method for a periodic and nonperiodic heterogeneous medium. *Computers and Structures*, 1992. to appear.

[38] J. Fish, A. Wagiman, and P. Nayak. Adaptive multiscale finite element method for a locally nonperiodic heterogeneous medium. *Journal of Computational Mechanics*, 1992. submitted to.

[39] Dassault Systems, IBM Corporation, 11601 Wilshire Boulevard, LA, CA. *CATIA Solids Geometry - Geometry Interface Reference Manual; CATIA Solids Geometry - Mathematical Subroutine Package Reference Manual; and CATIA Base - Mathematical Subroutine Package Reference Manual*, 1988. Pub. Nums. SH50-0059-0; SH50-0058-0; SH50-0089-0.

[40] R. Wentorf, A. Budhiraja, R. R. Collar, M. S. Shephard, and P. L. Baehmann. Two prototypes testing the use of an expert system in the control of structural analysis idealizations. In E. N. Houstis, J. R. Rice, and R. Vichnevetsky, editors, *Intelligent Scientific Software*, pages 283–326. North Holland, Amsterdam, 1992.

[41] M. S. Shephard and M. K. Georges. Automatic three-dimensional mesh generation by the Finite Octree technique. *Int. J. Numer. Meth. Engng.*, 32(4):709–749, 1991.

[42] Hibbitt, Karlsson and Sorensen, Inc., 100 Medway Street, Providence, RI. *ABAQUS Theory and User's Manual*, July 1985.

[43] M. W. Beall and M. S. Shephard. Advanced finite element formulations for composite shells. In *Proceeding of the Sixth Techanical Conference on Composite Materials*. American Society for Composites, 1991.

[44] A. K. Noor, W. S. Burton, and J. M. Peters. Predictor-corrector procedures for stress and free vibration analysis of multilayered composite plates and shells. *Comp. Meth. Appl. Mech. Engng.*, 82(6):341–363, 1990.

NDE-Vol. 10, Enhancing Analysis Techniques
For Composite Materials
ASME 1991

LAMINA LEVEL NONLINEAR COMPOSITE MIXING MODEL IN FINITE ELEMENT COMPUTATIONS

Mark W. Beall, Jer-Fang Wu, and Mark S. Shepard
Department of Mechanical Engineering, Aeronautical
Engineering and Mechanics
and
Department of Civil Engineering
Scientific Computation Research Center
Rensselaer Polytechnic Institute
Troy, New York

ABSTRACT

The inclusion of an advanced nonlinear mixing model for the determination of composite constitutive relations in finite element formulations for the analysis of composite structures is considered. The nonlinear mixing model considered is based on the bimodal plasticity model. This material model is being implemented into various forms of finite element idealizations including solid elements and laminated shell finite elements employing different through-the-thickness kinematic assumptions. At the time this paper was due a complete set of results was not available. They will be presented in the associated presentation and published subsequently.

NOMENCLATURE

$d\sigma$	stress increment
$d\varepsilon$	strain increment
M	instantaneous compliance matrix
L	instantaneous stiffness matrix
c_f	fiber volume fraction
c_m	matrix volume fraction
B	instantaneous stress concentration matrix
A	instantaneous strain concentration matrix
W	fiber stress concentration for a dilute solution
T	fiber strain concentration for a dilute solution
G	plastic compliance matrix
n	unit normal vector
s	slip direction vector
τ	shear stress
β	slip plane angle
θ	slip direction angle
D	material stiffness matrix

INT 'ODUCTION

The accurate modeling of structures constructed of advanced high temperature composite materials requires consideration of inelastic material behavior. The accurate prediction of the inelastic behavior of these materials requires the explicit consideration of the inelastic behavior of the constituent materials. The mixing models for fibrous composites that consider the inelastic behavior of the constituents have been developed [Teply and Dvorak, 1988], [Dvorak and Bahei-El-Din, 1987], [Bahei-El-Din, and Dvorak, 1989]. This effort is considering the application of one of these models, the bimodal plasticity model [Dvorak and Bahei-El-Din, 1987] into various levels of spatial discretization as applied in the finite element analysis of composite structures.

Since most composite structures have one dimension which is substantially smaller than the other two, it is desirable to employ a spatial discretization assumption which reduces the amount of computation needed in this small dimension. This dimensional reduction process is particularly complex in the case of laminated structures constructed from thin orthotropic layers. This process is further complicated when lamina level nonlinear material behavior is considered.

The purpose of our efforts is to examine the influence of the type of modeling on the accuracy and computational expense of analysis of composite shell structures with lamina level nonlinear behavior. Lamina level nonlinear behavior is represented using the bimodal plasticity theory [Dvorak and Bahei-El-Din, 1987] which is defined by the inner envelope of a fiber dominated mode (FDM) and a matrix dominated mode (MDM).

The next section gives a brief overview of the bimodal plasticity theory. The associated presentation and subsequent publications will describe its implementation into various levels of finite element idealizations and present the results obtained.

INTRODUCTION TO BIMODAL PLASTICITY

Bimodal plasticity is a semi-phenomenological model which describes the plastic deformation of fibrous composites consisting of elastic fibers and an elastic-plastic, rate-independent matrix [Dvorak and Bahei-El-Din, 1987]. The theory assumes that the deformation of such a composite can be described in terms of one of two deformation modes, the fiber-dominated mode (FDM) or the matrix-dominated mode (MDM). In the fiber-dominated mode, both phases deform together in the elastic and plastic range and the composite aggregate is treated in the context of heterogeneous media elasticity and plasticity. In the matrix-dominated mode, plastic deformation is caused by slip on matrix planes which are parallel to the fiber axis. The yield condition corresponding to each mode gives a yield surface in the overall stress space. The overall yield surface of the composite is

then given by the inner envelop of the yield surfaces of the two modes.

The dominant deformation mode is determined by the elastic moduli of the phases, in particular the longitudinal shear modulus, and the overall loads. In the plane stress space, the matrix-dominated mode is active in composites where the ratio of the longitudinal elastic shear modulus of the fiber and the matrix is large, eg. B/Al and SiC/Al composites. The fiber-dominated mode is common in composite systems where the fiber longitudinal shear modulus is comparable or smaller than the matrix elastic shear modulus. This mode also occurs when stress in the fiber axis is the dominant loading. Recent experiments on a B/Al composite system have verified the existence of the deformation modes postulated by the bimodal plasticity theory. Following is a brief description of both of the deformation modes.

Fiber-Dominated Mode

Plastic deformation in the fiber-dominated mode is described by averaging models originally introduced for elastic phases [Hill, 1963]. The constitutive relations of the phases are assumed to be known for the volume average of the local fields. Under isothermal loads, the phase strain average $d\varepsilon_r$ and the stress average $d\sigma_r$, are related by:

$$d\sigma_r = L_r\, d\varepsilon_r$$

$$d\varepsilon_r = M_r\, d\sigma_r$$

where

r = f (fiber phase) or m (matrix phase)

L_r = instantaneous stiffness matrix phase r.

$M_r = L_r^{-1}$ = instantaneous compliance matrix phase r

Similar relations can be written for the composite overall uniform field

$$d\sigma = L\, d\varepsilon$$

$$d\varepsilon = M\, d\sigma$$

The volume average of the local stress and strain increments are related to their overall counterparts by

$$d\sigma = c_f\, d\sigma_f + c_m\, d\sigma_m$$

$$d\varepsilon = c_f\, d\varepsilon_f + c_m\, d\varepsilon_m$$

where

c_f, c_m = fiber and matrix volume fraction $c_f + c_m = 1$.

In addition, the local fields are assumed to be related to the overall fields by:

$$d\sigma_r = B_r\, d\sigma$$

$$d\varepsilon_r = A_r\, d\varepsilon$$

where

B_r = instantaneous stress concentration phase r.

A_r = instantaneous strain concentration phase r.

Thus, the overall stiffness and compliance matrices can be written as

$$L = c_f L_f A_f + c_m L_m A_m$$

$$M = c_f M_f B_f + c_m M_m B_m$$

In the elastic range, the concentration factors of the phases can be found from an averaging model. In the present work, the method developed by Mori and Tanaka [1973] was used to evaluate the elastic concentration factors. The fiber stress concentration factor is then

$$B_f = W\,(c_m I + c_f W)^{-1}$$

where W is the fiber stress concentration factor of a dilute solution:

$$W = L_f T M_m$$

T is the fiber strain concentration factor of the dilute solution:

$$T = [\, I + P\,(L_f - L_m)]^{-1}$$

where P is a constant matrix that depends on the shape of the fibers and the elastic properties of the matrix.

In the plastic range, for composites with elastic fibers, the plastic strain increment in the matrix phase ($d\varepsilon_m^p$) is related to the overall plastic strain increment ($d\varepsilon^p$) by

$$d\varepsilon^p = c_m\, B_{me}^T\, d\varepsilon_m^p$$

where B_{me}^T is the transpose of the matrix elastic stress concentration factor.

The plastic strain increment of the matrix phase is related to the matrix stress increment ($d\sigma_m$) through the plastic compliance matrix (G)

$$d\varepsilon_m^p = G\, d\sigma_m$$

where G is derived from the constitutive model of the matrix, which in this case is described by a two surface plasticity theory.

The explicit form the instantaneous stress concentration factor (B_m^{inst}) can then be shown to be:

$$B_m^{inst} = \left[(M_{me} - M_f) + (I - B_{me}^T)\, G\right]^{-1} (M_e - M_f)/c_m$$

where

M_e is the composite overall elastic compliance matrix.

M_{me} is the matrix elastic compliance matrix.

M_f is the fiber compliance matrix (assumed always elastic)

The fiber instantaneous concentration factor (B_f^{inst}) and matrix instantaneous concentration factor (B_m^{inst}) can then be related:

$$B_f^{inst} = \left(I - c_m\, B_m^{inst}\right)^{-1}/c_m$$

It can be shown that the phase stress concentration factor and strain concentration factor are related as:

$$A_r = M_r\, B_r\, L$$

where L is the composite overall stiffness matrix.

Thus, once the instantaneous stress concentration factors of the phases are found, the overall stiffness matrix of the composite can be determined.

Matrix-dominated mode

In the matrix dominated mode the deformation in the plastic range is derived from plastic slip along plane parallel to the fiber direction. Consider a typical slip system shown in Fig. 1. The unit normal n defines the slip plane, and s is the slip direction,

$$n = [\, 0 \;\; \cos\beta \;\; -\sin\beta\,]^T$$

$$s = [\, \cos\theta \;\; \sin\beta \sin\theta \;\; \cos\beta \sin\theta\,]^T$$

The resolved shear stress on the plane with normal n in the direction s is then:

$$\tau_{ns} = n_i\, \sigma_{ij}\, s_j$$

or

$$\tau_{ns} = 1/2 \sin 2\beta \sin\theta\,(\sigma_{22} - \sigma_{33}) + \cos\beta \cos\theta\, \sigma_{21}$$

$$- \sin\beta \cos\theta\, \sigma_{31} + \cos 2\beta \sin\theta\, \sigma_{32}$$

We now transform the coordinate system by rotating by β about the fiber axis. In this new coordinate system we denote σ_{21} and σ_{23} by τ_1 and τ_2, respectively.

$$\tau_1 = \cos\beta\,\sigma_{21} - \sin\beta\,\sigma_{31}$$

$$\tau_2 = 1/2 \sin 2\beta\,(\sigma_{22} - \sigma_{33}) + \cos 2\beta\,\sigma_{32}$$

The resolved shear stress can be written as:

$$\tau_{ns} = \tau_1^2 + \tau_2^2$$

The onset of yielding occurs when the magnitude of the resolved shear stress τ_{ns} equals the matrix yield stress in simple shear. Thus the slip planes are found by evaluating the maxima of $\tau_{ns}(\beta)$.:

$$\frac{\partial\tau_{ns}}{\partial\beta} = \left[\frac{(\sigma_{22} - \sigma_{33})^2}{4} - \sigma_{32}^2\right] \sin 4\beta + \sigma_{32}(\sigma_{22} - \sigma_{33}) \cos 4\beta$$

$$- \frac{(\sigma_{21}^2 - \sigma_{31}^2)}{2} \sin 2\beta - \sigma_{21}\,\sigma_{31} \cos 2\beta = 0$$

Some trigonometric simplification of this condition leads to the following quartic equation for β's corresponding to the maximum resolved shear stress.

$$\alpha_1 y^4 + \alpha_2 y^3 + \alpha_3 y^2 + \alpha_4 y + \alpha_5 = 0$$

where

$$\alpha_1 = 4(A^2 + B^2)$$
$$\alpha_2 = -4(AC + BD)$$
$$\alpha_3 = -4(A^2 + B^2 - C^2 - D^2)$$
$$\alpha_4 = 2(2AC + BD)$$
$$\alpha_5 = B^2 - C^2$$

and

$$A = \frac{1}{4}(\sigma_{22} - \sigma_{33})^2 - \sigma_{32}^2$$
$$B = \sigma_{32}(\sigma_{22} - \sigma_{33})$$
$$C = \frac{1}{2}(\sigma_{21}^2 - \sigma_{31}^2)$$
$$D = \sigma_{21}\,\sigma_{31}$$

Thus once the roots of the quartic equation are known, the possible slip planes are given by:

$$\beta = \pm \cos^{-1}\sqrt{\frac{y+1}{2}}$$

A more complete derivation and a discussion of the specific plasticity theory used can be found in Wu [1991].

ACKNOWLEDGMENTS

This work was supported by a grant from the Office of Naval Research under grant number N000014-85-K-0733, Dr. Yapa Rajapakse, project monitor. We also thank Hibbitt, Karlsson and Sorensen, Inc., for the use of the ABAQUS program on this project.

REFERENCES

Bahei-El-Din, Y.A. and Dvorak, G.J. , 1989, "New Results in Bimodal Plasticity of Fibrous Composite Materials", *Proc. Plasticity* '89 pp. 121-127.

Dvorak, G.J. and Bahei-El-Din, Y.A. , 1987, "A Bimodal Plasticity Theory of Fibrous Composite Materials", *Acta Mechanica*, Vol. 69, pp. 219-241.

Hill, R, 1963, "Elastic properties of reinforced solids: some theoretical principles" *J. Mech. Phys. Solids*, Vol. 11 pp. 357-372.

Teply, J.L., and Dvorak, G.J., 1988, "Bounds on Overall Instantaneous Properties of Elastic Plastic Composites, *J. Mech. Phys. Solids*, Vol. 36, pp. 29-58.

Mori, T. and Tanaka, K., 1973, "Average Stress in Matrix and Average Elastic Energy of Materials with Misfitting Inclusions", *Acta Metallurgica*, Vol. 21, pp. 571.

Wu, J.F., 1991, "Numerical Techniques for Elastic-Plastic Analysis of Fibrous Metal Matrix Composites", Ph.D. Thesis, Rensselaer Polytechnic Institute.

Shephard

NDE-Vol. 10

ENHANCING ANALYSIS TECHNIQUES FOR COMPOSITE MATERIALS

presented at
THE WINTER ANNUAL MEETING OF
THE AMERICAN SOCIETY OF MECHANICAL ENGINEERS
ATLANTA, GEORGIA
DECEMBER 1-6, 1991

sponsored by
THE NDE ENGINEERING DIVISION,
THE APPLIED MECHANICS DIVISION, AND
THE AEROSPACE DIVISION, ASME

edited by
LEN SCHWER
APTEK, INC.

J. N. REDDY
VIRGINIA POLYTECHNIC INSTITUTE AND STATE UNIVERSITY

AJIT MAL
UNIVERSITY OF CALIFORNIA

THE AMERICAN SOCIETY OF MECHANICAL ENGINEERS
345 East 47th Street United Engineering Center New York, N. Y. 10017

Advanced Finite Element Formulations for Composite Shells

Mark W. Beall and Mark S. Shephard

SCOREC Report #10-1991
Scientific Computation Research Center

To appear: *ASC 6th Technical Conference on Composite Materials Proceedings*

Scientific Computation Research Center
Rensselaer Polytechnic Institute
Troy, NY 12180-3590
voice 5182766795
fax 5182764886

ADVANCED FINITE ELEMENT FORMULATIONS FOR COMPOSITE SHELLS

Mark W. Beall*
Mark S. Shephard**

ABSTRACT

This paper considers the application of advanced nonlinear mixing models for the determination of composite constitutive relations in finite element analysis of composite plates and shells. The nonlinear mixing model considered is based on the bimodal plasticity model. This material is used in conjunction with two spatial discretizations: solid finite elements and layerwise linear kinematic deformations through the thickness in first order shear deformation shell finite elements. Initial numerical results are presented.

INTRODUCTION

Accurate modeling of structures constructed with advanced high temperature composite materials requires consideration of the inelastic behavior of these materials. The accurate prediction of the inelastic behavior of composites requires explicit consideration of the inelastic behavior of their constituent materials. Mixing models for fibrous composites that consider the inelastic behavior of the constituents have been developed [1,2,3]. This paper considers the utilization of one of these models, the bimodal plasticity model [2], with various levels of spatial discretization in the finite element analysis of composite structures.

Since most composite structures have one dimension which is substantially smaller than the other two, it is desirable to employ a spatial discretization assumption which reduces the amount of computation needed in the small dimension. This dimensional reduction process is particularly complex in the case of laminated structures constructed from thin orthotropic layers. This process is further complicated when lamina level nonlinear material behavior must be considered. This paper considers two spatial discretizations: solid finite elements and layerwise linear kinematic deformations through the thickness in first order shear deformation shell finite elements.

For composite materials that are generally characterized by linear material responses, such as epoxy matrix composites, this issue of accuracy has been investigated for many different laminated shell models. Noor and Burton [4] give a complete review of the subject. However, in some composite systems, for example metal matrix composites, there is significant nonlinearity in the material response, i.e. matrix plasticity, long before the useful strength of the material is reached. For these materials the nonlinear response of the matrix material and thus the composite as a whole, must be accounted for.

**Professor, Dept. of Mechanical Eng., Aeronautical Eng. and Mechanics, Director, Scientific Computation Research Center, Rensselaer Polytechnic Institute, Troy, NT 12180-3590.
*Research Assistant, Dept. of Mechanical Eng., Aeronautical Eng. and Mechanics, RPI.

COMPOSITE SHELL MODELS

Due to the complex nature of laminated composites there are many different manners in which they may be modeled. Many papers, surveys and reviews have been published on this subject, for a recent reviews see Noor and Burton [4] and Reddy [5]. Each type of model provides good engineering accuracy for different types of problems. The increase in computational expense incurred by increasing the modeling accuracy can be quite significant. Therefore, it is important to understand the bounds of validity of each of the models.

The most complete way to model a composite structure is with full 3-D solid modeling. In this way no specific kinematic assumptions are introduced regarding the behavior of the structure. Assuming a correct material model, the only source of error is the discretization error, which can be easily quantified and controlled. This type of modeling, however, is computationally expensive, especially with thin curved structures. A typical composite may have dozens of layers, each of which requires one or more element through the thickness.

One way to derive formulations for the behavior of shells is to apply specific kinematic constraints to the full three-dimensional elasticity equations. This 'degeneration' of the three-dimensional elasticity equations is the basis for many shell formulations. A common kinematic assumption on the behavior of shells is that the in-plane displacement components vary linearly in the thickness direction. In particular, if we assume a linear variation through the thickness of the in-plane displacement quantities in each layer (equivalently, constant transverse shear strains in each layer) we arrive at a first-order discrete layer theory. In this formulation, if we neglect the generally small direct strain in the thickness direction, there are 2N +3 displacement parameters through the thickness, where N is the number of layers, which can be a significant reduction compared to 3-D modeling. Since the transverse stresses are constant in each layer, the continuity of these stresses is not satisfied at the layer interfaces and they are generally not zero at the top and bottom surface of the shell. This set of assumptions will be referred to as discrete layer theory (DLT) throughout this paper although there are many different shell theories that also fall into this category.

Another common simplification that is made is to apply the assumption of a single linear variation of the in-plane displacement quantities through the entire shell thickness, rather than to each individual layer. In this way the layered shell is replaced by an equivalent single-layer anisotropic shell. This type of formulation, generally called a first-order shear deformation theory, is computationally advantageous since the number of displacement parameters is independent of the number of layers, but gives poor results for transverse stress distributions [4].

The analyses performed in this investigation utilized the ABAQUS finite element program [6]. This program provides a simple interface to add user routines that are run during an analysis. In this work both a user element, for the discrete layer theory shell, and a user material, for the nonlinear material model, bimodal plasticity, were used.

The 3-D solid modeling was performed using the ABAQUS C3D20 element. This is a 20-noded quadratic displacement element. Both the fully integrated (3 x 3 x 3) and version and the reduced integration (2 x 2 x 2) version of this element were used. The reason for using the reduced integration element was to reduce the computation time for models with several elements through the thickness of each layer for problems where the reduced integration did not introduce errors into the solution.

The discrete layer theory element, called LCSLFC, was developed by K. Dorninger [7]. It employs C^0 linear segments for the through the thickness deformation of each layer. The LCSLFC element is based on the degeneration principle. The element is a 16-noded shell using cubic shape functions for the in-plane displacement quantities.

The implementation of the LCSLFC element allows considerable flexibility in modeling composite laminates. The shell thickness may be varied through each element. Each layer may have a different orientation, thickness and material. In this study a user defined material is incorporated into the element.

BIMODAL PLASTICITY

Bimodal plasticity is a semi-phenomenological model which describes the plastic deformation of fibrous composites consisting of elastic fibers and an elastic-plastic matrix [2]. The theory assumes that the deformation of such a composite can be described in terms of one of two deformation modes, the fiber-dominated mode (FDM) or the matrix-dominated mode (MDM). In the fiber-dominated mode, both phases deform together in the elastic and plastic range and the composite aggregate is treated in the context of heterogeneous media elasticity and plasticity. In the matrix-dominated mode, plastic deformation is caused by slip on matrix planes which are parallel to the fiber axis. The yield condition corresponding to each mode gives a yield surface in the overall stress space. The overall yield surface of the composite is then given by the inner envelope of the yield surfaces of the two modes.

The dominant deformation mode is determined by the elastic moduli of the phases, in particular the longitudinal shear modulus, and the overall loads. In the plane stress space, the matrix-dominated mode is active in composites where the ratio of the longitudinal elastic shear modulus of the fiber and the matrix is large, e.g. B/Al and SiC/Al composites. The fiber-dominated mode is common in composite systems where the fiber longitudinal shear modulus is comparable or smaller than the matrix elastic shear modulus. This mode also occurs when stress in the fiber axis is the dominant loading. Recent experiments on a B/Al composite system have verified the existence of the deformation modes postulated by the bimodal plasticity theory [8]. Following is a brief description of the both of the deformation modes [9].

Fiber-Dominated Mode

Plastic deformation in the fiber-dominated mode is described by averaging models originally introduced for elastic phases [10]. The constitutive relations of the phases are assumed to be known for the volume average of the local fields. Under isothermal loads, the phase strain average $d\varepsilon_r$ and the stress average $d\sigma_r$, are related by:

$$d\sigma_r = L_r\, d\varepsilon_r \tag{1}$$

$$d\varepsilon_r = M_r\, d\sigma_r \tag{2}$$

where

r = f (fiber phase) or m (matrix phase)

L_r = instantaneous stiffness matrix of phase r.

$M_r = L_r^{-1}$ = instantaneous compliance matrix of phase r

Similar relations can be written for the composite overall uniform field

$$d\sigma = L\, d\varepsilon \tag{3}$$

$$d\varepsilon = M\, d\sigma \tag{4}$$

The volume average of the local stress and strain increments are related to their overall counterparts by

$$d\sigma = c_f\, d\sigma_f + c_m\, d\sigma_m \tag{5}$$

$$d\varepsilon = c_f\, d\varepsilon_f + c_m\, d\varepsilon_m \tag{6}$$

where

c_f, c_m = fiber and matrix volume fraction, $c_f + c_m = 1$.

In addition, the local fields are assumed to be related to the overall fields by:

$$d\sigma_r = B_r\, d\sigma \tag{7}$$

$$d\varepsilon_r = A_r\, d\varepsilon \tag{8}$$

where

B_r = instantaneous stress concentration of phase r.

A_r = instantaneous strain concentration of phase r.

Thus, the overall stiffness and compliance matrices can be written as

$$L = c_f\, L_f\, A_f + c_m\, L_m\, A_m \tag{9}$$

$$M = c_f M_f B_f + c_m M_m B_m \tag{10}$$

In the elastic range, the concentration factors of the phases are found from an averaging model. In the present work, the method developed by Mori and Tanaka [11] was used to evaluate the elastic concentration factors.

In the plastic range, for composites with elastic fibers, the plastic strain increment in the matrix phase ($d\varepsilon_m^p$) is related to the overall plastic strain increment ($d\varepsilon^p$) by

$$d\varepsilon^p = c_m B_{me}^T d\varepsilon_m^p \tag{11}$$

where B_{me}^T is the transpose of the matrix elastic stress concentration factor.

The plastic strain increment of the matrix phase is related to the matrix stress increment ($d\sigma_m$) through the plastic compliance matrix (G)

$$d\varepsilon_m^p = G\, d\sigma_m \tag{12}$$

where G is derived from the constitutive model of the matrix, which in this case is described by a two surface plasticity theory.

The explicit form of the matrix instantaneous stress concentration factor (B_m^{inst}) can then be shown to be:

$$B_m^{inst} = \left[(M_{me} - M_f) + \left(I - B_{me}^T\right) G\right]^{-1} (M_e - M_f)/c_m \tag{13}$$

where

M_e is the composite overall elastic compliance matrix.

M_{me} is the matrix elastic compliance matrix.

M_f is the fiber compliance matrix (assumed always elastic)

The fiber instantaneous concentration factor (B_f^{inst}) and matrix instantaneous concentration factor (B_m^{inst}) can then be related:

$$B_f^{inst} = \left(I - c_m B_m^{inst}\right)^{-1}/c_m \tag{14}$$

The phase stress concentration factor and strain concentration factor are related as:

$$A_r = M_r B_r L \tag{15}$$

where L is the composite overall stiffness matrix.

Thus, once the instantaneous stress concentration factors of the phases are found, the overall stiffness matrix of the composite can be determined.

Matrix-dominated mode

In the matrix dominated mode the deformation in the plastic range is derived from plastic slip along planes parallel to the fiber direction. Consider a typical slip system shown in Fig. 1. The unit normal n defines the slip plane, and s is the slip direction,

$$n = [0 \;\cos\beta \;-\sin\beta]^T \tag{16}$$

$$s = [\cos\theta \;\sin\beta\sin\theta \;\cos\beta\sin\theta]^T \tag{17}$$

The resolved shear stress on the plane with normal n in the direction s is then:

$$\tau_{ns} = n_i \sigma_{ij} s_j \tag{18}$$

or

$$\tau_{ns} = 1/2 \sin 2\beta \sin\theta (\sigma_{22} - \sigma_{33}) + \cos\beta\cos\theta\sigma_{21} - \sin\beta\cos\theta\sigma_{31} + \cos 2\beta \sin\theta\sigma_{32} \tag{19}$$

We now transform the coordinate system by rotating by β about the fiber axis. In this new coordinate system we denote σ_{21} and σ_{23} by τ_1 and τ_2, respectively.

$$\tau_1 = \cos\beta\sigma_{21} - \sin\beta\sigma_{31} \tag{20}$$

$$\tau_2 = 1/2 \sin 2\beta (\sigma_{22} - \sigma_{33}) + \cos 2\beta \sigma_{32} \tag{21}$$

The resolved shear stress can be written as:

$$\tau_{ns} = \tau_1^2 + \tau_2^2 \tag{22}$$

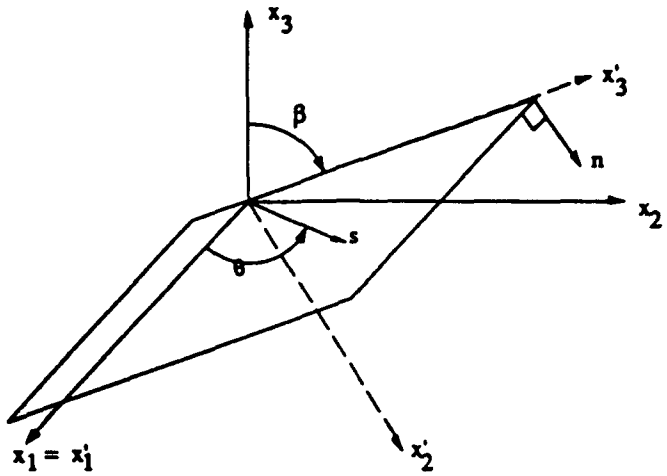

Figure 1. Slip Plane in Matrix Dominated Mode

The onset of yielding occurs when the magnitude of the resolved shear stress τ_{ns} equals the matrix yield stress in simple shear. Thus the slip planes are found by evaluating the maxima of $\tau_{ns}(\beta)$.:

$$\frac{\partial \tau_{ns}}{\partial \beta} = \left[\frac{(\sigma_{22} - \sigma_{33})^2}{4} - \sigma_{32}^2\right] \sin 4\beta + \sigma_{32}(\sigma_{22} - \sigma_{33}) \cos 4\beta - \frac{(\sigma_{21}^2 - \sigma_{31}^2)}{2} \sin 2\beta - \sigma_{21}\sigma_{31} \cos 2\beta = 0 \tag{23}$$

Some trigonometric simplification of this condition leads to the following quartic equation for β's corresponding to the maximum resolved shear stress.

$$\alpha_1 y^4 + \alpha_2 y^3 + \alpha_3 y^2 + \alpha_4 y + \alpha_5 = 0 \tag{24}$$

where

$$\alpha_1 = 4(A^2 + B^2)$$
$$\alpha_2 = -4(AC + BD)$$
$$\alpha_3 = -4(A^2 + B^2 - C^2 - D^2)$$
$$\alpha_4 = 2(2AC + BD)$$
$$\alpha_5 = B^2 - C^2$$

and

$$A = \frac{1}{4}(\sigma_{22} - \sigma_{33})^2 - \sigma_{32}^2$$
$$B = \sigma_{32}(\sigma_{22} - \sigma_{33})$$
$$C = \frac{1}{2}(\sigma_{21}^2 - \sigma_{31}^2)$$
$$D = \sigma_{21}\sigma_{31}$$

Once the roots the quartic equation are known, the possible slip planes are given by:

$$\beta = \pm \cos^{-1} \sqrt{\frac{y + 1}{2}} \tag{25}$$

A complete derivation and a discussion of the specific plasticity theory used can be found in Wu [9].

IMPLEMENTATION OF BIMODAL PLASTICITY INTO LAMINATED SHELL ELEMENTS

The original bimodal plasticity formulation considered a six dimensional stress-strain space. Therefore it is necessary, in the implementation of bimodal plasticity into shell elements, to eliminate the stress and strain terms that do not occur in the shell formulation.

The shell formulation used here assume that each layer is in a state of plane stress, that is $\sigma_3 = 0$. This condition was enforced by modifying the stiffness matrix (D) into a plane stress stiffness matrix (D^*) as follows.

$$D^*_{ij} = D_{kl} - \frac{D_{2k}\, D_{2l}}{D_{22}} \tag{26}$$

where the correspondence between i,j and k,l is given by:

i,j	1	2	3	4	5
⇓	↓	↓	↓	↓	↓
k,l	1	2	4	5	6

The strain increments passed into the material model are also modified to properly reflect the assumed state of the material. For this case the proper increment of ε_3 must be passed to the material model such that the model returns $\sigma_3 = 0$. this strain increment is calculated as:

$$d\varepsilon_3 = \frac{D_{ij}\, d\varepsilon_i}{D_{33}} \quad i = 1,2,4,5,6 \tag{27}$$

This transformation of the stiffness matrix is performed between the element routine and the bimodal plasticity routine. Thus, the same code can be used for the material model in both the shell elements and the solid elements.

RESULTS

The material properties in Table 1 were used for all examples.

Fiber		Matrix	
axial stiffness	689655	axial stiffness	72395.4
axial shear stiffness	15517.2	axial shear stiffness	27216.3
axial Poisson's ratio	0.2	axial Poisson's ratio	0.33
transverse stiffness	0.41	transverse stiffness	72395.4
transverse shear stiffness	2068.97	transverse shear stiffness	27216.3
volume fraction	0.5	yield stress	70.0

Table 1. Material Properties

Simply supported flat plate under uniform pressure load

For these problems, one-quarter of a simply supported plate, under a uniform load was modeled using shell elements and solid elements. The solid models used a 5 by 5 mesh for the quarter plate, with symmetry conditions, with 2 or 4 elements through the thickness of each ply. The shell models employed a 4 by 4 mesh for the quarter plate.

For all the plots presented below, stresses are given in the global axis system as shown in Fig. 2. The fiber orientations are measured with respect to the x_1 axis.

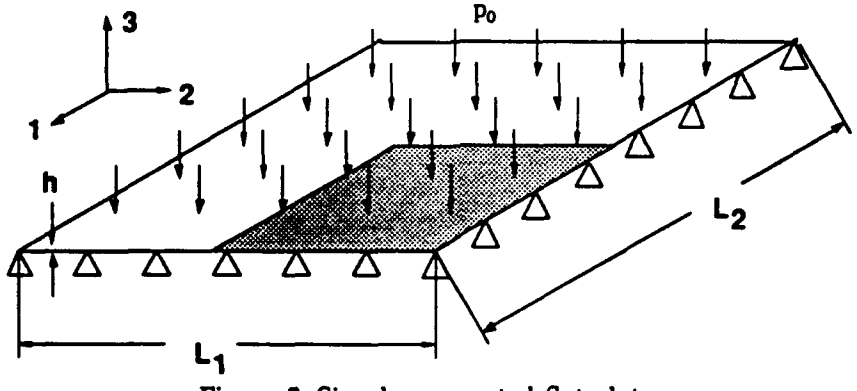

Figure 2. Simply supported flat plate.

$(0/90)_s$ square plate

For this problem $L_1 = L_2 = 2$. Although, for all the cases tested with this layup, there was significant material nonlinearity, load-deflection curves were very nearly linear. This implies that the overall response is primarily governed by the elastic response of the fibers.

For this layup the solid model and the discrete layer model produce essentially the same displacement results. The stress distributions obtained from the solid and discrete layer models, for a plate thickness h = 0.1, are shown in figures 3 and 4, ζ is the normalized thickness coordinate. For both models the in-plane stress distributions are in good agreement, while the transverse stress distributions show a significant difference, as would be expected since the discrete layer model assumes constant transverse strains through the thickness of each layer.

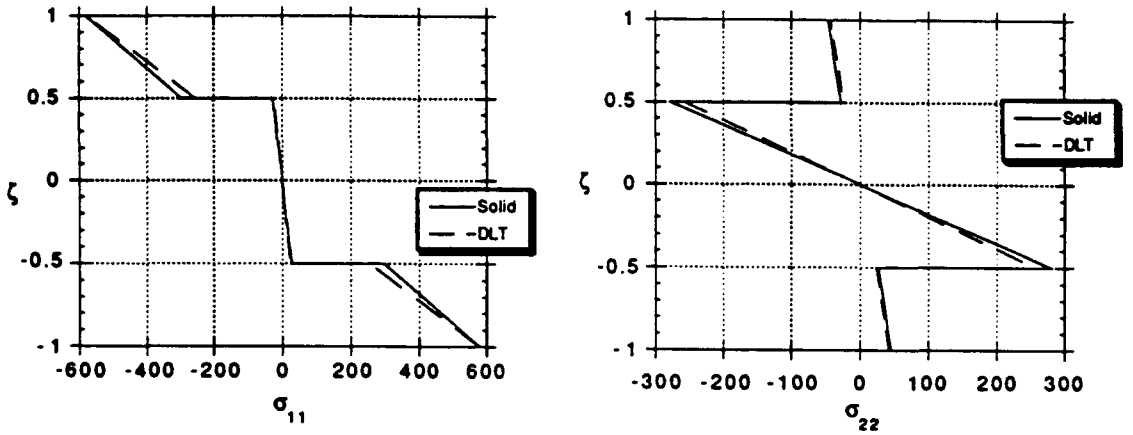

Figure 3. In-plane stress distributions for solid and discrete layer model. h = 0.1, Load = 2 MPa.

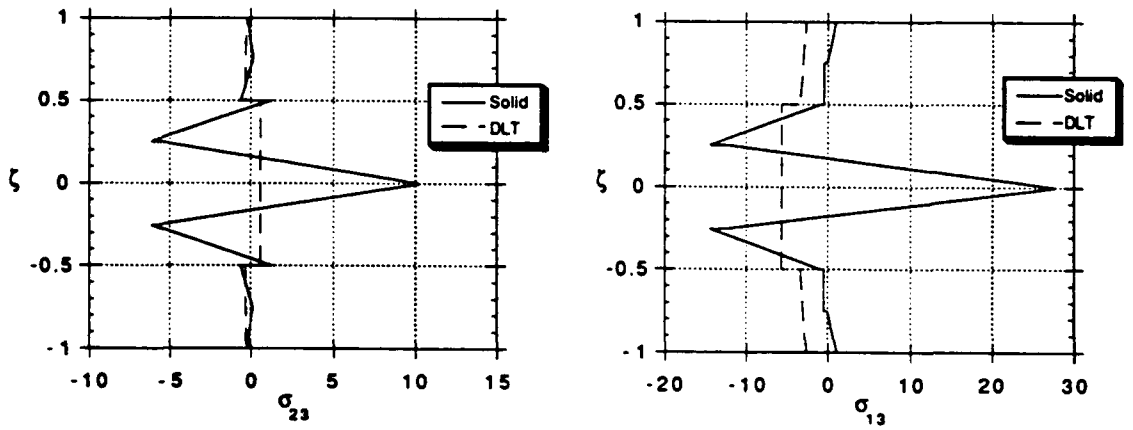

Figure 4. Transverse shear stress distributions for solid and discrete layer model. h = 0.1, Load = 2 MPa.

In Fig. 4 it can be seen that the transverse shear stresses in the discrete layer model are not constant. The transverse shear strain components are assumed constant through the layer but the other strain component vary through the thickness. Thus, for a nonlinear material the shear moduli may change through the thickness resulting in stress that are not constant. This in an important consideration in the formulation of shell elements for use with nonlinear material models.

$(\pm 45)_s$ square plate

For this problem $L_1 = L_2 = 2$. The thickness, h, was taken to be 0.1. The load-deflection curves for this laminate showed much more nonlinearity than those for the $(0/90)_s$ laminate. This implies that the overall response was significantly affected by the nonlinear behavior of the matrix.

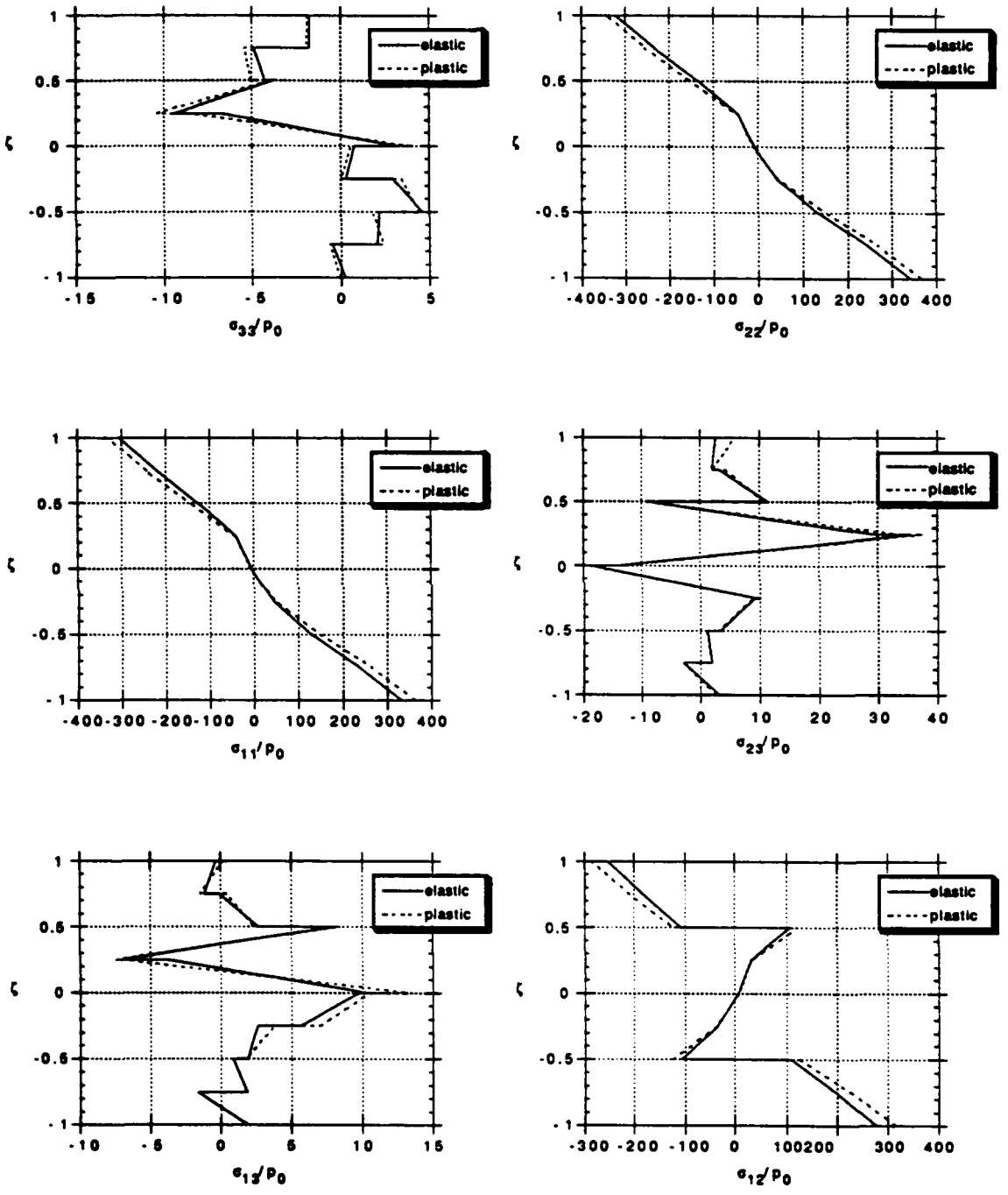

Figure 5. Stress distributions for $(\pm 45)_s$ laminate, solid model, 2 elements through thickness per layer

Figure 5 shows the stress distributions through the thickness for the laminate in both the elastic and plastic ranges for the solid model with 2 elements through the thickness. The stresses have been normalized by the applied load. The inplane stress quantities show similar distributions in both the elastic and plastic ranges. The transverse stress quantities, both direct and shear, show some significant differences between the elastic and plastic cases. The differences in the distributions increased with increasing load.

The transverse shear distribution through the thickness of the laminate for the shell model are shown in Fig. 6. These stress distributions show a significant difference from those obtained from the solid element. There is also a significant change in the stress distribution between the elastic and plastic stress distributions. The inplane stress quantities are similar to those from the solid model and have similar distributions in both the elastic and plastic range.

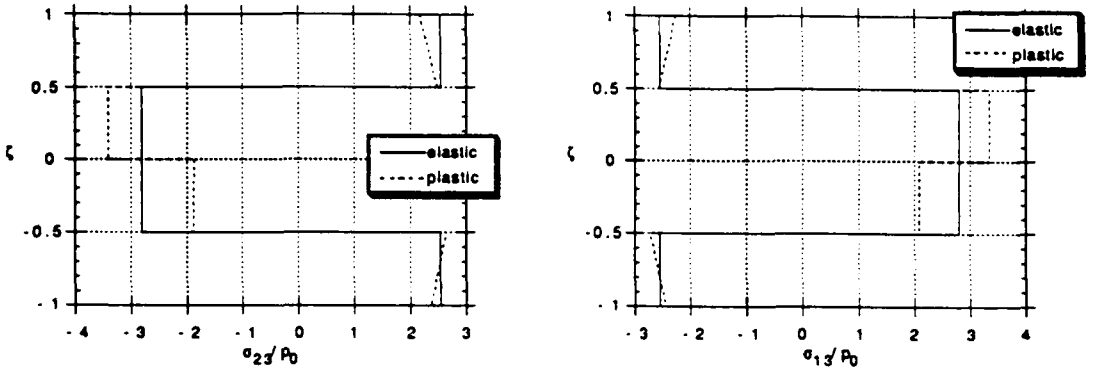

Figure 6. Transverse shear stress distributions, shell model.

Since the response of this material is dominated by the in-plane stiffness of the laminate and not the detailed transverse shear stress distribution, a first order shear deformation model, might be expected to give reasonable results. Combining this model with a predictor-corrector approach, such as that proposed by Norr, et. al. [12], could be expected to give good results with a significant reduction in computation time. Also since the response, for the layups tested, was dominated by the elastic properties of the fiber, it may be possible to use the elastic properties of the composite in the predictor phase and then incorporate the nonlinear material properties into the corrector phase.

ACKNOWLEDGMENTS

This work was supported by a grant from the Office of Naval Research under grant number N000014-85-K-0733, Dr. Yapa Rajapakse, project monitor. We also thank Hibbitt, Karlsson and Sorensen, Inc., for the use of the ABAQUS program on this project.

REFERENCES

[1] Teply, J.L., and Dvorak, G.J., "Bounds on Overall Instantaneous Properties of Elastic Plastic Composites, *J. Mech. Phys. Solids*, Vol. 36, pp. 29-58, 1988.

[2] Dvorak, G.J. and Bahei-El-Din, Y.A., "A Bimodal Plasticity Theory of Fibrous Composite Materials", *Acta Mechanica*, Vol. 69, pp. 219-241 , 1987.

[3] Bahei-El-Din, Y.A. and Dvorak, G.J. , "New Results in Bimodal Plasticity of Fibrous Composite Materials", *Proc. Plasticity* '89 pp. 121-127, 1989.

[4] Noor, A.K. and Burton W.S., "Assessment of computational models for multilayered composite shells", *Appl. Mech. Rev.*, Vol. 43, pp. 67 - 97, 1990.

[5] Reddy, J.N., "On Refined Computational Models of Composite Laminates", *Int. J. Num. Meth. Engng.*, Vol. 27, pp. 361-382, 1989.

[6] ABAQUS Version 4-8 Manuals, Hibbit, Karlsson & Sorrensen Inc., Providence, RI, 1989.

[7] Dorninger, K. "A Nonlinear Layered Shell Finite Element with Improved Transverse Shear Behavior", SCOREC Report #3-1991.

[8] Dvorak, G.J., Bahei-El-Din, Y., Macheret, Y. and Liu, C.H., "An Experimental Study of Elastic-Plastic Behavior of a Fibrous Boron-Aluminum Composite", *J. Mech. Phys. Solids*, Vol. 36, pp. 655-687, 1988.

[9] Wu, J.F., "Numerical Techniques for Elastic-Plastic Analysis of Fibrous Metal Matrix Composites", Ph.D. Thesis, Rensselaer Polytechnic Institute, 1991.

[10] Hill, R, "Elastic properties of reinforced solids: some theoretical principles" *J. Mech. Phys. Solids*, Vol. 11 pp. 357-372, 1963.

[11] Mori, T. and Tanaka, K., "Average Stress in Matrix and Average Elastic Energy of Materials With Misfitting Inclusions", *Acta Metallurgica*, Vol. 21 pp. 571, 1973.

[12] Noor, A.K., Burton S. and Peters, J.M., "Predictor-Corrector Procedures for Stress and Free Vibration Analyses of Multilayered Composite Plates and Shells", *Comp. Meth. in Applied Mech. and Eng.*, Vol. 82, pp. 341-363, 1990.

Analysis Idealization Control for Composite Materials with Nonlinear Behavior

M.S. Shephard, M.W. Beall
Scientific Computation Research Center, Rensselaer Polytechnic Institute, Troy, NY 12180-3590, U.S.A.

1. INTRODUCTION

Reliable modeling of the physical behavior of composite structures requires the balanced consideration of each of the analysis idealizations used to go from the physical description of the composite system to the numerical analysis models used to predict the behavior. Specification and categorization of the idealization steps associated with the analysis of nonlinear composite materials is complicated by both the complexity of the idealizations needed and the close interrelationships among the idealization steps.

Prediction of the performance of composite structures must explicitly account for the physical scales that control the behavior of interest. There are a variety of methodologies available to account for these physical scales in an analysis. Of particular interest in composites with nonlinear constituents are the methodologies used to account for the micromechanical nonlinear behavior. Another analysis idealization important to the analysis of composite structures is dimensional reductions.

This paper begins with a brief review of the issues associated with the control of analysis idealizations and outlines a modeling system being developed to provide this control. This is followed by a more detailed discussion of the idealizations associated with the thermo-mechanical analysis of composite structures. Finally some results which make comparisons between specific idealizations and emphasize the application of the bimodal plasticity model for nonlinear composites are given.

2. CONTROL OF ANALYSIS IDEALIZATIONS

Analysis Idealization

The application of engineering analysis typically employs a number of idealizations to reduce a physical behavior to a set of algebraic equations that can be solved manually or on a computer. Each step of idealization used in an engineering analysis process introduces some level of approximation. The reliability of an analysis depends on the ability to understand and control the approximation errors introduced by each step of idealization [1, 2, 3].

The accuracy of a solution is a function of the measure(s) of accuracy you are interested in. For example, the results of a finite element solution to the equations of elasticity for a given problem may yield values of the reactions and displacements with sufficient accuracy, while the predictions of the peak stresses are unacceptably inaccurate. It is therefore important to qualify the error of interest in an appropriate norm. Typically several norms of the solution results are of interest.

The first step in estimating the errors in engineering analysis is to enumerate the contributing sources which in the thermo-mechanical analysis of composites include: the basic mathematical model selected to represent the physical behavior of interest; the physical scale the mathematical model is solved upon and the alterations to the basic mathematical model associated with representation of lower scales; the dimensional reductions and associated alterations to the mathematical model to eliminate physical dimensions; the domain of the analysis; the material property parameters; the boundary conditions (also initial conditions when time is one of the dimensions of the problem); and the discretizations used for the analysis. Section 3 discusses each source with respect to the thermo-mechanical modeling of composites.

Since the exact solution to a requested analysis is generally not known, it is only possible to obtain estimates to the solution error. The goal of idealization error control is to ensure that reliable estimates of the errors of interest can be obtained and that these estimated errors are forced to be less than a user specified limit for that analysis.

The techniques available to aid in the control of idealization errors include analytically-based error estimation, hierarchic model comparisons, analytically-based results for ideal situations, sensitivity analysis, statistical methods, comparison to known physical limits, test results and reasonable limits, and rules based on experience and intuition [2]. Analytically-based error estimation and hierarchic model comparisons provide the greatest promise for the reliable estimation of the idealization error contributions. Analytically-based error estimators have been developed to provide reliable control of some of the finite element discretization errors. However, techniques of similar reliability are not readily available to control other idealization error contributions. The combination of analytically-based error estimation and hierarchic model comparisons is a promising approach for the control of the other idealizations critical to the analysis of composite structures.

Framework for Analysis Idealization Control in Engineering Design

The ability to apply idealization control during engineering design requires a system framework which can house various levels of analysis idealization control with intelligent design methodologies and engineering analysis tools. The framework of an engineering modeling system for mechanical objects (IDEALZ) that is specifically structured to support the idealizations used in engineering modeling and analysis is described in references [4, 5]. The system architecture is consistent with the architectures being considered to support design modeling systems in reference [6].

The heart of the system is the representation of the object being designed and the modelers that support that representation. To support the functions necessary in the design evolution of an object, its representation is housed in

linked functional and geometric model structures, each of which are controlled by the appropriate modelers. The other operational components of the modeling system are the applications. The applications include analysis procedures to answer performance questions, algorithms to alter the design based on analysis results, and procedures to plan the manufacturing processes, etc. Applications are separated into two groups based on the technology underlying their implementation, not on the functions addressed. The first group is analytically-based applications. The majority of the applications in this group are numerical analysis and optimization procedures. The second group is knowledge-based applications. Knowledge-based applications operate from codified heuristics placed in rule sets.

The task of analysis idealization control falls to the goal manager and the analysis strategist, which guide the operation of the system. The goal manager and the analysis strategist interact with the models, applications, and databases to track the various activities that have been performed and guide the application of those that are requested. The first task of the goal manager is to accept a request to perform an operation, and determine if the basic information and capabilities required to perform the task exist. It then invokes the strategist which is responsible for formulating and controlling the idealization steps required to perform the requested analysis. The goal manager is responsible for maintaining information about the status of the analysis goals used for the design and the goals that have been performed previously.

3. ANALYSIS IDEALIZATION CONTROL FOR COMPOSITE MATERIALS

This section outlines the analysis idealizations that should be considered in the analysis of composite structures and gives a brief indication of how the idealization processes can be addressed. The close interaction of the methods of idealization control applied to composite materials tends to make one idealization process flow into the next and makes the idealization processes dependent upon each other. Although this makes the process of idealization categorization difficult, and in some cases seemingly arbitrary, it affords an opportunity to employ idealization evaluation processes that can provide useful insight on multiple idealization steps. This possibility is being specifically considered in the current research program.

Mathematical Model

The derivation of the base mathematical model begins with a clear enumeration of the physical laws deemed critical to the description of the physical behavior at hand. In the case of the thermo-mechanical behavior of heterogeneous materials, the minimum scale that must be addressed in any analysis idealization must be considered. In structural composites of the overall size scale considered here, the minimum level is assumed to be orders of magnitude above that of individual atomic units. This assumption allows us to employ classic continuum mechanics in terms of i) equilibrium of mechanical forces, ii) kinematic relationships relating internal deformations (strains) to displacements, and iii) constitutive relations between internal forces and deformations. These relationships must be satisfied at any scale for which they are constructed. They are valid down to constituent levels where the minimum dimensions of the constituents considered are well above atomic dimensions.

Such assumptions may not be reasonable in extremely small scale structures such as micromachines or ultra-thin multichip interconnects. Since the definition of the mathematical model as used here is the fundamental starting point for an analysis process, the only idealization evaluation measure available is comparison to measured physical behavior.

Physical Scale of the Solution and Representation of Lower Scales

By their very nature, the thermo-mechanical analysis of heterogeneous materials at a macromechanical level must explicitly account for the micromechanical structure and properties of the constituents. In some simple linear cases, this consideration may be through simple homogenization models which are easy to apply. However, in more complicated situations much more explicit consideration of micromechanical behavior is needed. For example, metal matrix composites can not be properly designed without explicit consideration of the material nonlinearities. These materials demonstrate nonlinear behavior early in the load-deformation process, and the extension of linear results past the limit of linearity is not conservative [7, 8].

The determination of a homogenization method and its bounds of validity appropriate for the problem at hand must consider:

1. the accuracy level required for the terms in the homogenized constitutive model developed
2. the geometry of the microstructure
3. the well-posedness of the mathematical model due to the possible loss of ellipticity of local damage models
4. the material behavior of the constituents
5. the need to use the information generated during the homogenization process to predict local field information after the global field is determined
6. the gradients in the solution parameters with respect to the size of the constituents used in the homogenization process

A number of analytic procedures are available to perform the homogenization of idealized micromechanical geometries when the constituent materials are linear elastic [9]. In many cases these procedures can be shown to produce tight bounds on the macromechanical constitutive relations. However, they often do not provide accurate estimates of the detailed local stresses and strains for other than the idealized geometric configuration assumed. In cases of linear material problems, where these techniques do not provide accurate macromechanical constitutive properties or where accurate local solution quantities are important, more detailed micromechanical level homogenization analyses based on finite element techniques are possible [10].

When one or more of the constituent materials becomes nonlinear, analytically derived homogenization expressions require solution through numerical iteration. One such model is the vanishing fiber diameter model which has the two deficiencies of not being able to accurately model behavior dominated by transverse behavior and not being able to provide accurate local values.

Numerical models using more realistic micro-geometries have recently received considerable attention for the homogenization of nonlinear constituents. One such model is the periodic hexagonal array model [11] in which a local finite element discretization is used in the construction of a macromechanical constitutive model based on the constituent properties. Although a computationally demanding model, the periodic hexagonal array model does provide accurate prediction of the overall properties, and, if the local discretization is fine enough, a good estimation of the local field quantities for the idealized micro-geometry.

An alternative approach to the development of homogenization procedures in the presence of nonlinear constituents are phenomenological micromechanic models such as bimodal plasticity [7]. This model employs the inner envelop of a micromechanical level fiber dominated mode and matrix dominated mode. The numerical implementation of such a procedure can be made quite efficient, however, it is not likely that such an approach will provide accurate predictions of local field quantities.

Most homogenization procedures rely on a level of uniformity of the local fields at each point of evaluation. If the gradients of the critical solution parameters are too high, the accuracy and validity of the homogenization process is in question.

The ability to evaluate the idealization errors associated with homogenization is strongly dependent on the homogenization process used. Mathematical analysis procedures can be used in some cases to bound specific elastic constants. The ability to define such bounds is often lost with the introduction of nonlinear material behavior of the constituents. The use of finite element techniques for the solution of the homogenized problem provides an interesting method to employ discretization error control techniques to evaluate the homogenization errors [10].

Separate evaluation procedures are required when the high local gradients invalidate the micromechanical uniform periodicity of the entire homogenization process. As indicated below, this area is one that will receive specific consideration in the current research.

Dimensional Reductions

Since the effective use of composite materials must account for the directional nature of the material, most composite components are thin in at least one direction. Therefore, the development of analysis idealizations must deal with the reduction of the through the thickness direction. This introduces all the complexities of the plate and shell theories which all have at least one representational inconsistency which leads to complexities in the representation of transverse shear and introduces representational difficulties at boundaries and junctures in shells. These problems become even more critical in composite materials [12].

One approach to the control of idealization errors associated with dimensional reduction is to convert it into a discretization process. Instead of stating specific assumptions on the through the thickness direction, a convergent discretization through the thickness is used which allows the development of estimates of the error introduced by truncating the expansion at a given point [13, 14, 15, 16]. Since many of the finite element discretizations

of laminated shells [17] employ semi-discretizations where laminate level through the thickness discrete assumptions are applied, the use of an expansion through the thickness is possible.

Often the need to improve the through the thickness idealization is limited to critical areas. In these cases it is advisable to employ different levels of through the thickness idealization locally. For example, at shell boundaries or at junctures, complete three-dimensional representations could be used to improve the solution accuracy [18]. Alternatively, two level models can be used to determine local parameters and to provide feedback to locally improve the through the thickness idealization. Noor has successfully demonstrated such a procedure [19] for composite shells.

Domain

Domain simplifications in the analysis of composite materials can arise at each scale level considered. At the macromechanical level there are the standard domain simplifications. An additional concern in the evaluation of the influence of these procedures is the directional nature of composites which complicates the evaluation of idealization procedures. For example, typical dimensions for assuming Saint-Venant's principle holds can be much greater in an anisotropic material.

At the micromechanical scale it is common to employ geometric simplifications of the shape of the constituents in the specification of the idealization used in the homogenization process. Consideration must be given to the influence of these approximations on the determination of macromechanical material parameters. Often the approximations used have a small influence on these parameters. In some cases, consideration must also be given to the influence of micromechanical domain approximations on the estimation of local quantities such as stress concentration factors that may be used in criteria to estimate the initiation of local nonlinear behavior.

Material Properties

The accuracy of the material parameters in a macromechanical constitutive relation are a function of the homogenization process and the accuracy of the constituent constitutive parameters, including the representation of interfaces or interphases. Therefore, the accuracy of representation of the material parameters must consider the constituents and the representation, if any, of the constituent interfaces. Once the constituent material parameters have been combined through homogenization to produce a macromechanical constitutive relation, it is necessary to examine the ability of that relationship to represent the material behavior.

Although the mathematical model places constraints on the overall form of the constituent constitutive relations, there are a wide range of possible representational models that can be selected when material nonlinearities must be represented. The selection of these models must consider both the model's ability to represent the experimentally measured material response, and the validity and influence of that model on the nonlinear solution processes that must be applied to that model during thermo-mechanical analyses. At this time there has been a limited amount of work on the qualification of the idealization errors associated with nonlinear material models [20, 21].

Boundary and Initial Conditions

The representation of boundary conditions must account for the homogenization and dimensional reduction processes. The dimensional reduction processes introduce a number of problems in the specification of boundary conditions [22]. The issues of boundary condition representation become even more complex in composite materials if edge effects are considered. Another issue associated with the specification of boundary conditions of particular importance to this research is when a local micromechanical level analysis needs to obtain boundary conditions determined by a global macromechanical analysis. However in engineering analysis the choice of boundary conditions is usually a modeling decision between several alternatives. If this is the case for a particular problem then the choice leading to the smoother solution is preferable since it increases the rate of convergence of the solution [14].

Discretization

The control of discretization errors for composite materials at a particular level become complicated by the desire to control the discretization errors as they relate to variables at different scales where different discretizations may be used at the different levels of scale. Even with these complications it is clear that error control based on a posteriori error estimation is the most reliable method to qualify and control idealizations.

4. APPLICATION OF NONLINEAR MIXING MODEL WITH AND WITHOUT DIMENSIONAL REDUCTION

The following sections present some initial results comparing idealizations of the material model and idealizations involving dimensional reductions. First, an overview of the nonlinear material model, bimodal plasticity, is presented. Next the specific dimensional reductions used are discussed. Finally, some initial results of the effect of these idealizations on the prediction of the behavior of a transversely loaded plate are presented.

Bimodal Plasticity Material Model

Bimodal plasticity is a semi-phenomenological model which describes the plastic deformation of fibrous composites consisting of elastic fibers and an elastic-plastic matrix [23, 7]. The theory assumes that the deformation of such a composite can be described in terms of one of two deformation modes, the fiber-dominated mode (FDM) or the matrix-dominated mode (MDM). In the fiber-dominated mode, both phases, fiber and matrix, deform together in the elastic and plastic range and the composite aggregate is treated in the context of heterogeneous media elasticity and plasticity. In the matrix-dominated mode, plastic deformation is caused by slip on matrix planes which are parallel to the fiber axis. The yield condition corresponding to each mode gives a yield surface in the overall stress space. The overall yield surface of the composite is then given by the inner envelope of the yield surfaces of the two modes.

The dominant deformation mode is determined by the elastic moduli of the phases, in particular the longitudinal shear modulus, and the overall loads. In the plane stress space, the matrix-dominated mode is active in composites where the ratio of the longitudinal elastic shear modulus of the fiber and the matrix is large, e.g. B/Al and SiC/Al composites. The fiber-dominated mode is common in composite systems where the fiber longitudinal shear modulus is

comparable or smaller than the matrix elastic shear modulus. This mode also occurs when stress in the fiber axis is the dominant loading. Recent experiments on a B/Al composite system have verified the existence of the deformation modes postulated by the bimodal plasticity theory [23, 7]. Following is a brief description of both of the deformation modes [24].

Fiber-Dominated Mode Plastic deformation in the fiber-dominated mode is described by averaging models originally introduced for elastic phases [25]. The constitutive relations of the phases are assumed to be known for the volume average of the local fields.

The overall stiffness and compliance matrices can be written as functions of the phase volume fractions, phase properties and stress concentrations. In the elastic range, the concentration factors of the phases are found from an averaging model. In the present work, the method developed by Mori and Tanaka [26] is used to evaluate the elastic concentration factors. In the plastic range, for composites with elastic fibers, the plastic strain increment in the matrix phase is described by a two surface plasticity theory.

The explicit form of the matrix instantaneous stress concentration factor in the plastic range can be found. Once the instantaneous stress concentration factors of the phases are found, the overall stiffness matrix of the composite can be determined.

Matrix-Dominated Mode In the matrix dominated mode the deformation in the plastic range is derived from plastic slip along planes parallel to the fiber direction. The active slip planes are determined by finding the planes parallel to the fibers on which the resolved shear stress is a maximum. The onset of matrix yielding occurs when the magnitude of the resolved shear stress along one of the slip planes equals the matrix yield stress in simple shear. The plastic strain on each active slip plane is found from the associated flow rule and the normality requirement. The overall plastic strain is then found by the summation of the plastic strain on each active slip plane. A complete derivation and a discussion of the specifics of the implementation can be found in reference [24].

Dimensional Reduction and Finite Element Discretizations

One of the most important idealizations in the analysis of composite laminates is dimensional reduction. Dimensional reduction can significantly reduce the number of degrees of freedom required to model a given problem. This process is practical since a typical composite structure is usually relatively thin. However, the accuracy of the dimensional reduction process used depends on the particular problem to be analyzed and it is generally difficult to make a priori statements about its accuracy.

Dimensional reduction can be performed in several different manners. In reference [17] four general approaches for constructing two-dimensional theories for multilayered shells are identified. These four approaches are: 1) the method of hypotheses, 2) the method of expansion, 3) asymptotic integration techniques, 4) iterative methods and methods of successive corrections.

Of the above four methods the one that is most commonly used in engineering applications is the method of hypothesis. In this approach a priori

assumptions are introduced regarding the variation of displacements, stresses or strains through the thickness. This approach has the advantage of being intuitive and easily extendible to large displacements and nonlinear materials. However the theory does not provide an estimate of the error in the response predictions.

The other three methods have the advantage of producing, within the scope of the theory, some kind of estimate of the error introduced by the approximations. One recent theory [14] results in a set of hierarchic models that have the properties that the exact solution of the hierarchic series of models converge to the solution of the corresponding problem in elasticity for a fixed laminate thickness, and that the exact solution of each model in the series converges to the same limit as the solution of the corresponding problem in elasticity as the laminate thickness approaches zero. The lowest order model of the theory corresponds to Reissner-Mindlin plate theory.

The dimensional reduction used in this paper is a discrete layer shell with assumptions of a piecewise linear approximation for the in-plane displacements and constant transverse displacements in the thickness direction. This element is formulated using the degeneration principle, where the three dimensional elasticity equations are reduced to two dimensions by assuming a certain displacement behavior through the thickness of the shell. This approximation generally gives good results for in-plane quantities but since the transverse shear strains are constant within each layer, the continuity of the transverse shear stresses is not satisfied at layer interfaces.

A recent development in this area is a layerwise plate theory by Reddy [27]. This theory allows arbitrary piecewise representation of displacements through the thickness of each lamina. This theory has been shown to produce accurate results, even for thick plates [28]. It has also been extended by Barbero to account for multiple delaminations between layers including geometric nonlinearity to capture layer buckling [29].

Results of a Transversely Loaded Plate

This section demonstrates some of the effects of idealizations of the material model and the finite element formulation on the analysis of a transversely loaded plate. In each case, two analyses, which differ by only one of the idealizations used, are performed. Comparing the results of the two analyses shows the effect of that idealization.

The first set of results deals with the effects of idealizations on the global behavior of the model. Specifically, the effect of the material model used in the analysis is investigated. This is done by comparing the displacements and the stress resultants predicted using an elastic material model and those predicted using bimodal plasticity.

The later results deal with the effects of idealizations on local behavior of the model. The effect of the material model is first shown with a comparison of transverse shear values using elastic material model and bimodal plasticity. Also the effect of the finite element formulation on the prediction of transverse shear stresses is examined.

Some recent articles by Noor, et. al. [30, 17, 12, 19] provide a very good overview of many different plate and shell theories and their effects on the

accuracy of various analysis results, although all of their results are for elastic materials.

The results shown here are raw finite element data, no attempt was made to smooth the data or use various procedures to post process the data to improve the results. Predictor-corrector procedures [31] have been shown to be effective in obtaining better estimates of global and local response quantities for composites incorporating elastic materials. If these methods can be effectively implemented for composites with nonlinear materials much better local stress distributions could be found. The predictor-corrector procedures in reference [31] use a first-order shear deformation shell theory to obtain initial estimates of the solution to a problem (predictor). The results of the predictor are then used in conjunction with the three-dimensional equilibrium and constitutive equations to calculate a more detailed estimate of the solution. This result is then used either to calculate a corrected transverse shear stiffness for the shell or to directly calculate the functional dependence of the displacement components on the thickness coordinate.

The procedures used in the predictor-corrector methods were developed for linear elastic materials and take advantage of this fact by being implemented in a 'post-processing' manner. For elastic-plastic materials such procedures may have to be implemented in the solution procedure. The path dependence of such materials may preclude the correction of the stress and strains unless this is done within each load increment before any stress update procedures.

The specific problem analyzed is a flat plate with clamped edges as shown in Fig. 1. The plate is Boron/Aluminum with a $(0/90)_s$ lay-up. The parameters for the problem, unless otherwise noted are: L=2.0, h=0.1, and p_0=2.0. In the following results the loads are normalized to the load that causes initial yielding in the matrix. The finite element meshes used to produce the results varied from example to example. In all cases a uniformly refined mesh was used which was refined until the solution quantities of interest had converged.

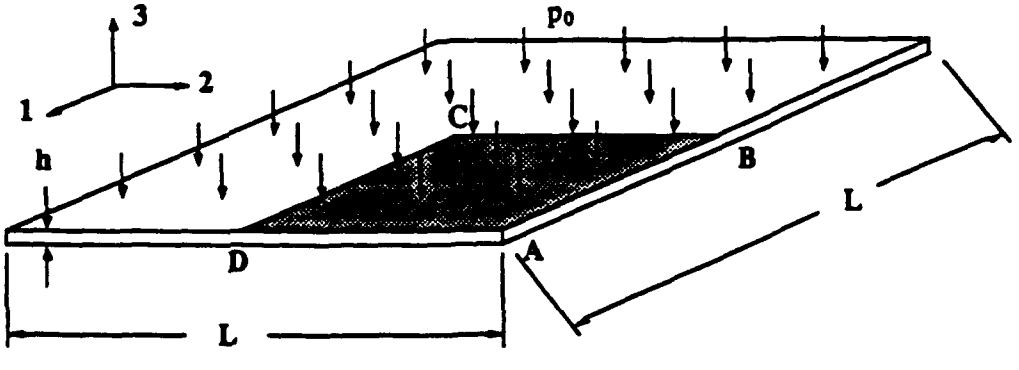

Figure 1. Flat square plate with clamped edges.

Global solution Figure 2 shows the effect of the material model on the overall solution. The difference in the displacements at the center of the plate does not become significant until almost three times the initial yield load and there is only a 4% difference at four times the initial yield load. As expected, the bimodal plasticity model shows softening behavior at higher loads.

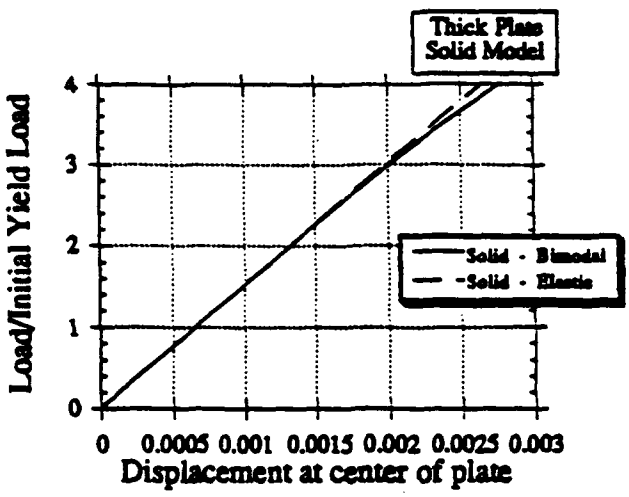

Figure 2. Effect of material model on displacement at center of plate.

Figure 3 shows the displacement at the center of a thin plate (h=0.01, p_0= 0.05). Again, the difference between the two solutions is only a few percent even up to eight times the initial yield load. The geometric nonlinearity, due to the large displacements, is much more significant than material nonlinearity for this problem. In both the thick and thin plates the linear response of the fibers, rather than the plastic response of the matrix, dominates the displacement behavior.

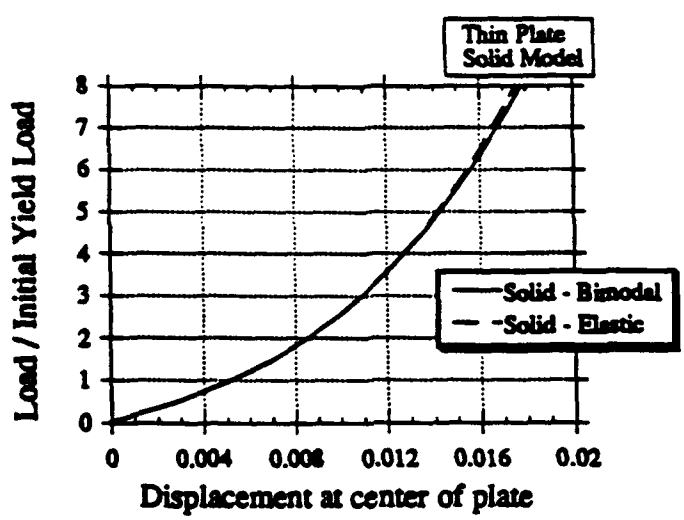

Figure 3. Effect of material model on displacement at center of plate. (thin plate: h=0.01, p_0= 0.05)

Figures 4 and 5 show another example of the effect of the material model on the overall solution. This result shows the resultant moment along edges A-B and A-D of the plate. The moment predicted by using the bimodal plasticity model is significantly different from that predicted by the same analysis using a linear elastic material model. As the load is increased past the elastic limit the moment does not change uniformly along the edge of the plate, rather there is a significant redistribution of moments. Edge A-D of the plate shows a similar

result but with the moments predicted using bimodal plasticity being higher than those predicted with the elastic material model.

This redistribution of moment occurs when yielding of the matrix limits the load carrying capability of a lamina. As the load is increased the reaction moments along the edges increase proportionally until one or more of the layers begins to yield. At this point the layer cannot maintain the increase in load, but the laminate must still be in overall equilibrium with the applied load. Thus, the increased compliance of the yielded portion of the laminate causes the load to be transferred to other portions of the plate.

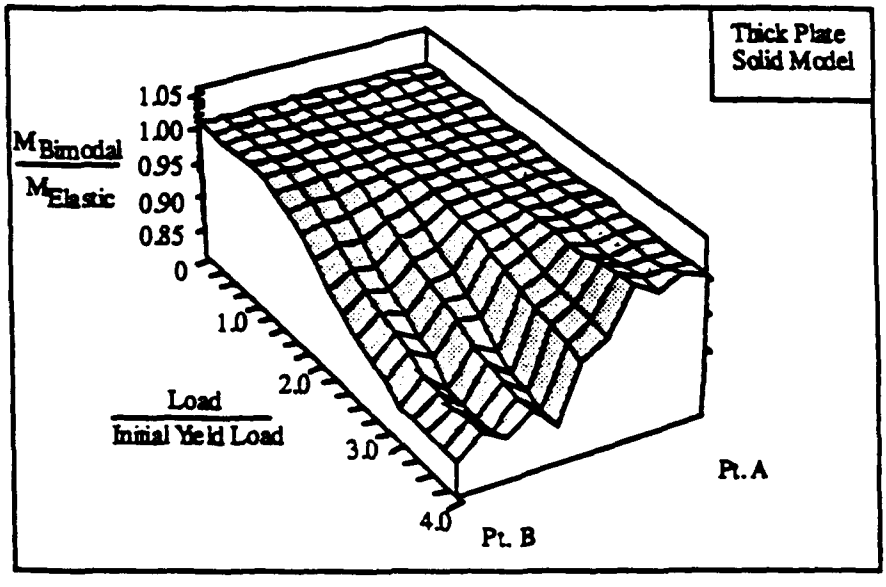

Figure 4. Bending moment distribution along edge A-B.

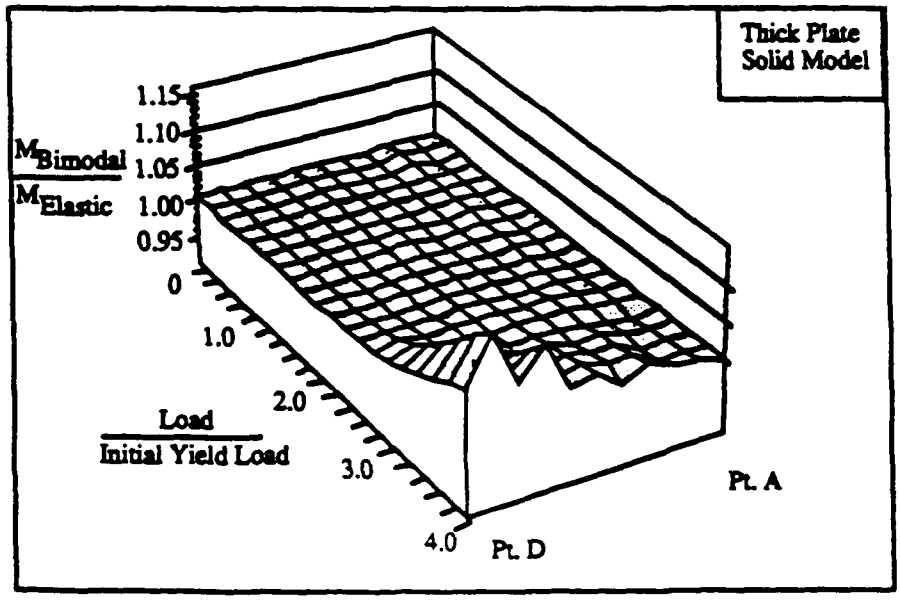

Figure 5. Bending moment distribution along edge A-D.

Local solution The effect of the material model on the local solution is shown in Fig. 6. In this figure the transverse shear stress, an important quantity in determining the initiation of delaminations, is plotted through the thickness of the plate. Generally, this example shows a decrease in the transverse shear stress everywhere except the bottom of the third layer of the plate. In some areas, the local values of stress change significantly after onset of matrix plasticity. In this example the significant changes are generally decreases.

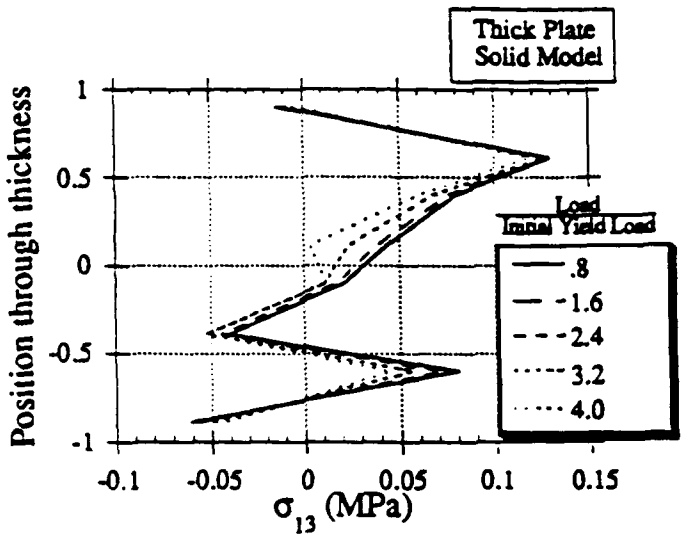

Figure 6. Changes in transverse shear stress due to nonlinear material model.

Next, the effects of finite element formulation on the local solution are investigated. The problem analyzed for these results has the same geometry as shown in Fig. 1. The material is Graphite/Aluminum with a $(\pm 45)_3$ lay-up. In these results the problem was modeled with both a solid element model and a discrete layer shell model, in both cases the bimodal plasticity material model was used.

The inplane stress values agree well between the discrete layer shell and the solid model, as would be expected. However, as shown in Fig. 7, the discrete layer shell assumption of layerwise constant transverse strains produces poor local values for the transverse stresses. The transverse shear stresses are not constant due to the nonlinear material model. This arises because the direct stress quantities are allowed to vary linearly through the thickness of each layer. Thus, although the transverse strains are constant through each layer, the point in overall stress space may change through the thickness of each layer. This results in different points through the thickness following different loading paths. With a plastic material model the response of the material is path dependent and a different loading path results in different material properties. The result of this is that the transverse shear stiffness may change through the thickness of each layer. The varying material properties through the thickness give rise to changes in stress even when the strain is constant.

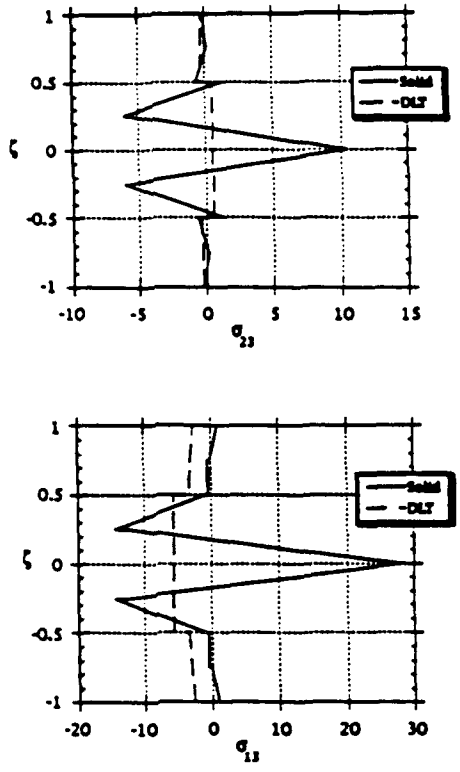

Figure 7. Effect of finite element formulation on transverse shear stress distribution (solid model and discrete layer model).

Bimodal plasticity

The next two figures show the evolution of the different plasticity modes throughout the loading history of an analysis. The load indicated in the figures is the actual load normalized to the initial yield load. In each figure one quarter of the plate is shown with the center being in the upper right corner (point C). The deformation mode predicted by the bimodal plasticity model is indicated by the shading in the figures. Elastic behavior is indicated by white, fiber dominated mode (FDM) is shown as gray and matrix dominated mode (MDM) is shown as black. In each case the data is shown for the bottom of the lower two layers in the laminate.

Figure 8 shows the results for a thin plate (h=0.01, p_0= 0.05). For this case the primary stresses are inplane loading due to bending-stretching coupling and bending behavior around the edge of the plate. The first inelastic behavior is FDM deformation at the center of the plate and along edge A-B near point B. The first appearance of MDM is at a load of 3.0 times the initial yield load on edge A-D near point D. This load is also when inelastic behavior is first indicated in layer 3. The inelastic deformation in layer 3 first appears as FDM near the center of the plate. Subsequently, areas of inelastic behavior can be seen to spread out from these initial areas. There are several areas that undergo unloading at one time or another, this shows up as an area of elastic behavior where there was previously FDM or MDM. At a load of 7.0 times the initial yield load layer 4 is almost totally inelastic and approximately one half of layer 3 is inelastic.

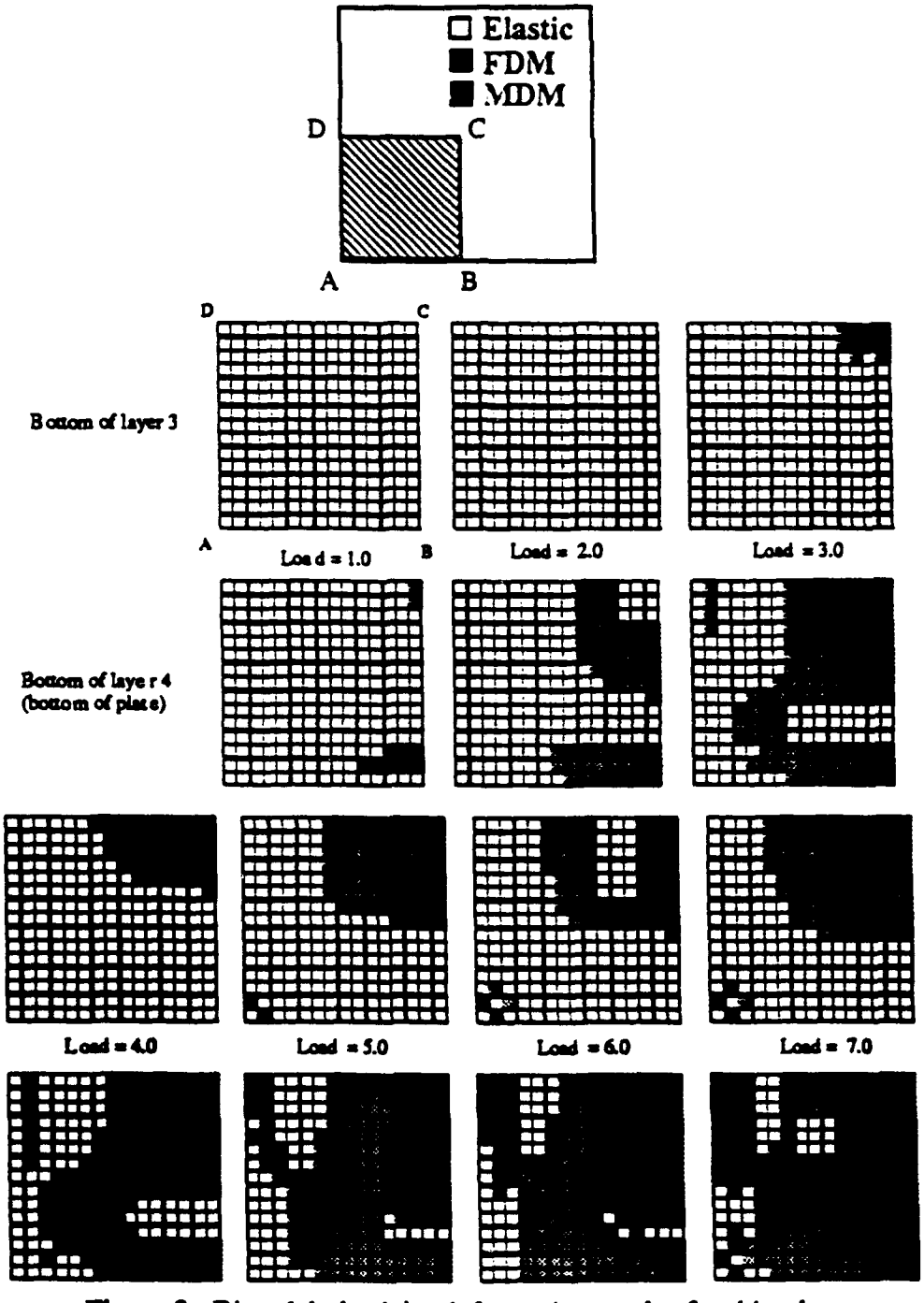

Figure 8. Bimodal plasticity deformation modes for thin plate.

Figure 9 shows the results for the thick plate. For this case the plate resists the load primarily by bending forces around the edge of the plate and near the center. As would be expected the initial inelastic behavior appears in the areas where the stresses causing these bending moments are highest: in layer 4 at the edges and center of the plate. Again in this case the initial deformation mode is FDM. The first appearance of inelastic behavior in layer 3 is at 2.0 times the initial yield load. By 3.4 times the initial yield load almost all of layer 4 and about 35% of layer 3 is behaving inelasticly.

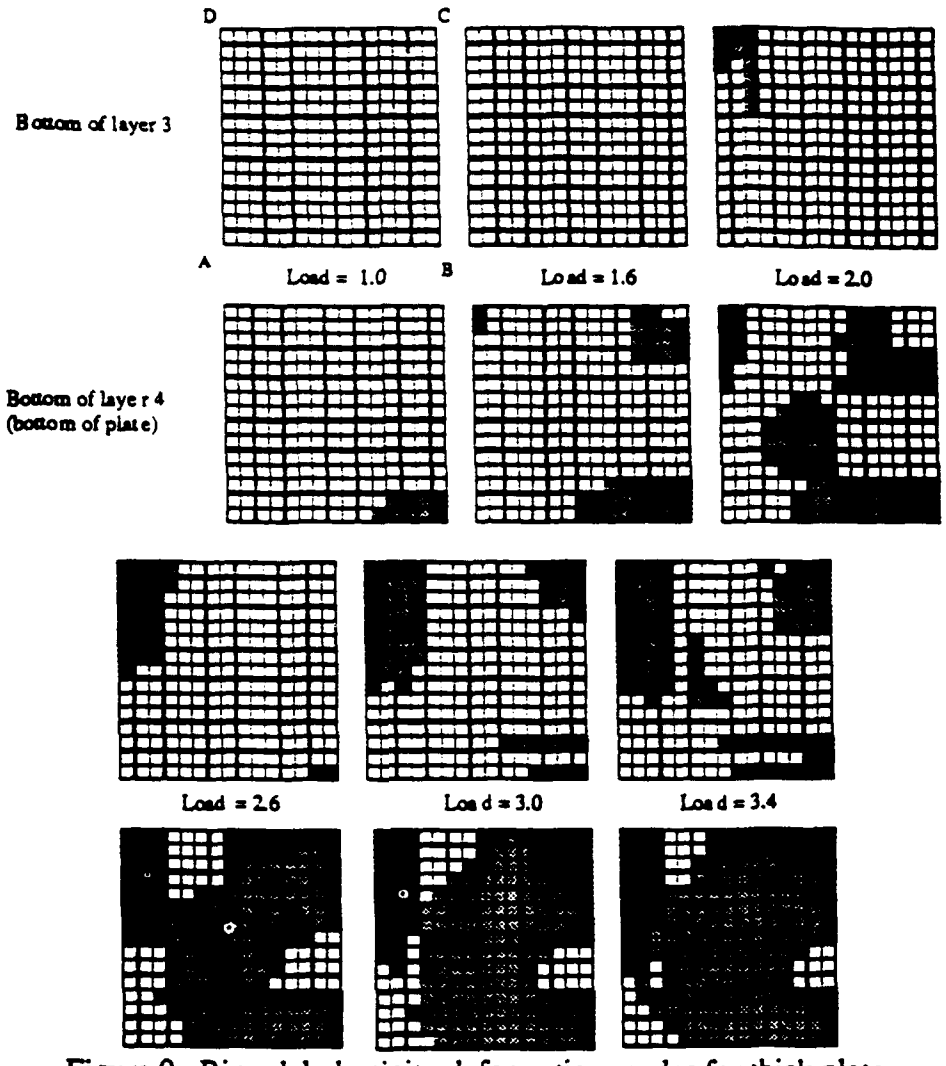

Figure 9. Bimodal plasticity deformation modes for thick plate.

5. CLOSING REMARKS

Reliable modeling of composite structures must take into consideration the idealizations used at each step of the process. Reliable estimates of the error introduced at each step in the idealization process is required to indicate the applicability of a given solution. Some progress has been made by various researchers in developing theories which give an estimate of the error for some types of idealizations for specific linear cases. These techniques must be extended to include nonlinear constituents in order to reliably predict their response characteristics.

This paper indicated the analysis idealizations important for the analysis of composite structures and outlined a system for the control of analysis idealizations in engineering design. Specific results were presented to illustrate some of the effects of idealizations on the analysis of composite laminates.

6. ACKNOWLEDGMENTS

The work on the development of finite element analysis capabilities for composites including nonlinear material mixing models was supported by the Office of Naval Research under grant N000014-85-K-0733, Dr. Yapa Rajapakse, Project Monitor. The work on the development of the analysis idealization control framework is supported by the Affiliates of the Scientific Computation Research Center.

7. REFERENCES

1. Babuska, I., "Adaptive Mathematical Modeling", in *Adaptive Methods for Partial Differential Equations*, P. J. Paslow, J. E. Flaherty, M. S. Shephard and J. D. Vasilakis, eds., p. 1-14, SIAM, 1989.
2. Shephard, M.S., Baehmann, P.L., Georges, M.K. and Korngold, E.V., "Framework for the Reliable Generation and Control of Analysis Idealizations", *Comp. Meth. in Appl. Mech. Eng.*, **82** p. 257-280, 1990.
3. Szabo, B.A., "On Errors of Idealization in Finite Element Analysis of Structural Connections", in *Adaptive Methods for Partial Differential Equations*, P. J. Paslow, J. E. Flaherty, M. S. Shephard and J. D. Vasilakis, eds., p. 15-28, SIAM, 1989.
4. Shephard, M.S., Korngold, E.V. and Wentorf, R., "Design Systems Supporting Engineering Idealizations", in *Geometric Modeling for Product Engineering*, North-Holland, Amsterdam, p. 279-300, 1990.
5. Wentorf, R. and Shephard, M.S., "Automated Analysis Idealization Control", in *CONCURRENT ENGINEERING: Automation, Tools, and Techniques*, John Wiley, New York, 1992.
6. Dixon, J.R., Libardi, E.C. and Nielsen, E.H., "Unresolved Research Issues in Development of Design-With-Features.", in *Geometric Modeling for Product Engineering*, North-Holland, Amsterdam, p. 183-196, 1990.
7. Dvorak, G.J. and Bahei-El-Din, Y.A., "A Bimodal Plasticity Theory of Fibrous Composite Materials", *Acta Mechanica*, **69** p. 219-241, 1987.
8. Teply, J.L. and Dvorak, G.J., "Bounds on the Overall Instantaneous Properties of Elastic-Plastic Composites", *J. Mech. Phys. Solids*, 1988, **36**(1) p. 29-58.
9. Christensen, R.M., *Mechanics of Composite Materials*, John Wiley, New York, 1979
10. Guedes, J.M. and Kikuchi, N., "Preprocessing and Postprocessing for Materials Based on the Homogenization Method with Adaptive Finite Element Methods", *Comp. Meth. in Appl. Mech. Eng.*, **83** p. 143-198, 1990.
11. Dvorak, G.J. and Teply, J.A., "Periodic Hexagonal Array Models for Plasticity of Composite Materials", in *Plasticity Today: Modeling, Methods and Applications*, Elsevier, Amsterdam, p. 623-642, 1985.
12. Noor, A.K. and Burton, W.S., "Assessment of Shear Deformation Theories for Multilayered Composite Plates", *Applied Mechanics Review*, **42**(1) p. 1-13, 1990.
13. Babuska, I. and Li, L., "Hierarchic Modeling of Plates", *Computers & Structures*, **40**(2) p. 419-430, 1991.
14. Babuska, I., Szabo, B. and Actis, R., "Heirarchic Models for Laminated Composites", *Int. J.. Num. Meth. Eng.*, 33 p. 503-535, 1992.

15. Szabo, B.A., "Hierarchic Plate and Shell Models Based on p-Extension", in *Analytical and Computational Models of Shells*, A.K. Noor, T. Belytschko, J. C. Simo, eds., ASME, New York, p. 317-331, 1989.
16. Vogelius, M., "On Mathematical Modeling - Dimensional Reduction", Institute for Physical Science and Technology, University of Maryland, College Park, Maryland, Tech. Note BN-940, 1980.
17. Noor, A.K. and Burton, W.S., "Assessment of Computational Models for Multilayered Composite Shells", *Appl. Mech. Review*, 43 p. 67-97, 1990.
18. Bathe, K.J., Lee, N.S. and Bucalem, M.L., "On the Use of Hierarchical Models in Engineering Analysis", *Comp. Meth. in Appl. Mech. Eng.*, 82 p. 5-26, 1990.
19. Noor, A.K. and Peters, J.M., "A Posteriori Estimates for Shear Correction Factors in Multilayered Composite Cylinders", *J. Eng. Mech.*, 115(6) p. 1225-1244, 1989.
20. Desai, C.S., Wathugala, G.W., Sharma, K.G. and Woo, L., "Factors Affecting Reliability ofComputer Solutions with Hierarchical Single Surface Constitutive Models.", *Comp. Meth. in Appl. Mech. and Eng.*, 82 p. 115-137, 1990.
21. Dvorak, G.J., "Plasticity Theories for Fibrous Composite Materials", in *Metal Matrix Composites, Vol. 2, Mechanisms and Properties*, Academis Press, 1990.
22. Babuska, I., "The Problem of Modeling the Elastomechanics in Engineering", *Comp. Meth. in Appl. Mech. Eng.*, 82 p. 155-182, 1990.
23. Dvorak, G.J., Bahei-El-Din, Y., Macheret, Y. and Liu, C.H., "An Experimental Study of Elastic-Plastic Behavior of a Fibrous Boron-Aluminum Composite", *J. Mech. Phys. Solids*, 36 p. 655-687, 1988.
24. Wu, J.F.,"Numerical Techniques for Elastic-Plastic Analysis of Fibrous Metal Matrix Composites", Ph.D. Thesis, Rensselaer Polytechnic Institute, 1991.
25. Hill, R., "Elastic Properties of Reinforced Solids: Some Theoretical Principles", *J. Mech. Phys. Solids*, 11 p. 357-372, 1963.
26. Mori, T. and Tanaka, K., "Average Stress in Matrix and Average Elastic Energy of Materials with Misfitting Inclusions", *Acta Metallurgica*, 21 p. 571, 1973.
27. Reddy, J.N., "A Generalization of Two-Dimensional Theories of Laminated Composite Plates", *Commum. Appl. Numer. Methods*, 3 p. 113-180, 1987.
28. Barbero, E.J. and Reddy, J.N., "An Accurate Determination of Stresses in Thick Laminates Using a Generalized Plate Theory", *Int. J. Num. Meth. in Eng.*, 29 p. 1-14, 1990.
29. Barbero, E.J. and Reddy, J.N., "Modeling of Delamination in Composite Laminates Using a Layer-wise Plate Theory", *Int. J. Solids Structures*, 28(3) p. 373-388, 1991.
30. Noor, A.K. and Burton, W.S., "Assessment of Computational Models for Multilayered Anisotropic Plates", *Composite Structures*, 14 p. 233-265, 1990.
31. Noor, A.K., Burton, W.S. and Peters, J.M., "Predictor-Corrector Procedures for Stress and Free Vibration Analyses of Multilayered Composite Plates and Shells", *Comp. Meth. in Appl. Mech. Eng.*, 82 p. 341-363, 1990.

Computer Aided Design in Composite Material Technology III

Editors:
S.G. Advani, University of Delaware, U.S.A.
W.R. Blain, Wessex Institute of Technology, U.K.
W.P. de Wilde, Free University of Brussels, Belgium
J.W. Gillespie, Jr., University of Delaware, U.S.A.
O.H. Griffin, Jr., Virginia Polytechnic Institute and State University, U.S.A.

Computational Mechanics Publications
Southampton Boston

Co-published with

Elsevier Applied Science
London New York

Reprinted from:

METAL MATRIX COMPOSITES:
Mechanisms and Properties

Edited by R.K. Everett and R.J. Arsenault

Academic Press, Boston, 1991

Plasticity Theories for Fibrous Composite Materials

GEORGE J. DVORAK

Department of Civil Engineering and
Institute Center for Composite Materials and Structures
Rensselaer Polytechnic Institute
Troy, New York

I Introduction 1
II Elastic Response 2
A Overall Properties and Local Fields 2
B Micromechanical Models 5
C Transformation Strain 11
III Elastic-Plastic Response 17
A Homogeneous Materials 17
B Heterogeneous Materials 23
IV Conclusion 71
Acknowledgments 73
Appendix 74
References 75

I. Introduction

Fabrication, processing, and effective use of metal matrix composites often cause inelastic deformations in the material. In many actual systems, the elastic-strain range of the elastic–plastic matrix is much smaller than the failure strain of the elastic-brittle fiber. Similarly, the temperature changes that may cause yielding in a stress–free composite are often smaller than those encountered in service. However, the total strains seen in fibrous systems are also small, i.e., they seldom exceed the failure strain of the fiber, which is usually found in the range of 0.01–0.02. Therefore, in contrast to metals, plasticity of fibrous composites is usually limited to small strains, but it may affect much of the useful load-bearing capacity of structural parts designed to utilize the high strength of the fibers.

Copyright © 1991 by Academic Press, Inc.
All rights of reproduction in any form reserved.
ISBN 0-12-341833-X

The purpose of this chapter is to give a brief review of the elastic-plastic response of fiber composites and of its implications for the mechanical behavior of these materials. First, we shall discuss some general features of thermoelastic behavior, such as evaluation of overall thermomechanical properties, phase concentration factors, thermal concentration factors, and transformation stress and strain concentration factors. Next, the elastic-plastic behavior of macroscopically homogeneous metals and composites is outlined. This provides a basis for a discussion of the plasticity of fiber composites, which includes a number of new, exact results. Then, some specific micromechanical models for plasticity analysis are described, together with their experimental verification and implementation in finite element programs for structural analysis.

The approach is based on micromechanics of heterogeneous media. The objective is to evaluate overall instantaneous properties of the medium from information about local properties and microstructural geometry and to establish various general connections between local and overall response. The consequences of plasticity in such phenomena as dimensional stability, fatigue, and fracture of fibrous metal matrix laminates are briefly described.

The notation used is similar to that introduced by Hill [1, 2]. Vectors are denoted by lower-case boldface letters, e.g., $\boldsymbol{\sigma}$, $\boldsymbol{\varepsilon}$, $\mathbf{a}$, $\mathbf{b}$; matrices are denoted by upper-case boldface Roman letters, e.g., $\mathbf{L}$, $\mathbf{M}$. In the contracted notation used, those will typically be (6×1) vectors and (6×6) matrices. $\mathbf{L}^{-1}$ denotes the inverse of $\mathbf{L}$, defined if it exists to satisfy $\mathbf{L}\mathbf{L}^{-1} = \mathbf{I} = \mathbf{L}^{-1}\mathbf{L}$, where $\mathbf{I}$ is the unit matrix. Further details of the notation are explained in the Appendix.

II. Elastic Response

4. *Overall Properties and Local Fields*

We start the exposition with an outline of a general procedure for the evaluation of overall thermomechanical properties of two-phase composite media in terms of thermoelastic constants and volume fractions of the phases. The elastic response contributes to the total strain during plastic loading, and it is the sole source of this strain in any elastic unloading step.

Consider a fibrous composite material consisting of two distinct continuous phases of cylindrical shape, which are aligned parallel to the x_1-axis of a Cartesian coordinate system. The phases remain bonded and are free of voids and cracks during deformation. A representative volume V with surface S is chosen so that under certain boundary conditions, it represents the macroscopic response of the composite. Within V, each phase $r = \alpha, \beta$ occupies a volume V_r, and the volume fractions $c_r = V_r/V$ satisfy $c_\alpha + c_\beta = 1$.

The volume V is subjected to certain uniform overall stresses $\bar{\boldsymbol{\sigma}}$ or strains $\bar{\boldsymbol{\varepsilon}}$, and to a uniform temperature change θ. Suppose that the constitutive relations of the phases are known, e.g., from experiments on neat matrix samples and on the fibers, and are written in the form

$$\boldsymbol{\sigma}(\mathbf{x}) = \mathbf{L}_r\boldsymbol{\varepsilon}(\mathbf{x}) + \mathbf{l}_r\theta, \qquad \boldsymbol{\varepsilon}(\mathbf{x}) = \mathbf{M}_r\boldsymbol{\sigma}(\mathbf{x}) - \mathbf{m}_r\theta. \tag{1}$$

where $\mathbf{L}_r$, $\mathbf{M}_r$ are instantaneous stiffness and compliance matrices, which have full diagonal symmetry: $\mathbf{L}_r = \mathbf{L}_r^T$, $\mathbf{M}_r = \mathbf{M}_r^T$; $\mathbf{LM} = \mathbf{I}$; $\mathbf{l}_r$ and $\mathbf{m}_r$ are the thermal stress and strain vectors, such that $\mathbf{l}_r = -\mathbf{L}_r\mathbf{m}_r$. As long as the phase remains elastic, the coefficients of these matrices are constant in V_r. Note that the components of $\mathbf{m}_r$ are the linear coefficients of thermal expansion of the phase, which are not affected by deformation and are assumed to be independent of temperature.

The local fields in (1) are generally not uniform. Therefore, it is often convenient to work with volume averages of the nonuniform fields defined by the integral

$$\{\cdot\}_{V'} = \frac{1}{V'}\int_{V'} (\cdot)\,dV. \tag{2}$$

Phase volume averages of local fields follow from (2) if one takes $V' = V_r$ and integrates both sides in (1),

$$\boldsymbol{\sigma}_r = \mathbf{L}_r\boldsymbol{\varepsilon}_r + \mathbf{l}_r\theta, \qquad \boldsymbol{\varepsilon}_r = \mathbf{M}_r\boldsymbol{\sigma}_r + \mathbf{m}_r\theta. \tag{3}$$

where

$$\boldsymbol{\sigma}_r = \{\boldsymbol{\sigma}(\mathbf{x})\}_{V_r}, \tag{4}$$

$$\boldsymbol{\varepsilon}_r = \{\boldsymbol{\varepsilon}(\mathbf{x})\}_{V_r}. \tag{4'}$$

Since $\mathbf{L}_r$, $\mathbf{M}_r$ are constant in V_r, (3) are exact analogs of (1) for phase volume averages. One can also obtain the overall stresses and strains as averages of the respective local quantities over the representative volume V and write the overall constitutive relations as

$$\bar{\boldsymbol{\sigma}} = \mathbf{L}\bar{\boldsymbol{\varepsilon}} + \mathbf{l}\theta, \qquad \bar{\boldsymbol{\varepsilon}} = \mathbf{M}\bar{\boldsymbol{\sigma}} + \mathbf{m}\theta, \tag{5}$$

where

$$\bar{\boldsymbol{\sigma}} = \{\boldsymbol{\sigma}(\mathbf{x})\}_V, \tag{6}$$

$$\bar{\boldsymbol{\varepsilon}} = \{\boldsymbol{\varepsilon}(\mathbf{x})\}_V. \tag{6'}$$

The implication is that the representative volume V of the composite aggregate is regarded as a macroscopically homogeneous medium and that under uniform overall stress or strain, the $\mathbf{L}$, $\mathbf{M}$ are the elastic overall stiffness and compliance matrices, and $\mathbf{m}$, $\mathbf{l} = -\mathbf{Lm}$ are the overall thermal strain and stress vectors of this composite medium.

To determine $\mathbf{L}$, $\mathbf{M}$, $\mathbf{l}$, and $\mathbf{m}$ of an elastic composite, one can proceed as follows. Suppose that for the composite system considered, one could evaluate the actual local fields (1) and write them in the form

$$\boldsymbol{\sigma}(\mathbf{x}) = \mathbf{B}_r(\mathbf{x})\bar{\boldsymbol{\sigma}} + \mathbf{b}_r(\mathbf{x})\theta, \qquad \boldsymbol{\varepsilon}(\mathbf{x}) = \mathbf{A}_r(\mathbf{x})\bar{\boldsymbol{\varepsilon}} + \mathbf{a}_r(\mathbf{x})\theta. \tag{7}$$

Of course, in many practical situations, one cannot find the actual fields, but it is usually possible to evaluate an estimate of average local fields in the two phases under the prescribed load increment. The result is the integral (2) of (7), taken over V_r,

$$\boldsymbol{\sigma}_r = \mathbf{B}_r\bar{\boldsymbol{\sigma}} + \mathbf{b}_r\theta, \qquad \boldsymbol{\varepsilon}_r = \mathbf{A}_r\bar{\boldsymbol{\varepsilon}} + \mathbf{a}_r\theta. \tag{8}$$

where $\mathbf{A}_r$, $\mathbf{B}_r$, $\mathbf{a}_r$, $\mathbf{b}_r$ are certain mechanical and thermal strain and stress concentration factors. If those are known, one can utilize (2) to write for $r = \alpha, \beta$,

$$\bar{\boldsymbol{\sigma}} = c_\alpha\boldsymbol{\sigma}_\alpha + c_\beta\boldsymbol{\sigma}_\beta, \tag{9}$$

$$\bar{\boldsymbol{\varepsilon}} = c_\alpha\boldsymbol{\varepsilon}_\alpha + c_\beta\boldsymbol{\varepsilon}_\beta. \tag{9'}$$

Then, for $\theta = 0$, equations (3), (8), and (9) give the overall mechanical properties

$$\begin{aligned} \mathbf{L} &= \mathbf{L}_\alpha + c_\beta(\mathbf{L}_\beta - \mathbf{L}_\alpha)\mathbf{A}_\beta, \qquad \mathbf{M} = \mathbf{M}_\alpha + c_\beta(\mathbf{M}_\beta - \mathbf{M}_\alpha)\mathbf{B}_\beta, \\ \mathbf{L} &= c_\alpha\mathbf{L}_\alpha\mathbf{A}_\alpha + c_\beta\mathbf{L}_\beta\mathbf{A}_\beta, \qquad \mathbf{M} = c_\alpha\mathbf{M}_\alpha\mathbf{B}_\alpha + c_\beta\mathbf{M}_\beta\mathbf{B}_\beta, \end{aligned} \tag{10}$$

together with the results

$$c_\alpha\mathbf{A}_\alpha + c_\beta\mathbf{A}_\beta = \mathbf{I}, \qquad c_\alpha\mathbf{B}_\alpha + c_\beta\mathbf{B}_\beta = \mathbf{I},$$

$$\mathbf{A}_r\mathbf{M} = \mathbf{M}_r\mathbf{B}_r, \qquad \mathbf{B}_r\mathbf{L} = \mathbf{L}_r\mathbf{A}_r.$$

This sequence, first outlined by Hill [1, 2], enables evaluation of the overall instantaneous $\mathbf{L}$ and $\mathbf{M}$ in terms of one mechanical concentration factor. The overall thermal strain and stress vectors $\mathbf{m}$ and $\mathbf{l}$ can be evaluated from known overall mechanical moduli and compliances or from local properties and concentration factors [3–7]. Convenient forms are

$$\mathbf{m} = c_\alpha\mathbf{B}_\alpha^T\mathbf{m}_\alpha + c_\beta\mathbf{B}_\beta^T\mathbf{m}_\beta \tag{11}$$

$$= (\mathbf{M} - \mathbf{M}_\beta)(\mathbf{M}_\alpha - \mathbf{M}_\beta)^{-1}\mathbf{m}_\alpha + (\mathbf{M} - \mathbf{M}_\alpha)(\mathbf{M}_\beta - \mathbf{M}_\alpha)^{-1}\mathbf{m}_\beta \tag{11'}$$

$$= c_\alpha(\mathbf{M}_\alpha\mathbf{b}_\alpha + \mathbf{m}_\alpha) + c_\beta(\mathbf{M}_\beta\mathbf{b}_\beta + \mathbf{m}_\beta), \tag{11''}$$

$$\mathbf{l} = c_\alpha\mathbf{A}_\alpha^T\mathbf{l}_\alpha + c_\beta\mathbf{A}_\beta^T\mathbf{l}_\beta \tag{11'''}$$

$$= (\mathbf{L} - \mathbf{L}_\beta)(\mathbf{L}_\alpha - \mathbf{L}_\beta)^{-1}\mathbf{l}_\alpha + (\mathbf{L} - \mathbf{L}_\alpha)(\mathbf{L}_\beta - \mathbf{L}_\alpha)^{-1}\mathbf{l}_\beta \tag{11''}$$

$$= c_\alpha(\mathbf{L}_\alpha\mathbf{a}_\alpha + \mathbf{l}_\alpha) + c_\beta(\mathbf{L}_\beta\mathbf{a}_\beta + \mathbf{l}_\beta). \tag{11'}$$

Using (10), one can establish that the first two forms are equivalent.

In a recent paper, Benveniste and Dvorak [8] had shown that the local thermal fields in the phases can be derived from the mechanical fields. Their result is

$$\begin{aligned} \mathbf{a}_r(\mathbf{x}) &= [\mathbf{I} - \mathbf{A}_r(\mathbf{x})](\mathbf{L}_s - \mathbf{L}_g)^{-1}(\mathbf{l}_g - \mathbf{l}_s), \\ \mathbf{b}_r(\mathbf{x}) &= [\mathbf{I} - \mathbf{B}_r(\mathbf{x})](\mathbf{M}_s - \mathbf{M}_g)^{-1}(\mathbf{m}_g - \mathbf{m}_s). \end{aligned} \tag{12}$$

Of course, since all local and overall properties are assumed to be constant, (12) can be integrated as in (2) to find the thermal concentration factors in terms of the mechanical concentration factors. In each case, these factors are phase volume averages of the fields $\mathbf{A}_r(\mathbf{x})$, $\mathbf{B}_r(\mathbf{x})$, $\mathbf{a}_r(\mathbf{x})$, or $\mathbf{b}_r(\mathbf{x})$ in (7).

B. Micromechanical Models

1. Inclusion Problems

In Section II.A, the averages of local fields and the overall elastic properties have been found in terms of stress or strain concentration factors. These factors can be evaluated in several different ways. First we describe an approach based on the solution of an inclusion problem, which will be useful in some of the micromechanical models discussed in the following.

A single inclusion of ellipsoidal shape is embedded in a large volume of a different homogeneous elastic material. There is a perfect bond between the phases, hence the tractions and displacements must be continuous across the interface. A circular cylindrical fiber is a particular example of such an inclusion. Let $\mathbf{L}'$ and $\mathbf{L}''$ denote the stiffness matrices of the inclusion and the surrounding medium, neither of which need to be isotropic. These matrices have full diagonal symmetry, and their inverses are denoted by $\mathbf{M}'$ and $\mathbf{M}''$, respectively. The surrounding medium is subjected to a uniform stress $\bar{\boldsymbol{\sigma}}$ or strain $\bar{\boldsymbol{\varepsilon}}$ at infinity. The objective is to find the stresses and strains in the inclusion.

Eshelby [9, 10] pointed out that in problems of this kind, the stress and strain fields in the inclusion are also uniform. Therefore, one can write the result in a form analogous to (8) as

$$\begin{aligned} \boldsymbol{\sigma}' &= \mathbf{B}'\bar{\boldsymbol{\sigma}}, \qquad \boldsymbol{\varepsilon}' = \mathbf{A}'\bar{\boldsymbol{\varepsilon}}, \\ \boldsymbol{\sigma}'' &= \mathbf{B}''\bar{\boldsymbol{\sigma}}, \qquad \boldsymbol{\varepsilon}'' = \mathbf{A}''\bar{\boldsymbol{\varepsilon}}, \end{aligned} \tag{13}$$

where $\boldsymbol{\sigma}$ and $\boldsymbol{\varepsilon}$ denote the uniform stresses and strains in the inclusion, and $\boldsymbol{\sigma}''$ and $\boldsymbol{\varepsilon}''$ the averages of the fields in the surrounding medium. Since the inclusion causes only a local perturbation of the overall field, its contribution to the overall averages $\bar{\boldsymbol{\sigma}}$ and $\bar{\boldsymbol{\varepsilon}}$ is vanishingly small, and it follows that $\mathbf{A}'' = \mathbf{B}'' = \mathbf{I}$.

The evaluation of $\mathbf{B}'$ was outlined by Eshelby, and in a more general case by Kinoshita and Mura [11]; a recent survey of pertinent results appears in Mura's monograph [12]. Here we limit our attention to a particularly simple approach to the solution proposed by Hill [2]. The fact that the inclusion fields are uniform suggests that the medium surrounding the inclusion is loaded at the interface by certain surface tractions derived from a uniform stress field. Therefore, it is useful to formulate an auxiliary problem in which the inclusion is removed from the medium, the wall of the ellipsoidal cavity is loaded by certain surface tractions derived from a unit uniform stress field $\boldsymbol{\sigma}^*$, and the remotely applied stresses vanish. Suppose that the unit stress components that generate the surface tractions are applied in a sequential manner and that six such solutions are obtained. For each solution, one can find the displacements of the cavity wall and convert them into strain components $\boldsymbol{\varepsilon}^*$, which represent a uniform strain of the ellipsoidal cavity. The result can thus be written as

$$\boldsymbol{\sigma}^* = -\mathbf{L}^*\boldsymbol{\varepsilon}^*, \qquad \boldsymbol{\varepsilon}^* = -\mathbf{M}^*\boldsymbol{\sigma}^*, \tag{14}$$

where each column of $\mathbf{L}^*$ was generated by one of the six solutions. Both $\mathbf{L}^*$ and $\mathbf{M}^*$ have full diagonal symmetry, and their coefficients depend on the aspect ratios of the ellipsoid and on the moduli $\mathbf{L}''$ of the surrounding medium; they may be regarded as stiffness and compliance matrices of the cavity. In Hill's terminology, $\mathbf{L}^*$ is the overall constraint tensor.

The solution of the inclusion problem then follows from that of the auxiliary problem if one replaces the inclusion in the surrounding medium and writes

$$\boldsymbol{\sigma}' - \bar{\boldsymbol{\sigma}} = -\mathbf{L}^*(\boldsymbol{\varepsilon}' - \bar{\boldsymbol{\varepsilon}}), \qquad \boldsymbol{\varepsilon}' - \bar{\boldsymbol{\varepsilon}} = -\mathbf{M}^*(\boldsymbol{\sigma}' - \bar{\boldsymbol{\sigma}}). \tag{15}$$

Then, from the local constitutive relations and (13),

$$\mathbf{A}' = (\mathbf{L}^* + \mathbf{L}')^{-1}(\mathbf{L}^* + \mathbf{L}''), \qquad \mathbf{B}' = (\mathbf{M}^* + \mathbf{M}')^{-1}(\mathbf{M}^* + \mathbf{M}''). \tag{16}$$

Note that if the local properties $\mathbf{L}'$ and $\mathbf{L}''$ are known, $\mathbf{L}^*$ alone yields the solution. It is advantageous to separate that part of the solution that depends only on $\mathbf{L}''$, or $\mathbf{M}''$ and to write

$$\mathbf{P} = (\mathbf{L}^* + \mathbf{L}'')^{-1}, \qquad \mathbf{Q} = (\mathbf{M}^* + \mathbf{M}'')^{-1}. \tag{17}$$

This suggests that $\mathbf{P} = \mathbf{P}^T$, $\mathbf{Q} = \mathbf{Q}^T$. One can also establish that $\mathbf{P}\mathbf{L}'' + \mathbf{M}''\mathbf{Q} = \mathbf{I}$.

The forms of $\mathbf{P}$ that correspond to different ellipsoidal shapes in various anisotropic materials can be found in the literature [11–15]. Of particular interest here is the result for an inclusion in the shape of a circular cylinder and for the surrounding medium, which is transversely isotropic about x_1.

the cylinder axis. This result can be recorded as follows:

$$P_{22} = P_{33} = \frac{k'' + 4m''}{8m''(k'' + m'')}, \qquad P_{23} = P_{32} = \frac{-k''}{8m''(k'' + m'')},$$
$$P_{44} = P_{55} = \frac{1}{2p''}, \qquad P_{66} = \frac{k'' + 2m''}{2m''(k'' + m'')}, \tag{18}$$

where k'', m'', and p'' are Hill's [16] elastic moduli of the surrounding transversely isotropic medium, which belong to $\mathbf{L}''$ and are defined in the Appendix. The remaining P_{ij} vanish.

2. The Self-Consistent Method

So far, we have considered only the problem of a single inclusion, embedded in an elastic medium, as a stepping stone to the more important problem of finding the stresses in the constituents of a composite medium. The latter problem can be solved in several different ways. One approach is based on the self-consistent approximation [2, 17–19], which assumes that the stress and strain field averages in the fiber are equal to those found in the inclusion problem above, provided that the fiber is embedded in a homogeneous medium that has the properties of the composite. In the notation of Section II.B.1, the $\mathbf{L}''$, $\mathbf{M}''$ are identified with the overall properties $\mathbf{L}$ and $\mathbf{M}$, and the $\mathbf{L}'$ and $\mathbf{M}'$ with the fiber properties, which we denote here by $\mathbf{L}_\alpha$, and $\mathbf{M}_\alpha$. The matrix properties are denoted by $\mathbf{L}_\beta$, $\mathbf{M}_\beta$.

Rewrite (9) in the form

$$c_\alpha(\boldsymbol{\sigma}_\alpha - \bar{\boldsymbol{\sigma}}) + c_\beta(\boldsymbol{\sigma}_\beta - \bar{\boldsymbol{\sigma}}) = \mathbf{0}, \qquad c_\alpha(\boldsymbol{\varepsilon}_\alpha - \bar{\boldsymbol{\varepsilon}}) + c_\beta(\boldsymbol{\varepsilon}_\beta - \bar{\boldsymbol{\varepsilon}}) = \mathbf{0}. \tag{19}$$

The above postulate of the self-consistent method and (15), (19) suggest that

$$(\boldsymbol{\sigma}_\alpha - \bar{\boldsymbol{\sigma}}) = -\mathbf{L}^*(\boldsymbol{\varepsilon}_\alpha - \bar{\boldsymbol{\varepsilon}}), \qquad (\boldsymbol{\sigma}_\beta - \bar{\boldsymbol{\sigma}}) = -\mathbf{L}^*(\boldsymbol{\varepsilon}_\beta - \bar{\boldsymbol{\varepsilon}}). \tag{20}$$

It is now apparent that both phases are regarded on the same footing, i.e., the concentration factor for the matrix phase is derived from the same $\mathbf{L}^*$ as the concentration factor of the fiber. The expressions follow from (16) and (17),

$$\mathbf{A}_r^{-1} = \mathbf{I} + \mathbf{P}(\mathbf{L}_r - \mathbf{L}), \qquad \mathbf{B}_r^{-1} = \mathbf{I} + \mathbf{Q}(\mathbf{M}_r - \mathbf{M}), \tag{21}$$

where $\mathbf{P}$ is given by (18) provided that the moduli k'', m'', p'' are replaced by the unknown overall moduli k, m, and p. Since the coefficients in (18) were derived for a transversely isotropic medium, the substitution of this particular form into (21) is permissible only if the fibrous composite itself conforms to the usual assumption of overall transverse isotropy.

Equations (21) and (10) yield estimates of overall moduli of the composite.

$$\mathbf{L} = \mathbf{L}_\alpha + c_\beta(\mathbf{L}_\beta - \mathbf{L}_\alpha)[\mathbf{I} + \mathbf{P}(\mathbf{L}_\beta - \mathbf{L})]^{-1},$$
$$\mathbf{M} = \mathbf{M}_\alpha + c_\beta(\mathbf{M}_\beta - \mathbf{M}_\alpha)[\mathbf{I} + \mathbf{Q}(\mathbf{M}_\beta - \mathbf{M})]^{-1}. \tag{22}$$

Self-consistency of the result can be established by showing that $\mathbf{L}^{-1} = \mathbf{M}$. Note, however, that (22) is a system of six implicit algebraic equations for the overall moduli. For fibrous composites that are transversely isotropic and are made of two transversely isotropic phases, Hill [19] derived a different set of equations for evaluations of the self-consistent estimates of the overall moduli, which yield the same results as (22):

$$\frac{c_\alpha k_\alpha}{k_\alpha - m} - \frac{c_\beta k_\beta}{k_\beta - m} = 2\left[\frac{c_\alpha m_\beta}{m_\beta - m} - \frac{c_\beta m_\alpha}{m_\alpha - m}\right],$$
$$\frac{1}{2p} = \frac{c_\alpha}{p - p_\beta} + \frac{c_\beta}{p - p_\alpha}, \tag{23}$$
$$\frac{1}{k - m} = \frac{c_\alpha}{k_\alpha - m} + \frac{c_\beta}{k_\beta - m}.$$

In addition, Hill [16] shows that regardless of the method used to obtain their estimates, only three of the five overall moduli of such composites are actually independent. The moduli, k, l, and n are related by so-called universal connections,

$$\frac{k - k_\alpha}{l - l_\alpha} = \frac{k - k_\beta}{l - l_\beta} = \frac{l - c_\alpha l_\alpha - c_\beta l_\beta}{n - c_\alpha n_\alpha - c_\beta n_\beta} = \frac{k_\alpha - k_\beta}{l_\alpha - l_\beta}, \tag{24}$$

between overall and phase moduli and volume fractions. Therefore, only one of the three moduli is independent. Relations (23) reflect this; they provide a cubic equation for m, and quadratic equations for p and k, the latter in terms of m. Once k is known, l and n follow from (24). If one or both phases are isotropic, then there are only two independent moduli in each such phase, and k_r, l_r, n_r, m_r, and p_r can be written in terms of the engineering phase moduli, as shown in the Appendix. Hill also gives a proof that the estimates (23) lie between rigorous bounds on the moduli, discussed below.

3. The Mori–Tanaka Method

Another and somewhat simpler approach to the evaluation of phase concentration factors of composite media was proposed by Mori and Tanaka [20] and restated recently in a more tractable form by Benveniste [21]. In a binary, matrix-based composite system, the method assumes that the stress or strain in the inclusion can be evaluated from a solution of the problem in Section II.B.1, provided that $\mathbf{L}_\alpha$ is identified with the inclusion stiffness

$\mathbf{L}'$, $\mathbf{L}''$ with the matrix stiffness $\mathbf{L}_\beta$, and the matrix average stress $\boldsymbol{\sigma}_\beta$ is applied in place of $\bar{\boldsymbol{\sigma}}$ at infinity.

This suggests that one must first find the partial concentration factors

$$\boldsymbol{\varepsilon}_r = \mathbf{T}\boldsymbol{\varepsilon}_\beta, \qquad \boldsymbol{\sigma}_r = \mathbf{W}\boldsymbol{\sigma}_\beta, \tag{25}$$

which follow from (16) as

$$\mathbf{T} = (\mathbf{L}^* - \mathbf{L}_r)^{-1}(\mathbf{L}^* + \mathbf{L}_\beta), \qquad \mathbf{W} = (\mathbf{M}^* + \mathbf{M}_r)^{-1}(\mathbf{M}^* + \mathbf{M}_\beta), \tag{26}$$

where the $\mathbf{L}^*$ and $\mathbf{M}^*$ are now functions of the coefficients $\mathbf{L}_\beta$ and $\mathbf{M}_\beta$ and are derived from (17). $\mathbf{P}$ is again found from (18) if the moduli k', m', p' are replaced by k_β, m_β, p_β, respectively.

Once $\mathbf{T}$ and $\mathbf{W}$ are known, one can utilize (9) and (25) to establish that

$$\boldsymbol{\sigma}_\beta = [c_r\mathbf{W} - c_\beta\mathbf{I}]^{-1}\bar{\boldsymbol{\sigma}}, \qquad \boldsymbol{\varepsilon}_\beta = [c_r\mathbf{T} - c_\beta\mathbf{I}]^{-1}\bar{\boldsymbol{\varepsilon}}. \tag{27}$$

Finally, using (10), the overall properties can be obtained in the form

$$\begin{aligned} \mathbf{L} &= \mathbf{L}_r - c_\beta(\mathbf{L}_\beta - \mathbf{L}_r)[c_r\mathbf{T} - c_\beta\mathbf{I}]^{-1}, \\ \mathbf{M} &= \mathbf{M}_r - c_\beta(\mathbf{M}_\beta - \mathbf{M}_r)[c_r\mathbf{W} - c_\beta\mathbf{I}]^{-1}. \end{aligned} \tag{28}$$

Note that in contrast to (22), these are explicit algebraic equations for the overall properties. Proofs of self-consistency $\mathbf{LM} = \mathbf{I}$ and full diagonal symmetry of $\mathbf{L}$, $\mathbf{M}$ for binary fibrous media are available; also, the estimates (28) lie within rigorous bounds on overall moduli [21–23].[1]

As yet unpublished results of Chen and Dvorak [24] give explicit expressions of the Mori–Tanaka estimates of the overall moduli for a transversely isotropic fibrous medium made of transversely isotropic phases. With $r = \alpha$ representing the fiber, and $r = \beta$ the matrix, these expressions are

$$\begin{aligned} k &= \frac{k_\alpha k_\beta + m_\beta(c_\alpha k_\alpha + c_\beta k_\beta)}{c_\alpha k_\beta + c_\beta k_\alpha + m_\beta}, \\ l &= \frac{c_\alpha l_\alpha(k_\beta + m_\beta) + c_\beta l_\beta(k_\alpha + m_\beta)}{c_\alpha(k_\beta + m_\beta) + c_\beta(k_\alpha + m_\beta)}, \\ n &= c_\alpha n_\alpha + c_\beta n_\beta + (l - c_\alpha l_\alpha - c_\beta l_\beta)\frac{l_\alpha - l_\beta}{k_\alpha - k_\beta}, \\ m &= \frac{m_\alpha m_\beta(k_\beta + 2m_\beta) + k_\beta m_\beta(c_\alpha m_\alpha + c_\beta m_\beta)}{k_\beta m_\beta + (k_\beta + 2m_\beta)(c_\alpha m_\beta + c_\beta m_\alpha)}, \\ p &= \frac{2c_\alpha p_\alpha p_\beta + c_\beta(p_\alpha p_\beta + p_\beta^2)}{2c_\alpha p_\beta + c_\beta(p_\alpha + p_\beta)}. \end{aligned} \tag{29}$$

[1] See also a more recent paper by Benveniste *et al.* [103].

These are analogous to (23) and also satisfy the universal connections (24). Again, if needed, the expressions in the Appendix may be used to evaluate the phase moduli of isotropic phases in terms of engineering elastic constants.

4 Bounds on Overall Moduli

The methods discussed in the previous two sections lead to simple estimates of local fields and overall properties, but they are heuristic in nature and thus do not provide an assurance of accuracy of the results. The legitimacy of the self-consistent, Mori–Tanaka, and similar estimates is derived from proofs that show that, in certain cases of practical interest, the estimates are bracketed by rigorous bounds on overall moduli. A simple illustration of the bounding procedure is the derivation of the Voigt and Reuss bounds [1]. The Voigt assumption is that the strain field in the entire representative volume V is uniform, i.e., $\mathbf{A}_r = \mathbf{I}$ in (8). If this field is derived from continuous displacements that coincide with the prescribed surface displacements on S, it is a kinematically admissible field, and the principle of minimum potential energy then gives the inequality $\bar{\boldsymbol{\varepsilon}}\mathbf{L}\bar{\boldsymbol{\varepsilon}} < \bar{\boldsymbol{\varepsilon}}(c_\alpha\mathbf{L}_\alpha - c_\beta\mathbf{L}_\beta)\bar{\boldsymbol{\varepsilon}}$, where the first term is the potential energy of the actual state, and the second term is the energy of the admissible state. There follows an upper bound on $\mathbf{L}$,

$$\mathbf{L} < \mathbf{L}_V = c_\alpha\mathbf{L}_\alpha + c_\beta\mathbf{L}_\beta, \tag{30}$$

where $\mathbf{L}_V$ is the Voigt estimate of the overall stiffness.

The dual assumption, introduced by Reuss, is that the stress field in V is uniform, i.e., $\mathbf{B}_r = \mathbf{I}$ in (8). The overall field that is in equilibrium with the surface tractions is a statically admissible field, and the principle of minimum complementary energy leads to the inequality that gives an upper bound on $\mathbf{M}$,

$$\mathbf{M} < \mathbf{M}_R = c_\alpha\mathbf{M}_\alpha + c_\beta\mathbf{M}_\beta. \tag{31}$$

Each of the principles actually gives dual bounds that can be summarized as

$$\mathbf{L}_R < \mathbf{L} < \mathbf{L}_V, \qquad \mathbf{M}_R > \mathbf{M} > \mathbf{M}_V. \tag{32}$$

Of course, the Voigt and Reuss bounds are insensitive to microstructural geometry and thus not particularly sharp. More restrictive bounds, which reflect essential features of the geometry, were originally derived by Hashin and Shtrikman [*25–28*], and for fibrous composites by Hashin and Rosen [*29*]. Alternative derivations were given by Hill [*16, 30*], Walpole [*31, 32*], Willis [*33, 34*], and Milton and Kohn [*35*]; they also appeared in Christensen's monograph [*36*] and in several reviews [*34, 37–39*]. The procedure again relies on the elastic extremum principles and on certain polarization stress and

strain fields that are estimated from solutions of inclusion problems in a homogeneous comparison material of stiffness $\mathbf{L}_0$, compliance $\mathbf{M}_0 = \mathbf{L}_0^{-1}$, from which follow the constraint tensors $\mathbf{L}_0^*$, $\mathbf{M}_0^*$ in (14–17). Walpole [*31, 32, 37*] gives a particularly simple form of the bounds:

$$\begin{aligned} [\textstyle\sum c_r(\mathbf{L}_r - \mathbf{L}_0^*)^{-1}]^{-1} - \mathbf{L}_0^* > \mathbf{L} \quad &\text{if} \quad \mathbf{L}_0 > \mathbf{L}_r. \\ [\textstyle\sum c_r(\mathbf{M}_r - \mathbf{M}_0^*)^{-1}]^{-1} - \mathbf{M}_0^* > \mathbf{M} \quad &\text{if} \quad \mathbf{M}_0 > \mathbf{M}_r. \end{aligned} \tag{33}$$

where $\mathbf{L}_r$ and $\mathbf{M}_r$ can be assembled from the appropriate terms of either $\mathbf{L}_r$ or $\mathbf{M}_r$.

C. *Transformation Strain*

1 Uniform Strain Fields in Fibrous Media

Local and overall deformation in elastic composite media can be caused either by mechanical loads or by transformation strains in the phases. Thermal changes and phase transformations are the most common sources of such strains; however, both local and overall plastic strains also can be regarded as transformation strains.

Problems of this kind are best analyzed with the help of uniform fields in fibrous composite media, which were recently discovered by Dvorak [*7, 40*]. To introduce the subject, we rewrite (3) in the more general form

$$\boldsymbol{\varepsilon}_r(\mathbf{x}) = \mathbf{M}_r\boldsymbol{\sigma}_r(\mathbf{x}) + \boldsymbol{\mu}_r. \tag{34}$$

$$\boldsymbol{\sigma}_r(\mathbf{x}) = \mathbf{L}_r\boldsymbol{\varepsilon}_r(\mathbf{x}) + \boldsymbol{\lambda}_r. \tag{34'}$$

where $\boldsymbol{\mu}_r$ denotes uniform transformation strains in the phases, which would be the only strains present if the phases were free to deform without mutual constraints, and $\boldsymbol{\lambda}_r = -\mathbf{L}_r\boldsymbol{\mu}_r$. The corresponding form of the overall relation (5) is

$$\bar{\boldsymbol{\varepsilon}} = \mathbf{M}\bar{\boldsymbol{\sigma}} + \boldsymbol{\mu}, \tag{35}$$

$$\bar{\boldsymbol{\sigma}} = \mathbf{L}\bar{\boldsymbol{\varepsilon}} + \boldsymbol{\lambda}, \tag{35'}$$

where $\bar{\boldsymbol{\sigma}}$, $\bar{\boldsymbol{\varepsilon}}$, $\boldsymbol{\lambda}$, and $\boldsymbol{\mu}$ are the overall volume averages of stress and strain, $\mathbf{L}$ and $\mathbf{M}$ are the tensors of elastic moduli and compliances, and $\boldsymbol{\lambda} = -\mathbf{L}\boldsymbol{\mu}$. Note that if the medium were unloaded in an elastic manner, then $\boldsymbol{\mu}$ would be the remaining overall strain caused by the eigenstrains $\boldsymbol{\mu}_r$; $\boldsymbol{\lambda}$ is the overall stress caused by $\boldsymbol{\mu}_r$ in a fully constrained medium.

In the presence of both mechanical overall stress or strain, and uniform

phase eigenstrains, the local fields in the phases can be written as

$$\begin{aligned}\boldsymbol{\varepsilon}_r(\mathbf{x}) &= \mathbf{A}_r(\mathbf{x})\bar{\boldsymbol{\varepsilon}} + \mathbf{D}_{r\alpha}(\mathbf{x})\boldsymbol{\mu}_\alpha + \mathbf{D}_{r\beta}(\mathbf{x})\boldsymbol{\mu}_\beta,\\ \boldsymbol{\sigma}_r(\mathbf{x}) &= \mathbf{B}_r(\mathbf{x})\bar{\boldsymbol{\sigma}} + \mathbf{F}_{r\alpha}(\mathbf{x})\boldsymbol{\lambda}_\alpha + \mathbf{F}_{r\beta}(\mathbf{x})\boldsymbol{\lambda}_\beta.\end{aligned} \tag{36}$$

where $\mathbf{D}_{r\alpha}(\mathbf{x})$ and $\mathbf{D}_{r\beta}(\mathbf{x})$ are the strain fields caused in the phases by unit phase transformation strains while the representative volume V of the aggregate is under zero overall strain. Similarly, $\mathbf{F}_{r\alpha}(\mathbf{x})$ and $\mathbf{F}_{r\beta}(\mathbf{x})$ are stress fields in the respective phases due to unit phase transformation stresses $\boldsymbol{\lambda}_r$ in V when the overall stress is zero.

With these definitions, we pose the following problem: For a fibrous two-phase composite medium that is subjected to uniform transformation strains $\boldsymbol{\mu}_r$ in the phases, find an overall stress $\hat{\boldsymbol{\sigma}}$ such that the superposed local strains are uniform in the entire volume V and equal to the overall strain $\hat{\boldsymbol{\varepsilon}}$.

$$\hat{\boldsymbol{\varepsilon}}_\alpha(\mathbf{x}) = \hat{\boldsymbol{\varepsilon}}_\beta(\mathbf{x}) = \hat{\boldsymbol{\varepsilon}}. \tag{37}$$

The problem can be solved with the following decomposition procedure. The phases are separated and subjected to the respective transformation strains and to as yet unknown surface tractions that cause only uniform stresses $\hat{\boldsymbol{\sigma}}_r$ in the separated phases. Before reassembly, the tractions must be in equilibrium at the cylindrical interfaces such that the auxiliary phase and overall stresses satisfy the conditions

$$\begin{aligned}&\hat{\sigma}_1^\alpha \neq \hat{\sigma}_1^\beta \qquad && \hat{\sigma}_j^\alpha = \hat{\sigma}_j^\beta \quad \text{for} \quad j = 2, 3, \ldots 6,\\ &\hat{\sigma}_1 = c_\alpha\hat{\sigma}_1^\alpha + c_\beta\hat{\sigma}_1^\beta \qquad && \hat{\sigma}_j = \hat{\sigma}_j^\alpha = \hat{\sigma}_j^\beta \quad \text{for} \quad j = 2, 3, \ldots 6\end{aligned} \tag{38}$$

in the usual contracted notation. This means that the axial normal stress may be piecewise uniform in V, whereas all other stress components are uniform in V.

The components of the unknown overall stress then follow from (34_1), (37), and the above equilibrium conditions.

$$M_{i1}^\alpha\hat{\sigma}_1^\alpha - M_{i1}^\beta\hat{\sigma}_1^\beta + \sum_{j=2}^{6}(M_{ij}^\alpha - M_{ij}^\beta)\hat{\sigma}_j + \mu_i^\alpha - \mu_i^\beta = 0; \quad i = 1, 2, \ldots 6. \tag{39}$$

There are seven unknown stresses in this system of six equations; if a solution is found, it guarantees the existence of a uniform strain in the aggregate under $\boldsymbol{\mu}_r$ and $\hat{\boldsymbol{\sigma}}$. In general, even the homogeneous set associated with (39) has a solution that gives a proportional overall stress path that creates a uniform field in the medium when $\boldsymbol{\mu}_r = \mathbf{0}$.

Whereas the solution of (39) may be obtained for any material symmetry of the phases, we restrict our attention to systems in which both phases are transversely isotropic about x_1. Of course, one or both phases may be

isotropic if the elastic moduli of the phases are defined as indicated in the Appendix. In any case, the phases and the aggregate share the same transverse plane of symmetry, the x_2x_3-plane. This is the only symmetry condition that must be satisfied on the macroscale; in single-crystal elasticity, it is associated with monoclinic crystals. For this system, the solution of (39) was obtained by Dvorak [40]; here, we only summarize the results in the following form.

$$\dot{\sigma} = \dot{\sigma}_0 - \dot{\sigma}_u, \qquad \dot{\sigma}_r = \dot{\sigma}_r^0 - \dot{\sigma}_r^u, \qquad \dot{\varepsilon} = \dot{\varepsilon}_0 - \dot{\varepsilon}_u, \tag{40}$$

such that for $\mu_r = 0$,

$$\dot{\sigma}_u = \dot{\sigma}_r^u = 0, \qquad \dot{\varepsilon}_u = 0. \tag{41}$$

The homogeneous solution is

$$\dot{\sigma}_0 = \mathbf{f}_0 S_T, \qquad \dot{\sigma}_r^0 = \mathbf{f}_r^0 S_T, \qquad \dot{\varepsilon}_0 = \mathbf{d}_0 S_T, \tag{42}$$

where $S_T = (\dot{\sigma}_2 - \dot{\sigma}_3)/2$ is selected as a free parameter in the solution. The coefficients of the above vectors are obtained in terms of Hill's moduli of transversely isotropic solids defined in the Appendix. Also, the following additional symbols are used:

$$\Delta k = k_\alpha - k_\beta, \qquad m^* = m_\alpha m_\beta/(m_\beta - m_\alpha); \quad m_\alpha \neq m_\beta,$$

$$\Delta l = l_\alpha - l_\beta, \qquad p^* = p_\alpha p_\beta/(p_\beta - p_\alpha); \quad p_\alpha \neq p_\beta,$$

$$q^{-1} = (l_\alpha k_\beta - k_\alpha l_\beta) = 2k_\alpha k_\beta(v_L^\alpha - v_L^\beta) \neq 0.$$

Then, the nonvanishing coefficients of $\mathbf{f}_0$, $\mathbf{f}_r^0$, and $\mathbf{d}_0$ are

$$\begin{aligned} f_1^0 &= q[c_\alpha(l_\alpha\Delta l - n_\alpha\Delta k) + c_\beta(l_\beta\Delta l - n_\beta\Delta k)], \qquad f_2^0 = f_3^0 = 1, \\ (f_r^0)_1 &= q(l_r\Delta l - n_r\Delta k), \qquad (f_r^0)_2 = (f_r^0)_3 = 1, \\ d_1^0 &= -q\Delta k, \qquad d_2^0 = d_3^0 = q\Delta l/2. \end{aligned} \tag{43}$$

The terms $\dot{\sigma}_u$, $\dot{\sigma}_r^u$, and $\dot{\varepsilon}_u$ in (40) can be expressed in the form

$$\dot{\varepsilon}_u = \mathbf{K}_\alpha\mu_\alpha + \mathbf{K}_\beta\mu_\beta = -\mathbf{K}_\alpha\mathbf{M}_\alpha\lambda_\alpha - \mathbf{K}_\beta\mathbf{M}_\beta\lambda_\beta, \tag{44}$$

$$\dot{\sigma}_u = \mathbf{N}_\alpha\mu_\alpha + \mathbf{N}_\beta\mu_\beta = -\mathbf{N}_\alpha\mathbf{M}_\alpha\lambda_\alpha - \mathbf{N}_\beta\mathbf{M}_\beta\lambda_\beta, \tag{45}$$

$$\dot{\sigma}_r^u = \mathbf{N}_{r\alpha}\mu_\alpha + \mathbf{N}_{r\beta}\mu_\beta = -\mathbf{N}_{r\alpha}\mathbf{M}_\alpha\lambda_\alpha - \mathbf{N}_{r\beta}\mathbf{M}_\beta\lambda_\beta, \tag{46}$$

where the nonvanishing coefficients of $\mathbf{K}_r$, $\mathbf{N}_r$, $\mathbf{N}_{r\alpha}$, $\mathbf{N}_{r\beta}$ are

$$\begin{aligned} &K_{11}^\alpha = ql_\alpha k_\beta, && K_{12}^\alpha = K_{13}^\alpha = qk_\alpha k_\beta, && K_{21}^\alpha = -ql_\alpha l_\beta/2, \\ &K_{22}^\alpha = -m^*/2m_\beta - qk_\alpha l_\beta/2, && && K_{23}^\alpha = m^*/2m_\beta - qk_\alpha l_\beta/2, \\ &K_{31}^\alpha = K_{21}^\alpha, && K_{32}^\alpha = K_{23}^\alpha, && K_{33}^\alpha = K_{22}^\alpha, \\ &K_{44}^\alpha = -m^* m_\beta, && K_{55}^\alpha = -p^* p_\beta, && K_{66}^\alpha = K_{55}^\alpha, \end{aligned}$$

and

$$N^{\alpha}_{11} = q(c_\alpha k_\alpha l_\beta E^{\alpha}_L + c_\beta k_\beta l_\alpha E^{\beta}_L),$$
$$N^{\alpha}_{12} = N^{\alpha}_{13} = qk_\alpha k_\beta (c_\alpha E^{\alpha}_L + c_\beta E^{\beta}_L),$$
$$N^{\alpha}_{ij} = N^{\alpha}_{ji} \quad \text{for} \quad i \neq 1.$$

together with

$$N^{\alpha\beta}_{11} = qk_\rho E^{\rho}_L l_\rho, \quad (\rho = \alpha \text{ if } r = \beta; \quad \rho = \beta \text{ if } r = \alpha),$$
$$N^{\alpha\beta}_{12} = N^{\alpha\beta}_{13} = qk_\rho E^{\rho}_L k_\rho, \qquad N^{\alpha\beta}_{22} = -N^{\alpha\beta}_{23} = -m^*,$$
$$N^{\alpha\beta}_{32} = -N^{\alpha\beta}_{33} = -N^{\alpha\beta}_{44} = m^*, \qquad N^{\alpha\beta}_{55} = N^{\alpha\beta}_{66} = -p^*.$$

In addition, one can establish that

$$\mathbf{K}_\alpha - \mathbf{K}_\beta = \mathbf{I}. \tag{47}$$

$$\mathbf{N}_\alpha - \mathbf{N}_\beta = \mathbf{0}. \qquad \mathbf{N}_{r\alpha} - \mathbf{N}_{r\beta} = \mathbf{0}. \tag{48}$$

$$\mathbf{N}_r = c_\alpha \mathbf{N}_{r\alpha} - c_\beta \mathbf{N}_{r\beta}. \tag{49}$$

A similar solution could be obtained for other material symmetries of the phases; of course, the coefficients in the matrices in (43) to (49) would change. This is also true for the case of $q^{-1} = 0$.

2. Local and Overall Effects

The existence of the uniform fields opens the way for the derivation of local fields caused by the uniform phase eigenstrains, and of the overall stress λ and strain μ in (35). Consider a two-phase fibrous system that is initially stress free and introduce uniform eigenstrains into the phases. Apply overall auxiliary stress or strain that makes the strain field uniform in V. With reference to (40), disregard the homogeneous solution and use only the overall stress $\hat{\boldsymbol{\sigma}}_\mu$ or strain $\hat{\boldsymbol{\varepsilon}}_\mu$ in this loading step. Finally, reduce the overall strain or stress to zero.

In terms of the overall quantities, this sequence can be recorded as

$$\begin{aligned} \hat{\boldsymbol{\varepsilon}}_\mu - \mathbf{M}\hat{\boldsymbol{\sigma}}_\mu &= \boldsymbol{\mu}, \\ \hat{\boldsymbol{\sigma}}_\mu - \mathbf{L}\hat{\boldsymbol{\varepsilon}}_\mu &= \boldsymbol{\lambda}, \end{aligned} \tag{50}$$

and in local terms as

$$\begin{aligned} \boldsymbol{\varepsilon}_r(\mathbf{x}) &= \hat{\boldsymbol{\varepsilon}}^{\mu}_r - \mathbf{A}_r(\mathbf{x})\hat{\boldsymbol{\varepsilon}}_\mu = (\mathbf{I} - \mathbf{A}_r(\mathbf{x}))\hat{\boldsymbol{\varepsilon}}_\mu, \\ \boldsymbol{\sigma}_r(\mathbf{x}) &= \hat{\boldsymbol{\sigma}}^{\mu}_r - \mathbf{B}_r(\mathbf{x})\hat{\boldsymbol{\sigma}}_\mu, \end{aligned} \tag{51}$$

with reference to (37).

Next, substitute into (50) for the auxiliary quantities from (44) to (46) and recover the following explicit forms of (35), with the overall μ and λ being expressed in terms of local and overall moduli and the phase eigenstrains.

$$\boldsymbol{\varepsilon} = \mathbf{M}\boldsymbol{\sigma} + (\mathbf{K}_\alpha - \mathbf{M}\mathbf{N}_\alpha)\boldsymbol{\mu}_\alpha + (\mathbf{K}_\beta - \mathbf{M}\mathbf{N}_\beta)\boldsymbol{\mu}_\beta. \tag{52}$$

$$\boldsymbol{\sigma} = \mathbf{L}\boldsymbol{\varepsilon} - (\mathbf{L}\mathbf{K}_\alpha - \mathbf{N}_\alpha)\boldsymbol{\mu}_\alpha - (\mathbf{L}\mathbf{K}_\beta - \mathbf{N}_\beta)\boldsymbol{\mu}_\beta. \tag{52'}$$

Recall that (11) presented an analogous result, albeit for thermal phase strains. This can be generalized in a self-evident way to the case of general eigenstrains if $\mathbf{m}\theta$ and $\mathbf{m}_r\theta$ in (11) are replaced by $\boldsymbol{\mu}$ and $\boldsymbol{\mu}_r$, and $\mathbf{l}\theta$ and $\mathbf{l}_r\theta$ by λ and λ_r. Then, compare the result with (52) and extract the following expressions for the mechanical phase concentration factors:

$$\begin{aligned}
c_\alpha \mathbf{B}_\alpha^T &= \mathbf{K}_\alpha - \mathbf{M}\mathbf{N}_\alpha = \mathbf{I} - \mathbf{K}_\beta + \mathbf{M}\mathbf{N}_\beta, \\
c_\beta \mathbf{B}_\beta^T &= \mathbf{K}_\beta - \mathbf{M}\mathbf{N}_\beta = \mathbf{I} - \mathbf{K}_\alpha + \mathbf{M}\mathbf{N}_\alpha, \\
c_\alpha \mathbf{A}_\alpha^T &= (\mathbf{L}\mathbf{K}_\alpha - \mathbf{N}_\alpha)\mathbf{M}_\alpha = \mathbf{I} - (\mathbf{L}\mathbf{K}_\beta - \mathbf{N}_\beta)\mathbf{M}_\beta, \\
c_\beta \mathbf{A}_\beta^T &= (\mathbf{L}\mathbf{K}_\beta - \mathbf{N}_\beta)\mathbf{M}_\beta = \mathbf{I} - (\mathbf{L}\mathbf{K}_\alpha - \mathbf{N}_\alpha)\mathbf{M}_\alpha.
\end{aligned} \tag{53}$$

These equations give the same magnitudes of $\mathbf{A}_r$ and $\mathbf{B}_r$ as one would obtain from (10) or (11), but they can be easily expanded so that one can see the dependence of the individual coefficients A_{ij}, B_{ij} on L_{ij} and M_{ij}, respectively.

Proceed now to the evaluation of local fields and their phase averages. Substitute from (36) into (51) and use (44) to (46) for the evaluation of the auxiliary strain and stress. After some algebra, derive the following relations between transformation and mechanical fields in the phases

$$\begin{aligned}
\mathbf{D}_{r\alpha}(\mathbf{x}) &= (\mathbf{I} - \mathbf{A}_r(\mathbf{x}))\mathbf{K}_\alpha, \qquad \mathbf{F}_{r\alpha}(\mathbf{x}) = (\mathbf{B}_r(\mathbf{x})\mathbf{N}_\alpha - \mathbf{N}_{r\alpha})\mathbf{M}_\alpha, \\
\mathbf{D}_{r\beta}(\mathbf{x}) &= (\mathbf{I} - \mathbf{A}_r(\mathbf{x}))\mathbf{K}_\beta, \qquad \mathbf{F}_{r\beta}(\mathbf{x}) = (\mathbf{B}_r(\mathbf{x})\mathbf{N}_\beta - \mathbf{N}_{r\beta})\mathbf{M}_\beta,
\end{aligned} \tag{54}$$

together with the connections

$$\mathbf{D}_{r\alpha}(\mathbf{x}) + \mathbf{D}_{r\beta}(\mathbf{x}) = (\mathbf{I} - \mathbf{A}_r(\mathbf{x})), \qquad \mathbf{F}_{r\alpha}(\mathbf{x})\mathbf{L}_\alpha + \mathbf{F}_{r\beta}(\mathbf{x})\mathbf{L}_\beta = \mathbf{0}. \tag{55}$$

Find phase volume averages (2), (4) of the above fields and employ (53) to replace the mechanical concentration factors. This connects the eigenstrain and eigenstress concentration factors directly to the overall $\mathbf{L}$ and $\mathbf{M}$.

$$\begin{aligned}
c_r \mathbf{D}_{r\alpha}^T &= \mathbf{K}_\alpha^T[c_r\mathbf{I} - (\mathbf{L}\mathbf{K}_r - \mathbf{N}_r)\mathbf{M}_r], \qquad c_r \mathbf{F}_{r\alpha}^T = \mathbf{M}_\alpha[\mathbf{N}_\alpha^T(\mathbf{K}_r - \mathbf{M}\mathbf{N}_r) - c_r\mathbf{N}_{r\alpha}^T], \\
c_r \mathbf{D}_{r\beta}^T &= \mathbf{K}_\beta^T[c_r\mathbf{I} - (\mathbf{L}\mathbf{K}_r - \mathbf{N}_r)\mathbf{M}_r], \qquad c_r \mathbf{F}_{r\beta}^T = \mathbf{M}_\beta[\mathbf{N}_\beta^T(\mathbf{K}_r - \mathbf{M}\mathbf{N}_r) - c_r\mathbf{N}_{r\beta}^T].
\end{aligned} \tag{56}$$

One also finds that these factors satisfy

$$c_\alpha \mathbf{D}_{\alpha\alpha} + c_\beta \mathbf{D}_{\beta\alpha} = \mathbf{0}, \qquad c_\alpha \mathbf{F}_{\alpha\alpha} + c_\beta \mathbf{F}_{\beta\alpha} = \mathbf{0},$$
$$c_\alpha \mathbf{D}_{\alpha\beta} + c_\beta \mathbf{D}_{\beta\beta} = \mathbf{0}, \qquad c_\alpha \mathbf{F}_{\alpha\beta} + c_\beta \mathbf{F}_{\beta\beta} = \mathbf{0}. \tag{57}$$

These results, and particularly Eqns. (54), can be utilized in the evaluation of the local fields. Equations (36) are the key; they can be restated as follows:

The local strain fields in a composite subjected to an overall strain $\bar{\boldsymbol{\varepsilon}}$ and to the phase eigenstrains $\boldsymbol{\mu}_r$ are given by

$$\boldsymbol{\varepsilon}_r(\mathbf{x}) = \mathbf{A}_r(\mathbf{x})\bar{\boldsymbol{\varepsilon}} + \mathbf{D}_{r\alpha}(\mathbf{x})\boldsymbol{\mu}_\alpha + \mathbf{D}_{r\beta}(\mathbf{x})\boldsymbol{\mu}_\beta. \tag{58}$$

The local stress fields in a composite loaded by an overall stress $\bar{\boldsymbol{\sigma}}$ and by the phase eigenstresses $\boldsymbol{\lambda}_r = -\mathbf{L}_r\boldsymbol{\mu}_r$ are given by

$$\boldsymbol{\sigma}_r(\mathbf{x}) = \mathbf{B}_r(\mathbf{x})\bar{\boldsymbol{\sigma}} + \mathbf{F}_{r\alpha}(\mathbf{x})\boldsymbol{\lambda}_\alpha + \mathbf{F}_{r\beta}(\mathbf{x})\boldsymbol{\lambda}_\beta. \tag{59}$$

Phase averages of the local fields follow if $\mathbf{A}_r(\mathbf{x})$, $\mathbf{B}_r(\mathbf{x})$, $\mathbf{D}_{r\alpha}(\mathbf{x})$, etc., are replaced by $\mathbf{A}_r$, $\mathbf{B}_r$, $\mathbf{D}_{r\alpha}$, and so on.

3 Evaluation Procedures

Applications of the various relations that describe the elastic behavior of fibrous composites must be preceded by a specification of phase thermoelastic properties and volume fractions. The first step is the evaluation of mechanical stress and strain concentration factors and overall moduli. This can be done in two different ways that, for a given approximation, lead to identical results. The factors can be evaluated directly by either the self-consistent method from (21) or by the Mori–Tanaka procedure from (25) to (27). The overall moduli and compliances then follow from (22) or (28), respectively. A more direct way to this result is indicated by (23) and (29), which offer the magnitudes of the moduli. Using the equations in the Appendix, one can readily assemble the overall $\mathbf{L}$ and $\mathbf{M}$. Alternatively, (33) can be used to find bounds on these moduli. In any event, each set of moduli obtained from one of these approaches must conform with the universal connections (24). Also, each set may be substituted into (10) or (53), which yield the concentration factor tensors. Of course, if (53) is used, one must first find the coefficients of $\mathbf{K}_r$, $\mathbf{N}_r$, and so on, in (44) to (46). The relations following (10) and (47)–(49) may be used to verify the results.

The response to a uniform change in temperature can be described in terms of local thermoelastic properties and overall $\mathbf{L}$ or $\mathbf{M}$; equations (11) give the overall properties, and (12) give the local fields. These results represent exact connections between the various thermal and mechanical terms. However, the latter are not known exactly; they are known only in

terms of bounds or estimates. Hence the overall thermal properties and phase field averages are also approximations produced by the various procedures.

The effect of uniform transformation strains on overall stress or strain and on phase field averages can also be described by local and overall moduli and by mechanical concentration factors. Equations (52) indicate the overall stress and strain in terms of the concentration factors (53); and (58), (59) give the local fields. Of course, these results reduce to those caused by a temperature change if the transformation strains are replaced by phase thermal strains.

The overall thermoelastic properties and averages of local fields can be obtained with minimal information about the microstructural geometry of the fibrous medium, essentially in terms of local properties and phase volume fractions. A much more difficult problem is the evaluation of local fields in the phases. Obviously, the outcome depends very much on the details of the geometry of the phases, and as such it calls for solution of specific boundary-value problems for prescribed geometries. The actual local geometry usually varies in any given system, hence exact solutions are beyond reach. However, the parts of the local fields that are of interest in applications are usually located in the fiber and in the proximity of the fiber–matrix interfaces. Estimates of such fields cannot be found by the self-consistent method unless it is modified by introduction of a matrix interlayer to surround the fiber, nor can they be deduced from the bounds. Only the Mori–Tanaka method offers a direct estimate of the interface stress and of those in the surrounding matrix. Recall that the method is based on the solution of an inclusion problem in which the fiber is embedded in an infinite matrix subjected to the average matrix stress or strain (27) at infinity; this field can be used as an estimate of the actual field. The fields are not described herein, but can be found in available texts [*12*, *36*].

Once the estimate of the mechanical fields (27) is found, it is an easy matter to use it in the evaluation of the thermal stress fields via (12) or of the transformation fields (58) and (59), with the connections (54).

III. Elastic–Plastic Response

A. *Homogeneous Materials*

1. Yield and Relaxation Surfaces

When a metal or a metal composite part is loaded beyond a certain stress magnitude, the total strain at each material point may consist of both elastic and inelastic contributions. If the loading rates are such that the response

can be regarded as independent of time. the inelastic part is represented by a plastic strain. At a given applied stress. the plastic part of the total strain. if any. is defined as the strain that would remain after complete local unloading. in which the material would be constrained to deform only elastically. In other words. the plastic strain in a homogeneous volume of material under uniform stress is the difference between the total strain and the elastic strain that would be generated by the current applied stress in a completely elastic solid.

In polycrystalline solids that are assumed to be elastically homogeneous on the macroscale. the plastic strains caused by prescribed stress histories can be evaluated. in principle. within the framework of classical plasticity [41–44]. The results are useful in the formulation of constitutive equations for the plastically deforming phases in composite materials. Although the theory is largely phenomenological and thus not necessarily sensitive to the effects that the heterogeneous microstructure may have on overall behavior. its general aspects are relevant to the plasticity of composite materials. We are concerned only with situations where the total strains are small and where the thermoelastic properties are independent of temperature. The yield stress. however. may change with temperature. Only uniform temperature changes will be applied.

Consider a representative volume of an elastic–plastic solid such that the selected sample can be regarded as elastically homogeneous on the macroscale. Starting from an undeformed. stress-free state. apply uniform overall stresses along a prescribed path that terminates at the current state $\hat{\boldsymbol{\sigma}}$. In most metals and composites. there is an elastic domain in stress space where no plastic strains are generated by load cycles from the current stress. In principle. its boundary can be found as a locus of points that can be reached by purely elastic loading excursions from $\hat{\boldsymbol{\sigma}}$. The outcome is described by a scalar-valued yield or loading function $f(\hat{\boldsymbol{\sigma}}, H)$. which depends on the current stress and also on a functional of past history of inelastic deformation H. The function represents a closed surface in the six-dimensional stress space. If the sample is heterogeneous on the microscale. the surface may consist of a finite number of smooth branches.

Experimental evaluation of yield surfaces has been performed most extensively on polycrystalline metals. particularly on commercially pure aluminum. on some aluminum alloys. and on other metals [45–49]. Only recently have similar results become available for metal matrix composites [50]. The results suggest that the surface translates and distorts during plastic loading. The distortions are often much less pronounced than the translation; hence in the first approximation. they may be neglected. and

$$f(\hat{\boldsymbol{\sigma}}, H) = f(\hat{\boldsymbol{\sigma}} - \hat{\boldsymbol{\alpha}}), \tag{60}$$

where $\bar{\alpha}$ denotes the position of the center of the surface. In the absence of prior inelastic deformation, $\bar{\alpha} = \bar{0}$, and (60) defines the initial yield surface.

Alternatively, the material volume considered can be viewed as subjected to a macroscopically uniform state of strain. After a deformation sequence leading to the current state $\bar{\varepsilon}$, elastic strain excursions from the current state may be employed to determine the outer boundary of the elastic strain domain. For materials that obey (60), the outcome is represented by the relaxation surface in strain space

$$\phi(\bar{\varepsilon}, H) = \phi(\mathbf{M}\bar{\sigma} + \bar{\varepsilon}^p, H) = f(\bar{\sigma}, H), \tag{61}$$

where H, in an appropriate form, is again a functional of past plastic strain history.

The specific analytic forms of ϕ or f, which approximate experimental observations, are closely related to elastic symmetry of the material volume. In the undeformed state, and after deformation histories that do not cause internal rearrangements affecting material symmetry, the functions (60) and (61) must be form-invariant under the group of symmetry transformations associated with the particular solid. For example, most metals are usually regarded as macroscopically isotropic, and the functions are expressed in terms of the familiar isotropic stress or strain invariants. The assumption of plastic incompressibility eliminates the dependence on the first invariant, and thus on the stress $\bar{\sigma}$ in favor of the deviatoric stress $\bar{s}$. The third invariant of $\bar{s}$ is convenient in special situations, but its role is neglected in typical applications. This leaves only the second invariant $J_2 = s_{ij}s_{ij}/2$, and f is then represented by the Mises form of the yield function

$$f(\bar{\sigma} - \bar{\alpha}) \equiv (\bar{\sigma} - \bar{\alpha})^T\mathbf{C}(\bar{\sigma} - \bar{\alpha}) - Y^2 = 0, \tag{62}$$

where the nonvanishing coefficients of the (6×6) matrix $\mathbf{C}$ are

$$C_{11} = C_{22} = C_{33} = 1, \; C_{23} = C_{13} = C_{12} = -\tfrac{1}{2}, \; C_{44} = C_{55} = C_{66} = 3,$$

and Y is the yield stress in simple tension; its magnitude may depend on temperature and/or the plastic strain history.

In contrast to the isotropic metals, fibrous composite materials are usually transversely isotropic, i.e., their properties remain invariant under rigid body rotations about the fiber axis x_1 and also under the transformation $x_1 = -x_1$. Hill [41] and Mulhern *et al.* [51] point out that the functions (60) and (61) must then depend on the corresponding invariants. Green and Atkins [52] and Spencer [53] give the appropriate forms; for transverse

isotropy the stress invariants are

$$\begin{aligned} I_1 &= (\bar{\sigma}_{22} + \bar{\sigma}_{33})/2, \\ I_2 &= \bar{\sigma}_{11}, \\ I_3 &= (\bar{\sigma}_{31}^2 + \bar{\sigma}_{21}^2), \\ I_4 &= [\tfrac{1}{2}(\bar{\sigma}_{33} + \bar{\sigma}_{22})^2 - \bar{\sigma}_{32}^2]/2, \\ I_5 &= [(\bar{\sigma}_{33} - \bar{\sigma}_{22})(\bar{\sigma}_{31}^2 - \bar{\sigma}_{21}^2) + 4\bar{\sigma}_{21}\bar{\sigma}_{31}\bar{\sigma}_{32}]/2. \end{aligned} \tag{63}$$

Other appropriate sets must be selected for other than transversely isotropic composites. Such considerations impose specific restrictions on the admissible form of (60) and (61) that must be respected in modeling. In particular, $f(\bar{\boldsymbol{\sigma}}, H) = f(I_1, I_2, I_3, I_4, I_5, H)$. In properly constructed micromechanical models, this restriction should be automatically satisfied when the overall yield or relaxation surfaces reflect the onset of inelastic deformation, e.g., in the matrix phase.

2. Plastic Strains and Hardening

When the overall stress is taken as the independent variable, the plastic strain is defined as the difference between total strain and the elastic strain recovered during purely elastic unloading. Conversely, when the overall strain is independent, plastic deformation is associated with the existence of a relaxation stress $\bar{\boldsymbol{\sigma}}^R$, defined as the difference between the elastic and current stress at the prescribed overall strain. When this is applied to strain and stress increments, it suggests the additive decompositions

$$d\bar{\boldsymbol{\varepsilon}} = \mathbf{M}\, d\bar{\boldsymbol{\sigma}} + d\bar{\boldsymbol{\varepsilon}}^p, \tag{64}$$

$$d\bar{\boldsymbol{\sigma}} = \mathbf{L}\, d\bar{\boldsymbol{\varepsilon}} - d\bar{\boldsymbol{\sigma}}^R. \tag{64'}$$

Unlike $\mathbf{M}\, d\bar{\boldsymbol{\sigma}}$ or $\mathbf{L}\, d\bar{\boldsymbol{\varepsilon}}$, the $d\bar{\boldsymbol{\varepsilon}}^p$ or $d\bar{\boldsymbol{\sigma}}^R$ are not linear functions of stress or strain. Therefore, the total quantities generated under a prescribed load or deformation history must be found by integration along the actual path.

The transition from elastic to plastic deformation can be defined with reference to the loading or relaxation surfaces. In what follows, we focus on the stress space formulation; an analogous strain space formulation can be found in [54–56]. By definition, the surface (60) must always contain the loading point during plastic deformation; this is assured by the consistency condition

$$df = \left(\frac{\partial f}{\partial \bar{\boldsymbol{\sigma}}}\right)^T (d\bar{\boldsymbol{\sigma}} - d\bar{\boldsymbol{\alpha}}) + \frac{\partial f}{\partial H}\, dH + \frac{\partial f}{\partial \theta}\, d\theta = 0. \tag{65}$$

The possible states reached by loading excursions from the current elastic state are:

$$d\bar{\varepsilon}^p = 0 \text{ for } f \le 0, \quad \frac{\partial f}{\partial \bar{\sigma}} \cdot d\bar{\sigma} + \frac{\partial f}{\partial \theta} d\theta < 0 \quad \text{(elastic state or unloading)},$$

$$d\bar{\varepsilon}^p = 0 \text{ for } f = 0, \quad \frac{\partial f}{\partial \bar{\sigma}} \cdot d\bar{\sigma} + \frac{\partial f}{\partial \theta} d\theta = 0 \quad \text{(neutral loading)}, \tag{66}$$

$$d\bar{\varepsilon}^p \neq 0 \text{ for } f = 0, \quad \frac{\partial f}{\partial \bar{\sigma}} \cdot d\bar{\sigma} + \frac{\partial f}{\partial \theta} d\theta > 0 \quad \text{(plastic loading)}.$$

The direction of the plastic strain vector $d\bar{\varepsilon}^p$ can be established by following a load cycle that starts at some stress $\bar{\sigma}^*$ within the current loading surface, continues to the stress state $\bar{\sigma}$ on the yield surface where the excursion into the plastic range takes place, and then returns to $\bar{\sigma}^*$. The elastic work is recovered in the cycle, whereas the plastic work performed during the load cycle is

$$W_p = \int_{t_0}^{t_1} (\bar{\sigma} - \bar{\sigma}^*) \cdot d\bar{\varepsilon}^p \, dt \ge 0. \tag{67}$$

This result suggests that

$$(\bar{\sigma} - \bar{\sigma}^*) \cdot d\bar{\varepsilon}^p \ge 0, \tag{68}$$

where the equality is valid only for neutral loading. The relations indicate two important conclusions [42]. First, in materials that satisfy (68), the yield and loading surfaces are always convex. Second, at regular points of the loading surface, the plastic strain rate vector is always normal to the loading surface.

Thus one can write

$$d\bar{\varepsilon}^p = d\lambda \frac{\partial f}{\partial \bar{\sigma}}, \tag{69}$$

where the magnitude $d\lambda$ needs to be determined.

During plastic straining, the yield surface must follow the motion of the loading point to satisfy (65). This can be assured by a proper evolution equation for the vector $\bar{\alpha}$ in (60). A suitable general form of a kinematic hardening law is

$$d\bar{\alpha} = d\bar{\sigma} + d\bar{\gamma}, \tag{70}$$

where the magnitude of the vector $d\bar{\gamma}$ is specified by various rules. Well-known prescriptions were suggested by Prager and modified by Ziegler [57]. However, experimental results [45–48] indicate that in aluminum alloys

$d\tilde{\boldsymbol{\varepsilon}}^p$ is best approximated by selecting $d\tilde{\gamma} = 0$ in (60). This hardening law was first suggested by Phillips [45, 46] and Phillips and Lee [47].

An illustration of the strain evaluation procedure for a uniformly stressed metal sample is provided by the following example [58]. Let the loading surface be represented by the Mises form (62), but with a temperature dependent yield stress $Y = Y(\theta)$, and the hardening by the Phillips law. If the latter is written in the form

$$d\tilde{\boldsymbol{\alpha}} = \mu\, d\tilde{\boldsymbol{\sigma}}, \tag{71}$$

then the consistency equation suggests that

$$\mu = \left[\left(\frac{\partial f}{\partial \tilde{\boldsymbol{\sigma}}}\right)^T d\tilde{\boldsymbol{\sigma}}\right]^{-1}\left[\left(\frac{\partial f}{\partial \tilde{\boldsymbol{\sigma}}}\right)^T d\tilde{\boldsymbol{\sigma}} + \frac{\partial f}{\partial \theta}\, d\theta\right]$$

$$= [(\tilde{\boldsymbol{\sigma}} - \tilde{\boldsymbol{\alpha}})^T \mathbf{C}\, d\tilde{\boldsymbol{\sigma}}]^{-1}[(\tilde{\boldsymbol{\sigma}} - \tilde{\boldsymbol{\alpha}})^T \mathbf{C}\, d\tilde{\boldsymbol{\sigma}} - Y(\theta)Y'(\theta)\, d\theta], \tag{72}$$

where the second expression was derived from the Mises form (62).

The plastic strain magnitude is evaluated from Ziegler's equality

$$c\, d\tilde{\varepsilon}^p_{ij} \frac{\partial f}{\partial \tilde{\sigma}_{ij}} = d\tilde{\alpha}_{ij} \frac{\partial f}{\partial \tilde{\sigma}_{ij}}, \tag{73}$$

which gives

$$d\lambda = [c\mathbf{q}^T\mathbf{q}^*]^{-1}\left[\mathbf{q}^T d\tilde{\boldsymbol{\sigma}} + \frac{\partial f}{\partial \theta}\, d\theta\right] = \frac{1}{cQ}\left[\boldsymbol{\eta}^T d\tilde{\boldsymbol{\sigma}} - \frac{2Y(\theta)Y'(\theta)}{Q}\, d\theta\right], \tag{74}$$

where

$$\boldsymbol{\eta} = \frac{1}{Q}\mathbf{q}, \qquad Q = (\mathbf{q}^T\mathbf{q}^*)^{1/2},$$

$$q_1 = q_1^* = 2(\tilde{\sigma}_{11} - \tilde{\alpha}_{11}) - (\tilde{\sigma}_{22} - \tilde{\alpha}_{22}) - (\tilde{\sigma}_{33} - \tilde{\alpha}_{33}),$$

$$q_2 = q_2^* = -(\tilde{\sigma}_{11} - \tilde{\alpha}_{11}) + 2(\tilde{\sigma}_{22} - \tilde{\alpha}_{22}) - (\tilde{\sigma}_{33} - \tilde{\alpha}_{33}),$$

$$q_3 = q_3^* = -(\tilde{\sigma}_{11} - \tilde{\alpha}_{11}) - (\tilde{\sigma}_{22} - \tilde{\alpha}_{22}) + 2(\tilde{\sigma}_{33} - \tilde{\alpha}_{33}),$$

$$q_4 = 2q_4^* = 6(\tilde{\sigma}_{21} - \tilde{\alpha}_{21}), \qquad q_5 = 2q_5^* = 6(\tilde{\sigma}_{31} - \tilde{\alpha}_{31}),$$

$$q_6 = 2q_6^* = 6(\tilde{\sigma}_{32} - \tilde{\alpha}_{32}).$$

The magnitudes of c and H are sometimes defined from a simple tension test, this gives

$$c = 2H/3, \qquad H = (d\tilde{\sigma} - dY)/d\tilde{\varepsilon}^p,$$

but a much better agreement with experiments follows when H is found from one of the contemporary theories of plasticity discussed, for example, in [48, 49, 59].

B. *Heterogeneous Materials*

1 Initial Yielding and Hardening

In comparison with the analysis of elastic systems, micromechanics of elastic-plastic composites is much more difficult. Some of the earlier results apply, however, the instantaneous mechanical properties of the phases, such as stiffness and compliance are no longer known constants, instead they depend on the current stress and on past history of plastic deformation. Therefore, a plastically deforming phase that has experienced some nonuniform plastic straining is no longer homogeneous, its instantaneous properties change from point to point.

The plastic deformation process can be better understood if the medium is viewed as an aggregate of small volume elements $k = 1, 2, \ldots, N$, which subdivide both the matrix and the reinforcement phase, and in which the local strains are regarded as piecewise uniform. The refinement of such subdivision can be varied from two elements, one for each phase, to as many as desired. Since each subelement is replicated in numerous locations in the actual composite, it is appropriate to assume that local properties are similar to those that would be found in a neat polycrystalline matrix or fiber material that was exposed to the actual in situ processing sequence. Of course, in many instances such properties can be found only indirectly, but it is apparent that those that apply to the inelastic phase must fit into the same general framework as those of the phase material, described in Section III.A.

The inelastic response of such a subdivided composite to external loading will be studied in more detail with the micromechanical models in Section III.B.4. However, an example of their behavior will be presented now, as an introduction to the subject. The example is taken from the work of Lin and Dvorak [*60*], who examined an idealized periodic model geometry of a discontinuously reinforced fiber composite shown in Fig. 1. The fibers are cylinders of hexagonal cross section, arranged in a periodic hexagonal array in the transverse x_2x_3-plane. In the longitudinal x_1-direction, the fibers are distributed also in a periodic manner. Figure 2 shows a representative volume of the composite and its subdivision into finite elements. When appropriate periodic boundary conditions are prescribed, the deformation of a large volume of the composite under macroscopically uniform overall stress can be studied with one such representative volume element. Finite element analysis of the representative volume is usually used to obtain specific results.

Suppose that the fiber is always elastic but that the matrix is an elastic-plastic material of the type described in Section III.A. The composite is initially in a stress-free state, but loading excursions of sufficient magnitude may cause plastic yielding in parts of, or in the entire matrix volume. At

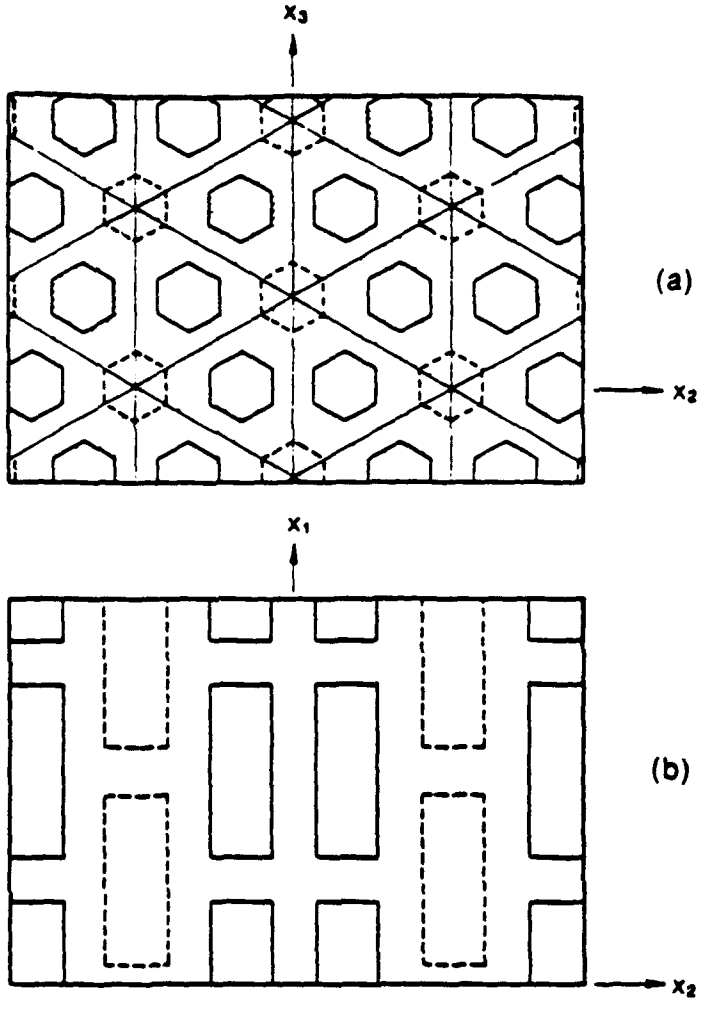

FIG. 1. Idealized microgeometry of a whisker-reinforced composite medium. (a) transverse plane. (b) longitudinal plane [60].

current overall stress, the boundary of the elastic region can be established by loading in many directions from this stress state. Onset of overall plastic deformation can be detected as a specific deviation from linearity in the stress–strain diagram. In Fig. 3, this has been done by many radial loading excursions from the origin. Then, the overall stress was changed along the path indicated from *A* to *B*. Many excursions were again made from *B* to find the next loading surface. This was repeated at *C*, and the path *CDE* was completed within the last surface.

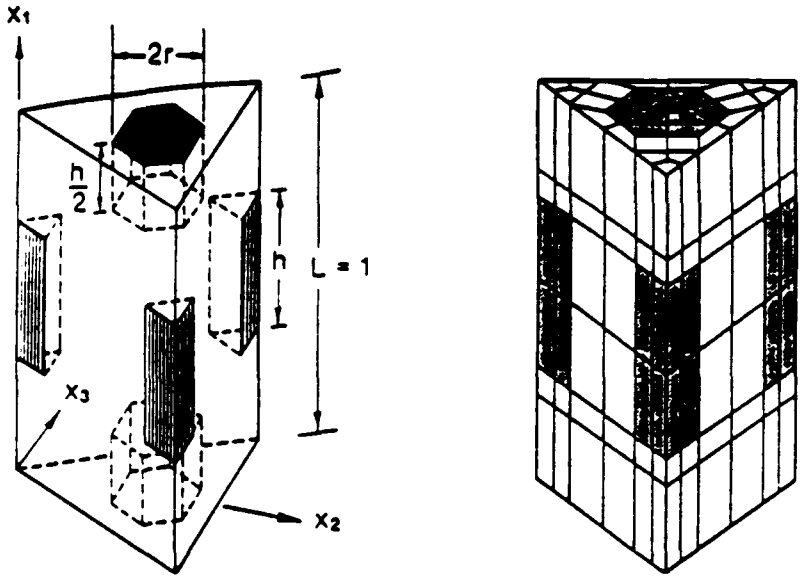

FIG 2 Geometry and finite element subdivision of the representative volume element [60]

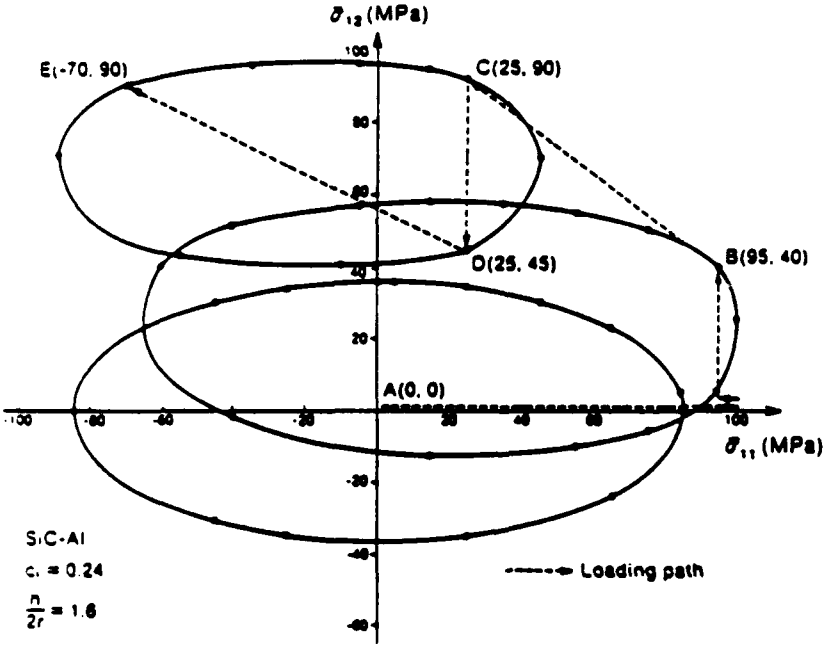

FIG 3 **Overall initial and subsequent yield surfaces of a whisker-reinforced composite in the axial tension ($\bar{\sigma}_{11}$), longitudinal shear ($\bar{\sigma}_{12}$) plane. The subsequent yield surfaces are given at loading points *B* and *C* [60].**

These overall surfaces reveal some aspects of plastic yielding, such as the essentially kinematic motion of the overall surface in the direction of the stress increment: this will be related to the Phillips-type kinematic hardening of the matrix. Also, there is some distortion, mostly expansion or contraction of the overall surface during plastic loading. In contrast, the yield surfaces of the kinematically hardening matrix do not change size.

A better insight into local and overall yielding can be derived from an examination of the local yield surfaces at integration points in the finite elements. To construct such local surfaces in the overall space, it is necessary to find the elastic stress concentration factors $\mathbf{B}_k$ of all elements. Each column of $\mathbf{B}_k$ is generated by a single component of the unit overall stress. Then, if the local surface of point k is given by $f_k(\boldsymbol{\sigma}_k, H_k) = 0$, in the local stresses, its image in the overall stress space is $g_k(\bar{\boldsymbol{\sigma}}, H_k) = f_k(\mathbf{B}_k\bar{\boldsymbol{\sigma}}, H_k) = 0$. With reference to (60), this can be written as

$$g_k(\bar{\boldsymbol{\sigma}} - \hat{\boldsymbol{\alpha}}_k) = f_k(\mathbf{B}_k(\bar{\boldsymbol{\sigma}} - \hat{\boldsymbol{\alpha}}_k)), \tag{75}$$

or, using (62),

$$g_k(\bar{\boldsymbol{\sigma}} - \hat{\boldsymbol{\alpha}}) = (\bar{\boldsymbol{\sigma}} - \hat{\boldsymbol{\alpha}}_k)^T\mathbf{B}_k^T\mathbf{C}\mathbf{B}_k(\bar{\boldsymbol{\sigma}} - \hat{\boldsymbol{\alpha}}_k) - Y^2 = 0. \tag{76}$$

Figure 4 shows a plane section of the cluster of local surfaces for the

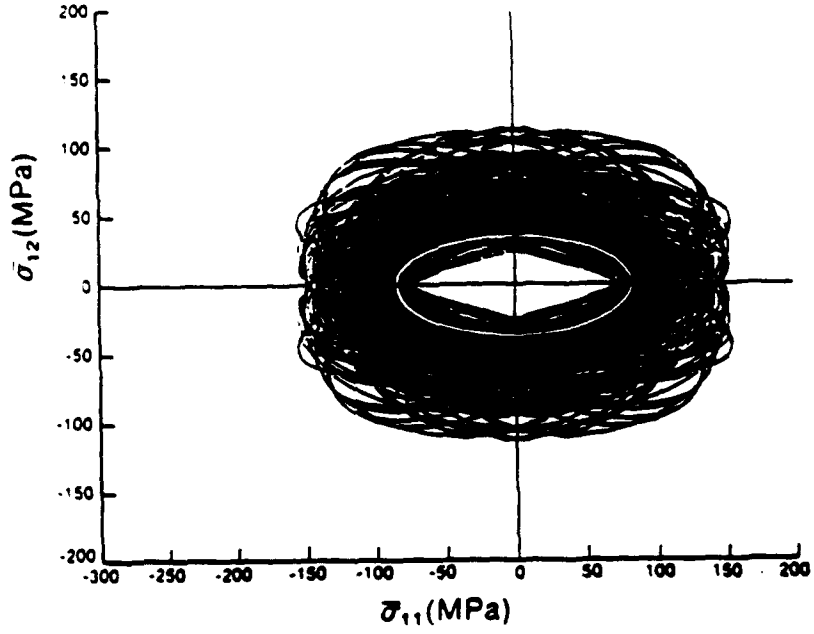

FIG. 4. Cluster of initial yield surfaces found in the overall $\bar{\sigma}_{11}\bar{\sigma}_{12}$-plane from local initial yield surfaces of the matrix phase. Overall yield surface found from deviation of the overall stress–strain response from linearity is superimposed [60].

integration points in Fig. 2, in the overall stress space for the undeformed state. The surface found from macroscopic deviations from linearity in Fig. 3 is superimposed. Figures 5 and 6 show similar clusters at points *B* and *C*, together with the corresponding surfaces from Fig. 3. Of course, the loading excursions designed to establish the points on the overall surface cause local plastic yielding and rearrangement of the clusters. In fact, even the seemingly elastic path *CDE* causes such rearrangement and plastic yielding. Figure 7 shows a detail of the cluster at point *C*. This is a section of a yield cone in the six-dimensional overall space. In the plane shown, it represents a corner; note the hinge-like arrangement which is typical after extended excursions. At the current point *C*, one can draw normals to the internal envelope and also evaluate the plastic strain increment. Hill [*61*] shows that the direction of the plastic strain must fall inside a cone of normals, this is illustrated by the plane section in Fig. 7.

The example indicates that it is not generally possible to derive the actual overall yield surface from a local yield condition. Instead, the overall surface that corresponds to measurable deviations from linearity is a locus of vertices

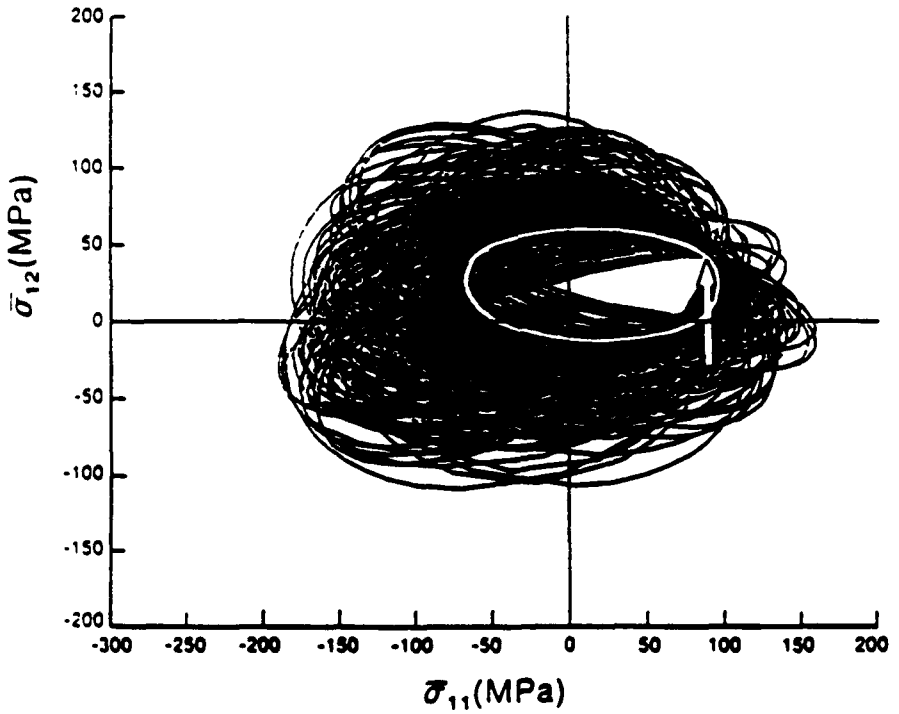

FIG. 5 Cluster of yield surfaces found at *B* in the overall $\bar{\sigma}_{11}\bar{\sigma}_{12}$-plane from local yield surfaces of the matrix phase. The loading path leading to *B* is indicated [*60*].

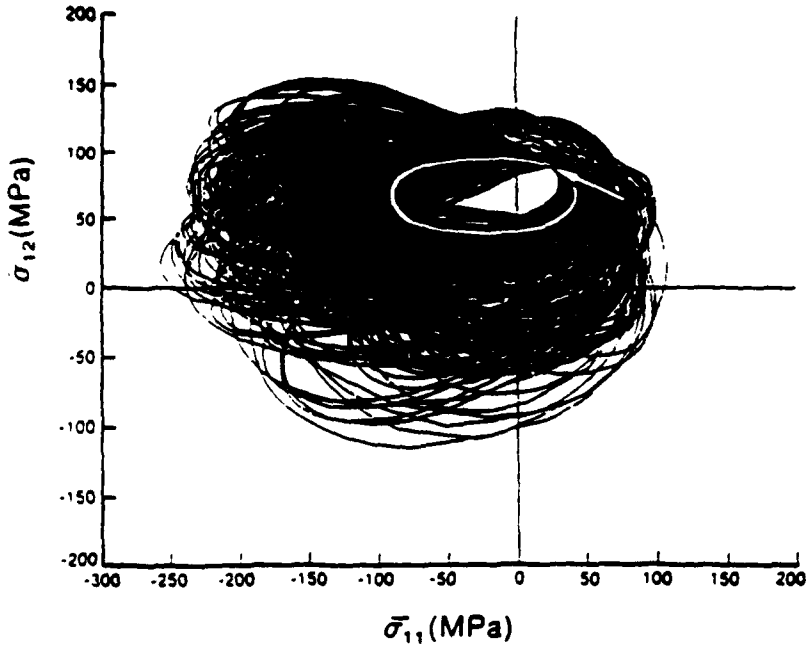

FIG. 6. Cluster of yield surfaces found at C in the overall $\bar{\sigma}_{11}\bar{\sigma}_{12}$-plane from local yield surfaces of the matrix phase [50]

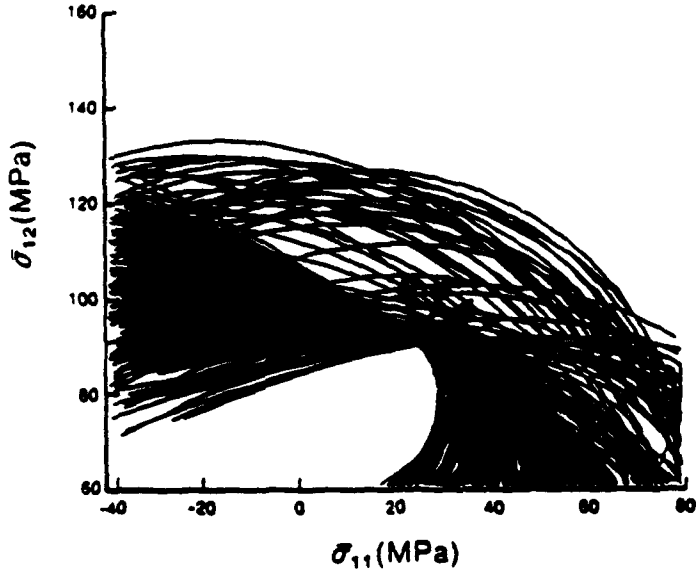

FIG. 7. Overall incremental plastic strain vector and cone of normals found at loading point C [50].

of local yield cones, with associated cones of normals that contain the plastic strain vectors.

From (75), one can read the following relation between the "radii" of local surfaces in the overall and element space.

$$(d\sigma_k - d\alpha_k) = \mathbf{B}_k(d\bar{\sigma} - d\bar{\alpha}_k). \tag{77}$$

In a kinematically hardening matrix, (70) applies to the stresses and translations in each element k. Together with (77), this specifies the direction of motion of the yield surface of each plastically deforming element k in the overall space as

$$d\bar{\alpha}_k = d\bar{\sigma} - \mathbf{B}_k^{-1}\, d\bar{\gamma}_k. \tag{78}$$

or

$$d\bar{\alpha}_k = d\bar{\sigma}$$

for the Phillips law. This last form is particularly simple in that it does not require any information about the local stresses or translations. Of course, it still applies only to surfaces of the plastic elements; hence it does not suggest an identical translation of all surfaces in the cluster.

Under certain limited circumstances that will be described in the sequel, the subdivision of the microstructure may be restricted to the two phases and the overall surface found from (77) and (78), with k replaced by the matrix subscript β, and $\mathbf{B}_\beta$ taken from the elastic estimates in Section II.B. However, an indiscriminate application of such a coarse subdivision of the representative volume may produce entirely misleading estimates of overall yield surfaces and hardening.

2. Plastic Constitutive Relations

An examination of the constitutive equations for the inelastic phase, Section III.A.2, suggests that they can be reduced to the form

$$\begin{aligned} d\sigma(\mathbf{x}) &= \mathscr{L}_r[\sigma(\mathbf{x}) - \beta(\mathbf{x}),\, H(\mathbf{x})]\, d\varepsilon(\mathbf{x}) + \ell_r[H(\mathbf{x})]\, d\theta, \\ d\varepsilon(\mathbf{x}) &= \mathscr{M}_r[\sigma(\mathbf{x}) - \alpha(\mathbf{x}),\, H(\mathbf{x})]\, d\sigma(\mathbf{x}) + m_r[H(\mathbf{x})]\, d\theta, \end{aligned} \tag{79}$$

where $\mathscr{M}_r[\sigma(\mathbf{x}) - \alpha(\mathbf{x}), H(\mathbf{x})]$ represents the instantaneous compliance of the inelastic phase, which can be constructed from (64), (69), and (74). The $\mathscr{L}_r[\varepsilon(\mathbf{x}) - \beta(\mathbf{x}), H(\mathbf{x})]$ is the instantaneous stiffness of the phase that follows from an analogous strain-space formulation. The vectors ℓ_r, m_r are composed from the temperature-dependent yield stress terms in (74), and from the thermal vectors $\mathbf{l}_r$, $\mathbf{m}_r$ taken from (1). These forms must replace (1) in the inelastic phase.

The phase volume averages (2) now are

$$d\boldsymbol{\sigma}_r = \frac{1}{V_r}\int_{V_r} \{\mathscr{L}_r[\boldsymbol{\varepsilon}(\mathbf{x}) - \boldsymbol{\beta}(\mathbf{x}), H(\mathbf{x})]\, d\boldsymbol{\varepsilon}(\mathbf{x}) + \boldsymbol{\ell}_r[H(\mathbf{x})]\, d\theta\}\, dV_r,$$
$$d\boldsymbol{\varepsilon}_r = \frac{1}{V_r}\int_{V_r} \{\mathscr{M}_r[\boldsymbol{\sigma}(\mathbf{x}) - \boldsymbol{\alpha}(\mathbf{x}), H(\mathbf{x})]\, d\boldsymbol{\sigma}(\mathbf{x}) + \boldsymbol{m}_r[H(\mathbf{x})]\, d\theta\}\, dV_r. \tag{80}$$

These equations replace (3), but they do not reduce to that simple form. Unless the local deformation is uniform, one cannot write the phase constitutive relations in terms of phase averages of stress and strain, because these are not connected by an instantaneous phase stiffness or compliance. Indeed, no such phase properties exist in the average sense. The phase constitutive relations must be satisfied pointwise, and this can be achieved only through integration of (79) in the phase volume along the prescribed overall stress or strain path. The fields cannot be found exactly for an actual or model geometry. An approximate evaluation is most conveniently done with the finite-element method, as indicated in the previous example.

Of course, there is a strong temptation to circumvent the difficulty associated with evaluation of the local fields. Typically, an attempt is made to reduce the actual phase constitutive relations (79) to the form

$$d\boldsymbol{\sigma}_r = \mathscr{L}_r(\boldsymbol{\varepsilon}_r, H_r)\, d\boldsymbol{\varepsilon}_r + \boldsymbol{\ell}_r(H_r)\, d\theta, \tag{81}$$
$$d\boldsymbol{\varepsilon}_r = \mathscr{M}_r(\boldsymbol{\sigma}_r, H_r)\, d\boldsymbol{\sigma}_r + \boldsymbol{m}_r(H_r)\, d\theta. \tag{81'}$$

where the instantaneous $\mathscr{L}_r$, $\boldsymbol{\ell}_r$, and $\mathscr{M}_r$, $\boldsymbol{m}_r$ relate the averages of phase stress and strain fields, as if these fields were always uniform. Such assumptions seem to be justified in modeling of the instantaneous properties of individual grains in elastic-plastic polycrystals [63]. Models of this kind regard the polycrystal as a multiphase medium, consisting of many differently orientated but otherwise identical grains, where it seems appropriate to view the deformation field as piecewise uniform. However, this view becomes untenable in two-phase systems where both the geometry and the elastic and elastic-plastic properties of the phases are entirely different. Usually, only the matrix phase deforms plastically, hence the phase properties grow even further apart in the plastic range.

A typical application of (81) is in variants of the self-consistent or Mori-Tanaka methods in plasticity. The schemes that have been proposed often employ composite cylinder or sphere inclusions in an effective medium, or other adjustments of geometry designed to improve the estimate of the local field in the matrix. We recall that in elastic analysis, these methods derive their legitimacy from proofs that show that their predictions of overall properties are bracketed by rigorous bounds. Such proofs are not available

in plasticity. Therefore, there is no assurance that the estimates are reliable. Errors introduced in this manner are easily compounded by integration of the incremental forms along a prescribed overall loading path. Additional problems may be introduced by a loss of consistency and/or symmetry of the estimates. Therefore, the approximation (81) should be either avoided altogether or used only in situations where it may be indicated by comparisons with experiments and more accurate micromechanical models. In two-phase fiber composites, such situations arise in the fiber-dominated deformation of the bimodal plasticity theory discussed in the following.

3 Exact Results

In most situations, the overall response of an inelastic composite is related to the nonuniform local fields, and those must be evaluated from an analysis of a specific micromechanical model. Such models are often based on simplified assumptions that may or may not be admissible in plasticity of heterogeneous media. To assist in model formulation, we now present certain exact results that are independent of the choice of model, and therefore, must be satisfied by all admissible models. They refer to overall and local plastic strains, to thermal hardening caused by a uniform change in temperature, and to normality and convexity of the overall yield surfaces. Except as noted, the results apply not only to two-phase composites, but to representative volumes of all inelastic heterogeneous media under homogeneous boundary conditions.

a. Local and Overall Plastic Strains

Suppose that an initially stress-free aggregate is subjected to a load cycle that starts and terminates at $\bar{\boldsymbol{\sigma}} = \mathbf{0}$, but reaches some intermediate level $\bar{\boldsymbol{\sigma}} = \bar{\boldsymbol{\sigma}}^0$ such that one or more phases undergoes plastic deformation. At each overall stress $\bar{\boldsymbol{\sigma}}^0$, the overall plastic strain is defined as the difference between the total overall strain and the strain caused by purely elastic unloading by $-\bar{\boldsymbol{\sigma}}^0$. As long as the local plastic strains are regarded in the usual continuum sense envisioned, for example by (79), a similar definition applies to each homogeneously stressed and strained material point of the inelastic phases. The local strain field in the inelastic phases consists of an elastic and plastic part, and the latter may be written as a sum of the phase volume average $\bar{\boldsymbol{\varepsilon}}_r^p$ and a variable plastic field $\tilde{\boldsymbol{\varepsilon}}_r^p(\mathbf{x})$. If $\boldsymbol{\sigma}(\mathbf{x})$ is the local stress under current uniform overall stress, the phase strain field is

$$\boldsymbol{\varepsilon}_r(\mathbf{x}) = \mathbf{M}_r\boldsymbol{\sigma}_r(\mathbf{x}) + \bar{\boldsymbol{\varepsilon}}_r^p + \tilde{\boldsymbol{\varepsilon}}_r^p(\mathbf{x}). \tag{82}$$

After complete elastic unloading to zero overall stress, these strains become

$$\boldsymbol{\varepsilon}_r(\mathbf{x}) = \mathbf{M}_r[\boldsymbol{\sigma}_r(\mathbf{x}) - \mathbf{B}_r(\mathbf{x})\bar{\boldsymbol{\sigma}}^0] + \bar{\boldsymbol{\varepsilon}}_r^p + \tilde{\boldsymbol{\varepsilon}}_r^p(\mathbf{x}), \tag{83}$$

where $\mathbf{B}_r(\mathbf{x})$ is related to the overall stress by the elastic influence function in (7), and $\mathbf{M}_r$ is the elastic phase compliance. The stress

$$\boldsymbol{\sigma}_r^e(\mathbf{x}) = \boldsymbol{\sigma}_r(\mathbf{x}) - \mathbf{B}_r(\mathbf{x})\bar{\boldsymbol{\sigma}}^0 \tag{84}$$

is the elastic stress field associated with the residual strain, which together with the plastic strain $\boldsymbol{\varepsilon}^p(\mathbf{x})$ creates a compatible field in the unloaded composite. The variable part of the plastic strain field has the property

$$\frac{1}{V_r}\int_{V_r} \tilde{\boldsymbol{\varepsilon}}_r^p(\mathbf{x})\, dV = \mathbf{0} \Rightarrow \frac{1}{V}\int_V \tilde{\boldsymbol{\varepsilon}}_r^p(\mathbf{x})\, dV = \mathbf{0}.$$

The phase volume average of the field (82) then is

$$\bar{\boldsymbol{\varepsilon}}_r = \mathbf{M}_r\bar{\boldsymbol{\sigma}}_r - \bar{\boldsymbol{\varepsilon}}_r^p \quad \text{where} \quad \bar{\boldsymbol{\varepsilon}}_r^p = \frac{1}{V_r}\int_{V_r} [\boldsymbol{\varepsilon}_r(\mathbf{x}) - \mathbf{M}_r\boldsymbol{\sigma}_r(\mathbf{x})]\, dV \tag{85}$$

The overall plastic strain $\bar{\boldsymbol{\varepsilon}}^p$ is defined as the volume average of the local strains (83) after complete elastic unloading from $\bar{\boldsymbol{\sigma}}^0$:

$$\bar{\boldsymbol{\varepsilon}}^p = \frac{1}{V}\int_V [\mathbf{M}_r\boldsymbol{\sigma}_r^e(\mathbf{x}) + \tilde{\boldsymbol{\varepsilon}}_r^p]\, dV. \tag{86}$$

In the alternative strain space formulation (64'), the overall strain $\bar{\boldsymbol{\varepsilon}}$ is regarded as the independent variable. At current $\bar{\boldsymbol{\varepsilon}}$, the local stress fields are

$$\boldsymbol{\sigma}_r(\mathbf{x}) = \mathbf{L}_r\boldsymbol{\varepsilon}_r(\mathbf{x}) - \bar{\boldsymbol{\sigma}}_r^R - \tilde{\boldsymbol{\sigma}}_r^R(\mathbf{x}) \tag{87}$$

and after elastic unloading leading to $\bar{\boldsymbol{\varepsilon}} = \mathbf{0}$:

$$\boldsymbol{\sigma}_r(\mathbf{x}) = \mathbf{L}_r[\boldsymbol{\varepsilon}_r(\mathbf{x}) - \mathbf{A}_r(\mathbf{x})\bar{\boldsymbol{\varepsilon}}] - \bar{\boldsymbol{\sigma}}_r^R - \tilde{\boldsymbol{\sigma}}_r^R(\mathbf{x}) = \mathbf{L}_r\boldsymbol{\varepsilon}_r^e(\mathbf{x}) - \bar{\boldsymbol{\sigma}}_r^R - \tilde{\boldsymbol{\sigma}}_r^R(\mathbf{x}). \tag{88}$$

The variable part of the phase relaxation stress $\tilde{\boldsymbol{\sigma}}_r^R(\mathbf{x})$ has the property

$$\frac{1}{V_r}\int_{V_r} \tilde{\boldsymbol{\sigma}}_r^R(\mathbf{x})\, dV = \mathbf{0} \Rightarrow \frac{1}{V}\int_V \tilde{\boldsymbol{\sigma}}_r^R(\mathbf{x})\, dV = \mathbf{0}, \tag{89}$$

and the average of the field (88) thus becomes

$$\bar{\boldsymbol{\sigma}}_r = \mathbf{L}_r\bar{\boldsymbol{\varepsilon}}_r - \bar{\boldsymbol{\sigma}}_r^R = \mathbf{L}_r(\bar{\boldsymbol{\varepsilon}}_r - \bar{\boldsymbol{\varepsilon}}_r^p). \tag{90}$$

The overall relaxation stress follows as

$$\bar{\boldsymbol{\sigma}}^R = \frac{1}{V}\int_V [\mathbf{L}_r\boldsymbol{\varepsilon}_r^p(\mathbf{x}) + \tilde{\boldsymbol{\sigma}}_r^R]\, dV \tag{91}$$

where

$$\bar{\boldsymbol{\sigma}}_r^R = \frac{1}{V_r}\int_{V_r} [\mathbf{L}_r\boldsymbol{\varepsilon}_r(\mathbf{x}) - \boldsymbol{\sigma}_r(\mathbf{x})]\, dV.$$

The variable parts of the local plastic strain and relaxation stress fields do not contribute to the overall strain or stress. Only the averages of the fields and the residual elastic fields make such contributions. However, the variable parts, together with the applied elastic fields, may have a very significant influence on the magnitude of plastic deformation which actually takes place in the phases, and thus on the magnitude of the averages. For example, Dvorak *et al.* [50, 62] show that extensive matrix-dominated plastic yielding may occur in an actual system under overall stress which would not satisfy a macroscopic yield condition based on average phase stresses.

We now proceed to derive a quantitative relationship between local and overall plastic strains that does not involve the residual field. A representative volume of a multiphase composite material under uniform overall stress or strain is again considered. The virtual work theorem is used: it states that the integral over a representative volume

$$\frac{1}{V}\int_V \boldsymbol{\sigma}(\mathbf{x})\cdot\boldsymbol{\varepsilon}'(\mathbf{x})\,dV = \bar{\boldsymbol{\sigma}}\cdot\bar{\boldsymbol{\varepsilon}}' \tag{92}$$

where $\boldsymbol{\sigma}(\mathbf{x})$ is any stress field that satisfies equations of equilibrium, with volume average (6) equal to $\bar{\boldsymbol{\sigma}}$. Similarly, $\boldsymbol{\varepsilon}'(\mathbf{x})$ is any strain field derivable from continuous displacements, with volume averaging (6') equal to $\bar{\boldsymbol{\varepsilon}}'$ [1].

The theorem is first applied to the elastic residual stress field in (84) and to the purely elastic strain field in a composite without plastic strains. The result is

$$\frac{1}{V}\int_V \boldsymbol{\sigma}^{\rho}(\mathbf{x})\cdot\mathbf{M}_r\mathbf{B}_r(\mathbf{x})\bar{\boldsymbol{\sigma}}'\,dV = \bar{\boldsymbol{\sigma}}^{\rho}\cdot\mathbf{M}\bar{\boldsymbol{\sigma}}' = 0 \tag{93}$$

because $\bar{\boldsymbol{\sigma}}^{\rho} = \mathbf{0}$.

Next, the theorem is applied to the elastic stress field in a composite without plastic strains and to the total strain field in the unloaded composite (83) and (86):

$$\frac{1}{V}\int_V \mathbf{B}_r(\mathbf{x})\bar{\boldsymbol{\sigma}}'\cdot[\mathbf{M}_r\boldsymbol{\sigma}^{\rho}(\mathbf{x}) + \boldsymbol{\varepsilon}_r^{\rho}(\mathbf{x})]\,dV = \bar{\boldsymbol{\sigma}}'\cdot\bar{\boldsymbol{\varepsilon}}^{\rho}. \tag{94}$$

With reference to (93), and to the symmetry $\mathbf{M} = \mathbf{M}^T$, one then finds the relation between local and overall plastic strains as

$$\bar{\boldsymbol{\varepsilon}}^{\rho} = \frac{1}{V}\int_{V_{\rho}} \mathbf{B}_r^T(\mathbf{x})\boldsymbol{\varepsilon}_r^{\rho}(\mathbf{x})\,dV \tag{95}$$

where V_{ρ} is the part of the total volume undergoing plastic deformation, where $\boldsymbol{\varepsilon}_r^{\rho} \neq \mathbf{0}$.

This is a general result valid for a heterogeneous medium with any number

of inelastic phases. Related but not identical relations have been derived by Hill [61] and Rice [67].

A dual relationship between the local and overall relaxation stresses in a composite subjected to a prescribed uniform deformation path is

$$\bar{\boldsymbol{\sigma}}^R = \frac{1}{V}\int_{V_r} \mathbf{A}_r^T(\mathbf{x})\boldsymbol{\sigma}_r^R(\mathbf{x})\,dV. \tag{96}$$

In many micromechanical models, the actual local fields are replaced by their piecewise uniform approximations. For example, the self-consistent model assumes that the local fields are uniform at each phase. In the Mori–Tanaka model and in the dilute approximation, uniform fields result in the inclusions, but not in the matrix. The unit cell models discussed in Section III.B.1 and in Section III.B.4.b, typically subdivide each phase into many finite elements with uniform or piecewise uniform strain and stress fields that are related by the elastic or inelastic phase constitutive relations. During plastic loading, each such uniformly strained subdomain will have different instantaneous properties and can be regarded as a separate inelastic phase. In practice, the fields evaluated by a finite element procedure represent the best available approximations of the actual fields.

Under such circumstances, both terms in the above integrals are constant within a certain subdomain k, and the integrals may be replaced by the sums

$$\bar{\boldsymbol{\varepsilon}}^p = \sum_{k_p} c_k \mathbf{B}_k^T \bar{\boldsymbol{\varepsilon}}_k^p, \tag{97}$$

$$\bar{\boldsymbol{\sigma}}^R = \sum_{k_p} c_k \mathbf{A}_k^T \bar{\boldsymbol{\sigma}}_k^R, \tag{97'}$$

taken over all k_p in which the local plastic fields exist. Note that only in elastically homogeneous media ($\mathbf{B}_r = \mathbf{I}$) is the overall plastic strain equal to the volume average of local plastic strains.

The above results can be expanded to include the effect of a uniform change in temperature and summarized as follows.

Under a given overall stress $\bar{\boldsymbol{\sigma}}$ and temperature change θ, the total overall strain is the sum of the elastic strain, the thermal strain, and the plastic strain:

$$\bar{\boldsymbol{\varepsilon}} = \mathbf{M}\bar{\boldsymbol{\sigma}} + \mathbf{m}\theta + \bar{\boldsymbol{\varepsilon}}^p. \tag{98}$$

Likewise, under fixed overall strain and temperature change θ, the overall stress is the sum of the following terms:

$$\bar{\boldsymbol{\sigma}} = \mathbf{L}\bar{\boldsymbol{\varepsilon}} + \mathbf{l}\theta - \bar{\boldsymbol{\sigma}}^R \tag{99}$$

with $\bar{\boldsymbol{\varepsilon}}^p$ and $\bar{\boldsymbol{\sigma}}^R$ related to local plastic strain by (95) to (97).

When written as relations between increments, the above relations are analogous to (64).

b. *Constitutive Relations for Two-Phase Fibrous Composites*

For each fiber composite system, there are certain loading conditions that promote the fiber-dominated deformation mode defined in Section III.B.4.c below. In this mode, the magnitude of the variable parts of the inelastic fields in (82) and (87) seems to be negligible. If this is the case, then one may simplify the analysis of such fibrous composite systems by assuming that the phase constitutive relations are satisfied by phase volume averages of the stress and strain fields, as indicated by (81). This suggests that the actual forms (82) and (87) of the local fields are now replaced by the much simpler forms (85) and (90), respectively. In other words, both the phase plastic strains and relaxation stresses are assumed to remain uniform during fiber-dominated deformation.

Now compare (85) with the phase average of (34), and (90) with the phase average of (34'). The implication is that the $\bar{\boldsymbol{\varepsilon}}_r^p$ can be identified with a uniform phase transformation strain $\boldsymbol{\mu}_r$, and $-\bar{\boldsymbol{\sigma}}_r^R$ with $\boldsymbol{\lambda}_r$. Similar connections exist between the overall transformation strain $\boldsymbol{\mu}$ in (35) and (52) and the overall plastic strain $\bar{\boldsymbol{\varepsilon}}^p$ derived from (97) and also between the overall transformation stress $\boldsymbol{\lambda}$ in (35') and (52') and the overall relaxation stress $-\bar{\boldsymbol{\sigma}}^R$ found from (97'). Therefore, (52) can be utilized to write the following result for a two-phase fiber system:

$$\begin{aligned} \bar{\boldsymbol{\varepsilon}}^p &= (\mathbf{K}_\alpha - \mathbf{M}\mathbf{N}_\alpha)\bar{\boldsymbol{\varepsilon}}_\alpha^p + (\mathbf{K}_\beta - \mathbf{M}\mathbf{N}_\beta)\bar{\boldsymbol{\varepsilon}}_\beta^p, \\ \bar{\boldsymbol{\sigma}}^R &= (\mathbf{L}\mathbf{K}_\alpha - \mathbf{N}_\alpha)\bar{\boldsymbol{\varepsilon}}_\alpha^p + (\mathbf{L}\mathbf{K}_\beta - \mathbf{N}_\beta)\bar{\boldsymbol{\varepsilon}}_\beta^p, \end{aligned} \tag{100}$$

which is analogous to (97), but employs the overall elastic moduli instead of the phase concentration factors. Another form of (97) follows from (53):

$$\bar{\boldsymbol{\varepsilon}}^p = c_\alpha \mathbf{B}_\alpha^T \bar{\boldsymbol{\varepsilon}}_\alpha^p + c_\beta \mathbf{B}_\beta^T \bar{\boldsymbol{\varepsilon}}_\beta^p, \tag{101}$$

$$\bar{\boldsymbol{\sigma}}^R = c_\alpha \mathbf{A}_\alpha^T \bar{\boldsymbol{\sigma}}_\alpha^R + c_\beta \mathbf{A}_\beta^T \bar{\boldsymbol{\sigma}}_\beta^R. \tag{101'}$$

where the relation employs again the elastic mechanical concentration factors. A comparison with the Levin [3] and Rosen–Hashin [4] formulae in (11) and (11^{IV}) serves to establish an analogy between the uniform thermal and plastic strains.

If only one of the phases does yield, then the relation can be inverted and the phase average of the plastic strain field can be evaluated in terms of the overall plastic strain. Thus, if $r = \beta$ is the inelastic phase,

$$\begin{aligned} \bar{\boldsymbol{\varepsilon}}_\beta^p &= (\mathbf{K}_\beta - \mathbf{M}\mathbf{N}_\beta)^{-1}\bar{\boldsymbol{\varepsilon}}^p = \frac{1}{c_\beta}(\mathbf{B}_\beta^T)^{-1}\bar{\boldsymbol{\varepsilon}}^p, \\ \bar{\boldsymbol{\sigma}}_\beta^R &= \mathbf{L}_\beta(\mathbf{L}\mathbf{K}_\beta - \mathbf{N}_\beta)^{-1}\bar{\boldsymbol{\sigma}}^R = \frac{1}{c_\beta}(\mathbf{A}_\beta^T)^{-1}\bar{\boldsymbol{\sigma}}^R, \end{aligned} \tag{102}$$

providing that the inverses exist.

When the local strains are assumed to be uniform in each of the phases, equations (100) and (101) relate the local and overall plastic strains in a two-phase fibrous composite.

We now derive *relations between local and overall total strains*. For the elastic composite, such relations are given by (8). Here we include the effect of a uniform temperature change θ in a similar way, but consider the plastic strains as separate eigenstrains, which by assumption are now uniform in the two phases. Recall that the effect of phase eigenstrains on the total phase strain or stress was evaluated in (58) or (59), respectively. With regard to the above connections between the uniform phase eigenstrains and plastic strains, or phase eigenstresses and relaxation stresses, and with the thermal strains taken from (8), the local and overall quantities are related as follows:

Under applied overall strain and temperature change:

$$\boldsymbol{\varepsilon}_r = \mathbf{A}_r\bar{\boldsymbol{\varepsilon}} + \mathbf{a}_r\theta + \mathbf{D}_{r1}\bar{\boldsymbol{\varepsilon}}_1^p + \mathbf{D}_{r\beta}\bar{\boldsymbol{\varepsilon}}_\beta^p. \tag{103}$$

Under a uniform overall stress and temperature change:

$$\boldsymbol{\sigma}_r = \mathbf{B}_r\bar{\boldsymbol{\sigma}} + \mathbf{b}_r\theta - \mathbf{F}_{r1}\bar{\boldsymbol{\sigma}}_1^R - \mathbf{F}_{r\beta}\bar{\boldsymbol{\sigma}}_\beta^R, \tag{104}$$

where the transformation concentration factors are given by (54) and (56). While both the overall $\bar{\boldsymbol{\varepsilon}}$ or $\bar{\boldsymbol{\sigma}}$, and the temperature change θ may have contributed to the local plastic strains, the two leading terms in the equations represent the elastic contribution to local averages; they may or may not be equal to the overall thermomechanical loads that produced the plastic strains. The relations are valid after a partial or complete unloading and in any circumstances where $\bar{\boldsymbol{\varepsilon}}$, $\bar{\boldsymbol{\sigma}}$, and θ cause no further plastic flow.

The average phase stress, which corresponds to the strain (103), follows from (34). When all contributions are included, one finds the local stresses in a constrained composite as:

$$\boldsymbol{\sigma}_r = \mathbf{L}_r\boldsymbol{\varepsilon}_r + \mathbf{l}_r\theta - \bar{\boldsymbol{\sigma}}_r^R = \mathbf{L}_r(\boldsymbol{\varepsilon}_r - \bar{\boldsymbol{\varepsilon}}_r^p) + \mathbf{l}_r\theta. \tag{105}$$

Alternatively, the constrained composite may be viewed as medium loaded by the overall stress $\bar{\boldsymbol{\sigma}}$, given by (99). Then, (104) and (101') may be utilized to find another form of (105):

$$\boldsymbol{\sigma}_r = \mathbf{B}_r\mathbf{L}\bar{\boldsymbol{\varepsilon}} + (\mathbf{b}_r + \mathbf{B}_r\mathbf{l})\theta + (c_1\mathbf{B}_r\mathbf{A}_1^T - \mathbf{F}_{r1})\bar{\boldsymbol{\sigma}}_1^R + (c_\beta\mathbf{B}_r\mathbf{A}_\beta^T - \mathbf{F}_{r\beta})\bar{\boldsymbol{\sigma}}_\beta^R. \tag{106}$$

The identity $\bar{\boldsymbol{\sigma}}_r^R = \mathbf{L}_r\bar{\boldsymbol{\varepsilon}}_r^p$ may be introduced if desired.

Next, we find the local strains in a composite under uniform overall stress, which coexist with the local stresses (104). According to (34), the result is:

$$\boldsymbol{\varepsilon}_r = \mathbf{M}_r\boldsymbol{\sigma}_r + \mathbf{m}_r\theta + \bar{\boldsymbol{\varepsilon}}_r^p. \tag{107}$$

Again, the overall uniform stress may be regarded as a consequence of the applied overall strain (98) that has the component (101') derived from the

local plastic strains. When this is utilized in (103), the local strain (107) assumes the form:

$$\boldsymbol{\varepsilon}_r = \mathbf{A}_r\mathbf{M}\bar{\boldsymbol{\sigma}} + (\mathbf{a}_r + \mathbf{A}_r\mathbf{m})\theta + (c_\alpha\mathbf{A}_r\mathbf{B}_\alpha^T + \mathbf{D}_{r\alpha})\bar{\boldsymbol{\varepsilon}}_\alpha^p + (c_\beta\mathbf{A}_r\mathbf{B}_\beta^T + \mathbf{D}_{r\beta})\bar{\boldsymbol{\varepsilon}}_\beta^p. \quad (108)$$

The above pairs of expressions for local stresses and strains, together with (9), (10), (85), and (90), provide the following general connections between the eigenstress and eigenstrain concentration factors:

$$\begin{aligned} &\mathbf{L}_r\mathbf{A}_r = \mathbf{B}_r\mathbf{L} \\ &\mathbf{F}_{rr} = \mathbf{L}_r[\mathbf{I} - c_r\mathbf{A}_r\mathbf{B}_r^T - \mathbf{D}_{rr}]\mathbf{M}_r \qquad (r = \alpha, \beta) \\ &\mathbf{F}_{r\rho} = -\mathbf{L}_r[c_\rho\mathbf{A}_r\mathbf{B}_\rho^T - \mathbf{D}_{r\rho}]\mathbf{M}_\rho \qquad (r\rho = \alpha\beta \text{ or } \beta\alpha). \end{aligned} \quad (109)$$

We remark that only (100) and (102) refer specifically to fiber systems, while all the other results from (101) to (109) apply to any two-phase composite for which the various concentration factors can be found. Exact connections between the mechanical and transformation concentration factors have been derived in [40], hence it is only necessary to find the elastic $\mathbf{A}_r$ and $\mathbf{B}_r$: this should be possible for most geometries of practical interest. For completeness, we reproduce the expressions that apply to any two-phase composite:

$$\begin{aligned} &\mathbf{D}_{r\alpha} = (\mathbf{I} - \mathbf{A}_r)(\mathbf{L}_\alpha - \mathbf{L}_\beta)^{-1}\mathbf{L}_\alpha, \qquad \mathbf{D}_{r\beta} = -(\mathbf{I} - \mathbf{A}_r)(\mathbf{L}_\alpha - \mathbf{L}_\beta)^{-1}\mathbf{L}_\beta, \\ &\mathbf{F}_{r\alpha} = (\mathbf{I} - \mathbf{B}_r)(\mathbf{M}_\alpha - \mathbf{M}_\beta)^{-1}\mathbf{M}_\alpha, \qquad \mathbf{F}_{r\beta} = -(\mathbf{I} - \mathbf{B}_r)(\mathbf{M}_\alpha - \mathbf{M}_\beta)^{-1}\mathbf{M}_\beta. \end{aligned} \quad (110)$$

For a fiber composite, these can be shown to represent another form of (54).

We now proceed to derive *macroscopic constitutive relations* for those two-phase composites that admit the approximate relations (81) for the phases. To this end, we utilize (81'):

$$d\boldsymbol{\varepsilon}_r = \mathscr{M}_r\, d\boldsymbol{\sigma}_r + \mathscr{m}_r\, d\theta \quad (81')$$

and the incremental forms of (104) and (107):

$$d\boldsymbol{\sigma}_r = \mathbf{B}_r\, d\bar{\boldsymbol{\sigma}} + \mathbf{b}_r\, d\theta - \mathbf{F}_{r\alpha}\mathbf{L}_\alpha\, d\bar{\boldsymbol{\varepsilon}}_\alpha^p - \mathbf{F}_{r\beta}\mathbf{L}_\beta\, d\bar{\boldsymbol{\varepsilon}}_\beta^p \quad (111)$$

$$d\boldsymbol{\varepsilon}_r = \mathbf{M}_r\, d\boldsymbol{\sigma}_r + \mathbf{m}_r\, d\theta + d\bar{\boldsymbol{\varepsilon}}_r^p. \quad (112)$$

From the first and third equation, one finds the average phase plastic strain:

$$d\bar{\boldsymbol{\varepsilon}}_r^p = (\mathscr{M}_r - \mathbf{M}_r)\, d\boldsymbol{\sigma}_r + (\mathscr{m}_r - \mathbf{m}_r)\, d\theta, \quad (113)$$

which we redefine to read as

$$d\bar{\boldsymbol{\varepsilon}}_r^p = \mathscr{g}_r\, d\boldsymbol{\sigma}_r + \mathscr{g}_r\, d\theta.$$

This is used in (112) to eliminate the local plastic strains and to write the following two equations for the unknown local stresses:

$$d\boldsymbol{\sigma}_r = \mathbf{B}_r\, d\bar{\boldsymbol{\sigma}} + \mathbf{b}_r\, d\theta - \mathbf{F}_{r\alpha}\mathbf{L}_\alpha(\mathcal{G}_\alpha\, d\boldsymbol{\sigma}_\alpha + \boldsymbol{\varphi}_\alpha\, d\theta) - \mathbf{F}_{r\beta}\mathbf{L}_\beta(\mathcal{G}_\beta\, d\boldsymbol{\sigma}_\beta + \boldsymbol{\varphi}_\beta\, d\theta) \tag{114}$$

for $r = \alpha, \beta$.

The solution is:

$$d\boldsymbol{\sigma}_r = \mathcal{B}_r\, d\bar{\boldsymbol{\sigma}} + \mathcal{b}_r\, d\theta. \tag{115}$$

where $\mathcal{B}_r$ and $\mathcal{b}_r$ are the instantaneous stress concentration factors given by

$$\mathcal{B}_\alpha = \left[\mathbf{I} - \mathbf{F}_{\alpha\alpha}\mathbf{L}_\alpha\mathcal{G}_\alpha - \frac{c_\alpha}{c_\beta}\mathbf{F}_{\alpha\beta}\mathbf{L}_\beta\mathcal{G}_\beta\right]^{-1}\left[\mathbf{B}_\alpha - \frac{1}{c_\beta}\mathbf{F}_{\alpha\beta}\mathbf{L}_\beta\mathcal{G}_\beta\right],$$

$$\mathcal{b}_\alpha = \left[\mathbf{I} - \mathbf{F}_{\alpha\alpha}\mathbf{L}_\alpha\mathcal{G}_\alpha - \frac{c_\alpha}{c_\beta}\mathbf{F}_{\alpha\beta}\mathbf{L}_\beta\mathcal{G}_\beta\right]^{-1}[\mathbf{b}_\alpha - \mathbf{F}_{\alpha\alpha}\mathbf{L}_\alpha\boldsymbol{\varphi}_\alpha - \mathbf{F}_{\alpha\beta}\mathbf{L}_\beta\boldsymbol{\varphi}_\beta], \tag{116}$$

$$\mathcal{B}_\beta = \left[\mathbf{I} + \mathbf{F}_{\beta\beta}\mathbf{L}_\beta\mathcal{G}_\beta - \frac{c_\beta}{c_\alpha}\mathbf{F}_{\beta\alpha}\mathbf{L}_\alpha\mathcal{G}_\alpha\right]^{-1}\left[\mathbf{B}_\beta - \frac{1}{c_\alpha}\mathbf{F}_{\beta\alpha}\mathbf{L}_\alpha\mathcal{G}_\alpha\right],$$

$$\mathcal{b}_\beta = \left[\mathbf{I} + \mathbf{F}_{\beta\beta}\mathbf{L}_\beta\mathcal{G}_\beta - \frac{c_\beta}{c_\alpha}\mathbf{F}_{\beta\alpha}\mathbf{L}_\alpha\mathcal{G}_\alpha\right]^{-1}[\mathbf{b}_\beta - \mathbf{F}_{\beta\alpha}\mathbf{L}_\alpha\boldsymbol{\varphi}_\alpha - \mathbf{F}_{\beta\beta}\mathbf{L}_\beta\boldsymbol{\varphi}_\beta]. \tag{117}$$

This applies when both phases experience plastic straining. If one phase remains elastic, say the α phase, then $\mathcal{G}_\alpha = \mathbf{0}$ and $\boldsymbol{\varphi}_\alpha = \mathbf{0}$.

The strain increments in the phases now follow by substitution of the above stress increments into (81'):

$$d\boldsymbol{\varepsilon}_r = \mathcal{M}_r\mathcal{B}_r\, d\bar{\boldsymbol{\sigma}} + (\mathcal{M}_r\mathcal{b}_r + \boldsymbol{\mu}_r)\, d\theta. \tag{118}$$

Finally, the overall constitutive relation for the total strains is obtained from (9') as

$$d\bar{\boldsymbol{\varepsilon}} = \mathcal{M}\, d\bar{\boldsymbol{\sigma}} + \boldsymbol{\mu}\, d\theta \tag{119}$$

where

$$\mathcal{M} = \sum_{r=\alpha,\beta} c_r\mathcal{M}_r\mathcal{B}_r, \qquad \boldsymbol{\mu} = \sum_{r=\alpha,\beta} c_r(\mathcal{M}_r\mathcal{b}_r + \boldsymbol{\mu}_r). \tag{120}$$

are analogous to the elastic forms in (10) and (11).

Another possible derivation of these results may utilize the general formula (101). Substitute (113) into (101) and write the overall instantaneous compliances as:

$$\mathcal{M} = \mathbf{M} + c_\alpha\mathbf{B}_\alpha^T\mathcal{G}_\alpha\mathcal{B}_\alpha + c_\beta\mathbf{B}_\beta^T\mathcal{G}_\beta\mathcal{B}_\beta$$
$$\boldsymbol{\mu} = \mathbf{m} + c_\alpha\mathbf{B}_\alpha^T(\mathcal{G}_\alpha\mathcal{b}_\alpha + \boldsymbol{\varphi}_\alpha) + c_\beta\mathbf{B}_\beta^T(\mathcal{G}_\beta\mathcal{b}_\beta + \boldsymbol{\varphi}_\beta). \tag{121}$$

where $\mathbf{M}$ and $\mathbf{m}$ are elastic, and the remaining terms are inelastic contributions that vanish for each elastic phase, when the particular $\boldsymbol{\varepsilon}_r = \mathbf{0}$.

In principle, the above results may be extended to a multiphase composite medium. The only requirement is to evaluate the additional transformation concentration factor terms, up to $-\mathbf{F}_{rn}\mathbf{L}_n\boldsymbol{\varepsilon}_n^p$ in (110). Once those are found, then the solution of n equations (114), if it exists, provides the instantaneous stress concentration factors for all n phases. Both (119) and (120) apply to any number of phases if additional phase terms are attached.

For a two-phase medium, the above results may be simplified. Recall that the phase transformation concentration factors are related to the mechanical concentration factors by (110). Therefore, in a two-phase medium (116) and (117) may be written without reference to the transformation concentration factors. The result may be derived in several ways. Here we recall the identities following (10) and restate them for the instantaneous concentration factors:

$$c_\alpha \mathcal{B}_\alpha + c_\beta \mathcal{B}_\beta = \mathbf{I} \qquad c_\alpha \mathcal{b}_\alpha + c_\beta \mathcal{b}_\beta = \mathbf{0}. \tag{122}$$

This is verified by the derivation leading to (116) and (117).

Next, compare the forms (120) and (121), and use (122) to eliminate one pair of the instantaneous concentration factors. Then, in turn, solve for the remaining instantaneous quantities to obtain

$$\begin{aligned}
\mathcal{B}_\alpha &= \frac{1}{c_\alpha}[\mathbf{M}_\alpha - \mathbf{M}_\beta - (\mathbf{B}_\alpha^T - \mathbf{I})\boldsymbol{\varepsilon}_\alpha + (\mathbf{B}_\beta^T - \mathbf{I})\boldsymbol{\varepsilon}_\beta]^{-1}[\mathbf{M} - \mathbf{M}_\beta + (\mathbf{B}_\beta^T - \mathbf{I})\boldsymbol{\varepsilon}_\beta] \\
\mathcal{b}_\alpha &= \frac{1}{c_\alpha}[\mathbf{M}_\alpha - \mathbf{M}_\beta - (\mathbf{B}_\alpha^T - \mathbf{I})\boldsymbol{\varepsilon}_\alpha + (\mathbf{B}_\beta^T - \mathbf{I})\boldsymbol{\varepsilon}_\beta]^{-1} \\
&\quad \times [-c_\alpha(\mathbf{B}_\alpha^T - \mathbf{I})\boldsymbol{\varepsilon}_\alpha - c_\beta(\mathbf{B}_\beta^T - \mathbf{I})\boldsymbol{\varepsilon}_\beta + c_\alpha\mathbf{m}_\alpha + c_\beta\mathbf{m}_\beta - \mathbf{m}]
\end{aligned} \tag{123}$$

for any two-phase system. Both are symmetric with respect to the exchange of α and β subscripts, and thus (122) is satisfied. It can be verified that this agrees with (116) and (117) if (110) is taken into account.

These results represent an explicit macroscopic constitutive relation for any two-phase composite in which the response of the phases is approximated by (81). Note that no material model has been used in the derivation. The only information about the microstructure is reflected in the elastic stress and strain concentration factors $\mathbf{A}_r$ and $\mathbf{B}_r$.

In all two-phase systems, the transformation concentration factors can be expressed in terms of $\mathbf{A}_r$ and $\mathbf{B}_r$; this is indicated by (54) and (110). If this route is chosen, then the self-consistent or Mori–Tanaka models may be adopted for convenient evaluation of $\mathbf{A}_r$ and $\mathbf{B}_r$. However, if the analysis proceeds from an independent evaluation of the overall elastic properties $\mathbf{L}$

and $\mathbf{M}$, e.g., via the Hashin–Shtrikman bounds (33), the concentration factors are derived from (10). For a fiber system, the factors also follow from (53) and (56). Then, the above constitutive relation is independent of the details of microstructural geometry and, therefore, is exact for any two-phase system that admits (81).

In summary, the above procedure gives closed-form expressions for the instantaneous overall properties in terms of instantaneous phase properties and overall elastic stiffness or compliance. In contrast, other available approaches usually evaluate the instantaneous concentration factors from approximate solutions of inelastic inclusion problems that often require extensive numerical computations. The estimates of $\mathscr{M}$ are usually implicit, and the plastic strains derived from these estimates may violate (95) to (97).

c *Thermal Hardening*

In an elastic composite, a uniform change in temperature will influence the local fields; this can be evaluated from (7) and (12). Even in the absence of plastic loading, such changes in local stresses and strains will affect the yield and relaxation surfaces in the overall stress or strain space. Under such circumstances, it is convenient to retain the representation of the yield surfaces suggested by (75) and (76) and to include the effect of temperature through additional parameters. For example, with reference to the illustration of local yielding in Section III.B.1. and Figs. 1 to 7, consider the effect of a small change $\Delta\theta$ on the overall yield surfaces of individual subelements k in the elastic–plastic matrix. Suppose that the overall stress, if any, is adjusted such that no plastic yielding is caused by the $\Delta\theta$. The average stress change in a subelement k is equal to $\Delta\boldsymbol{\sigma}_k = \mathbf{b}_k\Delta\theta$. There is no plastic loading, hence $d\boldsymbol{\alpha}_k = \mathbf{0}$, and $\Delta\boldsymbol{\sigma}_k$ is the only change in the local stress. Then, it follows from (77) that the translation of the overall yield surface of subelement k is equal to

$$\Delta\bar{\boldsymbol{\alpha}}_k = -\mathbf{B}_k^{-1}\Delta\boldsymbol{\sigma}_k. \tag{124}$$

The implication is that the change $\Delta\theta$ will cause a rigid body translation of all subelement yield surfaces in the overall space. This effect may be referred to as thermal hardening. Of course, it is present both in the elastic composite and during plastic deformation; in the latter case the translation in (101) must be added to the $\bar{\boldsymbol{\alpha}}_k$ during each loading step. Depending on the respective loading directions, the thermal change may accelerate or retard plastic deformation.

The result given is quite transparent, but not particularly convenient, as it involves the stress concentration factors. A more useful description follows from the decomposition procedure of Section II.C.1. Recall that this pro-

cedure admits eigenstrains in the phases and prescribes auxiliary overall stresses that make the strain field uniform in the entire aggregate, while the stresses become piecewise uniform. Moreover, if both the homogeneous and particular solutions (40) are combined, one can create a one-parameter family of such uniform fields. When each of the phases is isotropic in the transverse plane, i.e., isotropic or transversely isotropic, it is possible to adjust the parameter in such a way that the uniform auxiliary strain field is isotropic in the aggregate.

These considerations suggest the following strategy for evaluation of the effects of uniform changes in temperature on plastic deformation in composites with elastic–brittle fibers. In contrast to the example given, consider now a general plastic loading step from some current reference state in which a temperature change $d\theta$ is applied simultaneously with an overall stress $d\bar{\sigma}$. First, apply the temperature change and the auxiliary surface tractions that create the above isotropic uniform strain field. In an isotropic metal matrix that is plastically incompressible, such combined loading will cause only an isotropic stress increment but no plastic yielding; the local stress increment vector is parallel to the axis of the cylindrical local yield surface (75) or (76). Next, remove the auxiliary tractions and add the overall stress increment, if any, that has been prescribed together with the change $d\theta$. This modifies the current stress increment and the entire overall mechanical loading path. The effect of temperature is represented by a uniform and isotropic strain field together with a certain mechanical loading, which in superposition with the applied mechanical loads may cause plastic deformation of the aggregate.

This approach to thermal hardening was first outlined by Dvorak [7], without the benefit of the results in Section II.C.1. Here we utilize (40) and seek the magnitude of dS_T that guarantees an isotropic stress $d\hat{\sigma}_\beta$ in the metal matrix ($r = \beta$), which is assumed to be elastically isotropic and plastically incompressible. The thermal strains in the phases are uniform phase eigenstrains given by

$$d\mu_r = [\alpha_r, \beta_r, \beta_r, 0, 0, 0]^T \, d\theta, \tag{125}$$

where α_r and β_r denote the linear longitudinal and transverse coefficients of thermal expansion of the phases.

Substitute (125) into (40_2), and with the help of (42) to (46), evaluate the nonvanishing components of $d\hat{\sigma}_r$. The result is:

$$d\hat{\sigma}_1^\alpha = q(l_\alpha \Delta l - n_\alpha \Delta k)\, dS_T + qk_\alpha E_\alpha (l_\beta \Delta\alpha + 2k_\beta \Delta\beta)\, d\theta, \tag{126}$$

$$d\hat{\sigma}_1^\beta = q(l_\beta \Delta l - n_\beta \Delta k)\, dS_T + qk_\beta E_\beta (l_\alpha \Delta\alpha + 2k_\alpha \Delta\beta)\, d\theta, \tag{127}$$

$$d\hat{\sigma}_2^\alpha = d\hat{\sigma}_2^\beta = d\hat{\sigma}_3^\alpha = d\hat{\sigma}_3^\beta = dS_T. \tag{128}$$

Require that $d\hat{\sigma}_1^\beta = d\hat{\sigma}_2^\beta = d\hat{\sigma}_3^\beta$ and find

$$dS_T = \{qk_\beta E_\beta(l_\alpha \Delta\alpha + 2k_\alpha \Delta\beta)[1 - q(l_\beta \Delta l - n_\beta \Delta k)]^{-1}\}\, d\theta. \tag{129}$$

The overall auxiliary stress $d\hat{\boldsymbol{\sigma}}$ has the nonvanishing components

$$d\hat{\sigma}_1 = c_\alpha d\hat{\sigma}_1^\alpha + c_\beta d\hat{\sigma}_1^\beta = dS_A, \qquad d\hat{\sigma}_2 = d\hat{\sigma}_3 = dS_T. \tag{130}$$

Together with $d\theta$, this overall stress creates a uniform strain field in the aggregate. It also guarantees that the stress increment in the matrix is isotropic and thus causes no yielding.

Finally, the auxiliary stress must be removed. This is a mechanical loading step that also should include the actual stress $d\bar{\boldsymbol{\sigma}}$ that was prescribed together with the $d\theta$. After this step, the stress fields in the phases are

$$\begin{aligned} d\boldsymbol{\sigma}_\alpha(\mathbf{x}) &= d\hat{\boldsymbol{\sigma}}_\alpha + \mathcal{B}_\alpha(\mathbf{x})(d\bar{\boldsymbol{\sigma}} - d\hat{\boldsymbol{\sigma}}), \\ d\boldsymbol{\sigma}_\beta(\mathbf{x}) &= d\hat{\boldsymbol{\sigma}}_\beta + \mathcal{B}_\beta(\mathbf{x})(d\bar{\boldsymbol{\sigma}} - d\hat{\boldsymbol{\sigma}}). \end{aligned} \tag{131}$$

Inasmuch as plastic straining may be caused in the matrix during this step, the $\mathcal{B}_r(\mathbf{x})$ denote the instantaneous stress influence functions (116), (117) derived for a particular model geometry from an appropriate integration of (79) along the modified loading path. The implication is that the effect of temperature on local fields can be represented by a modification of the mechanical loading path from $d\bar{\boldsymbol{\sigma}}$ to $(d\bar{\boldsymbol{\sigma}} - d\hat{\boldsymbol{\sigma}})$, where $d\hat{\boldsymbol{\sigma}}$ depends on $d\theta$ as indicated by (126) to (130).

Similar conclusions apply to evaluation of the overall strain. In particular, the dS_T in (129) is substituted into (42_3) and the $d\hat{\boldsymbol{\varepsilon}}_0$ into (40_3); this gives the overall strain $d\hat{\boldsymbol{\varepsilon}}$ caused by $d\hat{\boldsymbol{\sigma}}$ and $d\theta$. Then, the strain caused by the mechanical loading $(d\bar{\boldsymbol{\sigma}} - d\hat{\boldsymbol{\sigma}})$ is added. The result is

$$d\bar{\boldsymbol{\varepsilon}} = d\hat{\boldsymbol{\varepsilon}} + \mathcal{M}(d\bar{\boldsymbol{\sigma}} - d\hat{\boldsymbol{\sigma}}), \tag{132}$$

where $\mathcal{M}$ is the instantaneous compliance of the aggregate (122).

During an elastic unloading step, the results (131) and (132) convert to their elastic counterparts, i.e., the $\mathcal{B}_r(\mathbf{x})$ are replaced by $\mathbf{B}_r(\mathbf{x})$, and $\mathcal{M}$ by $\mathbf{M}$.

Recall that such elastic loading by $\Delta\theta$ alone ($\Delta\hat{\boldsymbol{\sigma}} = \mathbf{0}$) was specified in the example leading to (124). We now reconstruct (124) in the following way. The change $\Delta\theta$ is applied together with $\Delta\hat{\boldsymbol{\sigma}}$, selected such that $\Delta\hat{\boldsymbol{\sigma}}_\beta$ is isotropic; i.e., (129) is used to evaluate ΔS_T. By definition, the Mises yield condition (62) or (76) does not depend on the hydrostatic stress component; hence $\Delta\hat{\boldsymbol{\sigma}}_\beta$ renders $\Delta\boldsymbol{\sigma}_k = \mathbf{0}$, and the $\Delta\theta$ is accounted for by application of the overall stress $-\Delta\hat{\boldsymbol{\sigma}}$, which does not vanish. As before, $\Delta\boldsymbol{\alpha}_k = \mathbf{0}$ because there is no plastic loading. Accordingly, (77) now becomes

$$\mathbf{0} = \mathbf{B}_k(\Delta\hat{\boldsymbol{\sigma}} - \Delta\bar{\boldsymbol{\sigma}}_k). \tag{133}$$

Therefore, instead of (124), we now obtain

$$\Delta\bar{\boldsymbol{\alpha}}_k = \Delta\hat{\boldsymbol{\sigma}}. \tag{134}$$

This is equivalent to (124), but it is now apparent that during elastic deformation, a temperature change $\Delta\theta$ causes a rigid-body translation of *all* subelement yield surfaces in the overall stress space by the same amount $\Delta\hat{\boldsymbol{\sigma}}$.

These results lead to several conclusions. First, unlike most polycrystals, composite materials may experience macroscopic plastic straining due to a sufficiently large change in temperature. The temperature change θ_Y, which will cause the onset of local yielding in an initially stress-free composite, can be evaluated from (134). The stress $\Delta\hat{\boldsymbol{\sigma}}$ is a function of temperature; (130) suggests that in the system considered, it is an axisymmetric overall stress consisting of an axial normal stress dS_A and transverse hydrostatic stress dS_T. The temperature needed to generate a certain dS_T follows from (129), and the axial components from (126), (127). Then, if the subelement yield surface is known in the overall stress space, or if the overall yield surface is derived from physical or numerically simulated experiments, the $d\hat{\boldsymbol{\sigma}}$ is integrated along the thermal loading path until $\theta = \theta_Y$, where $\hat{\boldsymbol{\sigma}}$ reaches the respective yield surface. Of course, in reality the yield surface of a stress-free composite undergoes a rigid-body translation equal to its diameter in the $\hat{\boldsymbol{\sigma}}$-direction in overall stress space. In the absence of an overall mechanical stress, the origin is the loading point, and plastic yielding starts when the overall surface comes into contact with this point. Similar conclusions apply to prestrained systems where the center of the yield surface is at some initial position distinct from the origin. A somewhat different treatment of such effects and specific examples can be found in [*64–66*].

In applications, it is useful to know that the effect of combined thermal and mechanical loads on plastic deformation of a fiber composite can be evaluated by prescribing only mechanical loading, but along a modified path. The uniform auxiliary fields must be added to the results. If the matrix yield stress depends on temperature, then it must be changed in each mechanical loading step that corresponds to a specific temperature change. With such adjustments, an existing model that was designed to predict overall response of a fiber composite under mechanical loading can be easily modified to accommodate both mechanical and thermal loads [*7*].

d. Normality and Convexity

Additional connections between local and overall behavior of composite materials can be established for certain work relations and for the direction of the plastic strain vector. The results summarized here were obtained mostly by Hill [*61*].

Consider the direction of the overall plastic strain vector. Suppose that the composite is subdivided into many small subelements, as in the example in Section III.B.1 above. Assume that each inelastic phase and therefore each subelement conforms with the Drucker postulate (68). Locally, the plastic strain rate vector coincides with the outside normal to the yield surface at the current local stress $\boldsymbol{\sigma}_k$. Any elastic stress increment $d\boldsymbol{\sigma}_k^*$ must be directed into the local surface, for example, if one takes $d\boldsymbol{\sigma}^* \approx (\boldsymbol{\sigma}^* - \boldsymbol{\sigma})$, then (68) indicates that

$$d\boldsymbol{\sigma}_k^*(d\boldsymbol{\varepsilon}_k - \mathbf{M}_r\, d\boldsymbol{\sigma}_k) \leq 0. \tag{135}$$

After some algebra, this can be recast into the form:

$$d\boldsymbol{\sigma}_k^*\, d\boldsymbol{\varepsilon}_k - d\boldsymbol{\sigma}_k\, d\boldsymbol{\varepsilon}_k^* \leq 0, \tag{136}$$

where $d\boldsymbol{\sigma}_k^*$ and $d\boldsymbol{\varepsilon}_k^*$ are elastic, while $d\boldsymbol{\sigma}_k$ and $d\boldsymbol{\varepsilon}_k$ are arbitrary.

Note that each of these terms is a product of an equilibrium stress field with a strain field derivable from continuous displacements. This opens the way to an application of (92) and to the result

$$d\bar{\boldsymbol{\sigma}}^*\, d\bar{\boldsymbol{\varepsilon}} - d\bar{\boldsymbol{\sigma}}\, d\bar{\boldsymbol{\varepsilon}}^* \leq 0. \tag{137}$$

The implication is that the plastic part of the overall strain rate lies within the cone of normals associated with the yield cone at the current vertex. Figure 7 shows an example of such a configuration of local yield surfaces, where the yield cone could be inscribed as an internal envelope of the local surfaces at the current loading point.

This property does not necessarily guarantee normality to a yield surface evaluated from numerical or physical experiments, such as those shown in Figs. 3 to 6, or in Fig. 25. Indeed, such surfaces are merely loci of vertices of adjacent yield cones, and at each loading point, normality limits the plastic rate vector only to the cone of normals.

Finally, consider the relation between the products of stress and plastic strain increments. Appeal again to the stability postulate (68) in the form

$$d\boldsymbol{\sigma}_k(d\boldsymbol{\varepsilon}_k - \mathbf{M}_r\, d\boldsymbol{\sigma}_k) \geq 0, \tag{138}$$

where the equality holds in the elastic subelements. This can be integrated over V to yield

$$d\bar{\boldsymbol{\sigma}}\, d\bar{\boldsymbol{\varepsilon}} \geq \frac{1}{V}\int_V d\boldsymbol{\sigma}_k(\mathbf{M}_r\, d\boldsymbol{\sigma}_k)\, dV. \tag{139}$$

If the actual stress field in the inelastic aggregate is regarded as an admissible field in equilibrium with $d\bar{\boldsymbol{\sigma}}$, and the strain field $\mathbf{M}_r\, d\bar{\boldsymbol{\sigma}}_k$ compatible with the strain $\mathbf{M}\, d\bar{\boldsymbol{\sigma}}$, then the principle of minimum complementary energy

in elasticity suggests that when $\mathbf{M}_r$ is positive-definite

$$d\bar{\boldsymbol{\sigma}}(\mathbf{M}\, d\bar{\boldsymbol{\sigma}}) < \frac{1}{V}\int_V d\boldsymbol{\sigma}_k(\mathbf{M}_r\, d\boldsymbol{\sigma}_k)\, dV, \tag{140}$$

where the left-hand side represents the energy of the actual field.

From the last two equations and from (92), one obtains the inequalities

$$d\bar{\boldsymbol{\sigma}}(d\bar{\boldsymbol{\varepsilon}} - \mathbf{M}\, d\bar{\boldsymbol{\sigma}}) > \frac{1}{V}\int_V d\boldsymbol{\sigma}_k(d\boldsymbol{\varepsilon}_k - \mathbf{M}_r\, d\boldsymbol{\sigma}_k)\, dV \geq 0, \tag{141}$$

under changing overall load $d\bar{\boldsymbol{\sigma}} \neq \mathbf{0}$. The sharp inequality guarantees that the overall plastic strain rate may vanish only in the absence of all local rates. It also suggests that in the absence of local strain hardening, when $d\boldsymbol{\sigma}_r = \mathbf{0}$ everywhere, the overall load must still increase. This is sometimes referred to as constraint hardening, since it arises from mechanical interactions between the phases.

Many additional aspects of the general structure of plasticity of heterogeneous media were discussed by Hill and Rice [*69*, *70*] and Rice [*67*, *68*].

4. Micromechanical Models

The discussion of elasticity and plasticity of heterogeneous media suggests that overall elastic properties can be estimated or bounded with relative ease and that the simplicity of elastic analysis is derived from the homogeneity of the phases during deformation. The elastic properties are known constants, hence volume averaging (2) of local fields (7) gives the relations (8), which provide the desired result (10). The estimates of $\mathbf{A}_r$ or $\mathbf{B}_r$ then follow from well-known approximate solutions of elastic inclusion problems, such as the self-consistent or Mori–Tanaka methods. Direct evaluation of bounds on elastic moduli can be made according to Section II.B.4.

When at least one phase deforms plastically, its homogeneity is lost. Local instantaneous stiffnesses and compliances are no longer known constants. Instead, they depend on current stress and on past history of plastic deformation, and as such they are functions of local coordinates. Although Sections III.B.2 and III.B.3 present many exact results, they do not address the influence of specific microstructural geometry on overall behavior. This can be accomplished only through evaluation of local fields along an incremental loading path. When the approximation (81) is no longer acceptable, evaluation of local fields becomes a necessary part of inelastic modeling of composite materials.

Before the advent of micromechanics, problems of this kind were sometimes approached by introduction of certain assumptions about the overall behavior of fibrous composites that were motivated by micromechanical

considerations. For example, in the model by Mulhern *et al.* [*51*] and Spencer [*71*], the fibers were taken to be inextensible and the composite plastically incompressible; and with these restrictions, the aggregate was regarded as a homogeneous medium. The early micromechanical models often employed simplified phase geometries in order to introduce actual mechanical properties of the phases. A natural goal was to adjust the geometry of the microstructure in such a way that the local fields became piecewise uniform. This was accomplished, for example, by the self-consistent method [*72*], or by assuming specific simple geometries of the matrix and fiber [*73–76*].

Each of these approximate models had certain advantages as well as drawbacks, but at least one of the early models, the vanishing-fiber-diameter model of Dvorak and Bahei-El-Din [*74*] permitted a simplified analysis of metal matrix composite structures. This model reduces the effect of the fiber to a unidirectional elastic constraint on the elastic–plastic matrix that is otherwise free to deform uniformly under uniform overall stress or strain. The model will not be reviewed here, but it is useful to recall its extension to plasticity of laminated plates [*75*], its implementation in a general purpose finite element program for structural analysis [*77*], and applications in the evaluation of stress fields at holes and notches in laminated composite plates [*78, 79*]. More recent extensions to thermoplasticity were discussed by Bahei-El-Din [*58*] and structural analysis applications in [*80*]. A strain-space form of the model [*56*] has been recently implemented into the ABAQUS program.

As an example of more recent work, we now describe two different approaches to plasticity analysis of fibrous composite media; one that provides bounds on certain instantaneous overall properties together with estimates of local fields, and one that takes advantage of certain newly recognized deformation mechanisms of fibrous composites.

a. Bounds on Overall Instantaneous Properties

Models of this kind typically utilize a particular geometry of the fibrous medium and derive bounds on instantaneous overall properties from estimates of local fields and minimum principles of plasticity [*44, 81–83*]. Here we briefly summarize the derivation introduced by Dvorak and Teply [*84, 85*]; an analogous model was later described by Accorsi and Nemat-Nasser [*86*].

In the minimum principle of plasticity for strain rates, one considers a representative volume V of a composite material that is subjected to overall uniform strain, applied along an incremental path that leads to the current strain point $\bar{\boldsymbol{\varepsilon}}$. It is assumed that the current state is represented by known actual local stress and strain fields in the phases and that these fields satisfy

the local constitutive equations, which are also assumed as known in the entire representative volume V at the current point $\bar{\boldsymbol{\varepsilon}}$ of the overall deformation path. At this current reference state, a uniform strain increment $d\bar{\boldsymbol{\varepsilon}}$ is applied through certain displacements $d\bar{\mathbf{u}}$, prescribed on the entire surface S of V. This creates local as well as overall stress changes that need to be determined. An exact solution is often beyond reach, but an approximate solution can be found with the help of suitably chosen trial functions. A kinematically admissible field $d\boldsymbol{\varepsilon}^*$ derived from a continuous velocity field is selected in V such that its volume average $\{d\boldsymbol{\varepsilon}^*\}_V = d\bar{\boldsymbol{\varepsilon}}^* = d\bar{\boldsymbol{\varepsilon}}$, is compatible with the surface displacements $d\bar{\mathbf{u}}^* = d\bar{\mathbf{u}}$ on $S = S_u$. This field is also supposed to satisfy the actual local constitutive equations in the current reference state, so that a certain stress field $d\boldsymbol{\sigma}^*$ can be found from the $d\boldsymbol{\varepsilon}^*$. Under such circumstances, the fields $d\boldsymbol{\sigma}^*$, $d\boldsymbol{\varepsilon}^*$, and $d\mathbf{u}^*$ represent a kinematically admissible set. The energy changes that would occur in the actual state (no asterisks), and those that take place in the admissible state are related through the minumum principle for strain rates

$$\int_V \tfrac{1}{2}\, d\boldsymbol{\varepsilon}\, d\boldsymbol{\sigma}\, dV - \int_{S_p} d\bar{\mathbf{p}}\, d\bar{\mathbf{u}}\, dS \leq \int_V \tfrac{1}{2}\, d\boldsymbol{\varepsilon}^*\, d\boldsymbol{\sigma}^*\, dV - \int_{S_p} d\bar{\mathbf{p}}\, d\bar{\mathbf{u}}^*\, dS, \quad (142)$$

where $S_p = S - S_u$. Body forces are neglected. Recall that displacements are prescribed on the entire surface $S = S_u$, hence the surface integrals vanish. The volume integrals can be written in terms of volume averages and work averages $\bar{\boldsymbol{\sigma}}\bar{\boldsymbol{\varepsilon}} = \{\boldsymbol{\sigma}\boldsymbol{\varepsilon}\}_V$. The result is

$$\tfrac{1}{2}\, d\bar{\boldsymbol{\varepsilon}}\mathbf{L}\, d\bar{\boldsymbol{\varepsilon}} \leq \tfrac{1}{2}\, d\bar{\boldsymbol{\varepsilon}}\mathbf{L}_e\, d\bar{\boldsymbol{\varepsilon}}. \quad (143)$$

If one prescribes the boundary conditions in terms of surface tractions rather than displacements, such that $d\bar{\boldsymbol{\sigma}}^* = d\bar{\boldsymbol{\sigma}}$ and $d\bar{\mathbf{p}}^* = d\bar{\mathbf{p}}$ on $S = S_p$, then one can obtain the inequality

$$-\tfrac{1}{2}\, d\bar{\boldsymbol{\sigma}}\mathbf{M}\, d\bar{\boldsymbol{\sigma}} \leq -\tfrac{1}{2}\, d\bar{\boldsymbol{\sigma}}\mathbf{M}_e\, d\bar{\boldsymbol{\sigma}}. \quad (144)$$

The $\mathbf{L}$ and $\mathbf{M}$ represent the actual instantaneous overall stiffness and compliance. The $\mathbf{L}_e$ and $\mathbf{M}_e$ are their approximations computed from the admissible field $d\bar{\boldsymbol{\varepsilon}}^*$.

In a similar way, one can specify a statically admissible stress field in the domain and use the minimum principle for stress rates to obtain lower bounds on energy rates. The final result can be summarized as

$$d\bar{\boldsymbol{\varepsilon}}\mathbf{L}_e\, d\bar{\boldsymbol{\varepsilon}} \geq d\bar{\boldsymbol{\varepsilon}}\mathbf{L}\, d\bar{\boldsymbol{\varepsilon}} \geq d\bar{\boldsymbol{\varepsilon}}\mathbf{L}_g\, d\bar{\boldsymbol{\varepsilon}} \geq 0 \quad (145)$$

and

$$d\bar{\boldsymbol{\sigma}}\mathbf{M}_g\, d\bar{\boldsymbol{\sigma}} \geq d\bar{\boldsymbol{\sigma}}\mathbf{M}\, d\bar{\boldsymbol{\sigma}} \geq d\bar{\boldsymbol{\sigma}}\mathbf{M}_e\, d\bar{\boldsymbol{\sigma}} \geq 0. \quad (146)$$

where $\mathbf{L}_\sigma$ and $\mathbf{M}_\sigma$ are the approximate values of instantaneous overall properties computed from the admissible stress field.

Since each of these terms is a positive-definite quadratic form, all the $\mathbf{L}$ and $\mathbf{M}$ matrices are also positive-definite. This property leads to the inequalities

$$d\bar{\boldsymbol{\varepsilon}}(\mathbf{L}_\varepsilon - \mathbf{L})\, d\bar{\boldsymbol{\varepsilon}} \geq 0, \qquad d\bar{\boldsymbol{\varepsilon}}(\mathbf{L} - \mathbf{L}_\sigma)\, d\bar{\boldsymbol{\varepsilon}} \geq 0, \tag{147}$$

where the equality signs apply only to the exact solution. Let

$$\mathbf{L}_\varepsilon - \mathbf{L} = \mathbf{H}, \qquad \mathbf{L} - \mathbf{L}_\sigma = \mathbf{D}, \tag{148}$$

and observe that all these matrices are positive-definite. In typical applications, these are (6×6) matrices with six eigenvalues, diagonal terms, and leading principal minors that are all positive. If the eigenvalues are arranged in nonincreasing order, then according to the monotonicity theorem for eigenvalues of symmetric matrices, the ordered eigenvalues of the above matrices, denoted here by lower-case kernel letters, are related by

$$l_i^\varepsilon \geq l_i - h, \qquad l_i \geq l_i^\sigma + d, \tag{149}$$

where

$$h_1 \geq h \geq h_n, \qquad d_1 \geq d \geq d_n,$$

and the ordered eigenvalues satisfy the inequalities

$$l_1^\varepsilon \geq l_2^\varepsilon \geq \cdots \geq l_6^\varepsilon > 0, \qquad h_1 \geq h_2 \geq \cdots \geq h_6 > 0, \text{ etc.}$$

This indicates that $h_n > 0$, $d_n > 0$, hence it follows that

$$l_i^\varepsilon \geq l_i \geq l_i^\sigma. \tag{150}$$

If the ordered eigenvalues are arranged in a nonincreasing order as diagonal terms, then one can write the bounds as

$$\operatorname{diag} l_i^\varepsilon \geq \operatorname{diag} l_i \geq \operatorname{diag} l_i^\sigma, \quad i = 1, 2, \ldots 6. \tag{151}$$

A similar procedure can be applied to (146) to find analogous bounds on the ordered eigenvalues of $\mathbf{M}$,

$$\operatorname{diag} m_i^\sigma \geq \operatorname{diag} m_i \geq \operatorname{diag} m_i^\varepsilon. \tag{152}$$

One also can find bounds on the diagonal terms of $\mathbf{L}$ and $\mathbf{M}$. Recall that these terms are also positive, and it follows from (147) that

$$L_{kk}^\varepsilon \geq L_{kk} \geq L_{kk}^\sigma, \qquad M_{kk}^\sigma \geq M_{kk} \geq M_{kk}^\varepsilon, \quad \text{(no sum on } k\text{)}. \tag{153}$$

However, no close bounds can be found for the off-diagonal terms of $\mathbf{L}$ and $\mathbf{M}$. That can be done only on the basis of known connections between the terms, such as those that exist, for example, in transversely isotropic and other elastic media.

If the bounds are used in an incremental evaluation of the overall properties of an elastic–plastic composite, e.g., by a finite-element analysis of the representative volume, then they must be qualified in the following way. We recall that the minimum principles compare the energy changes of the actual and admissible states from a current reference state that corresponds to the actual solution of the problem. This is assumed to be known, together with the actual local properties. However, in an incremental numerical solution, this condition is not met. Except in the elastic state, the local properties in each current state are not known exactly, they are known only in terms of the finite element approximations. The current state does not represent an admissible set, and it is not possible to find admissible local fields for the next plastic step. Therefore, the bounds do not apply to the actual composite system. Instead, they apply to a system in which the local properties have been replaced by those computed, say, in the finite element solution.

In a typical implementation, approximate upper bounds are computed from the displacement formulation of the finite element method, and approximate lower bounds are obtained from the hybrid formulation. Thus one follows a sequence of upper-bound solutions that also approximate the local properties, or a sequence of lower-bound solutions that give different approximations of the local properties. It remains to be established if either procedure is convergent.

b. Periodic Array Models

Evaluation of bounds on instantaneous overall properties of composite aggregates is best performed for a specific model material that approximates the microstructural geometry of the actual system. Although most microstructures are random, periodic distributions of the reinforcement are often used in the development of model materials. The advantage of this approach is that it may divide the composite into identical unit cells of smallest possible size, which are repeated throughout the representative volume. The cells are chosen so that one can prescribe for each cell certain periodic boundary conditions that correspond to uniform overall strain or stress states. The periodic representation appears to be justified in composites reinforced by continuous large-diameter ($\sim 150\ \mu$m) fibers, such as boron or silicon carbide, in which a nearly periodic distribution of the fibers is assured in manufacture. Models of this type are also useful in other fibrous systems, and in particulate composites, particularly at higher volume concentrations when interaction between phases becomes significant.

The model described here is the periodic hexagonal array (PHA) model [*84*, *85*]. Figure 8 shows the typical cross section of the model material in

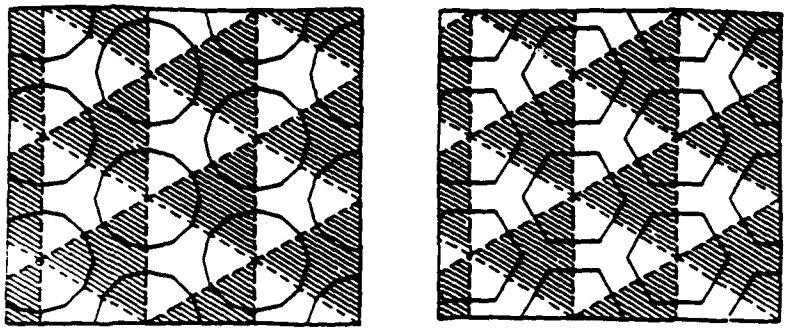

FIG. 8. Transverse cross-sections of periodic hexagonal array models of fibrous composites with hexagonal and dodecagonal cylindrical fibers. Reprinted with permission from *J. Mech. Phys. Solids* **36**, 29. J. L. Teply and G. J. Dvorak, © 1988, Pergamon Press plc.

the transverse plane. The medium consists of a matrix reinforced by aligned fibers of identical cross section, which is approximated by a regular $n \times 6$-sided polygon. As shown in the figure, the microstructure is divided into two sets of identical triangular prisms, with vertices in the fiber axes; these are selected as the unit cells.

Under uniform overall stress or strain, the deformation of the composite can be compared to that of a homogeneous effective medium that has the same overall properties. In particular, it is possible to identify a set of *contact points* in both the periodic and effective media, such that these points undergo exactly the same displacements when either medium is subjected to a given uniform overall deformation. For example, the previous choice of unit cells suggests that to each point $\mathbf{x}_0$ in a given cell, there correspond points $\mathbf{x}$ in all other cells of the same (shaded or unshaded) type, such that the local stresses and strains are equal at all such points. In the x_i system of Fig. 9, the coordinates of $\mathbf{x}$ are

$$\mathbf{x} = \mathbf{x}_0 + \mathbf{c}, \tag{154}$$

where $\mathbf{c} = c\,2(i, \bar{3}, j, 2s/c)$ and the values of i and j must be selected by an appropriate combination of the following:

$i = 0, j = \pm 2n$, for translation parallel to x_2

$i = j = \pm n$, for translation parallel to V_1V_3 direction

$i = -j = \pm n$, for translation parallel to V_1V_2 direction,

where n is an integer. Clearly, the relative displacements of all points (154) must be identical to those of the effective homogeneous medium, such points represent one set of possible contact points. Note that the fiber centers belong to this set.

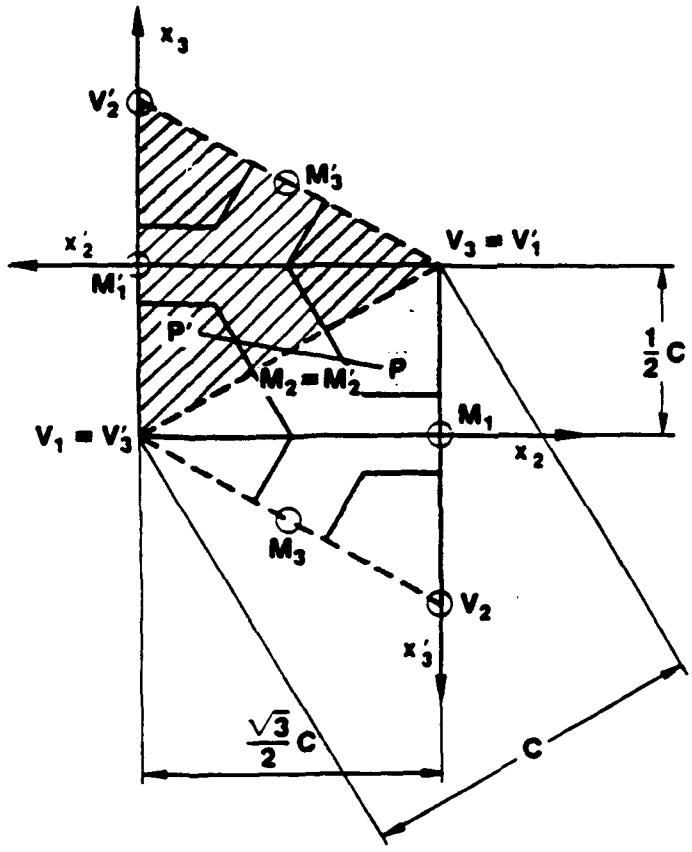

FIG. 9. Two adjacent unit cells and their local coordinate systems. Reprinted with permission from *J. Mech. Phys. Solids* **36**, 29. J. L. Teply and G. J. Dvorak, © 1988, Pergamon Press plc.

Next, one can show that the shaded and unshaded prisms are equivalent. In particular, the transformation

$$\mathbf{x}' = -\boldsymbol{\delta}\mathbf{x} + \mathbf{c}_0 \tag{155}$$

(where $\boldsymbol{\delta}$ is Kronecker's symbol and $\mathbf{c}_0$ is a particular value of $\mathbf{c}$) converts the shaded prisms into the unshaded ones and vice versa. Both the overall and local stresses and strains remain invariant under this transformation, and the surface tractions and displacements are identical in the $\mathbf{x}$ and $\mathbf{x}'$ coordinate systems.

Finally, the periodic displacement boundary conditions must be specified for the unit cells. For a uniform overall strain increment $\Delta\bar{\boldsymbol{\varepsilon}}$, Teply and Dvorak [*85*] show that, with reference to Fig. 9,

$$\Delta\mathbf{u}_{V'} - \Delta\mathbf{u}_V = \Delta\mathbf{u}'_{V'} - \Delta\mathbf{u}'_{V''} = \Delta\bar{\boldsymbol{\varepsilon}}\mathbf{c}_0, \tag{156}$$

where V and V' indicate pairs $V_1V'_1$, $V_2V'_2$, and so forth. Also, they find that

$$\Delta \mathbf{u}_M = \tfrac{1}{2}(\Delta \mathbf{u}_P + \Delta \mathbf{u}_{P'}) \tag{157}$$

for any pair of points P and P' selected on the boundary between two adjacent cells (Fig. 9). When $P \equiv V_3$ and $P' \equiv V_1$,

$$\Delta \mathbf{u}_M = \tfrac{1}{2}(\Delta \mathbf{u}_V + \Delta \mathbf{u}_{V'}) = \tfrac{1}{2}\Delta \bar{\boldsymbol{\varepsilon}} \mathbf{c}_0. \tag{158}$$

Hence,

$$\Delta \mathbf{u}_M - \Delta \mathbf{u}_V = \tfrac{1}{2}\Delta \bar{\boldsymbol{\varepsilon}} \mathbf{c}_0. \qquad \Delta \mathbf{u}'_M - \Delta \mathbf{u}'_V = \tfrac{1}{2}\Delta \bar{\boldsymbol{\varepsilon}} \mathbf{c}'_0. \tag{159}$$

Therefore, the displacements of V_i and M_i, $(i = 1, 2, 3)$, of the unit cell are related to $\Delta \bar{\boldsymbol{\varepsilon}}$ in the same way as the displacements of the same points

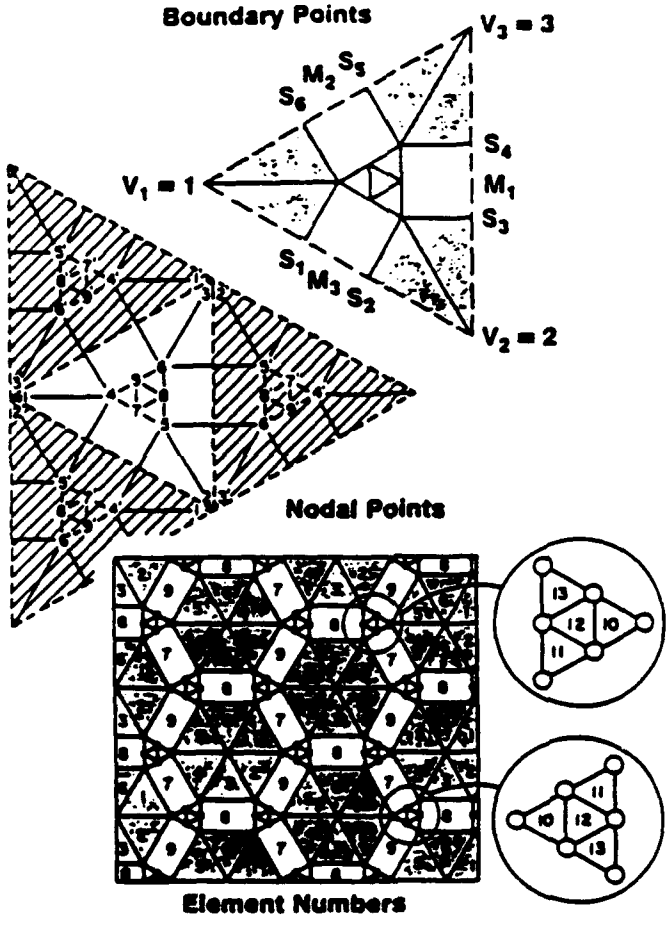

FIG. 10. Unit cell and the finite element mesh used in evaluation of upper bounds. Reprinted with permission from *J. Mech. Phys. Solids* 36, 29, J. L. Teply and G. J. Dvorak, © 1988, Pergamon Press plc.

located in the homogeneous effective medium. Accordingly, both sets represent contact points between the two media under uniform overall strain.

The subdivision of the unit cells into subelements is usually motivated by the particular purpose of the calculation. If only distant bounds on overall properties are needed, then one may prefer to choose the coarsest possible mesh that, however, still provides the number of degrees of freedom needed for plastic deformation. On the other hand, if one also wants to obtain some insight into the local fields, then a much more refined mesh is required.

Figure 10 shows the mesh used in evaluation of the upper-bound solutions for the PHA model. The number of subelements was determined with regard to the considerations in the previous section, and is suitable only for bounding of overall properties. Note that elements 7, 8, and 9 are shared by two unit cells. The actual upper-bound solution employs the displacement formulation of the finite element method, where the admissible strain-rate field is derived from a continuous, piecewise linear displacement field, prescribed in V. Figure 11 shows the actual solution domain and support conditions of the unit cell.

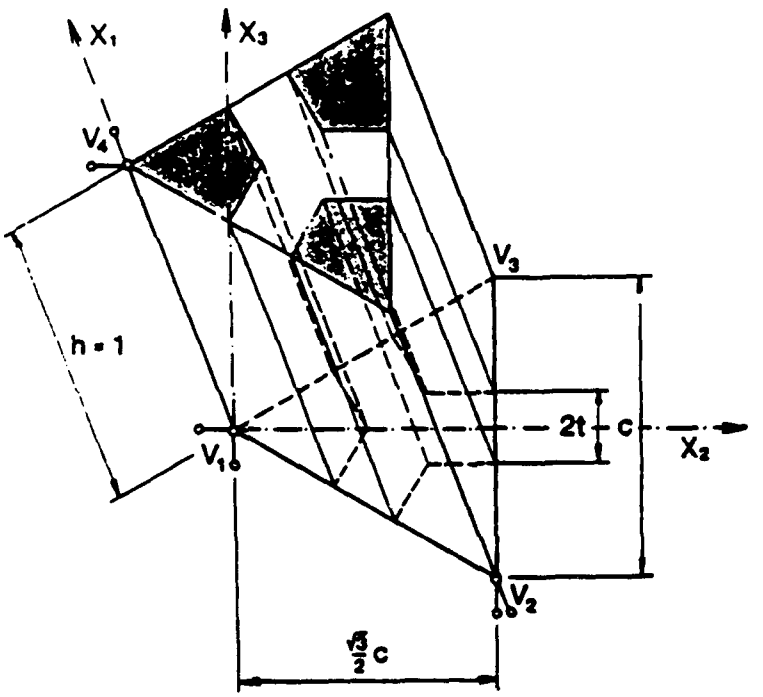

FIG. 11. Dimensions and support conditions of the unit cell in upper-bound evaluation. Reprinted with permission from *J. Mech. Phys. Solids* 36, 29, J. L. Teply and G. J. Dvorak, © 1988, Pergamon Press plc.

A complementary lower-bound solution was also obtained. A somewhat coarser mesh was used in this case, with elements 10–13 in Fig. 10 replaced by a single element. The equilibrium or hybrid formulation was used: the admissible stress field was specified as uniform in each element. Continuity of the field was satisfied by boundary tractions applied at nodal points selected at midside points of element boundaries. These tractions were balanced with Lagrange multipliers, identified with nodal displacements [87, 88, 89].

Figure 12 shows an example of the results found with the bounding approach implementation in the PHA model. A collection of stress–strain

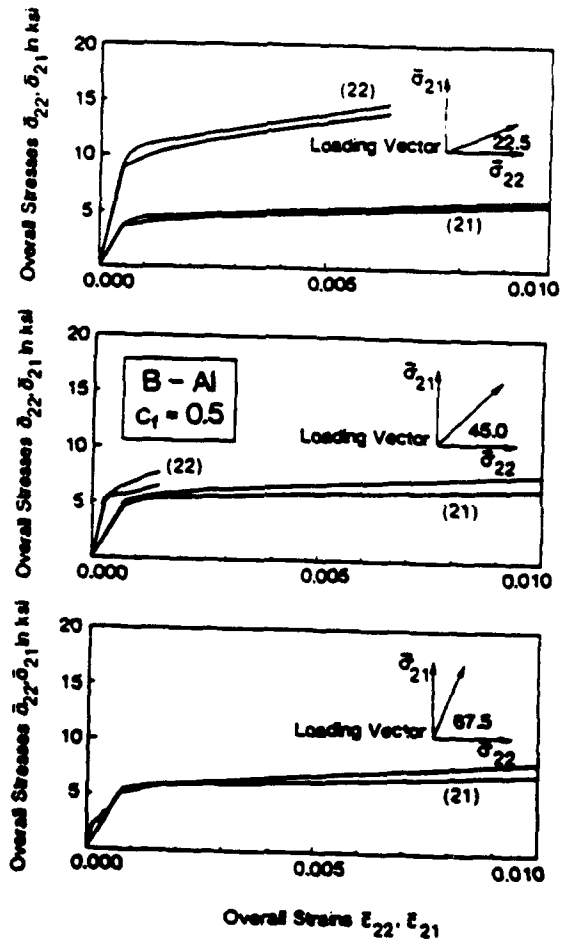

FIG. 12. Approximate bounds on overall response under proportional loading. Reprinted with permission from *J. Mech. Phys. Solids* 36, 29, J. L. Teply and G. J. Dvorak, © 1988, Pergamon Press plc.

curves was computed for a unidirectional fibrous material subjected to combined transverse tension and longitudinal shear stresses $\bar{\sigma}_{22}$ and $\bar{\sigma}_{21}$. A linearly hardening aluminum matrix and an elastic boron fiber were used in the unit cell. For the three proportional loading paths used in the evaluation, two stress–strain curves in close proximity were computed, one from the upper bound and one from the lower bound procedure. Note that both transverse normal and longitudinal shear strains appear in the first loading case. However, the second and third paths apparently promote preferential straining in shear. This turns out to be a demonstration of a so-called matrix deformation mode of fibrous composites, which is examined as a part of the bimodal plasticity theory in the following.

Local stress fields can be evaluated with more refined meshes in the PHA model unit cell. In the examples that follow, the cell was subdivided into 87 elements; the local stress fields were found and stress contours were plotted in the domain [*90*]. Figure 13 shows such fields for a boron–aluminum composite under transverse tension and longitudinal shear, at two overall stress levels. Figure 14 shows contours of local normal stress caused in the composite by uniform thermal change. At the lower levels of overall stress or temperature change, the matrix is strained only elastically, but it becomes fully plastic at the higher levels. Large gradients are present in each case.

The local fields can be utilized in a comparison of predictions of overall instantaneous properties by different micromechanical procedures. Of particular interest is the question of accuracy of those approaches that rely on averages of local fields, such as the self-consistent and the Mori–Tanaka methods. No attempt was actually made to reproduce either of the two techniques. Instead, the overall properties were found from averages of the fields found by the refined finite element analysis of the PHA unit cell. At many steps of each loading path, the local stresses in each element were integrated over the volume of each phase, as in (4). Then the specific forms of the constitutive equation (3) and (64) to (74), originally prescribed for the elastic and plastic strain increments in the matrix subelements, were applied to find the average total strain that would have been caused in the matrix by the average of the matrix stress field. A similar strain average was also evaluated in the elastic fiber. Finally, these phase strain averages were added as in (9') to arrive at the total overall strain. Figure 15 compares the overall response of the PHA model with that evaluated from the above averages of local fields. The agreement is quite poor in the B/Al system, but better in the T50–Gr/Al system. Similar comparisons were made for longitudinal shear loading of the two systems; the two methods gave reasonably close predictions, but the response computed from the averages was somewhat stiffer. Figure 16 shows the response under uniform thermal change. Again, the agreement of the two methods is not very satisfactory in the B/Al

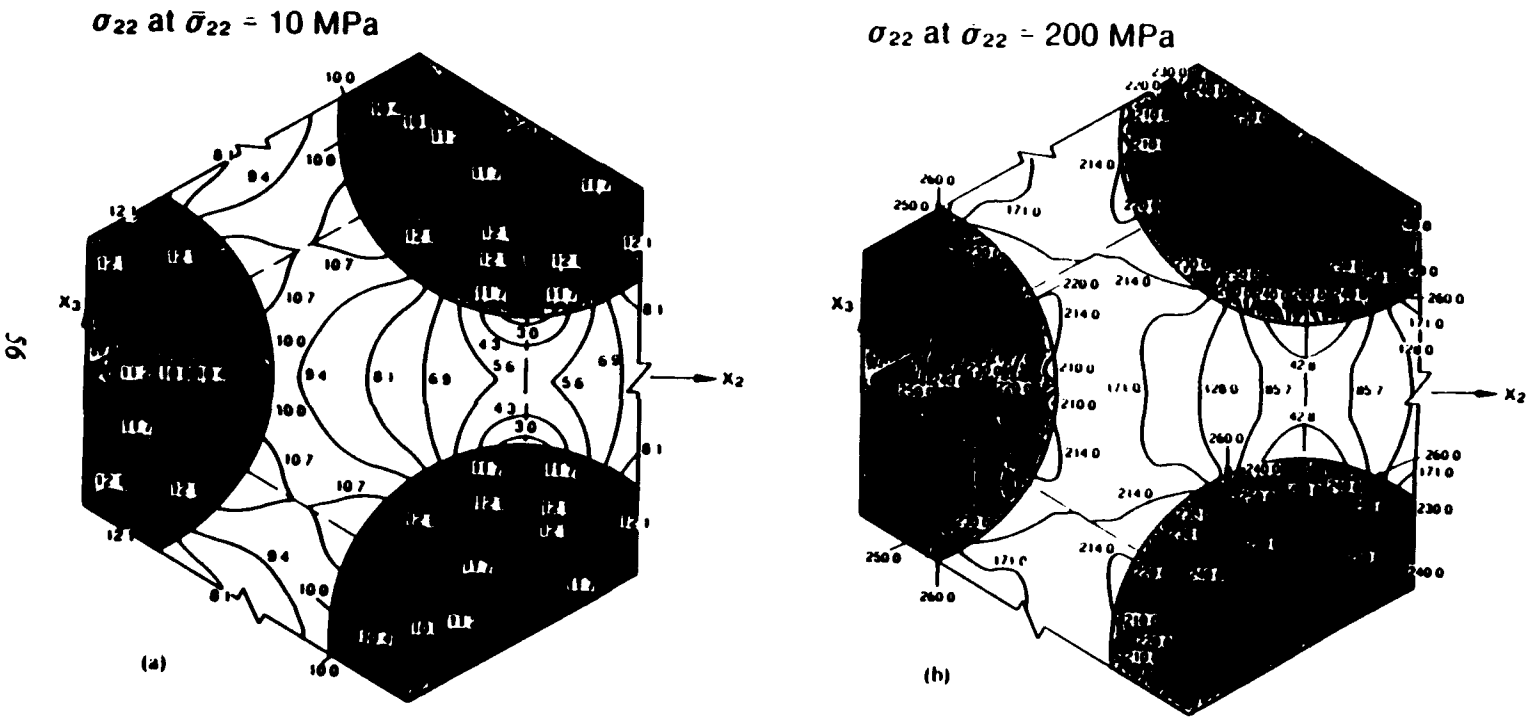
σ22 at σ̄22 = 10 MPa
σ22 at σ22 = 200 MPa
X3
X2
(a)
(b)

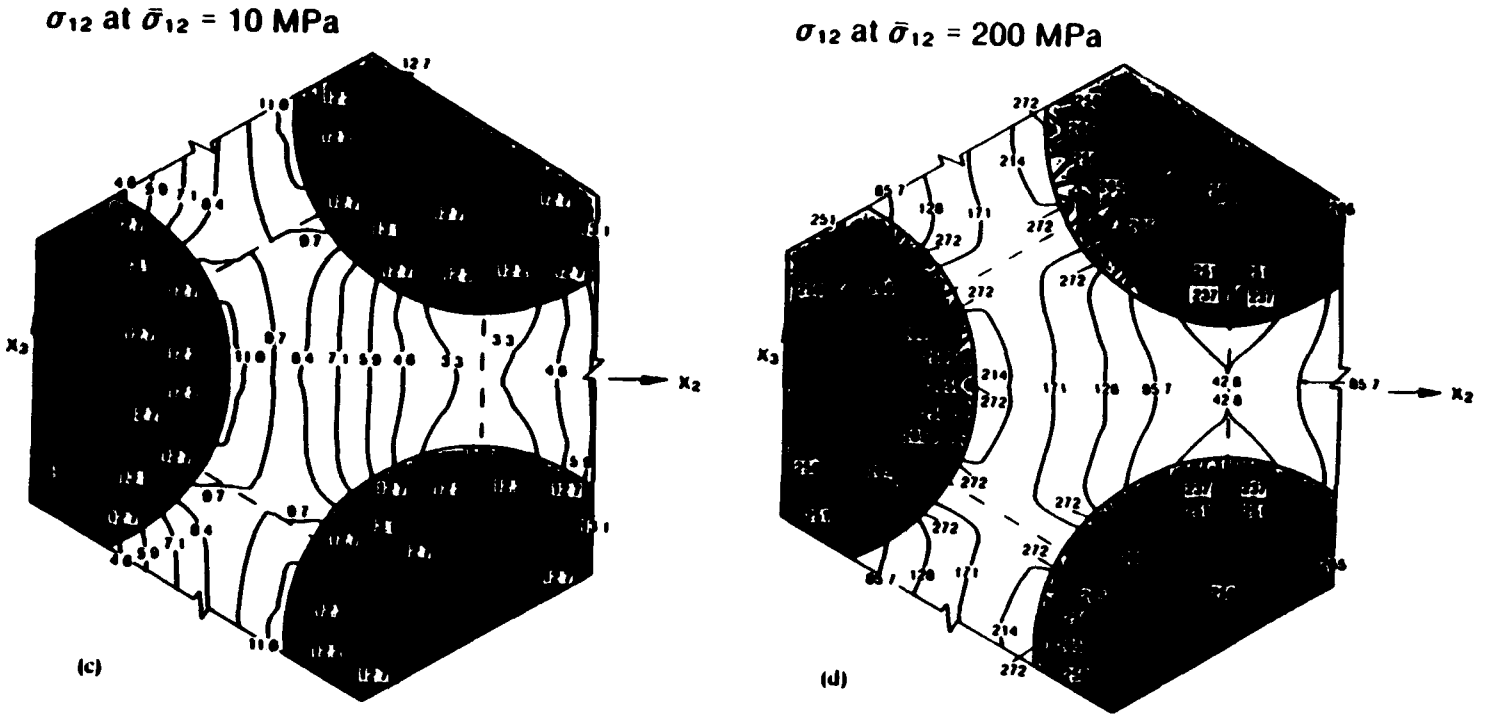

Fig. 13. Local stress contours in a B/Al composite subjected to mechanical load [90]. (a) Local transverse normal stress contours (σ_{22}) at $\bar{\sigma}_{22}$ = 10 MPa. Elastic state. (b) Same contours at $\bar{\sigma}_{22}$ = 200 MPa. Fully plastic state. (c) Local longitudinal shear stress contours (σ_{12}) at $\bar{\sigma}_{12}$ = 10 MPa. Elastic state. (d) Same contours at $\bar{\sigma}_{12}$ = 200 MPa. Fully plastic state.

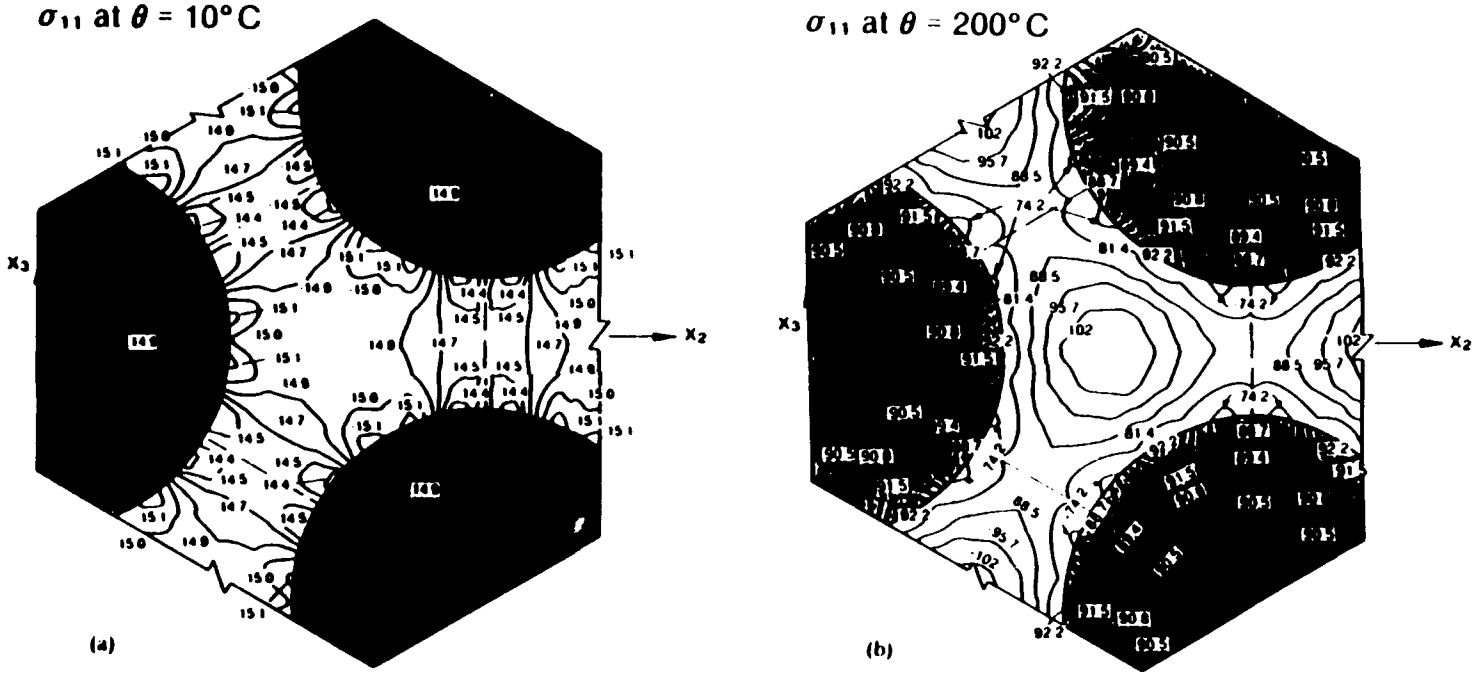
σ_{11} at θ = 10°C
σ_{11} at θ = 200°C
X_3
X_2
(a)
(b)

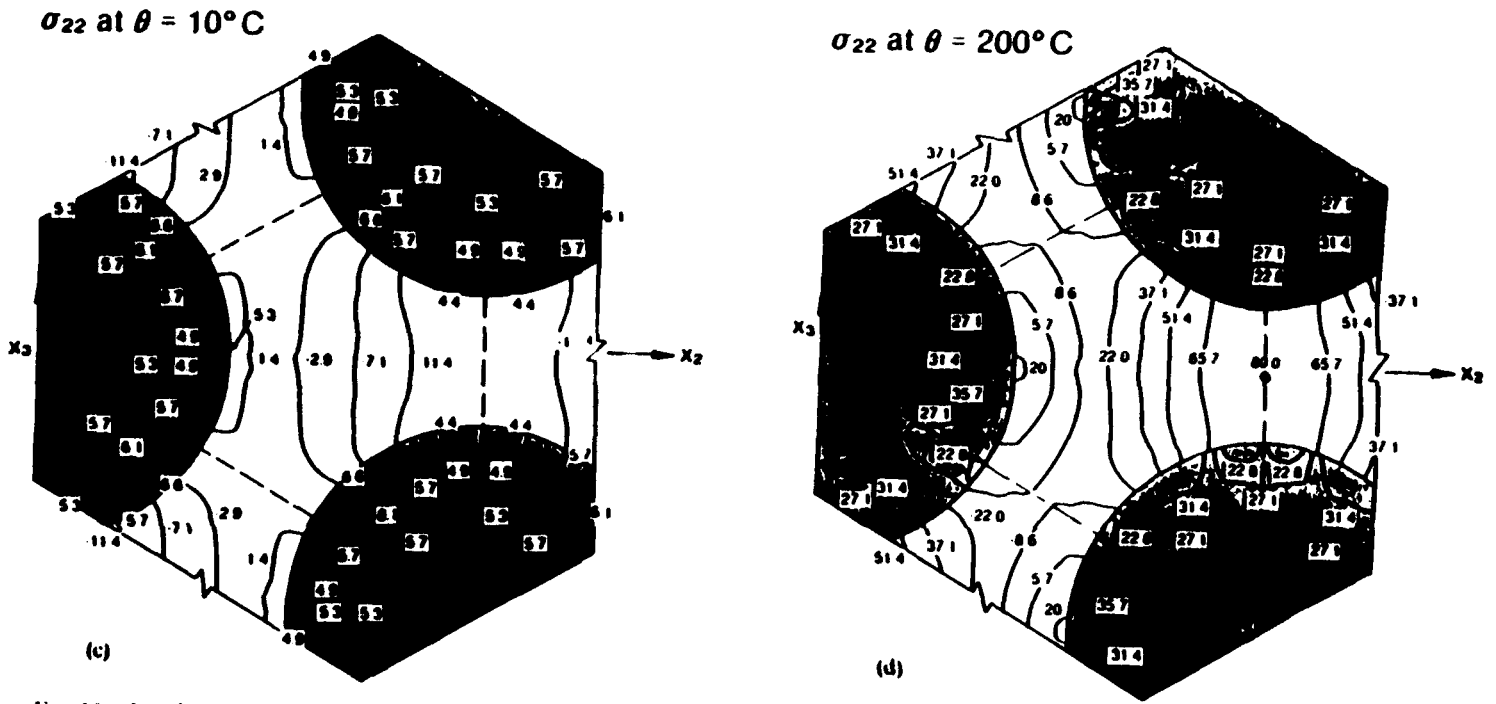

FIG. 14. Local stress contours in a B/Al composite subjected to a uniform thermal change [90]. (a) Axial stress (σ_{11}) at $\Delta\theta$ = 10°C. Elastic state. (b) Axial stress (σ_{11}) and $\Delta\theta$ = 200°C. Fully plastic state. (c) Transverse normal stress (σ_{22}) at $\Delta\theta$ = 10°C. Elastic state. (d) Transverse normal stress (σ_{22}) at $\Delta\theta$ = 200°C. Fully plastic state.

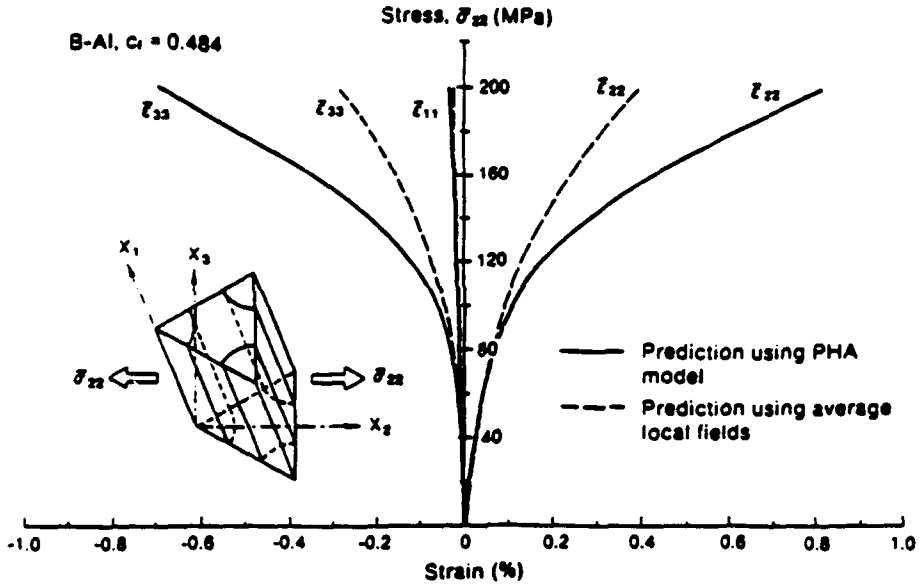

(a)

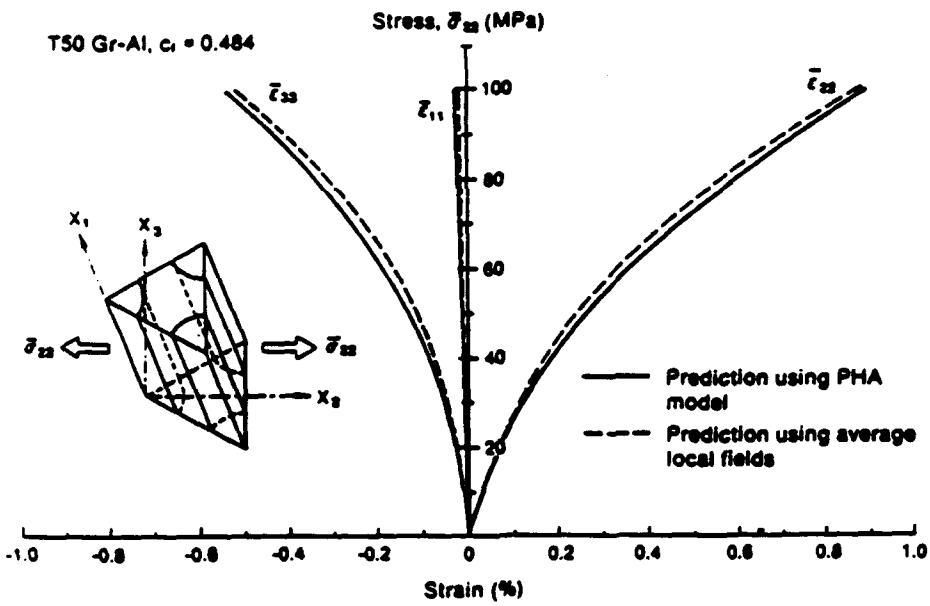

(b)

FIG. 15. Overall response under transverse tension $\bar{\sigma}_{22}$ [90]. (a) Of a B/Al system. (b) Of a Gr/Al system.

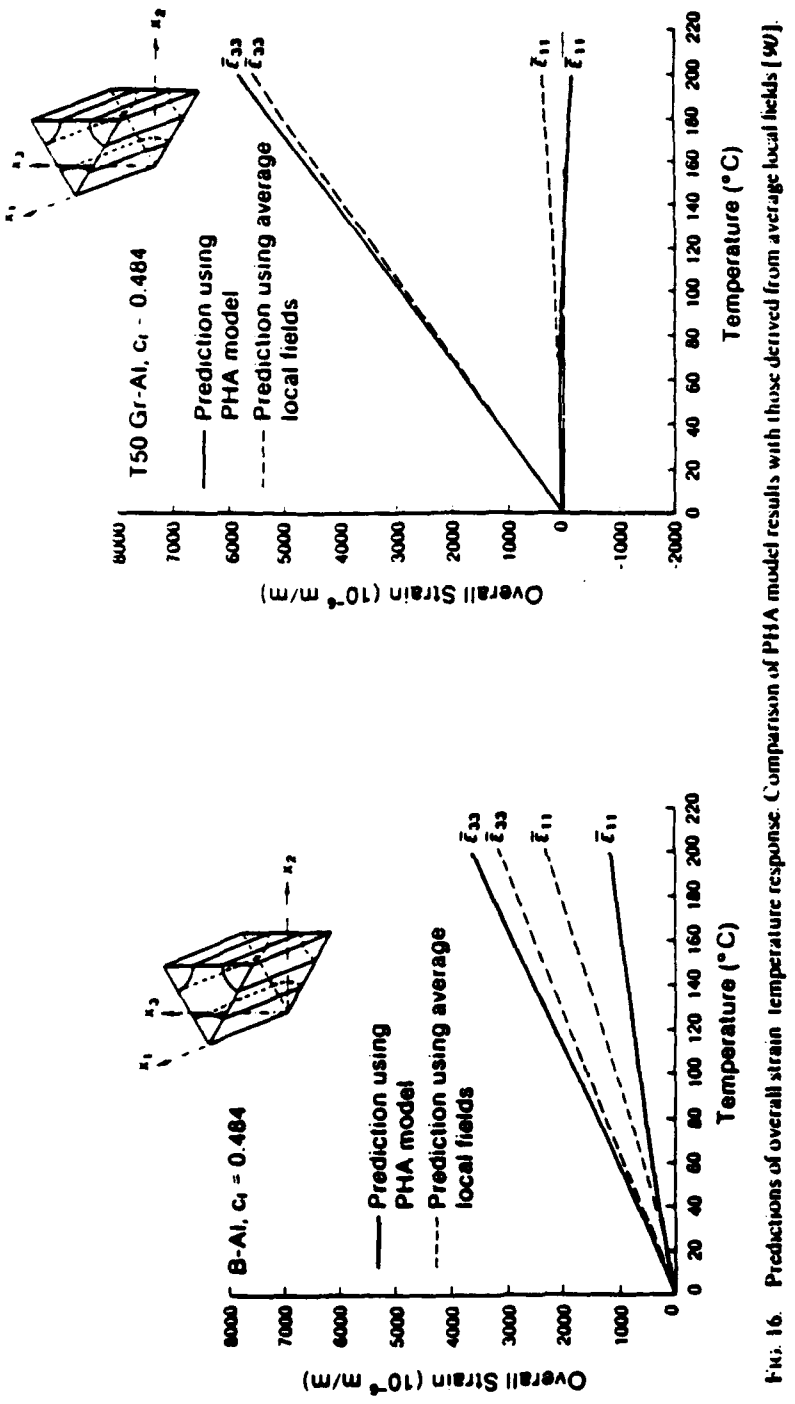

FIG. 16. Predictions of overall strain temperature response. Comparison of PHA model results with those derived from average local fields [90].

system. There appears to be a better agreement in the T50–Gr Al case, but in fact, the prediction of the axial strain by the averaging approach is entirely misleading, both in magnitude and in sign.

This example can serve as a salutory reminder of the possibly large errors that can be introduced by averaging; similar discrepancies would be found in analogous comparisons with the self-consistent or Mori–Tanaka schemes. Several other examples of such errors appear in the following.

We note that the PHA model has been implemented as a UMAT routine in the ABAQUS program [91] and can thus be used in structural applications. Also, the model opens an avenue to numerical experimentation, which is useful in the development of simpler constitutive theories and in interpretation of physical experiments. It is shown in the following that the PHA model agrees well with experimental results, provided that an accurate description of actual phase properties is specified. Finally, the PHA model serves as a check of accuracy of other approaches, such as the averaging scheme discussed earlier.

c *Bimodal Plasticity Theory*

Another approach to modeling of overall behavior of fibrous composites was motivated, in part, by the experimental results described in Section III.B.5, [50, 62]. The experiments suggest that a unidirectional fibrous layer under plane stress may exhibit two distinct deformation modes that affect only the inelastic response. If the overall stress increments have a large normal component in the fiber direction, then the material tends to deform in the fiber-dominated mode (FDM). In this mode, the composite appears to deform as described in Section III.B.3.b. In any event, the segments of the overall yield surface that correspond to this mode are well approximated if the matrix stress concentration factors derived from self-consistent estimates of local stresses. To this end, one finds the estimate of the elastic stress concentration factors in the matrix and relates the local averages to the overall stress. At yield, the overall stresses assume the magnitudes required to satisfy the Mises yield condition (62) by the stress averages in the matrix. This procedure leads to a single surface, given by (75) with $k = r = \beta$, for the matrix phase. The elastic concentration factor $\mathbf{B}_\beta$ in (75) is given by (21_2) for the self-consistent method and by the inverse of the coefficient matrix in (27_1) for the Mori–Tanaka method. Overall hardening follows from (77), $d\bar{\boldsymbol{\alpha}} = d\bar{\boldsymbol{\sigma}}$.

In the matrix-dominated mode (MDM), the theory postulates that the composite can be regarded as an elastic–plastic continuum in which plastic straining occurs in the form of smooth shearing deformations in the matrix, on certain hypothetical slip planes that are parallel to the fiber axis, and in certain preferred slip directions on these planes. This mode ignores the actual microstructural geometry. Instead, the matrix is regarded as a homogeneous

medium, and the fibers that occupy a finite volume fraction are assumed to constrain the matrix deformation to the slip planes. There is a similarity with continuum slip models of single-crystal plasticity, which ignore the discrete dislocation substructure of the crystal and postulate smooth shearing to take place on certain slip systems [92].

The MDM mode is illustrated by Fig. 17, which shows the admissible slip planes. The actual slip directions are determined by the requirement that the resolved shear stress reaches a maximum on the active slip systems. It is possible to show that there are always two conjugate systems that satisfy this requirement on planes parallel to the fiber axis, which is parallel to x_1. The corresponding MDM yield surface for an overall state of plane stress appears in Fig. 18. It is an infinite cylinder of the oval cross section shown, with generators parallel to the $\bar{\sigma}_{11}$ axis; hence the $\bar{\sigma}_{11}$ stress does not influence the onset of MDM yielding.

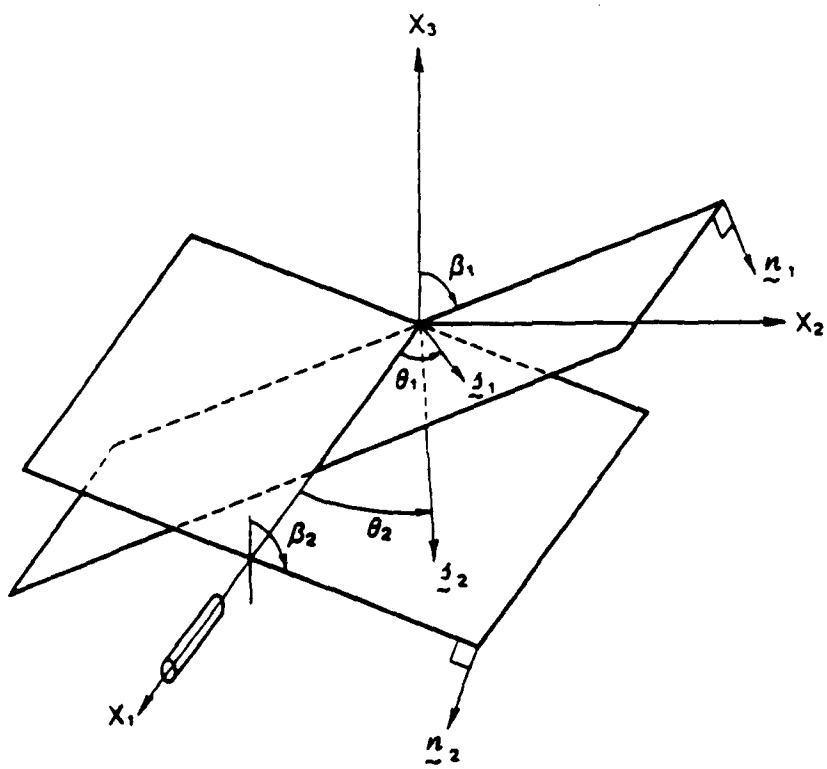

FIG. 17. Geometry of the two conjugate slip systems of the matrix-dominated mode (MDM). Reprinted with permission from Springer-Verlag, G. J. Dvorak and Y. A. Bahei-El-Din, *Acta Mechanica* 69, 219 (1987).

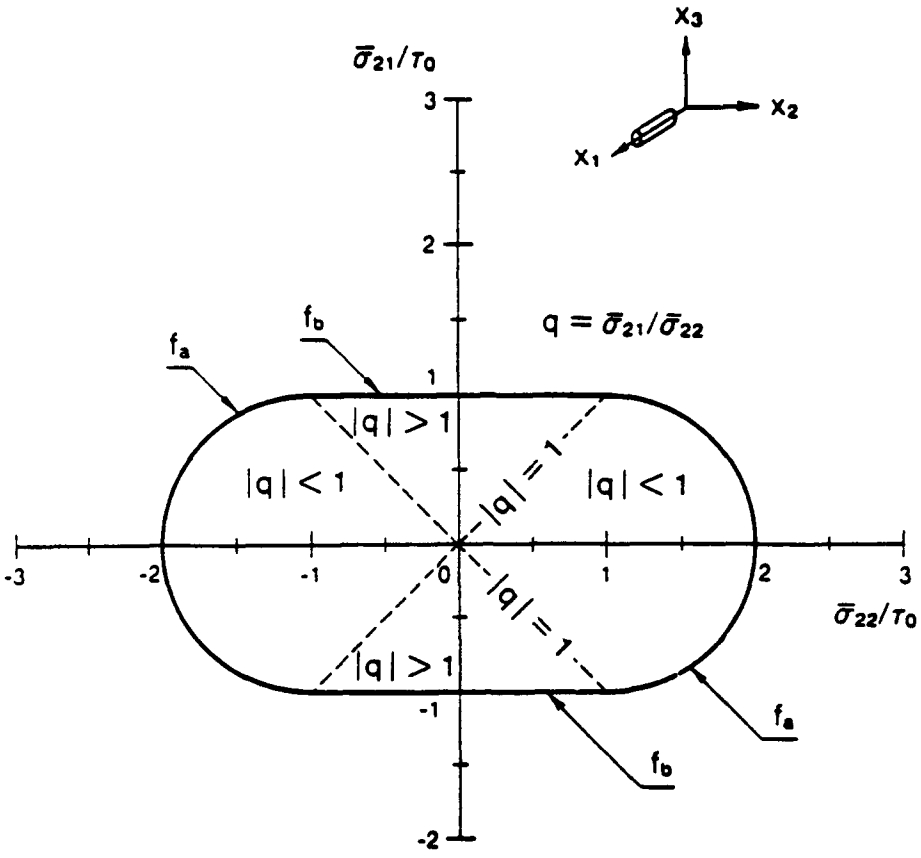

FIG. 18 Transverse cross section of the cylindrical overall yield surface of the matrix-dominated mode. Reprinted with permission from Springer-Verlag, G. J. Dvorak and Y. A. Bahei-El-Din, *Acta Mechanica* **69**, 219 (1987).

The surface consists of two segments defined by the equations

$$f_a \equiv (\bar{\sigma}_{21} - \tilde{x}_{21})^2/\tau_0 + [(\bar{\sigma}_{22} - \tilde{x}_{22})/\tau_0 \mp 1]^2 - 1 = 0 \qquad \text{for} \quad |q| \leq 1,$$
$$f_b \equiv (\bar{\sigma}_{21} - \tilde{x}_{21})^2 - \tau_0 = 0 \qquad \text{for} \quad |q| \geq 1, \tag{160}$$

where $q = (\bar{\sigma}_{21} - \tilde{x}_{21})/(\bar{\sigma}_{22} - \tilde{x}_{22})$, and $\tilde{x}_{ij} = 0$ for an initial yield surface.

Figures 19 and 20 show superimposed yield surfaces for the two modes and for two material systems. Figure 19 represents the section by the transverse normal stress $\bar{\sigma}_{22}$ and longitudinal shear $\bar{\sigma}_{21}$ plane. Fig. 20 by the axial normal stress $\bar{\sigma}_{11}$ and longitudinal shear plane. In both figures, the solid line indicates the MDM yield surface, which is not affected by phase elastic properties and is therefore unique for all systems. The various

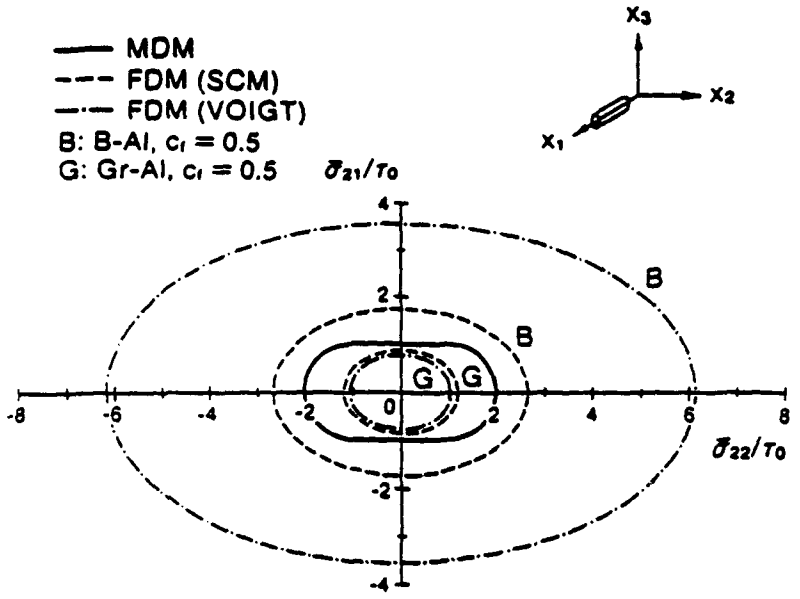

FIG. 19. Initial yield surfaces in the transverse tension ($\bar{\sigma}_{22}$) and longitudinal shear ($\bar{\sigma}_{21}$) plane. Comparison of the fiber-dominated (FDM) and matrix-dominated (MDM) yield modes in B Al and Gr Al composites. Reprinted with permission from Springer-Verlag, G. J. Dvorak and Y. A. Bahei-El-Din. *Acta Mechanica* **69**, 219 (1987).

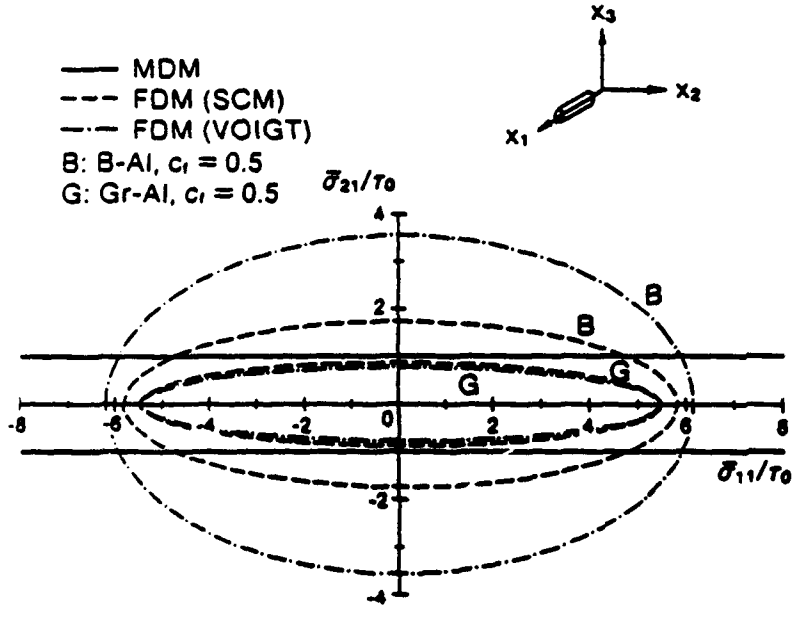

FIG. 20. Initial yield surfaces in the axial tension ($\bar{\sigma}_{11}$) and longitudinal shear ($\bar{\sigma}_{21}$) plane. Comparison of fiber-dominated (FDM) and matrix-dominated (MDM) yield modes in B Al and Gr/Al composite systems. Reprinted with permission from Springer-Verlag, G. J. Dvorak and Y. A. Bahei-El-Din, *Acta Mechanica* **69**, 219 (1987).

ellipses represent the FDM surfaces. Those were found for the B/Al and the T-50 Gr Al systems and are designated by letters *B* and *G*, respectively. The phase volume fractions were taken as equal to 0.5 in both systems. One set of the FDM surfaces was found using the self-consistent estimate of local stresses (SCM), and another set with the Voigt approximation, cf. (30).

Note that the B Al system yield surfaces have both MDM and FDM segments, the actual yield surface is the internal envelope of the segments. Within this envelope, the FDM segments can be regarded as end caps on the MDM oval cylinder. In the Gr Al system, the FDM surfaces are always within the MDM surface, hence the former is the active mode. Since only phase elastic properties are involved, one may ask which property makes a particular mode more or less prominent. In the example shown, the matrix is isotropic and its properties are identical in both systems. The B fiber is also isotropic, but the Gr fiber is transversely isotropic. Elastic constants used in the evaluation appear in Table 1.

The axial fiber moduli are very similar, but there is a large difference in the longitudinal shear modulus G_A, which is smaller in the graphite fiber than in the matrix and an order of magnitude smaller than the corresponding fiber modulus. The implication is that the MDM deformation is preferred in systems that have fibers of large shear stiffness, and the FDM modes are preferred in fibers that are compliant in shear. One may speculate that the stiff fiber tends to prevent plastic shearing on planes that intersect the fiber axis, and therefore encourages the slip pattern of Fig. 17. The more compliant fiber cannot do that, and thus the FDM mode may prevail.

Viewed from a different perspective, the results in Figs. 19 to 22 can be taken as a serious warning against indiscriminate use of averaging methods in plasticity of fibrous composites. Indeed, only the yield surface of the fiber mode may possibly be approximated by the self-consistent estimate of the local stresses, and then only under plane stress. Figure 14 tends to confirm this; note the agreement between the PHA and the averaging predictions in the Gr Al, which appear in Figs. 15 and 16. However, even in the seemingly simple case of uniform thermal change, averaging methods typically predict

TABLE 1
ELASTIC PROPERTIES OF SELECTED MATRIX AND FIBER MATERIALS

	E_A [GPa]	G_A [GPa]	ν_A	E_T [GPa]	G_T [GPa]
6061 Aluminum	72.5	27.2	0.33	72.5	27.2
Boron	400.0	166.8	0.20	400.0	166.8
T-50 Graphite	386.4	15.2	0.41	7.6	2.6

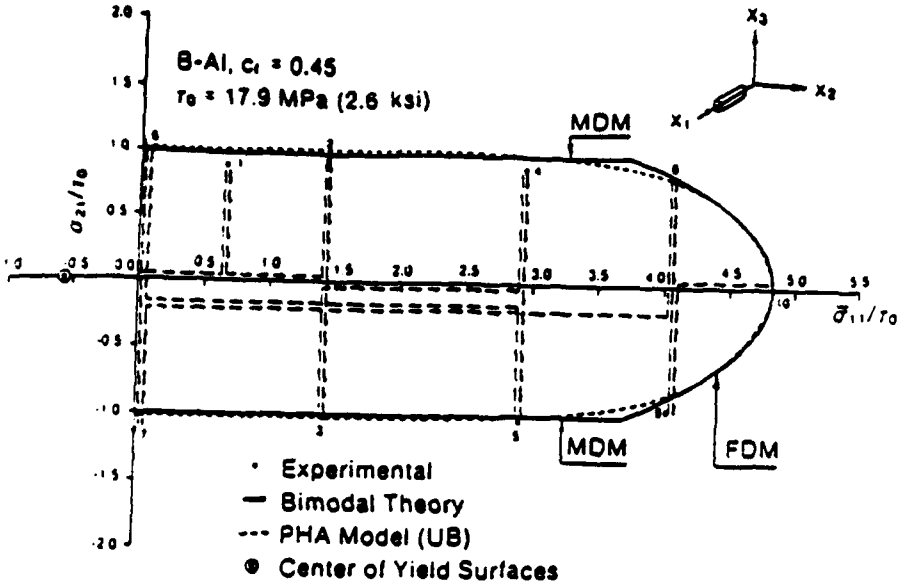

FIG. 21 Initial yield surface of a B-Al composite in the longitudinal plane. Comparison of experimental results with yield surfaces derived from the bimodal plasticity theory and the PHA model. Reprinted with permission from Springer-Verlag, G. J. Dvorak and Y. A. Bahei-El-Din, *Acta Mechanica* **69**, 219 (1987).

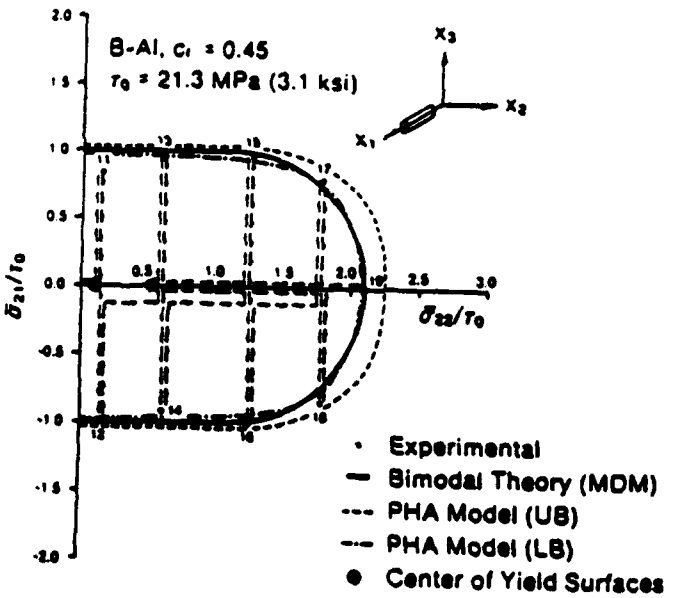

FIG. 22 Initial yield surface of the B-Al system in the transverse stress (σ_{22}) and longitudinal shear (σ_{21}) plane. Comparison of experimental results with surfaces derived from the PHA model, and from the matrix-dominated deformation mode (MDM). Reprinted with permission from Springer-Verlag, G. J. Dvorak and Y. A. Bahei-El-Din, *Acta Mechanica* **69**, 219 (1987).

an open cylindrical yield surface in the principal overall stress space [*72, 75*], whereas the actual overall yield surface is closed [*64, 66*]. Such disagreements in yield surface predictions then imply further problems in the evaluation of subsequent overall surfaces and plastic strains: this is illustrated in Fig. 16. The conclusion that emerges from these and other examples is that one may use the self-consistent or the Mori–Tanaka method with some confidence only in exceptional circumstances, which are currently limited to the plane stress FDM deformation.

We now turn our attention to the evaluation of plastic strains. Note first that the yield condition (160) suggests that the yield stress is independent of the slip system involved, which is confirmed by the experimental results that follow. Of course, that would be true in any case on the flat branches that engage only a single system. However, comparisons of the MDM results with the PHA model, and experimental measurements of flow stress, indicate that the slip direction, and perhaps even the direction of the stress increment, both influence the instantaneous overall properties in the plastic range if loading involves any of the semicircular segments of the MDM yield surface. The relevant connections have not yet been fully established, but work currently in progress indicates that good comparisons of predicted plastic strains with those measured in carefully conducted experiments are possible with the PHA model.

This is actually a part of a broader problem that remains unresolved in plasticity of both homogeneous and heterogeneous media, namely the formulation of reliable predictions of plastic strains during loading along an arbitrary path. A promising approach is offered by the contemporary multiple surface theories that are discussed, for example, in [*48, 49, 59*], but a definite treatment of this subject must await further research.

5. Comparison with Experimental Results

Whereas the theoretical aspects of elastic–plastic behavior of fibrous composites have been investigated rather extensively, only limited attention has been given to experimental investigations of the actual behavior of composite systems. To be useful in verification of a theory, the experiments must reflect overall response under multiaxial incremental loading. So far, only the recent study by Dvorak *et al.* [*50*] has been designed with this purpose in mind.

The work was conducted on thin-walled B/Al tubes, which were reinforced by continuous fibers aligned in the axial direction. Similar matrix tubes were tested as well. The tubes were loaded incrementally by combinations of an axial force, internal pressure, and torque; the in-plane strains were measured

and recorded. The purpose of the investigation was to establish initial and subsequent yield surfaces, and plastic strain magnitudes and directions, for several different loading programs.

Figures 21 and 22 show the initial yield surfaces in two stress planes. The coordinates have been normalized with respect to the composite yield stress τ_0 in longitudinal shear. The experimental points are connected by the arrows, which retrace the actual loading sequence. The solid line shows the MDM and FDM yield surface segments determined for the current τ_0. The dashed line is the prediction of the PHA model, with the same τ_0 and yield stress definition used in the experiments; the definition, we recall, relies on a back-extrapolation from few initial plastic steps. Both upper (UB) and lower (LB) bounds were computed in Fig. 22, but only the upper bound in Fig. 21. The agreement of the two predictions with experiments is satisfactory, and the existence of the flat segments of the surface is clearly confirmed. The positions of the centers of the surfaces do not coincide with the origin, which is believed to be caused by residual thermal stresses left after cooling from the annealing temperature. Note also that the values of τ_0 are different in the two figures. Such variations have been also observed in subsequent surfaces, both in the composite and in similar matrix specimens.

Many subsequent yield surfaces were evaluated. They were found to be of similar shape, but the size, i.e., the current τ_0, changed somewhat along the path. Similar changes were observed in the matrix surfaces. Figure 23 illustrates some of the results. The loading path connects points 87 and 88, then continues from 99 to 100, then from 113 to 114, from 136 to 127, and finally from 132 to 133. The intervening points define the loading surfaces established at the breaks in continuous loading. Note the similarity in shape, and also the adherence to the Phillips hardening rule (77, 78). An exception to the latter was found, however, for loading at the flat segments (Fig. 24). The normal stress component, which is parallel to the flat segment, exerts no influence on the translation, but reasserts itself if the loading vector is on the semicircular branch, *cf.* path 132–133 in Fig. 23b. A possible explanation of this behavior appears in [*50*]. The translation of the MDM surface is given, with reference to (160),

$$\begin{aligned} d\tilde{x}_{21} &= d\bar{\sigma}_{21}, \quad d\tilde{x}_{22} = d\bar{\sigma}_{22} \qquad \text{for} \quad f_a \equiv 0, \ |q| \le 1 \\ d\tilde{x}_{21} &= d\bar{\sigma}_{21} \qquad\qquad\qquad\quad \text{for} \quad f_b \equiv 0, \ |q| \ge 1. \end{aligned} \tag{161}$$

The strain increment vectors were found to follow the normality requirement along some but not all loading directions. An interpretation of the results is still in progress.

Figure 25 is another illustration of the agreement between the two theories

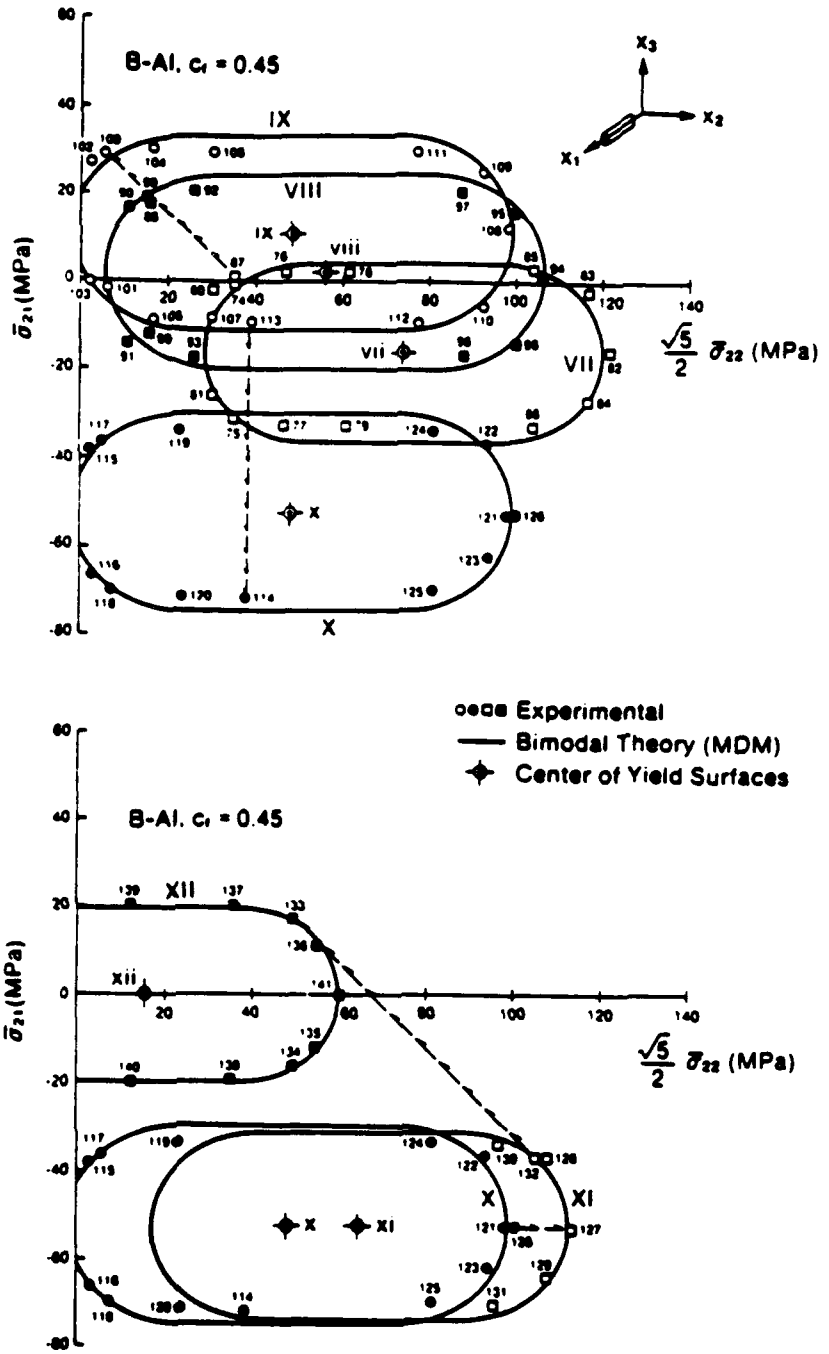

FIG. 23. Subsequent yield surfaces of the B/Al composite. Reprinted with permission from *J. Mech. Phys Solids* 36, 655, G. J. Dvorak, Y. A. Bahei-El-Din, Y. Macheret, and C. H. Liu, © 1988, Pergamon Press plc.

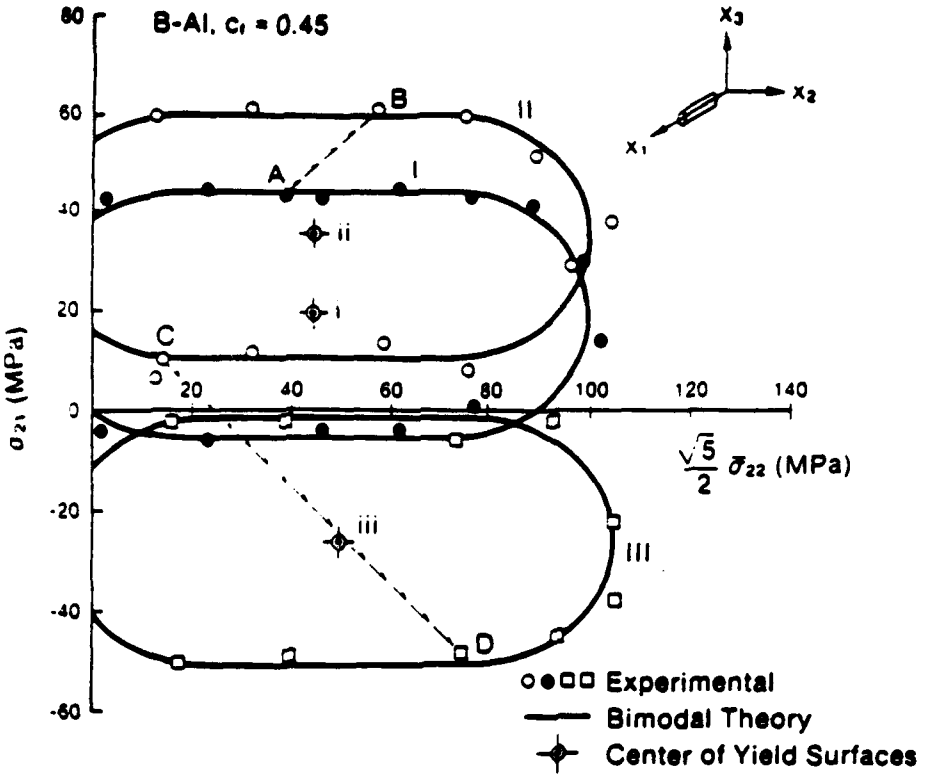

FIG. 24. Subsequent yield surfaces of the B/Al composite. Load is applied at the flat segments of the surface. Reprinted with permission from *J. Mech. Phys Solids* 36, 655. G. J. Dvorak, Y. A. Bahei-El-Din, Y. Macheret, and C. H. Liu, © 1988, Pergamon Press plc.

and experiments. For a cyclic loading path *ABCDEA*, which was retraced several times, we show the subsequent yield surfaces found by the different approaches. PHA-computed directions of the plastic strain vectors are shown as well. These are mostly normal to the current surface, whereas the experimentally measured plastic strains often have an additional longitudinal shear component.

IV. Conclusion

Space limitations prevent discussion of other aspects of plasticity of composites, and also of the applications of the above theories to practical problems. We note here related studies of fatigue behavior of B/Al laminates [*93*, *94*] that indicate that the onset and evolution of damage is closely related

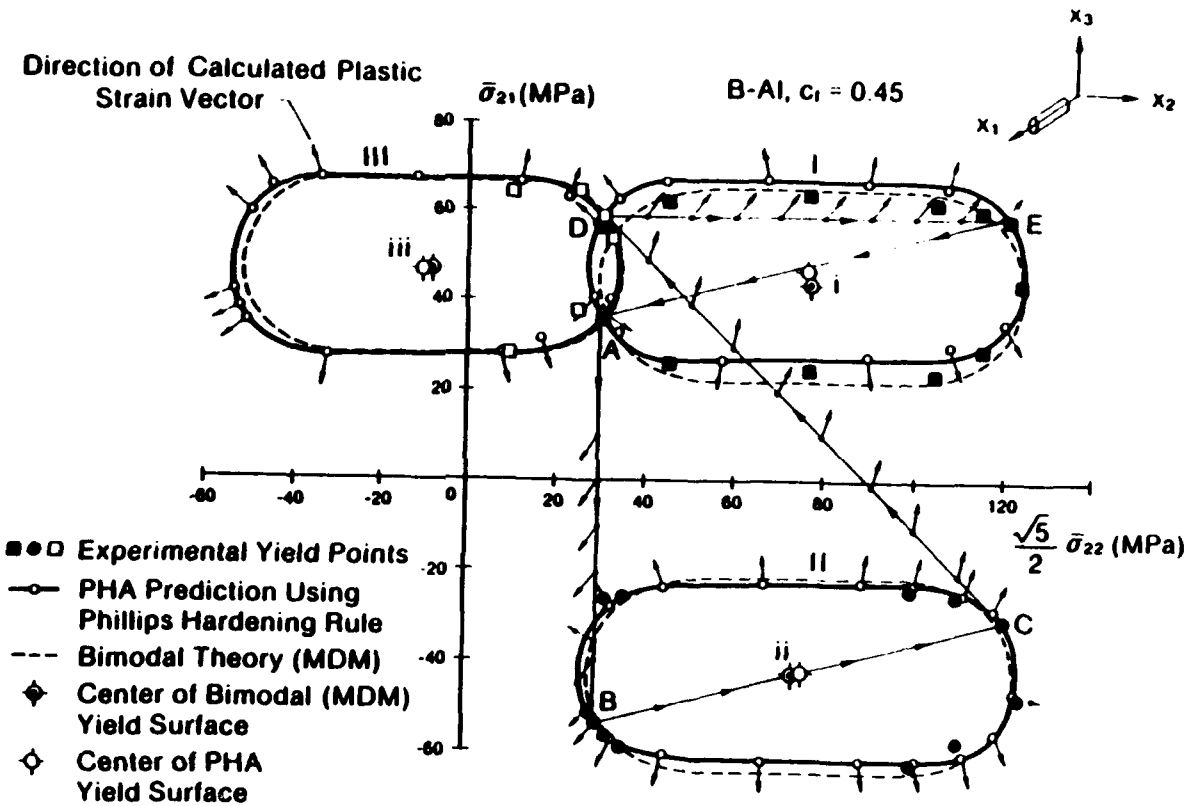

FIG. 25. Yield surfaces for a cyclic loading program *ABCDEA*. Comparison of experimental results with PHA and bimodal theory (MDM) predictions.

to shakedown of the laminate. The damage process is dominated by growth of low-cycle fatigue cracks in the matrix, on planes that are parallel to the fiber direction in each off-axis ply. Cracks perpendicular to the loading direction grow in the matrix of the axial 0° plies. Cyclic plastic straining of the matrix drives the cracks, and when it terminates by shakedown, the damage process reaches a saturation state. Laminate stiffness loss caused by damage saturation at a constant load amplitude has been predicted on these grounds and found to be in agreement with experimental measurements.

Another recent application of the theory has been in predictions of fracture strength of notched unidirectional B-Al plates [*95, 96*]. The matrix-dominated mode of deformation was identified there with discrete plastic zones that were observed to grow from notch tips, in the fiber direction, under increasing load. When plasticity was assumed to be limited to the matrix mode, the definition of zone geometry led to reliable predictions of local stresses ahead of the notch and to fracture strength estimates for the plates.

Current work that utilizes the PHA model includes a study in dimensional stability of Gr Al $\pm\theta$ laminates [*91*]. There we found that plastic deformation may improve dimensional stability in comparison with a purely elastic response in certain layups. The interaction between mechanical and thermal loads was also examined; particular combinations may enhance or impair dimensional stability.

Plasticity of particle- or whisker-reinforced composite materials is closely related to the present subject. In comparison to fibrous composites, the microstructural geometry of such systems is much more complex, and that makes modeling more difficult. The averaging techniques discussed earlier, such as the self-consistent and the Mori–Tanaka methods, are often likely to be employed in model development. Examples can be found in the work of Hutchinson [*97, 98*], Duva [*99*], Weng [*100*], Tandon and Weng [*101*], and McMeeking [*102*]. Experimental or computational verification is apparently not available in the literature.

Acknowledgments

Financial support for this work was provided by the Office of Naval Research. Professors Yehia A. Bahei-El-Din, Mark Shephard and Jerry Lin, Dr. Jan L. Teply, and graduate students, R. Shah and J. F. Wu, contributed to the recent work on plasticity of composite materials described herein.

Appendix

This is a brief summary of the relevant details of the notation used in the chapter. The constitutive relations of an elastic, transversely isotropic solid, with the axis of rotational symmetry x_1, has the form

$$\begin{Bmatrix} \varepsilon_1 \\ \varepsilon_2 \\ \varepsilon_3 \\ \varepsilon_4 \\ \varepsilon_5 \\ \varepsilon_6 \end{Bmatrix} = \begin{bmatrix} 1/E_L & -\nu_L/E_L & -\nu_L/E_L & 0 & 0 & 0 \\ & 1/E_T & -\nu_T/E_T & 0 & 0 & 0 \\ & & 1/E_T & 0 & 0 & 0 \\ & & & 1/G_T & 0 & 0 \\ & & & & 1/G_L & 0 \\ \text{SYM.} & & & & & 1/G_L \end{bmatrix} \begin{Bmatrix} \sigma_1 \\ \sigma_2 \\ \sigma_3 \\ \sigma_4 \\ \sigma_5 \\ \sigma_6 \end{Bmatrix}$$

$$\begin{Bmatrix} \sigma_1 \\ \sigma_2 \\ \sigma_3 \\ \sigma_4 \\ \sigma_5 \\ \sigma_6 \end{Bmatrix} = \begin{bmatrix} n & l & l & 0 & 0 & 0 \\ & (k+m) & (k-m) & 0 & 0 & 0 \\ & & (k+m) & 0 & 0 & 0 \\ & & & m & 0 & 0 \\ & & & & p & 0 \\ \text{SYM.} & & & & & p \end{bmatrix} \begin{Bmatrix} \varepsilon_1 \\ \varepsilon_2 \\ \varepsilon_3 \\ \varepsilon_4 \\ \varepsilon_5 \\ \varepsilon_6 \end{Bmatrix}.$$

The moduli E_L, G_L refer to straining in the longitudinal direction, and E_T, G_T in the transverse plane. Poisson's ratios are defined as $\nu_L = -\varepsilon_2/\varepsilon_1$, $\nu_T = -\varepsilon_3/\varepsilon_2$ under uniaxial tension σ_1, σ_2, respectively.

Hill's moduli k, l, n, m, and p are related to the moduli in the compliance matrix by the relations

$$k = [1/G_T - 4/E_T + 4\nu_L^2/E_L]^{-1},$$

$$l = 2k\nu_L,$$

$$n = E_L + 4k\nu_L^2 = E_L + l^2/k,$$

$$m = G_T, \qquad p = G_L.$$

Additional useful connections are

$$E_T = 2(1+\nu_T)G_T = 4km/(k+qm),$$

$$\nu_T = (k-qm)/(k+qm),$$

$$q = 1 + (4k\nu_L^2)/E_L.$$

If the solid is isotropic, with bulk modulus K and shear modulus G, then

$$k = G/(1-2\nu), \qquad l = K - 2G/3,$$

$$n = K + 4G/3, \qquad m = p = G.$$

References

1. R. Hill, *J. Mech. Phys. Solids*, **11**, 357 (1963).
2. R. Hill, *J. Mech. Phys. Solids*, **13**, 213 (1965).
3. V. M. Levin, *Mekh. Tverd. Tela.*, **2**, 88 (1967).
4. B. W. Rosen and Z. Hashin, *Int. J. Engng. Sci.*, **8**, 157 (1970).
5. N. Laws, *J. Mech. Phys. Solids*, **21**, 9 (1973).
6. Y. Takao and M. Taya, *J. Appl. Mech.*, **52**, 806 (1985).
7. G. J. Dvorak, *J. Appl. Mech.*, **53**, 737 (1986).
8. Y. Benveniste and G. J. Dvorak, in "Micromechanics and Inhomogeneity—The Toshio Mura Anniversary Volume," p. 65. Springer-Verlag, New York, 1989.
9. J. D. Eshelby, *Proc. Roy. Soc. London*, **A241**, 376 (1957).
10. J. D. Eshelby, in "Progress in Solid Mechanics" (I. N. Sneddon and R. Hill, eds.), Vol. II, p. 87. North-Holland Publ., Amsterdam, 1961.
11. M. Kinoshita and T. Mura, *Physica Status Solidi A*, **5**, 759 (1971).
12. T. Mura, "Micromechanics of Defects in Solids," Martinus Nijhoff Publ., The Hague, 1982.
13. L. J. Walpole, *Proc. Roy. Soc. London*, **A300**, 270 (1967).
14. L. J. Walpole, *J. Mech. Phys. Solids*, **17**, 235 (1969).
15. F. Ghahremani, *Mech. Res. Commun.*, **4**, 89 (1977).
16. R. Hill, *J. Mech. Phys. Solids*, **12**, 199 (1964).
17. A. V. Hershey, *J. Appl. Mech.*, **21**, 236 (1954).
18. B. Budiansky, *J. Mech. Phys. Solids.*, **13**, 223 (1965).
19. R. Hill, *J. Mech. Phys. Solids*, **13**, 189 (1965).
20. T. Mori and K. Tanaka, *Acta Metall.*, **21**, 571 (1973).
21. Y. Benveniste, *Mech. Mater.*, **6**, 147 (1987).
22. A. N. Norris, *J. Appl. Mech.*, **56**, 83 (1989).
23. G. J. Weng, *Int. J. Engng. Sci.*, **22**, 8945 (1984).
24. T. Chen and G. J. Dvorak, "On the Overall Elastic Moduli of Composite Materials by the Mori–Tanaka Scheme," to be published.
25. Z. Hashin, and S. Shtrikman, *J. Mech. Phys. Solids*, **10**, 335 (1962).
26. Z. Hashin, and S. Shtrikman, *J. Mech. Phys. Solids*, **10**, 343 (1962).
27. Z. Hashin, and S. Shtrikman, *J. Mech. Phys. Solids*, **11**, 127 (1963).
28. Z. Hashin, *J. Mech. Phys. Solids*, **13**, 119 (1965).
29. Z. Hashin, and B. W. Rosen, *J. Appl. Mech.*, **31**, 223 (1964).
30. R. Hill, in "Progress in Applied Mechanics, The Prager Anniversary Volume," Vol. 99, Macmillan, New York, 1963.
31. L. J. Walpole, *J. Mech. Phys. Solids*, **14**, 151 (1966).
32. L. J. Walpole, *J. Mech. Phys. Solids*, **14**, 289 (1966).
33. J. R. Willis, *J. Mech. Phys. Solids*, **25**, 185 (1977).
34. J. R. Willis, in "Advances in Applied Mechanics," Vol. 21, p. 1. Academic Press, New York, 1981.
35. G. W. Milton, and R. V. Kohn, *J. Mech. Phys. Solids*, **36**, 597 (1988).
36. R. M. Christensen, "Mechanics of Composite Materials," Wiley, New York, 1979.
37. L. J. Walpole, in "Advances in Applied Mechanics," Vol. 21, p. 169. Academic Press, New York, 1981.
38. L. J. Walpole, in "Fundamentals of Deformation and Fracture" (B. A. Bilby, K. J. Miller, and J. R. Willis, eds.), p. 91. Cambridge University Press, Cambridge, 1985.
39. Z. Hashin, *J. Appl. Mech.*, **50**, 481 (1983).
40. G. J. Dvorak, "On Uniform Fields in Heterogeneous Media," to be published in *Proc. Roy. Soc. London*, 1990.

41 R. Hill, "The Mathematical Theory of Plasticity," Oxford University Press, Oxford, 1950.
42 D. C. Drucker, in "Proc. 1st U. S. Natl. Congress Appl. Mech.," p. 487. ASME, New York, 1952.
43 P. M. Naghdi, in "Proc. Second Symp. Naval Structural Mechanics" (E. H. Lee and P. S. Symonds, eds.), p. 121. Pergamon Press, New York, 1960.
44 J. B. Martin, "Plasticity: Fundamentals and General Results," The MIT Press, Cambridge, Mass., 1975.
45 A. Phillips, C. S. Liu, and J. W. Justusson, *Acta Mechanica*, **14**, 119 (1972).
46 A. Phillips and H. Moon, *Acta Mechanica*, **27**, 91 (1977).
47 A. Phillips and C. W. Lee, *Int. J. Solids Structures*, **15**, 715 (1979).
48 D. L. McDowell, *J. Appl. Mech.*, **54**, 323 (1987).
49 J. L. Chaboche, *Int. J. Plasticity*, **2**, 149 (1986).
50 G. J. Dvorak, Y. A. Bahei-El-Din, Y. Macheret, and C. H. Liu, *J. Mech. Phys. Solids*, **36**, 655 (1988).
51 J. F. Mulhern, T. G. Rogers, and A. J. M. Spencer, *Proc. Roy. Soc. London*, **A301**, 473 (1967).
52 A. E. Green and J. E. Atkins, "Large Elastic Deformation," Oxford University Press, Oxford, 1960.
53 A. J. M. Spencer, "Theory of Invariants" in *Continuum Physics*, Vol. I (A. C. Eringen, ed.), p. 239. Academic Press, New York, 1971.
54 J. Casey and P. M. Naghdi, *J. Appl. Mech.*, **50**, 350 (1983).
55 P. J. Yoder and W. D. Iwan, *J. Appl. Mech.*, **48**, 773 (1981).
56 C. J. Wung and G. J. Dvorak, *Int. J. Plasticity*, **1**, 125 (1985).
57 H. Ziegler, *Q. Appl. Math.*, **17**, 55 (1959).
58 Y. A. Bahei-El-Din, "Plasticity Analysis of Fibrous Composite Laminates under Thermo-mechanical Loads," to appear in *ASTM-STP*.
59 Y. F. Dafalias and E. P. Popov, *J. Appl. Mech.*, **43**, 645 (1976).
60 J. Lin and G. J. Dvorak, "Local and Overall Elastic-Plastic Response of Particle-Reinforced Metal Matrix Composites," to be published.
61 R. Hill, *J. Mech. Phys. Solids*, **15**, 79 (1967).
62 G. J. Dvorak and Y. A. Bahei-El-Din, *Acta Mechanica*, **69**, 219 (1987).
63 R. Hill, *J. Mech. Phys. Solids*, **13**, 89 (1965).
64 G. J. Dvorak, M. S. M. Rao, and J. Q. Tarn, *J. Comp. Mater.*, **7**, 194 (1973).
65 G. J. Dvorak and M. S. M. Rao, and J. Q. Tarn, *J. Appl. Mech.*, **41**, 249 (1974).
66 G. J. Dvorak and M. S. M. Rao, *J. Appl. Mech.*, **43**, 619 (1976).
67 J. R. Rice, *J. Appl. Mech.*, **37**, 728 (1970).
68 J. R. Rice, *J. Mech. Phys. Solids*, **19**, 433 (1971).
69 R. Hill and J. R. Rice, *J. Mech. Phys. Solids*, **20**, 401 (1972).
70 R. Hill and J. R. Rice, *SIAM J. Appl. Math.*, **25**, 448 (1973).
71 A. J. M. Spencer, "Deformation of Fiber-Reinforced Materials," Oxford University Press, Oxford, 1972.
72 G. J. Dvorak and Y. A. Bahei-El-Din, *J. Mech. Phys. Solids*, **27**, 51 (1979).
73 G. J. Dvorak and Y. A. Bahei-El-Din, in "Proceedings of ARO/NSF Research Workshop on Mechanics of Composite Materials," (G. J. Dvorak, ed.), pp. 32–54. Duke University, Durham, N.C., 1978.
74 G. J. Dvorak and Y. A. Bahei-El-Din, *J. Appl. Mech.*, **49**, 327 (1982).
75 Y. A. Bahei-El-Din and G. J. Dvorak, *J. Appl. Mech.*, **49**, 740 (1982).
76 J. Aboudi, *Int. J. Engng Sci.*, **20**, 605 (1982).
77 Y. A. Bahei-El-Din, G. J. Dvorak, and S. Utku, *Computers and Structures*, **13**, 321 (1981).
78 Y. A. Bahei-El-Din and G. J. Dvorak, *J. Appl. Mech.*, **47**, 827 (1980).
79 W. S. Johnson, C. A. Bigelow, and Y. A. Bahei-El-Din, NASA Technical Paper 2187, 1983.

80. A. J. Svobodnik, H. J. Bohm and F. G. Rammerstorfer, in "Advances in Plasticity 1989" (A. S. Khan and M. Tokuda, eds.), p. 137, Pergamon Press, New York, 1989.
81. H. J. Greenberg, *Q. Appl. Math.*, 7, 85 (1949).
82. D. C. Drucker, in "Calculus of Variations and its Applications, Proceedings of Symposia in Applied Mathematics," Vol. VIII, p. 7, McGraw Hill, New York, 1958.
83. P. G. Hodge, Jr., in "Engineering Plasticity," (J. Heyman and F. A. Leckie, eds.), p. 237, Cambridge University Press, Cambridge, 1968.
84. G. J. Dvorak and J. L. Teply, in "Plasticity Today: Modelling, Methods and Applications, W. Olszak Memorial Volume" (A. Sawczuck and V. Bianchi, eds.), p. 623, Elsevier, London, 1985.
85. J. L. Teply and G. J. Dvorak, *J. Mech. Phys. Solids*, **36**, 29 (1988).
86. M. L. Accorsi and S. Nemat-Nasser, *Mechanics of Materials*, **5**, 209 (1986).
87. B. Fraeijs De Veubeke, "Stress Analysis" (O. C. Zienkiewicz and G. S. Hollister, eds.), Ch. 9, Wiley, New York, 1965.
88. O. C. Zienkiewicz, "The Finite Element Method," McGraw-Hill, London, 1977.
89. J. L. Teply, Ph.D. Thesis, University of Utah, Salt Lake City, 1984.
90. Y. A. Bahei-El-Din, G. J. Dvorak, J. Lin, R. S. Shah, and J. F. Wu, "Local Fields and Overall Response of Fibrous and Particulate Metal Matrix Composites," ALCOA Laboratories Report, 1987.
91. J. F. Wu, M. S. Shephard, G. J. Dvorak, and Y. A. Bahei-El-Din, *Composites Science and Technology*, **35**, 347 (1989).
92. J. F. W. Bishop and R. Hill, *Phil. Mag.*, **42**, 414 (1951).
93. G. J. Dvorak and W. S. Johnson, *Int. J. Fracture*, **16**, 585 (1980).
94. G. J. Dvorak and E. C. J. Wung, in "Strain Localization and Size Effect Due to Cracking and Damage" (J. Mazars and Z. P. Bazant, eds.), Elsevier Applied Science Publishers, London, 1989.
95. G. J. Dvorak, Y. A. Bahei-El-Din, and L. C. Bank, *Engng. Fracture Mech.*, **34**, 87 (1989).
96. Y. A. Bahei-El-Din, G. J. Dvorak, and J. F. Wu, *Engrg. Fracture Mech.*, **34**, 105 (1989).
97. J. W. Hutchinson, *Proc. Roy. Soc. London*, **A319**, 247 (1970).
98. J. W. Hutchinson, *Proc. Roy. Soc. London*, **A348**, 101 (1976).
99. J. M. Duva, *J. Engng. Materials and Technology*, **106**, 317 (1984).
100. G. Weng, *Intl. J. Plasticity*, **1**, 275 (1985).
101. G. P. Tandon and G. Weng, *J. Appl. Mech.*, **55**, 126 (1988).
102. R. M. McMeeking, in "Mechanics of Material Behavior—The Daniel C. Drucker Anniversary Volume" (G. J. Dvorak and R. T. Shield, eds.), p. 275, Elsevier Science Publishers, Amsterdam, 1984.
103. Y. Benveniste, G. J. Dvorak, and T. Chen, *Mech. of Mater.*, **305**, 8 (1989).

SECURITY CLASSIFICATION OF THIS PAGE

REPORT DOCUMENTATION PAGE

Form Approved OMB No. 0704-0188

1a. REPORT SECURITY CLASSIFICATION Unclassified	1b. RESTRICTIVE MARKINGS
2a. SECURITY CLASSIFICATION AUTHORITY	3. DISTRIBUTION/AVAILABILITY OF REPORT Approved for public release Distribution unlimited
2b. DECLASSIFICATION/DOWNGRADING SCHEDULE	
4. PERFORMING ORGANIZATION REPORT NUMBER(S)	5. MONITORING ORGANIZATION REPORT NUMBER(S)
6a. NAME OF PERFORMING ORGANIZATION Rensselaer Polytechnic Institute 6b. OFFICE SYMBOL (If applicable)	7a. NAME OF MONITORING ORGANIZATION
6c. ADDRESS (City, State, and ZIP Code) Troy, NY 12180-3590	7b. ADDRESS (City, State, and ZIP Code)
8a. NAME OF FUNDING/SPONSORING ORGANIZATION Mechanics Division Office of Naval Research 8b. OFFICE SYMBOL (If applicable)	9. PROCUREMENT INSTRUMENT IDENTIFICATION NUMBER
8c. ADDRESS (City, State, and ZIP Code) 800 North Quincy Street Arlington, Virginia 22217	10. SOURCE OF FUNDING NUMBERS PROGRAM ELEMENT NO. / PROJECT NO. / TASK NO. / WORK UNIT ACCESSION NO

11. TITLE (Include Security Classification)
Mechanics of Composite Materials for Spacecraft (unclassified)

12. PERSONAL AUTHOR(S)
George J. Dvorak, Mark S. Shephard

13a. TYPE OF REPORT	13b. TIME COVERED	14. DATE OF REPORT (Year, Month, Day)	15. PAGE COUNT
Final	FROM 6/1/91 TO 12/31/91	August 1992	

16. SUPPLEMENTARY NOTATION

17. COSATI CODES			18. SUBJECT TERMS (Continue on reverse if necessary and identify by block number)
FIELD	GROUP	SUB-GROUP	Composite materials, inelastic deformation, finite element analysis

19. ABSTRACT (Continue on reverse if necessary and identify by block number)

During this seven month project efforts continued on the development of advanced analytical and numerical techniques which can be effectively combined to provide advanced thermomechanical modeling of composite materials with nonlinear constituents. The areas of emphasis during this period were:

- development of thermoplastic and thermoviscoplastic models of composite materials using transformation strains;
- finite element formulation of bimodal plasticity model in combination with various forms of dimensional reduction;
- idealization control for composite materials.

20. DISTRIBUTION/AVAILABILITY OF ABSTRACT	21. ABSTRACT SECURITY CLASSIFICATION
☒ UNCLASSIFIED/UNLIMITED ☐ SAME AS RPT. ☐ DTIC USERS	
22a. NAME OF RESPONSIBLE INDIVIDUAL YAPA RAJAPAKSE	22b. TELEPHONE (Include Area Code) 202-696-4404 / 22c. OFFICE SYMBOL

DD Form 1473, JUN 86 Previous editions are obsolete. SECURITY CLASSIFICATION OF THIS PAGE